THE INFLUENCE OF RELATIVISTIC EFFECTS ON THE NUCLEAR MAGNETIC RESONANCE SPECTRA

Artur Wodyński

March 2015

Artur Wodyński, *The influence of relativistic effects on the Nuclear Magnetic Resonance Spectra*

Tytuł w języku polskim: *Wpływ efektów relatywistycznych na widma jądrowego rezonansu magnetycznego*

Ph. D. thesis under supervision of
dr hab. Magdalena Pecul-Kudelska, prof. UW
Faculty of Chemistry, University of Warsaw
Pasteura 1, 02-093 Warsaw, Poland
and
prof. Adam Gryff-Keller
Faculty of Chemistry, Warsaw University of Technology
Noakowskiego 3, 00-664 Warsaw, Poland

The results presented in this thesis were obtained with the generous financial support of MPD/2010/4 project, realized within the MPD programme of Foundation for Polish Science, cofinanced from European Union, Regional Development Fund.

to Marcin

Contents

Chapter 1

Introduction

The Nuclear Magnetic Resonance spectroscopy is a valuable source of structural information. This method is especially useful for biomolecules and their complexes, since in many cases they are difficult to crystallise and therefore the techniques based on X-Ray diffraction or neutron scattering cannot be used. Typically, NOE (Nuclear Overhauser Effects) approach is used to determine secondary structure of proteins and nucleic acids. However, in many cases also the values of the shielding constants and the spin-spin coupling constants can be employed for this purpose.

NMR spectroscopy of light nuclei like ^{1}H, ^{13}C, ^{15}N, and ^{31}P is nowadays a routine research tool in organic chemistry or biochemistry. In organometallic and bioorganometallic chemistry, ^{195}Pt, ^{199}Hg or ^{205}Tl NMR is employed too, since these isotopes also have ½ nuclear spins and thus give sharp signals. Moreover, they have a very wide range of chemical shifts. NMR spectra are routinely collected to confirm whether the synthesis led to a desired product, and to recognize specific structural features. In particular, the indirect spin-spin coupling constants of the heavy nucleus to the specific ligand nucleus can be used to confirm that a given fragment is within the coordination sphere.

In many cases quantum chemical calculations are essential to analyse the experimental NMR spectra, and to give deeper insight into the physical aspects of magnetic properties. These computations, at least for molecules containing light atoms (up to the second row elements), are nowadays a common research tool (see for example reviews [1, 2, 3, 4, 5, 6]), and are frequently performed even by non-specialists. However, predictions of NMR parameters for compounds containing heavier elements are still challenging. The shielding constants and spin-spin coupling constants of heavy nuclei are related to the atomic core region, where the average electron

velocities are the largest [7], which explains the requirement of accurate description of the relativistic effects in computations of these parameters. The standard computational methods based on the Schrödinger equation are not sufficient in this case.

The next section consists of a brief review of relativistic computations of NMR parameters, to show the state of knowledge in this area at the start of my PhD thesis. Since the thesis is focused on the influence of a heavy atom on the NMR parameters of light nuclei, the reseach done in this area is discussed in the following section.

1.1 Inclusion of the relativistic effects in the computations of NMR parameters

In general, the relativistic effects can be accounted for by means of various methods. The most important ones include those employing the relativistic or pseudorelativistic Hamiltonians, those based on perturbational treatment on top of the nonrelativistic wavefunction and those using pseudopotential approach. Below, recent developments in this area are discussed in order of increasing accuracy (and computational cost) of the method.

The computationally cheapest method of inclusion of the relativistic effects in *ab initio* calculations are pseudopotentials parametrized on the basis of all-electron relativistic calculations of heavy atoms. However, they cannot be applied for computations of NMR parameters of heavy nuclei since ECPs by definition do not allow for accurate modelling of electron density in the core region. One of the possible solution of this problem has been proposed recently. Development of gauge including projector augmented wave (GIPAW) method for shielding constants [8] or projector augmented wave (PAW) method for spin-spin coupling constants [9] make it possible for the NMR parameters in periodic systems to be calculated at all-electron accuracy within the planewave-pseudopotential DFT formalism. Unfortunately, this methodology is still not very popular.

The calculations of relativistic effects on the shielding constants by means of the perturbational theory based on the Breit-Pauli Hamiltonian and non-relativistic wave function were reported several times [10, 11, 12, 13] (see also Refs. [14, 15] for specialized reviews), but these methods cannot be used for computations of the NMR parameters of all systems. In the case of the spin-spin coupling constants, some terms diverge upon basis set expansion [14], whereas for the shielding constants of the heaviest nuclei (including 1/2-spin nuclei like ^{199}Hg or ^{205}Tl,

important in NMR spectroscopy) the non-relativistic wave function does not provide a good expansion point to the perturbation theory.

The best solution in the case of computations of the NMR parameters of heavy nuclei is an approach based on a relativistic or pseudorelativistic Hamiltonian, either four-component or two-component one. In the last two decades great progress has been made in the area of relativistic quantum chemical methodology and in development of computer codes for this purpose. Now, more and more molecular properties are being calculated using relativistic Hamiltonians. Four- and two-component Hamiltonians with DFT approach were used for the linear molecular polarizabilities [16, 17, 18, 19, 20], non-linear molecular polarizabilities, other high-order optical properties [21, 22, 23], the electron paramagnetic resonance parameters [24, 25, 26] and the electric field gradient [27, 28, 29].

It should be stressed that the calculations of the nuclear shielding constants and spin-spin coupling constants are associated with several difficulties. For the shielding constants calculated with finite basis sets the gauge invariance (independence of the calculated results on the gauge origin chosen for the vector potential) should be ensured, whereas in the case of the spin-spin coupling constants it is essential to describe the electron correlation at a sufficient level of theory. It is known (see for example [3]) that the non-relativistic Hartree-Fock approach often produces very poor results for the spin-spin coupling constants. For the relativistic computations the body of numerical evidence is much smaller (a comparison of the correlated and Hartree-Fock relativistic results can be found for example in Refs [30, 31]) but it seems that it is also true in this case. Additionally, computational costs of the spin-spin coupling constants calculations rises significantly with the system size. All of these have hampered the relativistic calculations of the spin-spin coupling constants until the methods based on density functional theory [32, 33, 34, 35, 36, 37] have been developed. There are available non-relativistic implementations using correlation methods (such as coupled cluster (CC) [38, 39, 40] or multiconfigurational self consistent field method (MCSCF) [41]), but currently only the DFT approach gives the possibility to simultaneously include the relativistic effects and electron correlation in computations of NMR parameters.

Several pseudorelativistic Hamiltonians were developed and many of them have been used in the relativistic calculations of the NMR properties, such as the zeroth-order regular approximation (ZORA) [42, 43], the infinite-order regular approximation with modified metric (IORAmm) [44] or the Douglas-Kroll-Hess (DKH) [31] Hamiltonians. All of them em-

ploy the elimination of the small spinor. Currently, the ZORA-DFT is the most popular approach at least for the computations of the spin-spin coupling constants (for instance J_{PtPt} [45], J_{PtTl}[46], J_{PtC}[46], J_{TlC} [46], the Hg couplings [47, 48], and the Ru couplings [49]). For the shielding constants, both ZORA[50] and the Douglas-Kroll-Hess[51] method have been developed and employed in many calculations, for example in the series of HgX_2 and $Hg(CH_3)X$ [52, 53] or HX (ZORA-DFT [54, 55] and DKH2-HF [52]) where X=Cl,Br,I. Not only organomercury compounds and halide derivatives, but also compounds containing ^{183}W [56], ^{207}Pb [56], ^{195}Pt [57], ^{235}U [58, 59] or ^{77}Se [60] have been investigated using the ZORA-DFT approach. Preliminary findings [61, 62, 63] have shown that ZORA approach reproduces well the chemical shifts at heavy nuclei but fails completely for the absolute shielding constants. It should be stressed that it is not a full list of the research papers where the ZORA Hamiltonian was employed in the computations of NMR parameters, since this approach becomes very popular in the last few years and more and more calculations are performed with this method. Recently, the newly developed paramagnetic ZORA approach [26] for computation of the shielding constants opens new possibilities for the computations of NMR parameters also for open-shell systems.

The four-component calculations of NMR parameters have been carried out so far mainly at the four-component Dirac-Hartree-Fock level of theory without electron correlation effects and the Breit correction. This approach has been examined for example for the spin-spin coupling constants in XH_4 (X=C, Si, Ge, Sn, Pb) and $Pb(CH_3)_3H$ [64], XH_3 (X=N,P,As,Sb,Bi) and XH_2 (X=O, S, Se, Te, Po) [65], and XF_n (n=2,4,6) [66] and for the shielding constants in HX (X=Cl, Br, I) [67, 68], H_2Y (Y=O, S, Se, Te) [69], H_3Y (Y=N, P, As, Sb, Bi) [70]. However, the lack of the electron correlation tends to lead to less than satisfactory results. Recently, the density functional methods have been implemented at the four-component level [71, 72] and the results are promising. The Dirac-Kohn-Sham method with London atomic orbitals (LAOs) [73] has been implemented also for the shielding constants [74, 72, 75] and has been used for HgL_2 (L = Cl, Br, I, CH_3) [62] and several other small molecules [76, 77, 78, 79, 80, 81, 82].

1.2 Importance of the relativistic effects in the computations of NMR parameters of light atoms in the vicinity of a heavy atom

The presence of a heavy nucleus in a molecule affects not only the Nuclear Magnetic Resonance (NMR) properties of the heavy nucleus, but also the shielding constants and the indirect spin-spin coupling constants of the nearby light nuclei. This phenomenon is called, after Pyykkö *et al.* [83], the heavy-atom-on-light-atom (HALA) effect.

The experimental NMR research for halide derivatives has shown that increasing charge of X=F, Cl, Br, I leads to decreasing shift of atoms in vicinity of X. This behaviour is known as "normal halogen dependence" (NHD) and is now one of the best known examples of the HALA effect. Probably, the first report explaining this effect on the basis of the spin-orbit coupling phenomenon (using the third-order perturbation theory at the semiempirical level) was presented in a domestic conference in Japan by Nakagawa *et al.* [84] and later in reports by Nomura *et al.* [85] and Morishima *et al.* [86] for hydrogen halides. In the postulated mechanism, strong spin-orbit coupling around highly charged nucleus of a heavy atom causes appearance of non-zero spin-density which is transmitted through chemical bond and interacts with nuclei via FC/SD mechanism (for more details see section 2.9.3). In 1978 Volodicheva *et al.* [87] reinvestigated hydrogen halides, whereas in 1980 Cheremisin *et al.* [88] estimated spin-orbit coupling terms for halide-substituted methane. In 1987 Pyykkö *et al.* [83] calculated the relativistic contributions using the relativistically parametrized extended Hückel theory.

The spin-orbit contribution to HALA effects have been reinvestigated in the late '90s by Kaupp *et al.* The research has been focused on the ^{13}C NMR chemical shifts in halomethyl cations [89] and iodo compounds [90] calculated with the DFT approach and the double perturbation theory. It was shown that decreasing of the ^{13}C NMR chemical shifts is related to increasing charge of heavy nuclei and to the change of s-character of the light atom in the vicinity of heavy atoms. The latter findings confirmed the mechanism suggested earlier by Nomura *et al* [85].

The sum-over-states expression for the spin-orbit coupling contribution to the HALA effect suggests its dependence on the inverse of the lowest excitation energy, assuming the dominant contribution arises from the HOMO-LUMO gap. The first studies in this area have been performed by Wolff *et al.* [91] but the results have shown a trend opposite than expected. In the same year, investigations in this area have been performed by Kaupp *et al.* [92], and they

have shown that the spin-orbit coupling contribution to the shielding constant is indeed inversely proportional to the energy gaps in a series of organomercury compounds. Later in 2009 Hyvärinen *et al.* [93] published a study of Co, Rh and Ir d^6 complexes, which also confirmed the expected trend.

A lot of other research was focused on the spin-orbit-induced HALA effects even for bigger systems (for example [94] or [95]), whereas much less is known about the parallel phenomenon occurring for the nuclear spin-spin coupling constants. There is a handful of papers dealing with the situation when a heavy atom mediates the geminal coupling between two light nuclei [96, 97, 98, 99, 100, 101]. All of them show that the total relativistic effect on the spin-spin coupling constants is usually dominated by the scalar term. However, to the best of my knowledge, there are no investigations concerning the situation where the heavy atom is not in the coupling path.

1.3 Outline of the thesis

The thesis consists of this introductory part, followed by a chapter presenting basics of the relativistic *ab initio* calculations and the computations of NMR parameters using relativistic or pseudorelativistic Hamiltonians (Part I). After that, the application calculations are presented, followed by a summary (Part II).

Part I consists of two chapters. Chapter 2 (the first one in Part I) starts from some basic definitions for the NMR methodology (see section 2.1 and 2.2). The following sections are focused on the inclusion of the relativistic effects in *ab initio* computations. The four-component Dirac Hamiltonian is described in section 2.3. The elimination of small component (ESC) technique and approximations to the four-component Dirac Hamiltonian are explained in section 2.4. The pseudopotential approach using the nonrelativistic Hamiltonian and the relativistic effective core potential is presented in section 2.5. In section 2.6 methods of description of the electron-electron interaction are discussed. Finally, in section 2.7, the inclusion of the magnetic field to Hamiltonian is described, whereas section 2.8 presents basics of NMR computations employing the nonrelativistic, one- and two-component ZORA and Dirac-Coulomb Hamiltonians. Additionally, in the same chapter (section 2.9) the perturbational treatment of the spin-orbit corrections to NMR parameters is outlined.

Chapter 3 describes basic aspects of the density functional theory (DFT) (section 3.1) and discusses the extension of the theory in the relativistic framework (section 3.2).

Since this work does not contain any method development, only a brief outline of the underlying theory will be given. For a more extended description, the reader is referred to the relevant papers and chapters in handbooks. For the basics of NMR computation the reader is referred to chapter 12.9 in [102], whereas for the discussion of the relativistic or pseudorelativistic Hamiltonian the chapter 13 in [103] is recommended. For more extended discussion of the pseudopotential approach the reader is referred for example to chapter 10 in [104]. A more detailed discussion of the magnetic field in molecular electronic relativistic Hamiltonian can be found in [105] and subsection 8.2.2 of [106]. Finally, the NMR methodology in relativistic framework can be found for example in [107].

The original research presented in this thesis is organised in three chapters of Part II. Chapter 4 describes computational details of the employed methods. In Chapter 5, the influence of a heavy atom on the shielding constants of light atoms (in particular the carbon and nitrogen nuclei) will be investigated. Transition metal cyanides, organomercury compounds as well as halide derivatives will be discussed. The chosen systems contain carbon atoms of different hybridizations and in different positions with respect to the heavy atom in question. The influence of these parameters on the change of the HALA effect will be investigated. The shielding constants obtained with the selected methods will be compared with experimental results if available.

In Chapter 6 the influence of a heavy atom on the spin-spin coupling constants of light atoms (carbon, nitrogen and hydrogen) will be discussed. Four types of coupling constants will be investigated: the $^1J_{CN}$ coupling constants in the transition metal cyanides, the $^1J_{CC}$ and $^1J_{CH}$ coupling constants in a series of the organometallic compounds and halide derivatives and finally the $^nJ_{CC}$ (n=2,3,4) coupling constants mediated by the 12th group or p-block heavy elements. The heavy atoms under study have been selected to cover a wide range of electron configurations and to allow the investigation of the influence of the charge of the heavy nucleus on the HALA effect. As in the case of the HALA effect in the series of shielding constants, the chosen systems contain carbon atoms of different hybridizations and in different positions with respect to the heavy atom.

It should be stressed that despite hybridization theory is a bit outdated, the electron spin density in position of nucleus is an important parameter in HALA mechanism involves FC/SD operator and should correlate well with the s-character of hybrid orbitals from hybridization

theory. Because of that, the hybridization theory is used in the thesis to classify molecules according to the electron configuration of the light atom under study.

The thesis is based on four papers (three already published), but in some cases, the results are supplemented with newly obtained ones (not published). The thesis is self-contained. The essential results published in Papers 1–4 can be found in Applications part. Only in few cases, the reader is referred to original papers, which are attached as supplements.

1.4 The main goals of the thesis

The main goal of the first part of the thesis is to reinvestigate the HALA effects on the ^{13}C shielding constants of halide derivatives using newly developed (and possibly more accurate) tools and to estimate the size of the HALA effects in the organomercury compounds since much less is known about this effects for the 6th row elements compounds. The physical nature of the relativistic effects (the relativistic scalar vs. spin-orbit coupling contributions) will be investigated. Additionally the potential causes of the variation of the relative size in a series of halide derivatives will be discussed.

The main goal of the second part of the thesis (concerning the spin-spin coupling constants) is to describe the influence of a heavy atom on the nuclear spin-spin coupling constants of light atoms, since this effect is almost unexploited in the literature. As in the part focused on the shielding constants, the interplay of the relativistic scalar and spin-orbit coupling contributions will be investigated. Atypically large spin-orbit coupling contribution for selected compounds will be rationalized.

Additionally in both applicational parts of the thesis some methodological aspects (comparison of selected Hamiltonians) will be discussed. One of the goals of the work is to check how the more approximate methods (ECP, ZORA) reproduce the results obtained with the more rigorous ones.

1.5 Hierarchy of the methods used in the thesis

Four types of Hamiltonians have been employed in the research. Before a detailed description of relativistic and pseudorelativistic Hamiltonians, it is worthwhile to explain relations between the methods (see Figure 1.1) and their function in the thesis.

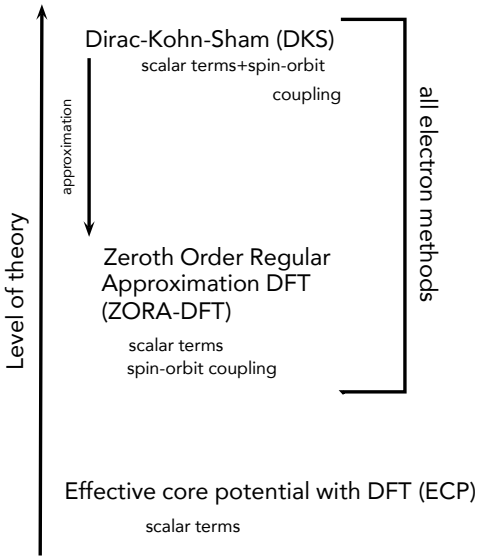

Figure 1.1: The comparison of the Hamiltonians used in the thesis.

In this thesis, the Dirac-Kohn-Sham (DKS) results have been used in most cases to estimate the relativistic contribution to the shielding constants and nuclear spin-spin coupling constants (by comparison with nonrelativistic results obtained with the same basis sets and functionals). The DKS results have been treated as benchmark data for the approximate methods since for some shielding constants and the spin-spin coupling constants no experimental data are available. The pseudorelativistic Hamiltonian discussed in this research is the Zeroth Order Regular Approximation (ZORA) Hamiltonian in the one- (includes only the scalar relativistic effects) and the two-component (includes the spin-orbit coupling term) variant. The additive form of the ZORA Hamiltonian gives the possibility to separate the scalar and the spin-orbit contribution to the shielding constants and the spin-spin coupling constants. Additionally, it is worthwhile to check how the ZORA-DFT method reproduces the more accurate DKS method in the computations of NMR parameters since ZORA is the most popular approach of the inclusion of the relativistic effects in the computational NMR research, at least for bigger systems.

The DKS and ZORA-DFT methods use all-electron approach, whereas ECPs employs the pseudopotential approximation on top of the nonrelativistic Hamiltonian. Even though the scalar ECP method fails in to reproduce of NMR parameters of heavy nuclei, it is expected that it works fine for NMR parameters of light atoms (since the core region of the atom under study is

properly described by all-electron basis set) in the vicinity of the heavy ones (described with the pseudopotential approach) at least when the scalar terms dominate the relativistic contribution. Verfication of this suspicions is important since ECP is still a popular and computationally cheap tool to include some relativistic effects in quantum chemical computations.

Part I

Theory

Chapter 2

Computations of NMR parameters

2.1 Definitions. The effective Hamiltonian[1]

The nuclear magnetic moment ($\boldsymbol{M}_K$) arises from the spin of the nucleus ($\boldsymbol{I}_K$)

$$\boldsymbol{M}_K = \gamma_K \hbar \boldsymbol{I}_K \tag{2.1}$$

(where γ_K is the gyromagnetic ratio of the nucleus and $\hbar$ is the reduced Planck constant) and interacts with the external magnetic field as well as the magnetic field of the other magnetic nuclei. The nuclear magnetic resonance spectroscopy measures the differences between the energy levels of nuclei in magnetic field.

In order to describe the NMR spectra in terms of molecular properties the effective Hamiltonian, where the nuclei are described by dipole magnetic moments, is used:

$$\mathcal{H}^{NMR} = -\sum_{\boldsymbol{K}} \boldsymbol{B^T}(\mathbf{1} - \boldsymbol{\sigma_K})\boldsymbol{M_K} + \frac{\mathbf{1}}{\mathbf{2}} \sum_{\boldsymbol{K \neq L}} \boldsymbol{M_K^T}(\boldsymbol{D_{KL}} + \boldsymbol{K_{KL}})\boldsymbol{M_L} \tag{2.2}$$

where:

$\boldsymbol{\sigma_K}$ — the shielding tensor,

$\boldsymbol{D_{KL}}$ — the direct (dipolar) spin-spin coupling tensor,

$\boldsymbol{K_{KL}}$ — the reduced indirect (scalar) spin-spin coupling tensor.

[1] This subsection has been written on the basis of chapter 12.9 in [102].

The shielding tensor describes the modification of the external magnetic field (B) on the nucleus by the presence of electrons. The effective (local) magnetic field can be written as:

$$\boldsymbol{B_K^{loc}} = (\mathbf{1} - \boldsymbol{\sigma_K})\boldsymbol{B}. \tag{2.3}$$

The direct spin-spin coupling constant describes the classical dipol-dipol interaction between two nuclear spin magnetic moments:

$$\boldsymbol{D_{KL}} = \frac{1}{c^2}\frac{3\boldsymbol{R_{KL}}\boldsymbol{R_{KL}} - \mathbf{1}\boldsymbol{R_{KL}^2}}{R_{KL}^5} \tag{2.4}$$

where R_{KL} is a position vector between nucleus K and L and c is the speed of light. The scalar spin-spin coupling constant describes interaction between two nuclear spin magnetic moments transmitted through electrons.

The NMR experiment can measure the scalar spin-spin coupling constants $\boldsymbol{J}_{KL}$ related to the reduced spin-spin coupling constants by:

$$\boldsymbol{J_{KL}} = h\frac{\gamma_K}{2\pi}\frac{\gamma_L}{2\pi}\boldsymbol{K_{KL}} \tag{2.5}$$

and the chemical shifts ($\boldsymbol{\delta}$) related to the shielding constant by

$$\boldsymbol{\delta_K} = \frac{\boldsymbol{\sigma_0} - \boldsymbol{\sigma_L}}{\mathbf{1} - \boldsymbol{\sigma_0}} \approx \boldsymbol{\sigma_0} - \boldsymbol{\sigma_K} \tag{2.6}$$

where $\boldsymbol{\sigma_0}$ is the shielding constant of reference and $\boldsymbol{\sigma_K}$ is the shielding constant of a sample.

For freely rotating molecules, the effective Hamiltonian is reduced to:

$$H_{iso}^{NMR} = -\sum_K B^T(1-\sigma_K)M_K + \frac{1}{2}\sum_{K\neq L} K_{KL}M_K^T M_L \tag{2.7}$$

where:

$$\sigma_K = \tfrac{1}{3}\mathrm{Tr}\boldsymbol{\sigma_K}, \quad K_{KL} = \tfrac{1}{3}\mathrm{Tr}\boldsymbol{K_{KL}}, \quad \mathrm{Tr}\boldsymbol{D_{KL}} = 0.$$

It should be stressed that $\boldsymbol{D_{KL}}$ is traceless which means that for freely rotating molecules only scalar coupling constants are measured.

2.2 Theoretical description of the NMR parameters

Perturbation theory is used for theoretical description of the spin-spin coupling constants and shielding constants. The energy of the molecule perturbed by the external magnetic field ($\boldsymbol{B}$) and the field of nuclei ($\boldsymbol{M}$) can be written as:

$$\begin{aligned} E(\boldsymbol{B},\boldsymbol{M}) = E_0 + \frac{\partial E(\boldsymbol{B},\boldsymbol{M})}{\partial \boldsymbol{B}}|_{\substack{\boldsymbol{B}=0,\\ \boldsymbol{M}=0}} \boldsymbol{B} + \sum_K \frac{\partial E(\boldsymbol{B},\boldsymbol{M})}{\partial \boldsymbol{M}_k}|_{\substack{\boldsymbol{B}=0,\\ \boldsymbol{M}=0}} \boldsymbol{M}_k + \frac{1}{2}\boldsymbol{B}^T \frac{\partial^2 E(\boldsymbol{B},\boldsymbol{M})}{\partial^2 \boldsymbol{B}}|_{\substack{\boldsymbol{B}=0,\\ \boldsymbol{M}=0}} \boldsymbol{B} \\ + \sum_K \boldsymbol{B}^T \frac{\partial^2 E(\boldsymbol{B},\boldsymbol{M})}{\partial \boldsymbol{B}\partial \boldsymbol{M}_K}|_{\substack{\boldsymbol{B}=0,\\ \boldsymbol{M}=0}} \boldsymbol{M}_K + \frac{1}{2}\sum_{L,K\neq L} \boldsymbol{M}_K^T \frac{\partial^2 E(\boldsymbol{B},\boldsymbol{M})}{\partial \boldsymbol{M}_K \partial \boldsymbol{M}_L}|_{\substack{\boldsymbol{B}=0,\\ \boldsymbol{M}=0}} \boldsymbol{M}_L + ... \end{aligned} \tag{2.8}$$

The first derivatives vanish for closed-shell systems. Comparison with the effective Hamiltonian shows a relation between the energy derivatives and the NMR parameters:

• the shielding constant:

$$\frac{\partial^2 E(\boldsymbol{B},\boldsymbol{M})}{\partial \boldsymbol{B}\partial \boldsymbol{M}_K}|_{\substack{\boldsymbol{B}=0,\\ \boldsymbol{M}=0}} = \boldsymbol{\sigma_k} - \mathbf{1}, \tag{2.9}$$

• the spin-spin coupling constant:

$$\boldsymbol{K}_{KL} = \frac{\partial^2 E(\boldsymbol{M}_1,\boldsymbol{M}_2,...)}{\partial \boldsymbol{M}_K \partial \boldsymbol{M}_L}|_{M_K=M_L=...=0}. \tag{2.10}$$

From computational point of view second order derivatives can be calculated as a sum of the expectation value and the sum-over-states expansion involving the appropriate operators:

$$\frac{\partial^2 E}{\partial X \partial Y} = \left\langle 0 \left| \frac{\partial^2 H}{\partial X \partial Y} \right| 0 \right\rangle + 2Re \sum_{n\neq 0} \frac{\left\langle 0 \left| \frac{\partial H}{\partial X} \right| n \right\rangle \left\langle n \left| \frac{\partial H}{\partial Y} \right| 0 \right\rangle}{E_0 - E_n}. \tag{2.11}$$

In the following sections selected Hamiltonians (including some relativistic effects) and the corresponding derivatives of the Hamiltonians will be discussed. Relativistic effects can be included in the *ab initio* calculations in several manners. The most accurate but also the most expensive method is the quantum electrodynamics (QED) theory, but because of the difficulties in implementation and computational cost its usage is limited to small systems composed of the lightest atoms. Only in a few cases QED has been employed to the computations of the relativistic corrections to the NMR shielding constants [108, 109, 110]. The state-of-art of NMR relativistic calculations employ instead the Dirac Hamiltonian.

2.3 The one-electron Dirac Hamiltonian[2]

The one-electron Dirac Hamiltonian can be written as:

$$H^D\Psi = (c\boldsymbol{\alpha}\cdot\boldsymbol{p}_i + \beta c^2 + V(\boldsymbol{r}))\Psi = E\Psi \tag{2.12}$$

where $\boldsymbol{\alpha}$ is a vector composed from 4×4 Dirac matrices:

$$\boldsymbol{\alpha} = (\alpha_1, \alpha_2, \alpha_3). \tag{2.13}$$

It is possible to write these matrices in terms of 2×2 sub-matrices:

$$\boldsymbol{\alpha}_k = \begin{pmatrix} \mathbf{0} & \boldsymbol{\sigma_k} \\ \boldsymbol{\sigma_k} & \mathbf{0} \end{pmatrix} \tag{2.14}$$

where k=1,2,3 and σ_k are the Pauli matrices:

$$\boldsymbol{\sigma_1} = \begin{pmatrix} 0 & 1 \\ 1 & 0 \end{pmatrix}, \boldsymbol{\sigma_2} = \begin{pmatrix} 0 & -i \\ i & 0 \end{pmatrix}, \boldsymbol{\sigma_3} = \begin{pmatrix} 1 & 0 \\ 0 & -1 \end{pmatrix}. \tag{2.15}$$

The β matrix (sometimes denoted as the Dirac matrix with k=0) is build from 2×2 identity matrices :

$$\alpha_0 = \beta = \begin{pmatrix} \boldsymbol{I_{2\times 2}} & \mathbf{0} \\ \mathbf{0} & -\boldsymbol{I_{2\times 2}} \end{pmatrix}. \tag{2.16}$$

Because of the matrix form of the Dirac equation, Ψ is no longer a one-component function but takes the form of a 4-component vector (bispinor):

$$\Psi = \begin{pmatrix} \psi_1 \\ \psi_2 \\ \phi_1 \\ \phi_2 \end{pmatrix} = \begin{pmatrix} \Psi_L \\ \Phi_S \end{pmatrix}. \tag{2.17}$$

For electronic states the Ψ_L spinor is called the large component whereas the Φ_S spinor is called the small component of the wave function. The composition of the bispinor can be interpreted

[2]This subsection has been written on the basis of chapter 3 in [102]

as superposition of the electron (spin-up and spin-down) and positron (spin-up and spin-down) states.

2.4 Elimination of the small spinor[3]

The small spinor (Φ_S) has limited influence on description of chemical problems and many approximations to Dirac equation are based on elimination of small component (ESC) strategy. The exact ESC equation for one-electron system can be derived from the matrix form of the Dirac equation:

$$\begin{pmatrix} V(\boldsymbol{r}) & c\boldsymbol{\sigma}\cdot\boldsymbol{p} \\ c\boldsymbol{\sigma}\cdot\boldsymbol{p} & V(\boldsymbol{r})-2c^2 \end{pmatrix} \cdot \begin{pmatrix} \Psi_L \\ \Phi_S \end{pmatrix} = \epsilon \begin{pmatrix} \Psi_L \\ \Phi_S \end{pmatrix} \tag{2.18}$$

where for convenience the energy has been shifted by c^2 ($\epsilon = E - c^2$). We can rewrite this equation as a coupled pair of equations:

$$V(\boldsymbol{r})\Psi_L + c\boldsymbol{\sigma}\cdot\boldsymbol{p}\Phi_S = \epsilon\Psi_L, \tag{2.19}$$

$$c\boldsymbol{\sigma}\cdot\boldsymbol{p}\Psi_L + (\upsilon(r) - 2c^2)\Phi_S = \epsilon\Phi_S. \tag{2.20}$$

After rewriting equation (2.20):

$$\Phi_S = (2c^2 - V(\boldsymbol{r}) + \epsilon)^{-1} c\boldsymbol{\sigma}\cdot\boldsymbol{p}\Psi_L \tag{2.21}$$

and substituting (Φ_S) in equation (2.19) we obtain:

$$V(\boldsymbol{r})\Psi_L + c\boldsymbol{\sigma}\cdot\boldsymbol{p}(2c^2 - V(\boldsymbol{r}) + \epsilon)^{-1} c\boldsymbol{\sigma}\cdot\boldsymbol{p}\Psi_L = \epsilon\Psi_L. \tag{2.22}$$

Finally, we can rewrite equation (2.22) in a more suitable form :

$$V(\boldsymbol{r})\Psi + \frac{1}{2}\boldsymbol{\sigma}\cdot\boldsymbol{p}K\boldsymbol{\sigma}\cdot\boldsymbol{p}\Psi_L = \epsilon\Psi_L \tag{2.23}$$

where $K = (1 + \frac{\epsilon - V(\boldsymbol{r})}{2c^2})^{-1}$.

[3] This section has been written on the basis of section 13.1 in [103]

Unfortunately, because the energy is present on both sides of the equation, it is no longer an eigenvalue problem. To overcome this issue many methods based on unitary transformation of the Dirac Hamiltonian matrix have been postulated, like Foldy–Wouthuysen Transformation (FW) [111] or Douglas-Kroll-Hess (DKH) [112, 113, 114, 115]. Alternatively approximations to K parameter like the Regular Approximation [116, 117] can be used.

2.4.1 The Foldy–Wouthuysen transformation

The most straightforward way to obtain a two-component Hamiltonian is to find the unitary transformation:

$$\hat{H} = U h^D U^{-1} \tag{2.24}$$

where $h^D(i)$ is the one electron Dirac Hamiltonian and the unitary matrices (U and U^{-1}) are:

$$U = \begin{pmatrix} \frac{1}{\sqrt{1+X^\dagger X}} & \frac{1}{\sqrt{1+X^\dagger X}} X^\dagger \\ -\frac{1}{\sqrt{1+X^\dagger X}} X & \frac{1}{\sqrt{1+X^\dagger X}} \end{pmatrix} \tag{2.25}$$

and

$$U^{-1} = \begin{pmatrix} \frac{1}{\sqrt{1+X^\dagger X}} & -X^\dagger \frac{1}{\sqrt{1+X^\dagger X}} \\ X \frac{1}{\sqrt{1+X^\dagger X}} & \frac{1}{\sqrt{1+X^\dagger X}} \end{pmatrix}. \tag{2.26}$$

The upper-left part of the transformed Hamiltonian is the Foldy–Wouthuysen Hamiltonian (H^{FW}):

$$H^{FW} = \frac{1}{\sqrt{1+X^\dagger X}} \times (c\boldsymbol{\sigma}\cdot\boldsymbol{p}X + X^\dagger c\boldsymbol{\sigma}\cdot\boldsymbol{p} - 2c^2 X^\dagger X + V(\boldsymbol{r}) + X^\dagger V(\boldsymbol{r}) X) \times \frac{1}{\sqrt{1+X^\dagger X}}. \tag{2.27}$$

The H Hamiltonian is off-diagonal if:

$$-XV - Xc\sigma\cdot pX + c\sigma\cdot p + (V - 2c^2)X = 0. \tag{2.28}$$

The solution (X) of this equation is not known for a general potential and some sort of approximation has to be used. One of the possible approximations is:

$$\frac{1}{\sqrt{1+X^\dagger X}} \approx \frac{1}{\sqrt{1+XX^\dagger}} \approx 1 \tag{2.29}$$

and

$$X = \frac{\boldsymbol{\sigma} \cdot \boldsymbol{p}}{2c}. \tag{2.30}$$

2.4.2 The nonrelativistic limit[4]

Another approach is based on an approximation to K. At the beginning let's suppose that $c \to \infty$ then $K \approx 1$ which gives:

$$V(\boldsymbol{r})\Psi_L + \frac{1}{2}(\boldsymbol{\sigma} \cdot \boldsymbol{p})(\boldsymbol{\sigma} \cdot \boldsymbol{p})\Psi_L = \epsilon\Psi_L. \tag{2.31}$$

Employing properties of the Pauli matrices, it is possible to write that

$$(\boldsymbol{\sigma} \cdot \boldsymbol{p})(\boldsymbol{\sigma} \cdot \boldsymbol{p}) = \boldsymbol{p}^2 1_{2x2}. \tag{2.32}$$

If we put (2.32) into equation (2.31), we obtain:

$$V(\boldsymbol{r})\Psi + \frac{1}{2}\boldsymbol{p}^2\Psi = \epsilon\Psi \tag{2.33}$$

which is nothing more than the nonrelativistic Schrödinger equation. Equation (2.31) is the Lévy-Leblond equation, sometimes called the nonrelativistic equation with spin because it is satisfied by the two-component spinor. It is one of the ways to show that the Dirac equation simplifies to the nonrelativistic equation if $c \to \infty$ is assumed.

2.4.3 The regular approximation[5]

Popular computational implementations employ yet another approximation to K, the so-called regular approximation. This approximation can be used to describe some of the relativistic effects.

We can rewrite K as:

$$K = \frac{-2c^2}{\epsilon}\frac{\epsilon}{V(\boldsymbol{r}) - 2c^2}\left(1 - \frac{\epsilon}{V(\boldsymbol{r}) - 2c^2}\right)^{-1} \equiv \frac{-2c^2}{\epsilon}x(1-x)^{-1} \quad \text{where } x = \frac{\epsilon}{V(\boldsymbol{r}) - 2c^2}. \tag{2.34}$$

[4] This section has been written on the basis of section 4.6 in [107].
[5] This section has been written on the basis of chapter 18 in [107].

Now we can use the expansion:

$$\frac{-2c^2}{\epsilon}x(1-x)^{-1} = \frac{-2c^2}{\epsilon}[x + x^2 + x^3 + \cdots] \quad \text{for} -1 < x < 1. \tag{2.35}$$

The regular approximation postulated by *Chang et al.* [116] and *Heully et al.* [117] has one very important advantage in comparison with other expansions (see subsection 2.9.1). The convergence of the series depends on the $\epsilon < 2c^2$ condition (since nuclear potential is always negative we can write $|\epsilon - 2c^2| > 2c^2$) which is true for all occupied and virtual states up to $2c^2$ which are in the scope of chemical research.

Zeroth order regular approximation

If the regular series is truncated after the first term, the zeroth order regular approximation is obtained:

$$K \approx \frac{-2c^2}{\epsilon}\frac{\epsilon}{V(\boldsymbol{r}) - 2c^2} = \frac{2c^2}{2c^2 - V(\boldsymbol{r})}. \tag{2.36}$$

This approximation leads to the ZORA Hamiltonian:

$$\boxed{H_{ZORA} = V(\boldsymbol{r}) + \frac{1}{2}\boldsymbol{\sigma}\cdot\boldsymbol{p}K\boldsymbol{\sigma}\cdot\boldsymbol{p}.} \tag{2.37}$$

If the Dirac relation is used:

$$(\boldsymbol{\sigma}\cdot\boldsymbol{u})(\boldsymbol{\sigma}\cdot\boldsymbol{v}) = (\boldsymbol{u}\cdot\boldsymbol{v})I_2 + i\boldsymbol{\sigma}\cdot(\boldsymbol{u}\times\boldsymbol{v}) \tag{2.38}$$

(where $\boldsymbol{u}$ and $\boldsymbol{v}$ are 2×2 arbitrary matrices and i is imaginary number) it is possible to split the ZORA Hamiltonian into the spin-free (scalar) and the spin-dependent (spin-orbit coupling) terms:

$$H_{ZORA} = H_{sc-ZORA} + H_{so-ZORA}, \tag{2.39}$$

$$\boxed{H_{sc-ZORA} = V(\boldsymbol{r}) + \boldsymbol{p}\frac{K}{2}\boldsymbol{p},} \tag{2.40}$$

$$\boxed{H_{so-ZORA} = \frac{K^2}{4c^2}\boldsymbol{\sigma}\cdot[\nabla\boldsymbol{V}\times\boldsymbol{p}].} \tag{2.41}$$

This equation can be also obtained with the unitary transformation using approximations:

$$\frac{1}{\sqrt{1+X^\dagger X}} \approx \frac{1}{\sqrt{1+XX^\dagger}} \approx 1 \tag{2.42}$$

and

$$X = \frac{\boldsymbol{c\sigma}\cdot\boldsymbol{p}}{2c^2 - V}. \tag{2.43}$$

2.5 Pseudopotential approach[6]

In the previous sections the *all-electron* approaches, where the relativistic effects are employed by the relativistic or pseudorelativistic Hamiltonians, have been discussed. It is also possible to include these effects by means of pseudopotential approach (relying on the use of the the effective core potentials) with the nonrelativistic pseudo-Hamiltonian. In this paragraph, the concept of pseudopotential approach will be discussed. The main idea of the approach is to treat the core and the valence electrons separately. It is based on the assumption that the core wave functions do not change significantly regardless of the environment (molecular bonds are built mainly by valence electron). That gives the possibility to replace the core electrons by properly fitted pseudopotentials.

2.5.1 Choice of the core region

Several parameters have to be considered to perform the proper core-valence separation:

- the overlap between the core and the valence densities should be relatively small,
- the static dipole polarizability of the core should be small ($\alpha_D < 1$ a.u.),
- removing or adding valence electrons should not change significantly the core density,
- the core should not be penetrated by valence electrons of other atoms in molecule.

2.5.2 The pseudopotential approximation

Systems built from closed-shell core orbitals and one valence electron will be discussed in this section but it is possible to generalize these considerations to many valence electrons system.

The main goal is to find the valence-only Fock operator. The Hartree-Fock equation for the valence electron is:

$$F\psi_v = \epsilon_v\psi_v \quad \text{and} \quad \langle\psi_v|\psi_c\rangle = 0 \tag{2.44}$$

[6] This section has been written on the basis of chapter 10 in [104]

where F is the Fock operator, ϵ is the energy of the ψ_v state, whereas ψ_c and ψ_v are the core and the valence one-electron wave functions, respectively. It is possible to write the Phillips-Kleinman ansatz mixing the core orbitals to the new valence orbital:

$$\phi_v = \psi_v + \sum_c a_{cv}\psi_c \quad \text{where } a_{cv} = \langle\psi_c|\phi_v\rangle. \tag{2.45}$$

Unfortunately, the obtained valence orbital has different energy in comparison to the original one:

$$\langle\phi_v|F\phi_v\rangle = \epsilon_v + \sum_c a_{cv}^2\epsilon_c. \tag{2.46}$$

We have to find the modified Fock operator (F') which satisfies the relationship:

$$F'\phi_v = \epsilon_v\phi_v. \tag{2.47}$$

After basic transformations it is possible to write:

$$F\phi_v = \epsilon_v\phi_v + \sum_c \langle\phi_v|\psi_c\rangle(\epsilon_c - \epsilon_v)\psi_c. \tag{2.48}$$

Second term can be moved to the left side of the equation which leads to (after inserting the a_{cv} coefficients):

$$[F + P_{core}]\phi_v = \epsilon_v\phi_v, \quad \text{where } P_{core} = \sum_c (\epsilon_v - \epsilon_c)|\psi_c\rangle\langle\psi_c|. \tag{2.49}$$

If we split the Fock (F) operator into two terms:

$$F = F_{valence} + F_{core}, \tag{2.50}$$

we can finally write:

$$V_{PP}(r) = F_{core} + P_{core} = -\frac{n_c}{r} + \sum_c (2J_c - K_c) + P_{core} \tag{2.51}$$

where $V_{PP}(r)$ is the pseudopotential operator.

One of the possible approximations to the pseudopotential operator (the most crude one) is to replace all operators by a linear combination of Gaussian functions:

$$V_{PP}(r) \cong V_{PP}^{local} + \sum_{l=0}^{L_{max}} V_{PP}^{l}(r) \sum_{m=-l}^{l} |lm\rangle\langle lm| = \sum_{n=1}^{N_L} A_n r^{k_n} e^{-\alpha_n r^2} + \sum_{l=0}^{L_{max}} \sum_{n=1}^{N_{SL}} B_{ln} r^{k_{ln}} e^{-\beta_{ln} r^2} \sum_{m=-l}^{l} |lm\rangle\langle lm| \quad (2.52)$$

where the last sum is an l-dependent operator projecting onto the Hilbert subspace of angular momentum l, and k is integer with $k >= -2$. Two sets of A_n, α_n, B_{ln} and β_{ln} coefficients have been used in the thesis:

a) *Energy consistent pseudopotentials*

Parameters are fitted to an atomic valence spectrum by least-squares fit:

$$\sum_i w_i (\Delta E_i^{AE} - \Delta E_i^{PP})^2 = \min \quad (2.53)$$

where w_i are weight factors. The ionization potentials, electron affinities and excitation energies (ΔE_i^{AE}) for atoms and ions are obtained from the relativistic or quasirelativistic atomic calculations. This method has been used in Stuttgart ECPs. Name of ECP type in this series indicates the type of the atomic calculation used in the fitting procedure (MDF means the Dirac-Fock method and MWB the Wood-Boring method [118, 119, 120, 121, 122, 123, 124, 125, 126, 127, 128, 129])

b) *Shape-consistent pseudopotentials*

In this method all-electron orbitals (obtained from relativistic atomic calculations) are modified to be nodeless in the core region ($R < R_c$) and pseudopotential coefficients are fitted to reproduce the shape of all-electron orbitals. This approach has been used in Los Alamos pseudopotentials (series of LANL ECPs [130, 131]).

2.6 The N-electron Hamiltonian. Description of the electron-electron interaction[7]

In nonrelativistic theory, the electron-electron and electron-nucleus interaction is described by the Coulomb interaction. The potential of the electron-electron interaction can be written as:

$$U_C(\boldsymbol{r}_{ij}) = -\frac{1}{r_{ij}} \tag{2.54}$$

The electron-electron or electron-nucleus interaction in this description is instantaneous (the velocity of the electromagnetic wave is assumed to be infinite) and the retardation effects are neglected. From the relativistic theory it is known that the velocity of the electromagnetic wave has a finite value (the speed of light) which means that the distance between particles changes during the interaction. This fact should be taken into account in the definition of the interaction potential in a N-electron relativistic or pseudorelativistic Hamiltonian. Unfortunately, the exact form of this potential is not known. One of the possible approximations is the Breit Hamiltonian, where the electron-nucleus interaction has the classical form (nuclei are treated as external potential) but the electron-electron interaction potential includes retardation effects.

$$U_B(\boldsymbol{r}_{ij}) = \frac{1}{r_{ij}} - \frac{1}{2r_{ij}}\left[\boldsymbol{\alpha}(i)\boldsymbol{\alpha}(j) + \frac{[\boldsymbol{\alpha}(i)\cdot\boldsymbol{r}_{ij}][\boldsymbol{\alpha}(j)\cdot\boldsymbol{r}_{ij}]}{r_{ij}^2}\right] \tag{2.55}$$

The Breit Hamiltonian for a N-electron system (also known as the Dirac-Coulomb-Breit Hamiltonian) is sum of the one-electron Dirac Hamiltonians and the Breit potentials:

$$\boxed{H_{DCB} = \sum_i h_i^D + \sum_{i<j} U_B(\boldsymbol{r}_{ij}).} \tag{2.56}$$

The retardation effects can be rejected by using the Coulomb interaction to describe not only the nucleus-electron interaction, but also the electron-electron interaction which leads to the N-electron Dirac-Coulomb Hamiltonian:

$$\boxed{H_{DC} = \sum_i H_i^D + \sum_{i<j} \frac{1}{\boldsymbol{r}_{ij}}.} \tag{2.57}$$

[7] This subsection has been written on the basis of chapter 3 in [102]

It should be stressed that in this thesis only the results where the electron-electron interaction has been approximated by the Coulomb interaction will be discussed.

2.7 Molecular electronic Hamiltonian in the magnetic field[8]

2.7.1 Minimal Coupling

To make an electronic Hamiltonian applicable to any kind of NMR calculations, the magnetic field has to be introduced into the Hamiltonian. This can be done via the vector potential ($\boldsymbol{A}(\boldsymbol{r})$) instead of the magnetic field ($\boldsymbol{B}(\boldsymbol{r})$) directly :

$$\boldsymbol{B}(\boldsymbol{r}) = \boldsymbol{\nabla} \times \boldsymbol{A}(\boldsymbol{r}). \tag{2.58}$$

The vector potential can be included in Hamiltonian using generalized momentum:

$$\boldsymbol{\pi} = \frac{\partial \mathcal{L}}{\partial \dot{\boldsymbol{r}}} \tag{2.59}$$

where $\mathcal{L}$ is a Lagrangian. In the presence of the electric and magnetic field Lagrangian at non-relativistic level can be written as:

$$\mathcal{L} = \frac{m}{2}\dot{\boldsymbol{r}} \cdot \dot{\boldsymbol{r}} + q\boldsymbol{A}(\boldsymbol{r}) \cdot \dot{\boldsymbol{r}} - q\varphi \tag{2.60}$$

or after inclusion of the relativistic effects as:

$$\mathcal{L} = -mc^2\sqrt{1 - \frac{\dot{\boldsymbol{r}} \cdot \dot{\boldsymbol{r}}}{c^2}} + q\boldsymbol{A}(\boldsymbol{r}) \cdot \dot{\boldsymbol{r}} - q\varphi. \tag{2.61}$$

Differentiation of the Lagrangian leads to the generalized momentum in the presence of the electric and magnetic field:

$$\boldsymbol{\pi}_i \equiv \boldsymbol{p}_i + q\boldsymbol{A}(\boldsymbol{r}). \tag{2.62}$$

Because of that in order to include the magnetic field, the substitution $\boldsymbol{p}_i \rightarrow \boldsymbol{\pi}_i$ in a Hamiltonian should be made.

[8] This section has been written on the basis of [105] and subsection 8.2.2 in [106].

2.7.2 The gauge invariance

The problem with the vector potential is that it is not uniquely defined by Eq. (2.58) (electric field and the scalar potential related to it will not be discussed in this section). One of the possible gauge choice is Coulomb gauge (where the divergence of $\boldsymbol{A}$ vanishes: $\boldsymbol{\nabla} \cdot \boldsymbol{A} = 0$). Under this condition the magnetic field ($\boldsymbol{B}(\boldsymbol{r})$) remains unchanged when the vector potential is transformed using an arbitrary scalar function ($\chi(r)$):

$$\boldsymbol{A}(\boldsymbol{r}) \rightarrow \boldsymbol{A}'(\boldsymbol{r}) = \boldsymbol{A}(\boldsymbol{r}) + \boldsymbol{\nabla}\chi(r). \tag{2.63}$$

This transformation is called gauge transformation, whereas $\chi(r)$ is the gauge function.

Gauge transformation yields a new Hamiltonian (H') where the generalized momentum ($\boldsymbol{\pi}_i$) is transformed in the following fashion:

$$\boldsymbol{\pi}_i \equiv \boldsymbol{p}_i + q\boldsymbol{A} \rightarrow \boldsymbol{\pi}_i \equiv \boldsymbol{p}_i + q\boldsymbol{A} + q\boldsymbol{\nabla}\chi(r_i). \tag{2.64}$$

The gauge-transformed Hamiltonian can be written as:

$$H' = e^{-i\sum_i \chi(r_i)} H e^{i\sum_i \chi(r_i)}. \tag{2.65}$$

Since $\boldsymbol{B}(\boldsymbol{r})$ remains unchanged after gauge transformation, it implies that all equations describing measurable physical properties should also be invariant under the transformation. It means that expectation values of both Hamiltonians should have the same value:

$$\langle \Phi | H | \Phi \rangle = \langle \Phi' | H' | \Phi' \rangle. \tag{2.66}$$

To meet this condition wave function should be simultaneously transformed according to

$$|\Phi\rangle \rightarrow |\Phi'\rangle = e^{-i\sum_i \chi(r_i)} |\Phi\rangle. \tag{2.67}$$

A popular gauge function is:

$$\chi(\boldsymbol{r_i}) = -\frac{\boldsymbol{B} \times \boldsymbol{R}_{G0} \cdot \boldsymbol{r}_i}{2} \tag{2.68}$$

where $\boldsymbol{R}_{G0}$ is an arbitrary gauge origin. Its divergence is:

$$\boldsymbol{\nabla}\chi(\boldsymbol{r}_i) = -\frac{\boldsymbol{B}\times\boldsymbol{R}_{G0}}{2} \tag{2.69}$$

which leads to:

$$\boldsymbol{A}^{B'}(\boldsymbol{r}_i) = \frac{1}{2}\boldsymbol{B}\times(\boldsymbol{r}_i - \boldsymbol{R}_{G0}). \tag{2.70}$$

The gauge transformed atomic orbitals are the so-called gauge invariant atomic orbitals (GIAO) and they are widely used in computation of the NMR shielding constants, since when finite basis sets are used with standard atomic orbitals the results depend on the selected origin of $\boldsymbol{A}(\boldsymbol{r})$.

2.7.3 The Hamiltonian after inclusion of the external and local magnetic fields

To make an electronic Hamiltonian applicable to NMR calculations the total vector potential should be expressed as:

$$\boldsymbol{A} = \boldsymbol{A}^{ext} + \sum_A \boldsymbol{A}_A^{\mu} \tag{2.71}$$

where $\boldsymbol{A}^{ext}$ is the vector potential of the external, homogeneous magnetic field ($\boldsymbol{B}^{ext}$):

$$\boldsymbol{A}^{ext} = \frac{\boldsymbol{B}^{ext}\times\boldsymbol{r_0}}{2} \tag{2.72}$$

and $\boldsymbol{A}_A^{\mu}$ is the vector potential of the point-like nuclear magnetic dipole ($\boldsymbol{\mu_A}$):

$$\boldsymbol{A}_A^{\mu} = \frac{1}{c^2}\frac{\boldsymbol{\mu_A}\times\boldsymbol{r_A}}{r_A^3} \tag{2.73}$$

The nonrelativistic Hamiltonian

After inclusion of the vector potential in the nonrelativistic Hamiltonian the magnetic term is obtained

$$H_{nrel}^{mag} = \frac{1}{2}[\boldsymbol{A}\boldsymbol{p} + \boldsymbol{p}\boldsymbol{A} + i\boldsymbol{\sigma}(\boldsymbol{p}\times\boldsymbol{A} + \boldsymbol{A}\times\boldsymbol{p}) + \boldsymbol{A}^2] \tag{2.74}$$

and after subsequent substitution of (2.71) it can be expressed as:

$$H_{nrel}^{mag}(\boldsymbol{B}^{ext}, \boldsymbol{\mu}) = \frac{1}{2}(\boldsymbol{A}^{ext})^2 + H^{OZ} + H^{SZ} + H^{OP} + H^{DS} + H^{FC} + H^{SD} + H^{OD} \tag{2.75}$$

where the individual terms have the following meaning:

- the orbital Zeeman term:

$$H^{OZ} = \frac{1}{2}\boldsymbol{B}^{ext} \cdot (\boldsymbol{r} \times \boldsymbol{p}) = \frac{1}{2}\boldsymbol{B}^{ext} \cdot \boldsymbol{L}, \tag{2.76}$$

- the spin Zeeman term:

$$H^{SZ} = \frac{1}{2}\boldsymbol{B}^{ext} \cdot \boldsymbol{\sigma}, \tag{2.77}$$

- the paramagnetic orbital term:

$$H^{PO} = \frac{1}{c^2}\sum_A \mu_A \left(\frac{\boldsymbol{r}_A}{r_A^3} \times \boldsymbol{p}\right), \tag{2.78}$$

- the diamagnetic term:

$$H^{DS} = \frac{1}{2c^2}\sum_A \left[(\mu_A \cdot \boldsymbol{B}^{ext})\left(\frac{\boldsymbol{r_A}}{r_A^3} \cdot \boldsymbol{r}\right) - (\mu_A \cdot \boldsymbol{r})\left(\boldsymbol{B}^{ext} \cdot \frac{\boldsymbol{r_A}}{r_A^3}\right)\right]. \tag{2.79}$$

- the Fermi contact and spin-dipole term:

$$H^{FC+SD} = \frac{1}{2c^2}\sum_A \boldsymbol{\sigma}\left[\mu_A\left(\nabla \cdot \frac{\boldsymbol{r_A}}{r_A^3}\right) - (\mu_A \cdot \nabla)\frac{\boldsymbol{r_A}}{r_A^3}\right], \tag{2.80}$$

- the diamagnetic orbital term:

$$H^{OD} = \frac{1}{2c^4}\sum_{B\neq A} \frac{(\boldsymbol{\mu_A} \cdot \boldsymbol{\mu_B})(\boldsymbol{r_A} \cdot \boldsymbol{r_B}) - (\boldsymbol{\mu_A} \cdot \boldsymbol{r_B})(\boldsymbol{\mu_B} \cdot \boldsymbol{r_A})}{r_A^3 r_B^3}. \tag{2.81}$$

The ZORA Hamiltonian

The magnetic part of the ZORA Hamiltonian is similar to the nonrelativistic form:

$$H^{mag}_{ZORA} = \frac{1}{2}[\boldsymbol{A}K\boldsymbol{p} + \boldsymbol{p}K\boldsymbol{A} + i\boldsymbol{\sigma}(\boldsymbol{p} \times (K\boldsymbol{A}) + \boldsymbol{A} \times (K\boldsymbol{p})) + K\boldsymbol{A}^2]. \tag{2.82}$$

After substitution, it is possible to find terms similar to the nonrelativistic ones, but including K and its derivatives. Because of the complicated form of the operators they are not discussed any further (the reader is referred to [53, 132]).

The Dirac Hamiltonian

The magnetic part of the Dirac Hamiltonian has a much simpler form than the nonrelativistic

or ZORA analogues:

$$H_{Dirac}^{mag}(\boldsymbol{B}^{ext},\boldsymbol{\mu}) = -\frac{c}{2}\boldsymbol{B}^{ext}\cdot(\boldsymbol{\alpha}\times\boldsymbol{r}) - \frac{1}{c}\sum_{A}\boldsymbol{\mu_A}\cdot\left(\boldsymbol{\alpha}\times\frac{\boldsymbol{r_A}}{r_A^3}\right), \tag{2.83}$$

since vector potential in the Hamiltonian is only to the first power.

2.8 Computations of the NMR parameters

The expectation value and the sum-over-states (see equation (2.11)) applied to the magnetic part of the Hamiltonian (2.75, 2.82, 2.83), leads to an expressions for the shielding constants and spin-spin coupling constants.

It should be stressed that notation used in this subsection has been simplified by writing operators in one electron form to preserve consistency with refs [53, 132].

2.8.1 Shielding constants

The nonrelativistic Hamiltonian[9]

At the nonrelativistic level the shielding constant can be written as:

$$\boldsymbol{\sigma}_K = 1 + \boldsymbol{\sigma}_K^{dia} + \boldsymbol{\sigma}_K^{para} \tag{2.84}$$

where:

- the diamagnetic contribution is the expectation value:

$$\boldsymbol{\sigma}_K^{dia} = \frac{1}{2c^2}\left\langle 0\left|\frac{(\boldsymbol{r}_K\cdot\boldsymbol{r}_0)\boldsymbol{I}-\boldsymbol{r}_K\boldsymbol{r}_0^T}{r_K^3}\right|0\right\rangle, \tag{2.85}$$

- the paramagnetic contribution in sum-over-states expression has the form:

$$\boldsymbol{\sigma}_K^{para} = \frac{1}{c^2}\sum_{n\neq 0}[\left\langle 0\left|\frac{\boldsymbol{r}_K}{r_K^3}\times\boldsymbol{p}\right|n\right\rangle\langle n\left|\boldsymbol{r_0}\times\boldsymbol{p}\right|0\rangle + \langle 0\left|\boldsymbol{r_0}\times\boldsymbol{p}\right|n\rangle\left\langle n\left|\frac{\boldsymbol{r}_K}{r_K^3}\times\boldsymbol{p}\right|0\right\rangle]/(E_0-E_n). \tag{2.86}$$

[9] This subsection has been written on the basis of chapter 11 in [133]

The ZORA Hamiltonian[10]

At the ZORA level the shielding constant can be written as:

$$\boldsymbol{\sigma}_K = 1 + \boldsymbol{\sigma}_K^{dia} + \boldsymbol{\sigma}_K^{para} + \boldsymbol{\sigma}_K^{SO}. \tag{2.87}$$

- The diamagnetic contribution is:

$$\sigma_{jk}^{dia}(K) = \frac{1}{2c^2} \left\langle 0 \left| \frac{K}{r_K^3} \left(\boldsymbol{r}_K \cdot \boldsymbol{r} \delta jk - r_{K,j} r_k \right) \right| 0 \right\rangle . \tag{2.88}$$

- The paramagnetic contribution can be expressed as:

$$\sigma_{jk}^{para}(K) = \frac{1}{4c^2} \sum_{n \neq 0} [\left\langle 0 \left| \frac{K}{r_K^3} \cdot (\boldsymbol{r}_{\boldsymbol{K}} \times \boldsymbol{p})_j + (\boldsymbol{r}_{\boldsymbol{K}} \times \boldsymbol{p})_j \cdot \frac{K}{r_K^3} \right| n \right\rangle \langle n | K \cdot (\boldsymbol{r} \times \boldsymbol{p})_k + (\boldsymbol{r} \times \boldsymbol{p})_k \cdot K | 0 \rangle +$$
$$\langle 0 | K \cdot (\boldsymbol{r} \times \boldsymbol{p})_k + (\boldsymbol{r} \times \boldsymbol{p})_k \cdot K | n \rangle \left\langle n \left| \frac{K}{r_K^3} \cdot (\boldsymbol{r}_{\boldsymbol{K}} \times \boldsymbol{p})_j + (\boldsymbol{r}_{\boldsymbol{K}} \times \boldsymbol{p})_j \cdot \frac{K}{r_K^3} \right| 0 \right\rangle] / (E_0 - E_n). \tag{2.89}$$

- The spin-orbit contribution has the form:

$$\sigma_{jk}^{SO}(K) = \frac{1}{4c^2} \sum_{n \neq 0} [\left\langle 0 \left| \sigma_j \boldsymbol{\nabla} \left(K \frac{\boldsymbol{r}_{\boldsymbol{K}}}{r_K^3} \right) - \nabla_j \left(K \cdot \boldsymbol{\sigma} \frac{\boldsymbol{r}_{\boldsymbol{K}}}{r_K^3} \right) \right| n \right\rangle \langle n | K \cdot (\boldsymbol{r} \times \boldsymbol{p})_k + (\boldsymbol{r} \times \boldsymbol{p})_k \cdot K | n \rangle +$$
$$\langle 0 | K \cdot (\boldsymbol{r} \times \boldsymbol{p})_k + (\boldsymbol{r} \times \boldsymbol{p})_k \cdot K) | n \rangle \left\langle n \left| \sigma_j \boldsymbol{\nabla} \left(K \frac{\boldsymbol{r}_{\boldsymbol{K}}}{r_K^3} \right) - \nabla_j \left(K \boldsymbol{\sigma} \cdot \frac{\boldsymbol{r}_{\boldsymbol{K}}}{r_K^3} \right) \right| n \right\rangle] / (E_0 - E_n). \tag{2.90}$$

At the nonrelativistic (K=1) or the scalar ZORA level, the spin-orbit contribution reduces to the Fermi contact and spin-dipolar terms. Without the spin-orbit coupling for closed shell systems the contributions to FC and SD terms from α and β spinorbitals cancel each other since in this formalism the external magnetic field does not induce appearance of non-zero electron spin-density.

[10] This subsection has been written on the basis of paper [53]

The Dirac Hamiltonian[11]

Sum-over-states expansion with the Dirac Hamiltonian leads to:

$$\sigma_K = 1 + \frac{1}{2}\sum_{n\neq 0}[\langle 0|(\boldsymbol{\alpha}\times\boldsymbol{r})|n\rangle\left\langle n\left|\frac{(\boldsymbol{\alpha}\times\boldsymbol{r_K})}{r_K^3}\right|0\right\rangle + \\ + \left\langle 0\left|\frac{(\boldsymbol{\alpha}\times\boldsymbol{r_K})}{r_K^3}\right|n\right\rangle\langle n|(\boldsymbol{\alpha}\times\boldsymbol{r})|0\rangle]/(E_0 - E_n). \quad (2.91)$$

We should remember that the Dirac Hamiltonian depends linearly on the vector potential and the diamagnetic term vanishes (there are no terms dependent on the magnetic field and the magnetic moments simultaneously). Nevertheless, it is possible to split the term into two contributions. The sum over positive-energy states ($|k\rangle$) can be interpreted as corresponding to the paramagnetic term, whereas the other sum over negative-energy states ($|v\rangle$) corresponds to the diamagnetic term.

$$\sum_{n\neq 0}[\langle 0|(\boldsymbol{\alpha}\times\boldsymbol{r})|n\rangle\left\langle n\left|\frac{(\boldsymbol{\alpha}\times\boldsymbol{r_K})}{r_K^3}\right|0\right\rangle]/(E_0 - E_n) = \\ = \sum_k[\langle 0|(\boldsymbol{\alpha}\times\boldsymbol{r})|k\rangle\left\langle n\left|\frac{(\boldsymbol{\alpha}\times\boldsymbol{r_K})}{r_K^3}\right|0\right\rangle]/(E_0 - E_k) \\ + \sum_v[\langle 0|(\boldsymbol{\alpha}\times\boldsymbol{r})|v\rangle\left\langle v\left|\frac{(\boldsymbol{\alpha}\times\boldsymbol{r_K})}{r_K^3}\right|0\right\rangle]/(E_0 - E_v) \quad (2.92)$$

2.8.2 Nuclear spin-spin coupling constants

The nonrelativistic Hamiltonian[12]

After applying the sum-over-states expansion and a straightforward rearrangement, we obtain several contributions to the scalar spin-spin coupling tensor:

- The diamagnetic spin-orbit contribution (DSO):

$$\boldsymbol{K_{KL}^{DSO}} = \frac{1}{2c^4}\left\langle 0\left|\frac{(\boldsymbol{r}_K\cdot\boldsymbol{r}_L)\boldsymbol{I} - \boldsymbol{r}_K\boldsymbol{r}_L^T}{r_K^3 r_L^3}\right|0\right\rangle \quad (2.93)$$

[11] This subsection has been written on the basis of section 13.6 in [107].
[12] This subsection has been written on the basis of chapter 11 in [133]

- The paramagnetic spin-orbit contribution (PSO):

$$\boldsymbol{K}_{\boldsymbol{KL}}^{\boldsymbol{PSO}} = \frac{1}{c^4}\sum_{n\neq 0}[\left\langle 0\left|\frac{\boldsymbol{r}_K}{r_K^3}\times\boldsymbol{p}\right|n\right\rangle\left\langle n\left|\frac{\boldsymbol{r}_L}{r_L^3}\times\boldsymbol{p}\right|0\right\rangle + \left\langle 0\left|\frac{\boldsymbol{r}_L}{r_L^3}\times\boldsymbol{p}\right|n\right\rangle\left\langle n\left|\frac{\boldsymbol{r}_K}{r_K^3}\times\boldsymbol{p}\right|0\right\rangle/(E_0-E_n). \quad (2.94)$$

This contribution describes the interaction between the nuclear (spin) magnetic moment and the orbital magnetic moments of the electrons.

- The Fermi contact term (FC):

$$\boldsymbol{K}_{\boldsymbol{KL}}^{\boldsymbol{FC}} = \frac{1}{c^4}\sum_{n\neq 0}[\left\langle 0\left|-\frac{8\pi}{3}\delta(\boldsymbol{r_K})\boldsymbol{m}\right|n\right\rangle\left\langle n\left|-\frac{8\pi}{3}\delta(\boldsymbol{r_L})\boldsymbol{m}\right|0\right\rangle + \left\langle 0\left|-\frac{8\pi}{3}\delta(\boldsymbol{r_L})\boldsymbol{m}\right|n\right\rangle\left\langle n\left|-\frac{8\pi}{3}\delta(\boldsymbol{r_K})\boldsymbol{m}\right|0\right\rangle]/(E_0-E_n) \quad (2.95)$$

where $\delta(\boldsymbol{r})$ is Dirac delta. The FC term describes the zero-distance interaction between the nuclear spin and the electron spin.

- The spin-dipolar (SD) contribution:

$$\boldsymbol{K}_{\boldsymbol{KL}}^{\boldsymbol{SD}} = \frac{1}{c^4}\sum_{n\neq 0}\left\langle 0\left|\frac{\boldsymbol{m}}{r_K^3}-3\frac{(\boldsymbol{m}\cdot\boldsymbol{r_K})\boldsymbol{r_K}}{r_K^5}\right|n\right\rangle\left\langle n\left|\frac{\boldsymbol{m}}{r_L^3}-3\frac{(\boldsymbol{m}\cdot\boldsymbol{r_L})\boldsymbol{r_L}}{r_L^5}\right|0\right\rangle \left\langle 0\left|\frac{\boldsymbol{m}}{r_L^3}-3\frac{(\boldsymbol{m}\cdot\boldsymbol{r_L})\boldsymbol{r_L}}{r_L^5}\right|n\right\rangle\left\langle n\left|\frac{\boldsymbol{m}}{r_K^3}-3\frac{(\boldsymbol{m}\cdot\boldsymbol{r_K})\boldsymbol{r_K}}{r_K^5}\right|0\right\rangle/(E_0-E_n) \quad (2.96)$$

The SD term describes interaction between the magnetic spin dipoles (nuclear and electronic).

- Mixed terms:

In many cases the SD and FC mixed term dominates the spin-spin coupling anisotropy but it is small for isotropic constants. The mixed terms of the PSO and SD or PSO and FC operators at nonrelativistic level is zero since ground state is a pure singlet state (see discussion of mixed terms at ZORA level).

The ZORA Hamiltonian[13]

After applying the same approach as before:

- The diamagnetic spin-orbit contribution (DSO) has the form:

$$K_{jk}^{ZDSO}(K,L) = \frac{K}{c^4}\left\langle 0\left|\frac{(\boldsymbol{r}_K\cdot\boldsymbol{r}_L)\delta_{jk}-\boldsymbol{r}_{Kj}\boldsymbol{r}_{Lk}}{r_K^3 r_L^3}\right|0\right\rangle. \tag{2.97}$$

The paramagnetic ZORA spin-orbit contribution (PSO) is:

$$\begin{aligned}&K_{jk}^{ZPSO}(KL) = \\ &\frac{1}{4c^4}\sum_{n\neq 0}[\left\langle 0\left|\frac{K}{r_K^3}\cdot(\boldsymbol{r_K}\times\boldsymbol{\nabla})_j+(\boldsymbol{r_K}\times\boldsymbol{\nabla})_j\cdot\frac{K}{r_K^3}\right|n\right\rangle\left\langle n\left|\frac{K}{r_L^3}\cdot(\boldsymbol{r_L}\times\boldsymbol{\nabla})_k+(\boldsymbol{r_L}\times\boldsymbol{\nabla})_k\cdot\frac{K}{r_L^3}\right|0\right\rangle+ \\ &\left\langle 0\left|\frac{K}{r_L^3}\cdot(\boldsymbol{r_L}\times\boldsymbol{\nabla})_k+(\boldsymbol{r_L}\times\boldsymbol{\nabla})_k\cdot\frac{K}{L_K^3}\right|n\right\rangle\left\langle n\left|\frac{K}{r_K^3}\cdot(\boldsymbol{r_K}\times\boldsymbol{\nabla})_j+(\boldsymbol{r_K}\times\boldsymbol{\nabla})_j\cdot\frac{K}{r_L^3}\right|0\right\rangle/(E_0-E_n).\end{aligned} \tag{2.98}$$

- The ZORA spin-orbit contribution (ZSO) can be written as:

$$\begin{aligned}&K_{jk}^{ZSO}(K,L) = \\ &\frac{1}{4c^4}\sum_{n\neq 0}[\left\langle 0\left|\sigma_j\boldsymbol{\nabla}\left(K\frac{\boldsymbol{r_K}}{r_K^3}\right)-\boldsymbol{\sigma}\nabla_j\left(K\frac{\boldsymbol{r_K}}{r_K^3}\right)\right|n\right\rangle\left\langle n\left|\sigma_k\boldsymbol{\nabla}\left(K\frac{\boldsymbol{r_L}}{r_L^3}\right)-\boldsymbol{\sigma}\nabla_k\left(K\frac{\boldsymbol{r_L}}{r_L^3}\right)\right|n\right\rangle+ \\ &\left\langle 0\left|\sigma_k\boldsymbol{\nabla}\left(K\frac{\boldsymbol{r_L}}{r_L^3}\right)-\boldsymbol{\sigma}\nabla_k\left(K\frac{\boldsymbol{r_L}}{r_L^3}\right)\right|n\right\rangle\left\langle n\left|\sigma_j\boldsymbol{\nabla}\left(K\frac{\boldsymbol{r_K}}{r_K^3}\right)-\boldsymbol{\sigma}\nabla_j\left(K\frac{\boldsymbol{r_K}}{r_K^3}\right)\right|n\right\rangle]/(E_0-E_n).\end{aligned} \tag{2.99}$$

The nonrelativistic limit of this term corresponds to the sum of the Fermi-contact and spin-dipolar term of the Ramsey's theory.

- Mixed terms:

At the scalar (spin-free) ZORA level of theory the mixed terms between the ZPSO and ZSO (FC+SD terms at scalar ZORA level) operators are zero, but after the inclusion of the spin-orbit coupling there appears a non-zero cross term involving the ZPSO and ZSO operators (in the thesis it will be denoted as ((FC+SD)/ PSO cross terms).

[13] This subsection has been written on the basis of paper [132]

The Dirac Hamiltonian[14]

Again, the spin-spin coupling tensor derived from the Dirac Hamiltonian has a much simpler form than the corresponding tensor at the nonrelativistic or ZORA level:

$$\boldsymbol{D}_{KL} + \boldsymbol{K}_{KL} = \frac{2}{c^2} \sum_{n \neq 0} [\left\langle 0 \left| \frac{(\boldsymbol{\alpha} \times \boldsymbol{r_K})}{r_K^3} \right| n \right\rangle \left\langle n \left| \frac{(\alpha \times r_L)}{r_L^3} \right| 0 \right\rangle + \left\langle 0 \left| \frac{(\alpha \times r_K)}{r_K^3} \right| n \right\rangle \left\langle n \left| \frac{(\boldsymbol{\alpha} \times \boldsymbol{r_L})}{r_L^3} \right| 0 \right\rangle] / (E_0 - E_n). \quad (2.100)$$

2.9 Perturbational treatment of the spin-orbit coupling[15]

Another approach to include the relativistic effect (the spin-orbit coupling contribution) into computation of the NMR parameters is based on the perturbation theory where the spin-orbit operator is treated as perturbation. The perturbation operator can be derived from the Breit-Pauli Hamiltonian.

2.9.1 The Pauli and Breit-Pauli Hamiltonians

The use of the Foldy–Wouthuysen transformation (see subsection 2.4.1) with approximations (2.29) and (2.30) for the N-electron Dirac-Coulomb Hamiltonian leads to two-component Pauli Hamiltonian, whereas the same approach with the Dirac-Coulomb-Breit Hamiltonian leads to Breit-Pauli Hamiltonian:

$$H^{Breit-Pauli} = H^{Nonrel} \underbrace{- \frac{1}{8c^2} \sum_i p_i^4}_{H^{MV}} \underbrace{+ \frac{\pi}{2c^2} \sum_K Z_K \sum_i \delta(r_{iK})}_{H^{D1}} \underbrace{- \frac{\pi}{2c^2} \sum_{i \neq j} \delta(r_{iK})}_{H^{D2}}$$
$$\underbrace{\frac{g_e}{4c^2} \left[\sum_K Z_K \sum_i \frac{\boldsymbol{\sigma}_i \cdot \boldsymbol{l}_{iK}}{r_{iK}^3} - \sum_{ij} \frac{(\boldsymbol{\sigma}_i + 2\boldsymbol{\sigma}_j) \cdot \boldsymbol{r}_{ij} \times \boldsymbol{p}_i}{r_{ij}^3} \right]}_{H^{SO}} + H^{SS} + H^{OO} \quad (2.101)$$

The H^{Nonrel} Hamiltonian is the nonrelativistic Hamiltonian. H^{MV} is the mass-velocity term which describes correction to the kinetic energy of the electrons due to the variations of electron mass with velocity. H^{D1} and H^{D2} are the one- and two-electron Darwin terms connected with the *Zitterbewegung* phenomenon. The H^{SS} term describes interaction of electronic spins

[14] This subsection has been written on the basis of section 13.6 in [107].
[15] This section has been written on the basis of [134].

whereas the H^{OO} term describes interaction between the orbital magnetic moments of electrons. The H^{SO} is the spin-orbit coupling operator and can be split into $H^{SO(1)}$ and $H^{SO(2)}$. The first operator ($H^{SO(1)}$) describes the interaction between the spin magnetic moment and the orbital magnetic moment of the same electron, whereas the second operator ($H^{SO(2)}$) describes the interaction between the spin magnetic moment of one electron and the orbital magnetic moment of another one.

Unfortunately the Breit-Pauli Hamiltonian can not be employed for a variational treatment. The variational minimization of the energy leads to situation when (close to nuclei) mass-velocity term dominates over the kinetic energy term. Since both terms in the core region have opposite signs, it would cause the wave function to collapse. It is one of the reasons why this Hamiltonian is only used with the perturbation theory.

2.9.2 The spin-orbit operator in the magnetic field

In the next subsections only the spin-orbit operator derived from Breit-Pauli Hamiltonian will be discussed. In the presence of the magnetic field (external or induced by nuclei) an additional contribution to the spin-orbit coupling operator should be included. For the external magnetic field:

$$H^{SO,B} = H^{SO,B(1)} + H^{SO,B(2)}, \tag{2.102}$$

$$H^{SO,B(1)} = \frac{g_e}{8c^2}\left[\sum_K Z_K \sum_i \boldsymbol{s}_i \frac{(\boldsymbol{r}_{iO}\cdot\boldsymbol{r}_{iK})\boldsymbol{I} - \boldsymbol{r}_i\boldsymbol{r}_{iK}^T}{r_{iK}^3}\cdot\boldsymbol{B}\right], \tag{2.103}$$

$$H^{SO,B(2)} = -\frac{g_e}{8c^2}\left[\sum_{ij}(\boldsymbol{s}_i + 2\boldsymbol{s}_j)\frac{(\boldsymbol{r}_{iO}\cdot\boldsymbol{r}_{ij})\boldsymbol{I} - \boldsymbol{r}_i\boldsymbol{r}_{ij}^T}{r_{ij}^3}\cdot\boldsymbol{B}\right], \tag{2.104}$$

whereas for the magnetic field induced by nuclei they are:

$$H^{SO,K} = H^{SO,K(1)} + H^{SO,K(2)}, \tag{2.105}$$

$$H^{SO,K(1)} = \frac{g_e}{4c^4}\left[\sum_M Z_M \sum_i \boldsymbol{s}_i \frac{(\boldsymbol{r}_{iK}\cdot\boldsymbol{r}_{iM})\boldsymbol{I} - \boldsymbol{r}_{iK}\boldsymbol{r}_{iM}^T}{r_{iK}^3 r_{iM}^3}\cdot\boldsymbol{m}_K\right], \tag{2.106}$$

$$H^{SO,K(2)} = -\frac{g_e}{4c^4}\left[\sum_{ij}(\boldsymbol{s}_i + 2\boldsymbol{s}_j)\frac{(\boldsymbol{r}_{iK}\cdot\boldsymbol{r}_{ij})\boldsymbol{I} - \boldsymbol{r}_{iK}\boldsymbol{r}_{ij}^T}{r_{ij}^3 r_{iK}^3}\cdot\boldsymbol{m}_K\right]. \tag{2.107}$$

In the following the linear (2.108) and quadratic (2.109) response functions will be used:

$$\langle\langle A;B\rangle\rangle_{\omega} = \sum_{P}\sum_{m\neq 0}\frac{\langle 0|A|m\rangle\langle m|B|0\rangle}{\omega_m-\omega}, \tag{2.108}$$

$$\langle\langle A;B,C\rangle\rangle_{\omega_B,\omega_C} = \sum_{P}\sum_{m\neq 0}\frac{\langle 0|A|m\rangle\langle m|\overline{B}|n\rangle\langle n|C|0\rangle}{(\omega_B+\omega_C-\omega_m)(\omega_C-\omega_n)} \tag{2.109}$$

where $\overline{B} = B - \langle 0|B|0\rangle$, P is the permutation operator, $|0\rangle$ is the reference state, whereas $|m\rangle$ and $|n\rangle$ are the excited states.

2.9.3 The spin-orbit corrections to the shielding constants

The total perturbational spin-orbit coupling correction to the shielding tensor is

$$\sigma_K^{SO} = \sigma_K^{SO-I} + \sigma_K^{SO-II}. \tag{2.110}$$

The first term sums the quadratic response functions for the FC and SD operators:

$$\sigma_K^{SO-I} = \sigma_K^{FC-I(1)} + \sigma_K^{FC-I(2)} + \sigma_K^{SD-I(1)} + \sigma_K^{SD-I(2)}, \tag{2.111}$$

$$\sigma_K^{FC-I(n)} \propto \langle\langle H^{K,FC}; H^{SO(n)}, H^{B}\rangle\rangle_{0,0}, \tag{2.112}$$

$$\sigma_K^{SD-I(n)} \propto \langle\langle H^{K,SD}; H^{SO(n)}, H^{B}\rangle\rangle_{0,0} \tag{2.113}$$

where:

$$H^{K,FC} = -\frac{8\pi}{3c^2}\frac{g_e}{2}\sum_i \delta(\boldsymbol{r_{Ki}})\boldsymbol{s_i} \tag{2.114}$$

is the Fermi contact operator,

$$H^{B} = \sum_i \boldsymbol{r_{0i}}\times\boldsymbol{p_i} \tag{2.115}$$

and

$$H^{K,SD} = \frac{1}{c^2}\frac{g_e}{2}\sum_i\left[\frac{\boldsymbol{s_i}}{r_{Ki}^3} - 3\frac{(\boldsymbol{s_i}\cdot\boldsymbol{r_{Ki}})\boldsymbol{r_{Ki}}}{r_{Ki}^5}\right] \tag{2.116}$$

is the spin-dipolar operator.

The second term sums the linear response functions for the FC and SD operators:

$$\sigma_K^{SO-II} = \sigma_K^{FC-II(1)} + \sigma_K^{FC-II(2)} + \sigma_K^{SD-II(1)} + \sigma_K^{SD(2)-II}, \tag{2.117}$$

$$\sigma_K^{FC-II(n)} = \langle\langle H^{K,FC}; H^{SO,B(n)} \rangle\rangle_0, \tag{2.118}$$

$$\sigma_K^{SD-II(n)} = \langle\langle H^{K,SD}; H^{SO,B(n)} \rangle\rangle_0 \tag{2.119}$$

where n=0,1.

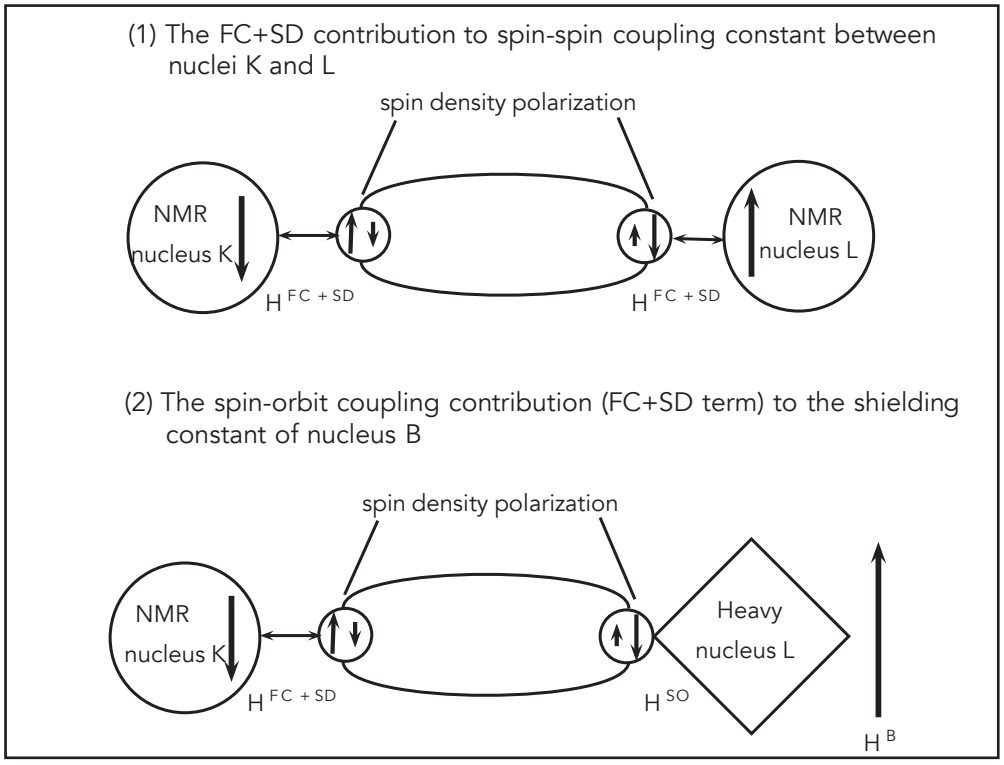

Figure 2.1: The diagram shows the analogy between the FC+SD contribution to the spin-spin constants and the spin-orbit coupling mechanism to the FC+SD contribution to shielding constant

The spin-orbit corrections involving the Fermi contact operator seem to be the most important contributions to the HALA effect. It can be rationalized using an analogy to the FC+SD contribution to the spin-spin constants (see Figure 2.1). In the FC+SD contribution to the spin-spin coupling constant (denoted in Figure 2.1 as (1)) the FC+SD operator at the L nucleus leads to the spin density polarization interacting with the nuclear spin of the K nucleus via the FC+SD

operator. In the case of the SO correction to the shielding constants (denoted in Figure 2.1 as (2)) the external magnetic field in the vicinity of a heavy nucleus induces electron spin density polarization (the spin-orbit coupling operator mixes the triplet state with the single ground state) interacting with the nuclear spin of the K nuclei via the FC+SD mechanism.

2.9.4 The spin-orbit corrections to the spin-spin coupling constants

The total spin-orbit coupling correction to the spin-spin coupling constant between the nuclei K and L is a sum of the quadratic response functions:

$$J_{KL}^{FC/PSO} \propto \langle\langle H^{K,FC}; H^{SO}, H^{L,PSO}\rangle\rangle_{0,0} + \langle\langle H^{L,FC}; H^{SO}, H^{K,PSO}\rangle\rangle_{0,0}, \tag{2.120}$$

$$J_{KL}^{SD/PSO} \propto \langle\langle H^{K,SD}; H^{SO}, H^{L,PSO}\rangle\rangle_{0,0} + \langle\langle H^{L,SD}; H^{SO}, H^{K,PSO}\rangle\rangle_{0,0} \tag{2.121}$$

and the linear response functions:

$$J_{KL}^{FC/SO} \propto \langle\langle H^{K,FC}; H^{SO,L}\rangle\rangle_{0} + \langle\langle H^{L,FC}; H^{SO,K}\rangle\rangle_{0}, \tag{2.122}$$

$$J_{KL}^{SD/SO} \propto \langle\langle H^{K,SD}; H^{SO,L}\rangle\rangle_{0} + \langle\langle H^{L,SD}; H^{SO,K}\rangle\rangle_{0} \tag{2.123}$$

where the SD and FC operators are defined by (2.116) and (2.114), respectively, and the PSO operator is:

$$H^{K,PSO} = \sum_i \frac{\boldsymbol{r}_{iK}}{r_{iK}^3} \times \boldsymbol{p}_i. \tag{2.124}$$

The quadratic response functions mix the FC+SD and PSO operators. At the nonrelativistic level of theory (or in general the one-component wave function) the cross term

$$\langle\langle H^{K,FC+SD}; H^{L,PSO}\rangle\rangle_0 = \sum_P \sum_{m\neq 0} \frac{\langle 0|H^{K,FC+SD}|m\rangle\langle m|H^{L,PSO}|0\rangle}{E_0 - E_m} \tag{2.125}$$

will be zero since $|0\rangle$ is a pure singlet state. The PSO operator does not operate on the spin and the $\langle|0|H^{PSO}|m\rangle$ integral has non-zero value when the $|m\rangle$ state is also singlet one. The

$\langle|n|H^{FC+SD}|0\rangle$ integral has zero value in these conditions since both the FC and the SD operator are spin operators. After inclusion of the spin-orbit coupling perturbation via the quadratic response function it can be easily seen that this is no longer true. We can write (using (2.109)):

$$\langle\langle H^{K,SD}; H^{SO}, H^{L,PSO}\rangle\rangle_{0,0} = \sum_{P} \sum_{m,n\neq 0} \frac{\langle 0|H^{K,SD}|m\rangle\langle m|\overline{H}^{SO}|n\rangle\langle n|H^{L,PSO}|0\rangle}{(E_0 - E_m)(E_0 - E_m)}. \tag{2.126}$$

From the previous discussion we know that $|n\rangle$ has to be a singlet state and $|m\rangle$ has to be a triplet one. If we meet this conditions, the third integral involving the SO operator will have non-zero value since SO operates on spin. It should be stressed that if we use the two- or four-component wave function as the ground state $|0\rangle$ in equation (2.125), this contribution also has non-zero value since the four- or two-component wave function is not a pure singlet.

Chapter 3

The density functional theory

3.1 Introduction to the DFT at the nonrelativistic level[1]

The first Hohenberg-Kohn theorem states that the ground state density ($\rho(\boldsymbol{r})$) in some external potential ($v(\boldsymbol{r})$) describes this potential and all properties of the system uniquely. This theorem is the fundamental principle of the density functional theory (DFT) where a system is described by the electron density (which depends on three component of the r vector) instead of the N-electron wave function ($\Psi(\boldsymbol{r}, \sigma_1, \boldsymbol{r_2}, \sigma_2 ... \boldsymbol{r_N}, \sigma_N)$).

$$\rho(\boldsymbol{r}) = N \sum_{\sigma_1=1/2}^{-1/2} \int d\tau_2 d\tau_3 ... d\tau_N |\Psi(\boldsymbol{r}, \sigma_1, \boldsymbol{r_2}, \sigma_2 ... \boldsymbol{r_N}, \sigma_N)|^2, \tag{3.1}$$

$$\int \rho(\boldsymbol{r}) d\boldsymbol{r} = N. \tag{3.2}$$

The second Hohenberg-Kohn theorem states that density functional assumes ($E_\nu^{HK}[\rho]$) its minimal value at the ground-state density :

$$E_\nu^{HK}[\rho] \geqslant E_\nu^{HK}[\rho_0] = E_0 \tag{3.3}$$

where ρ_0 is the exact density for the ground state (this is an analogue of the variational principle).

In the Kohn-Sham equations the system composed of non-interacting electrons with the same density as the system of interacting electrons is considered. All interactions inside the

[1] This section has been written on the basis of chapter 11 in [102].

system are included in a local effective (fictitious) external potential. In this approach the N-electron problem reduces to the one-electron problem:

$$\left(-1/2\boldsymbol{p}^2 + V_{eff}\right)\phi_i = \epsilon_i \phi_i \tag{3.4}$$

where ϕ_i are the Kohn-Sham spinorbitals. Using the Kohn-Sham spinorbitals it is possible to calculate the exact density, but first we have to know the form of V_{eff}.

The total energy is expressed as a functional of the charge density:

$$E = T_0 + \int V(\boldsymbol{r})\rho(\boldsymbol{r})d\boldsymbol{r} + J[\rho] + E_{xc}[\rho] \tag{3.5}$$

where $T_0[\rho]$ is kinetic energy of the fictitious Kohn-Sham system:

$$T_0[\rho] = \sum_{i=1}^{N} \int d\boldsymbol{r}\ \phi_i^*(\boldsymbol{r})\left(-1/2\boldsymbol{p}^2\right)\phi_i(\boldsymbol{r}). \tag{3.6}$$

The $\int V(\boldsymbol{r})\rho(\boldsymbol{r})d\boldsymbol{r}$ integral describes the interaction of the electron with the external potential, whereas the $J[\rho]$ integral describes self-interaction of the electron cloud:

$$J[\rho] = \frac{1}{2}\iint \frac{\rho(\boldsymbol{r_1})\rho(\boldsymbol{r_2})}{|\boldsymbol{r_{12}}|} d\boldsymbol{r_2} d\boldsymbol{r_2}. \tag{3.7}$$

Finally $E_{xc}[\rho]$ is the exchange-correlation energy. After proper transformation we can write the equation for the external potential (V_0) for the fictitious non-interacting system

$$V_{eff} = V + V_{coul} + V_{xc}, \tag{3.8}$$

$$V_{xc}(\boldsymbol{r}) = \frac{\delta E_{xc}}{\delta \rho(\boldsymbol{r})} \tag{3.9}$$

where V is the potential of the nuclei, V_{coul} is the Coulomb potential and V_{xc} is the exchange-correlation potential. Many approximations for V_{xc} have been postulated since the exact form of this potential is not known.

3.1.1 The local density approximation (LDA)

Local density approximation assumes local homogeneity of the electron density and uses the data obtained for the homogeneous electron gas.

$$E_{xc}^{\mathrm{LDA}}[\rho] = \int \rho(\boldsymbol{r})\epsilon_{xc}(\rho)\,\mathrm{d}\boldsymbol{r} \tag{3.10}$$

where $\epsilon_{xc}(\rho)$ is the exchange-correlation energy per particle.
It is also possible to take into account spin densities (using spin LDA variant-SLDA):

$$E_{xc}^{\mathrm{LDA}}[\rho_\alpha, \rho_\beta] = \int \rho(\boldsymbol{r})\epsilon_{xc}(\rho_\alpha, \rho_\beta)\,\mathrm{d}\boldsymbol{r}. \tag{3.11}$$

3.1.2 The generalized gradient approximations (GGA)

This approximation is still local but also includes gradients of the spin density:

$$E_{XC}^{GGA}[\rho_\alpha, \rho_\beta] = \int \epsilon_{XC}(n\rho_\alpha, \rho_\beta, \vec{\nabla}\rho_\alpha, \vec{\nabla}\rho_\beta)\rho(\vec{r})d\boldsymbol{r}. \tag{3.12}$$

Two types of GGA functionals (Becke-Perdew-BP86 [135, 136]; Perdew, Burke and Ernzerhof-PBE [137, 138]) have been used to obtain the results presented in the thesis.

3.1.3 The hybrid functionals

In this approximation a portion of the exact exchange from the Hartree-Fock theory is mixed with the correlation-exchange functional from other sources. The coefficients are chosen to obtain the best reproduction of the experimental results.

A well-known example is the B3LYP functional [139]:

$$E_{xc}^{B3LYP} = E_{xc}^{LDA} + a_0(E_x^{HF} - E_x^{LDA}) + a_x(E_x^{GGA} - E_x^{LDA}) + a_c(E_c^{GGA} - E_c^{LDA}) \tag{3.13}$$

where: $a_0 = 0.20, a_x = 0.72, a_c = 0.81$
In this thesis, the hybrid PBE0 [140] functional has also been used:

$$E_{xc}^{PBE0} = E_{xc}^{PBE} + 1/4(E_x^{HF} - E_x^{PBE}). \tag{3.14}$$

3.2 Some remarks about the relativistic density functional theory (RDFT)[2]

All of the calculation discussed in this thesis have been carried out using the non-relativistic exchange-correlation functionals. In this paragraph differences between the DFT and the relativistic DFT (RDFT) approaches will be discussed.

In the RDFT the system is described by the four-current density ($j^{\mu}(\boldsymbol{r})$) instead of electron density ($\rho(\boldsymbol{r})$) . It is possible to show that the ground state of the relativistic many-body system is uniquely described by the four-current (an analogue of the first Hohenberg-Kohn theorem) and the minimization of the functional $E_{tot}[j]$ leads to variational equations (an analogue of the second Hohenberg-Kohn theorem). Definition of four-current density is:

$$j^{\mu}(\boldsymbol{r}) = N \int \psi_i^{\dagger}(\boldsymbol{r}) c\alpha^{\mu} \psi_i(\boldsymbol{r}) d\boldsymbol{r} \tag{3.15}$$

where $\alpha^{\mu} = (\beta, \boldsymbol{\alpha})$. We can write:

$$j^{\mu}(\boldsymbol{r}) = (c\rho, \boldsymbol{j}). \tag{3.16}$$

It is possible to show [141] that when the Breit interaction is truncated after the first term (the Coulomb approximation is used to describe the electron-electron interaction) and there is no external magnetic field (vector potential) the relativistic four-current DFT reduces to the regular DFT (based on the electron density) form. For that reason there is no need to introduce the current density in the equations.

Unfortunately, incorporation of the vector potential in calculations of the NMR parameters is obligatory which means that the expectation value (energy) contains $\boldsymbol{\alpha}$ matrices:

$$E^A = \langle \Psi | c(\boldsymbol{\alpha} \cdot A) | \Psi \rangle = \int \boldsymbol{j}(\boldsymbol{r}) \cdot \boldsymbol{A}(\boldsymbol{r}) d\boldsymbol{r} \tag{3.17}$$

and the four-current density should be employed in the computations of NMR parameters at the relativistic level. However, because of the lack of the proper implementation of the relativistic current-dependent exchange-correlation functionals all calculation in the thesis have been performed with regular DFT.

[2] This section has been written on the basis of [141].

Part II

Applications

Chapter 4

Computational details

4.0.1 Geometry optimization

The geometric parameters of the cyanides under study have been obtained in a twofold way. For AgCN, CuCN, AuCN experimental chain structures X-C-N-X-C-N (X=Ag, Cu, Au) obtained in diffraction experiments [142, 143, 144] have been used. For the 12th group transition metals and thallium cyanides, the DFT geometry optimization has been carried out using the Amsterdam Density Functional (ADF) package [145, 146, 147] (version 2009 and 2010), scalar ZORA Hamiltonian [42, 43], VWN [148]+Becke88 [135] and Perdew86 [136] nonlocal gradient corrections (BVP86) as the exchange-correlation functional and the Slater-type TZ2P basis sets (the innermost atomic shells, namely 1s of carbon and nitrogen, 1s-2p of zinc, 1s-3d of cadmium, and 1s-4d of mercury and thallium, have been approximated by the frozen core densities).

For the organomercury compounds and the halogen derivatives (discussed in Chapter 5) the geometric parameters of the isolated molecules under study have been obtained using the same method as above but with the inclusion of the spin-orbit coupling effects. Again, the frozen core approximation has been employed (1s for carbon, 1s to 4d for mercury, 1s to 2p for chlorine, 1s to 3d for bromine and 1s to 4p for iodine). Additionally, another set of geometry parameters (used to estimate solvent effects) has been obtained using the same electron structure model as above and the conductor-like screening model (COSMO [149, 150, 151, 152]). Dielectric constants of 4.8 and 46.7 have been employed to describe $CHCl_3$ and DMSO, respectively, and the cavity has been built from the default van der Waals radii.

The geometric parameters of the derivatives discussed in Chapter 6 (except the transition metal cyanides) have been obtained using the complementary electronic structure model as before but the frozen-core approximation has not been employed.

4.0.2 Four-component calculations

The four-component Dirac-Kohn-Sham (DKS) calculations of the shielding constants for the cyanide derivatives containing heavy metals from the 5th and 6th row have been performed with the mDKS-RMB-GIAO module of the ReSpect program (version 3.1.0) [153], employing the generalized gradient approximation (GGA) Perdew, Burke and Ernzerhof (PBE [154]) functional. On the light atoms (nitrogen and carbon), the uncontracted pc-2 Gaussian basis set of Jensen [155, 156] has been attached, while the triple-ζ Dyall's [157] basis set has been used for the silver, cadmium, gold, mercury and thallium atoms. The restricted magnetic balance has been ensured by transformation of the Dirac Hamiltonian [74, 75], and the gauge invariant atomic orbitals (GIAOs) have been employed. The calculations have been further speeded up by the density fitting technique employing complementary auxiliary basis sets. All calculations have been performed with the Gaussian charge distribution model.

The shielding constants for the organomercury compounds and the halide derivatives have been computed using the same method as for the transition metal cyanides. The GGA PBE functional and the triple-ζ uncontracted pc-2 Gaussian basis set of Jensen [155, 156] for carbon, hydrogen and chlorine, and the triple-ζ Dyall's [157] for mercury, bromine and iodine basis set have been used. The calculated shielding constants (obtained using DKS and other employed methods) have been converted into relative shielding constants using benzene as a reference ($\Delta_{rel}\sigma = \sigma - \sigma_{benzene}$).

For the organometallic (cadmium and mercury) and halide derivatives, the DKS calculations of the spin-spin coupling constants have been carried out with a local version of the DIRAC program [158], including the recent developments by Saue [159]. The large and small components of the wave function have been connected by the unrestricted kinetic balance, as implemented in DIRAC [158]. The Perdew, Burke and Ernzerhof functional with Adamo and Barone's HF exchange contribution (PBE0) [160] has been used together with the uncontracted triple-ζ basis set with additional tight functions (aug-cc-pVTZ-J [161]) for carbon and hydrogen, and the uncontracted triple-ζ Dyall's basis set (dyall.v3z [157]) for mercury, cadmium, iodine and astatine.

All calculations have been performed with the Gaussian charge distribution model, as default in DIRAC.

The DKS calculations of the $^{n}J_{CC}$ (n=2,3,4) coupling constants have been carried out with the ReSpect program, including the recent modification by Křístková *et al.* [162]. The large and small components of the wave function have been connected by explicit magnetic balance approach of Komorovský *et al.* [74]. The Perdew, Burke and Ernzerhof functional (PBE) [154] has been used together with the uncontracted triple-ζ Jensen basis set with additional tight functions (upcJ-2[163] and upc-2 as auxiliary basis sets) for carbon and hydrogen, and the uncontracted triple-ζ Dyall's basis set (dyall.v3z [157]) for cadmium, indium, tin, antimony, tellurium, mercury, thallium, lead, bismuth and polonium. All calculations have been performed with the Gaussian charge distribution model.

4.0.3 ZORA calculations

For the transition metal cyanides, the one- and two-component ZORA calculations of the NMR properties have been carried out using the B3LYP and PBE (for comparison of the ZORA results with the DKS computations) functionals. The standard Slater TZP basis sets available in the ADF [147] program have been employed.

The NMR shielding constants for the organomercury compounds and the halogen derivatives have been calculated using the one- and two-component ZORA, with the standard PBE GGA functional and Perdew, Burke and Ernzerhof functional with Adamo and Barone's HF exchange contribution (the PBE0 hybrid functional) [160]. The standard TZP basis set have been used. In one set of calculations the conductor-like screening model (COSMO) with the same set of parameters as for the geometry optimization has been applied to include solvent effects.

The NMR spin-spin coupling constants have been calculated using the one- and two- component ZORA, employing the PBE0 hybrid functional (for the $^{1}J_{CC}$ coupling constants) and the PBE GGA functional (for the $^{n}J_{CC}$ (n=2,3,4) coupling constants). The triple-ζ Slater basis set with additional tight functions (jcpl [164]) for hydrogen, carbon, mercury, iodine, thallium, lead and TZ2P for cadmium, indium, tin, antimony, tellurium, bismuth, polonium and astatine have been used. All calculations have been performed with the Gaussian charge distribution model.

4.0.4 ECP calculations

The effective core potential results have been obtained using the Gaussian 03 program [165] for the shielding constants and the Gaussian 09 program [166] for the spin-spin coupling constants. The PBE functional has been employed for the calculations of the shielding constants and the $^{2}J_{CC}$ coupling constants, whereas the PBE0 functional has been employed for the calculations of the $^{1}J_{CC}$ coupling constants. Three types of basis sets for the light atoms (carbon and hydrogen) have been used: pc-2 for the shielding constants, aug-cc-pVTZ-J for the $^{1}J_{CC}$ coupling constants and pcJ-2 for the $^{2}J_{CC}$ coupling constants.

Several types of ECPs have been used during computations: LANL2DZ [130, 131] for cadmium, indium, tin, antimony, tellurium, iodine, mercury, thallium, lead, bismuth; MDF28 [118, 119, 120] for cadmium, indium, antimony and tellurium, iodine; MDF46 [121] for iodine; MWB28 [122, 123] for cadmium and indium; MWB46 [124, 125] for cadmium, indium, tin, antimony, tellurium, iodine; MDF60 [118, 126, 119, 120] for mercury, thallium, lead, bismuth, polonium and astatine; MWB60 [127, 128] for mercury and thallium; MWB78[129] for mercury, thallium, lead, bismuth, polonium and astatine; MDF78 [119, 121] for lead, bismuth, polonium and astatine. Additionally, for the shielding constants, calculations with the non-relativistic MHF60 [167] ECP have been performed to estimate the scalar relativistic effects as rendered by the relativistic ECPs.

4.0.5 Non-relativistic calculations

Two sets of the non-relativistic calculations have been performed. The first set has been carried out using DFT as implemented in the ADF program with the PBE or PBE0 functional. The basis sets used in this series of calculations have been the same as in the ZORA calculations. The second set of the calculations has been performed using DFT as implemented in Dalton 2011 [168] program. The PBE or PBE0 functional, the Gauss-type aug-cc-pVTZ-J or pcJ-2 basis set for carbon and hydrogen, and the uncontracted dyall.v3z basis set [157] for heavy elements have been used. All calculations have been used to estimate magnitude of the relativistic effects and to estimate the influence of basis set change (Slater-type vs. Gauss-type basis sets) in comparison DKS and ZORA results.

Chapter 5

The influence of the heavy atom on shielding constants of light atoms

The heavy atom on light atom (HALA) effect is well known for halide derivatives and have been investigated in the literature at several levels of theory (see section 1.2). However, in most cases HALA effects have been estimated using approximate method of inclusion of the relativistic effects. In the best case Dirac-Hartree-Fock [169] method has been used, where correlation effects have been neglected or estimated at nonrelativistic level of theory. For some time, methods based on the four-component Dirac Hamiltonian involving Kohn-Sham approach (DKS) have been developed for calculations of the NMR parameters, and now the HALA effects can be estimated relatively accurately, at least as far as the inclusion of the relativistic effects is concerned.

In the first part of my research, the NMR parameters for transition metal cyanides have been investigated. Among others, the shielding constants of carbon and nitrogen nuclei in vicinity of a transition metal have been computed. Next, my interest was focused on the ^{13}C shielding constants in halogen derivatives and organomercury compounds. The results have been obtained at several levels of theory, starting from the nonrelativistic approach, through one- (sc-ZORA) and two-components (so-ZORA) ZORA-DFT, and up to the DKS method. This approach allows to estimate the relativistic effects, to compare the spin-free and spin-dependent terms to the shielding constants, and finally to investigate the accuracy of the ZORA method in the reproduction of the relativistic effects for the shielding constants of light nuclei.

5.1 The shielding constants of the carbon and nitrogen nuclei in the transition metal cyanides

The molecules studied in this section are a series of closed-shell transition metal compounds (i.e. $Hg(CN)_2$, $Zn(CN)_4^{2-}$, $Cd(CN)_4^{2-}$, $Hg(CN)_4^{2-}$; $Tl(CN)_4^-$, CuCN, AgCN and AuCN) for which some experimental NMR data are available. The choice of cyanides has been motivated by the possibility to consider the relativistic effects not only for the spin-spin coupling constants and shielding constants of heavy metal nuclei, but also for the coupling constant between light nuclei in the vicinity of the metal atom ($^1J_{CN}$) (which will be discussed in the next chapter) and the shielding constants of the light nuclei (^{15}N, ^{13}C). Several experimental papers about the NMR properties of these compounds have been published [142, 143, 144, 170, 171, 172], but so far no systematic theoretical studies have been conducted.

For the 12th group elements and thallium compounds all the environmental effects (solvent effects) have been neglected. The 11th group (i.e. Cu, Ag, Au) cyanides exist as "infinite" linear chains in crystals, thus, for these compounds, mini-chain-like structures X-C-N-X-C-N (X=Ag, Cu, Au) have been used.

5.1.1 The estimation of the total relativistic term

The relativistic contributions to the shielding constants in a series of cyanide compounds (calculated as a difference between the so-ZORA and the nonrelativistic results) are shown in Figure 5.1. For the 4th and 5th row of the periodic table the relativistic contributions to the carbon and nitrogen shielding constants are small (less than (-)3 ppm, which constitutes 7% of the total value). However, for the 6th row they become sizeable: from about 10–16 ppm (20–25% of the total value) for σ_N and about (-8)–(-13) ppm (30% of the total value) for σ_C in $Me(CN)_4^{n-}$ anions to 23 ppm (48% of the total value) and 35 ppm (45% of the total value) for σ_C in $Hg(CN)_2$ and AuCNAuCN, respectively. Interestingly, for the 12th group elements, the relativistic effects lead to deshielding of the carbon nuclei, whereas for 11th group to an increased shielding of the carbon nuclei. Another interesting observation is that the relativistic contribution to shielding constants of the nitrogen nuclei in AuCNAuCN is very small.

5.1.2 The scalar and spin-orbit coupling terms

A comparison of the scalar (spin-free) and spin-orbit coupling (spin-dependent) contributions to the total relativistic effect (calculated using so-ZORA and sc-ZORA approach) is shown in

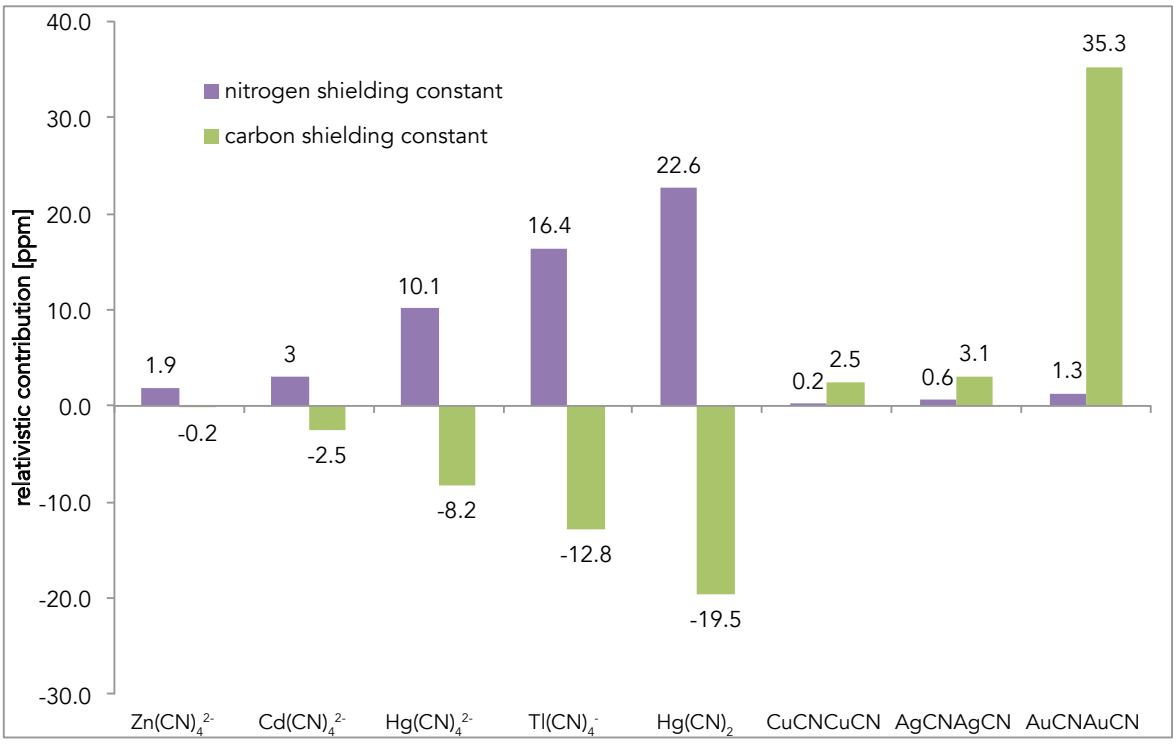

Figure 5.1: Comparison of the relativistic contributions (calculated as a difference between the so-ZORA and the nonrelativistic results) to the shielding constants [ppm] of the carbon and nitrogen nuclei in selected cyanides

Figure 5.2. Inspection of the results helps to elucidate the surprisingly small relativistic contribution in AuCNAuCN. It comes from mutual cancelling of the scalar and spin-orbit terms.

For the carbon and nitrogen nuclei in the molecules containing 11th group elements the inclusion of the scalar relativistic effects changes mainly the value of the paramagnetic term. The sum-over-states expressions for the term suggest its dependence on the inverse of the lowest singlet excitation energy, assuming the dominant contribution arises from this excitation. In the series the difference between the first and second singlet excitation energy is at least 0.3 eV, which supports the initial assumption. The first singlet excitation energy change after taking into account the scalar effects have been compared with the change of the paramagnetic term. The results are presented as a function of $(1/E_{singlet}^{nonrel} - 1/E_{singlet}^{sc-ZORA})$ in Figure 5.3. The quasi-linear dependence has been observed for both carbon and nitrogen shielding constants which suggests that some correlation between the chosen excitation and the discussed contribution exists. Inclusion of the scalar effects leads to a reduction of calculated singlet excitation energy. However, the paramagnetic term decreases as well, which suggests the transition moment (the numerator in the sum-over-states expansion) decreases more than the excitation energy.

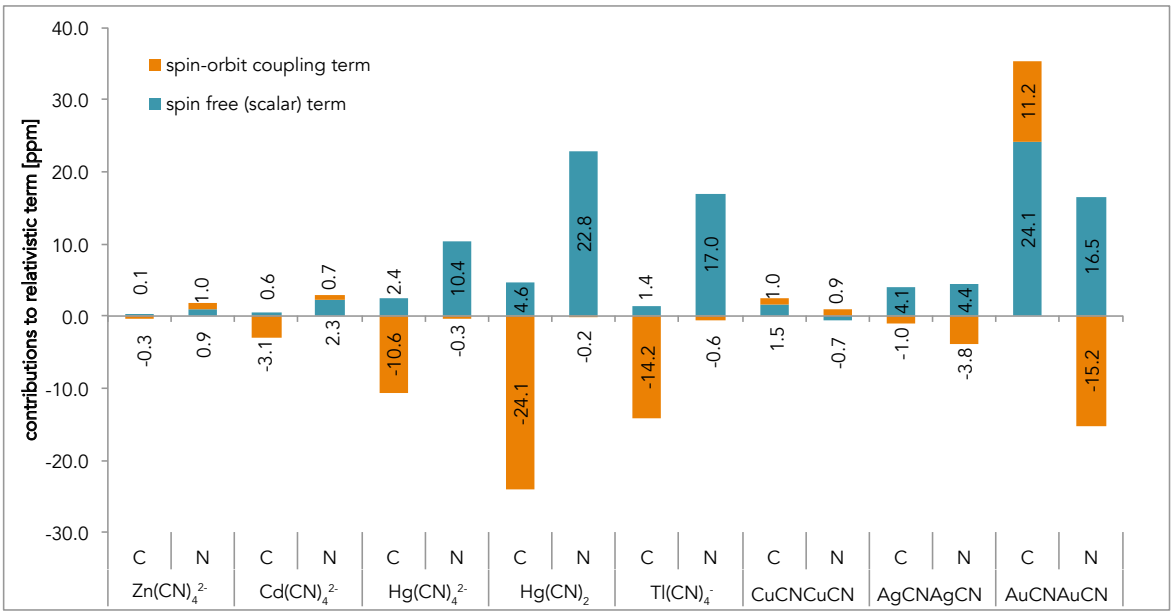

Figure 5.2: Comparison of the scalar and spin-orbit coupling corrections [ppm] calculated using the ZORA approach for the nitrogen and carbon shielding constants in selected cyanides

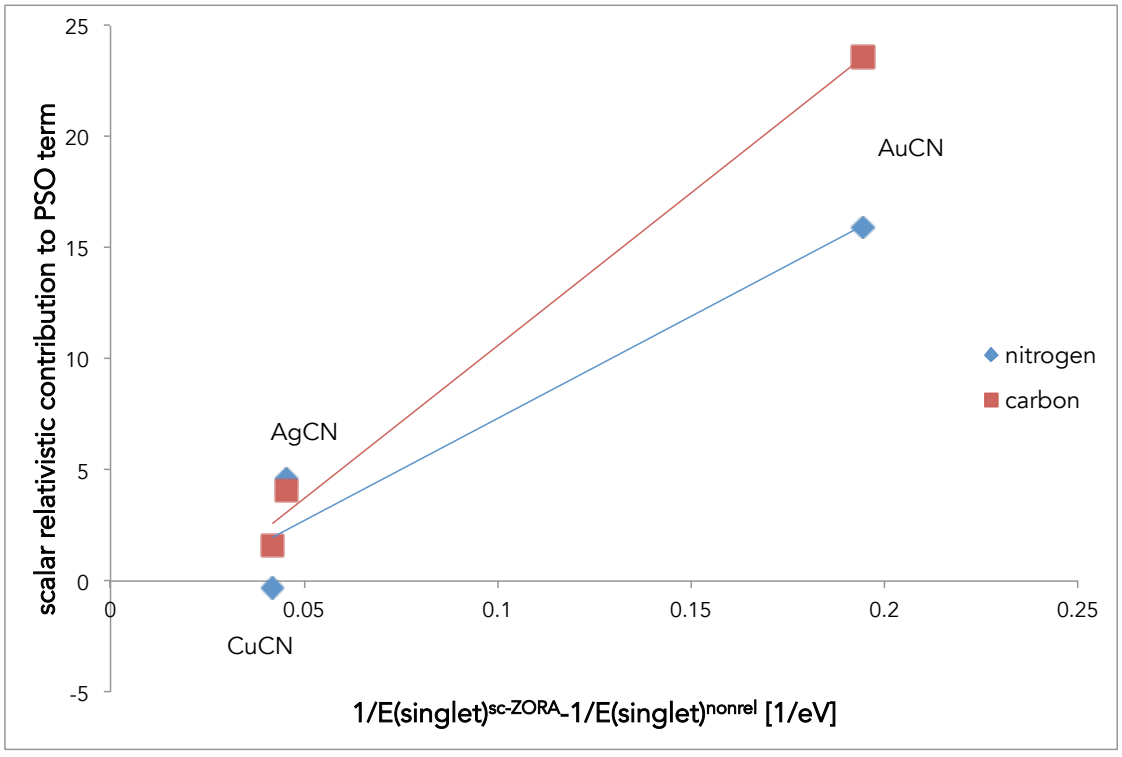

Figure 5.3: Comparison of the change of the first singlet excitation energy calculated as $(1/E^{nonrel}_{singlet} - 1/E^{sc-ZORA}_{singlet})$ with the change of the paramagnetic term after inclusion of the scalar relativistic effects

The spin-orbit coupling contribution can be explained by a mechanism analogous to the FC contribution to the spin-spin coupling constants. The electron spin density polarization is induced on a heavy atom by the spin-orbit operator and interacts with the spins of the light nuclei via the FC mechanism (this term is known as ZSO term — for more details see 2.9.3). The strong dependence of the term on the triplet excitation energy is therefore expected. However, this is not the case. For silver compound the triplet excitation (calculated using the so-ZORA Hamiltonian) is the smallest in the series whereas the value of the spin-orbit contribution is between the contributions for copper and gold analogues. Probably it is a result of the fact that the main contribution is not derived from the lowest triplet excitation (the first five triplet energy excitations differ less than 0.05 eV) and the initial assumption is not fulfilled. Interestingly, for the copper and silver compounds, the inclusion of the spin-orbit coupling induces ZSO term in the shielding constant whereas diamagnetic and paramagnetic terms remain unchanged. It is not true for gold cyanide where only a half of the spin-orbit coupling contribution comes from the ZSO term, whereas the second half is a result of the paramagnetic term change. Similar trends can be observed for the cyanides of the 12th group elements and will not be discussed here any further.

Another important observation is that for the 12th group the HALA effect is mostly caused by the spin-orbit effects for the σ_C and by the scalar effects for the σ_N shielding constants. It is known [173] that for the shieldings of the nuclei directly bonded with heavy atom the spin-orbit coupling effects are sizeable, but this is apparently not necessarily true for the shieldings of nuclei which are not in the immediate neighbourhood of a heavy atom.

5.1.3 DKS vs. ZORA results

Experimental data concerning nitrogen and carbon chemical shifts are not available for the considered cyanides. For that reason the quality of the chemical shifts obtained with ZORA Hamiltonian has been investigated by comparison with the results of the four-component Dirac-Coulomb Hamiltonian calculations. Chemical shifts have been obtained with respect to the carbon and nitrogen nuclei in HCN molecule as a reference.

For molecules containing the 5th row metals, the differences between the carbon chemical shifts obtained using ZORA and DKS are from 2 ppm to 6 ppm. For molecules containing the 6th row metals, the differences are from 5 to 8 ppm in the case of $Hg(CN)_4^{2-}$ and $Tl(CN)_4^{-}$ (they are 16% of the DKS result) and about 10 ppm for $Hg(CN)_2$ and AuCNAuCN (it is 27% and

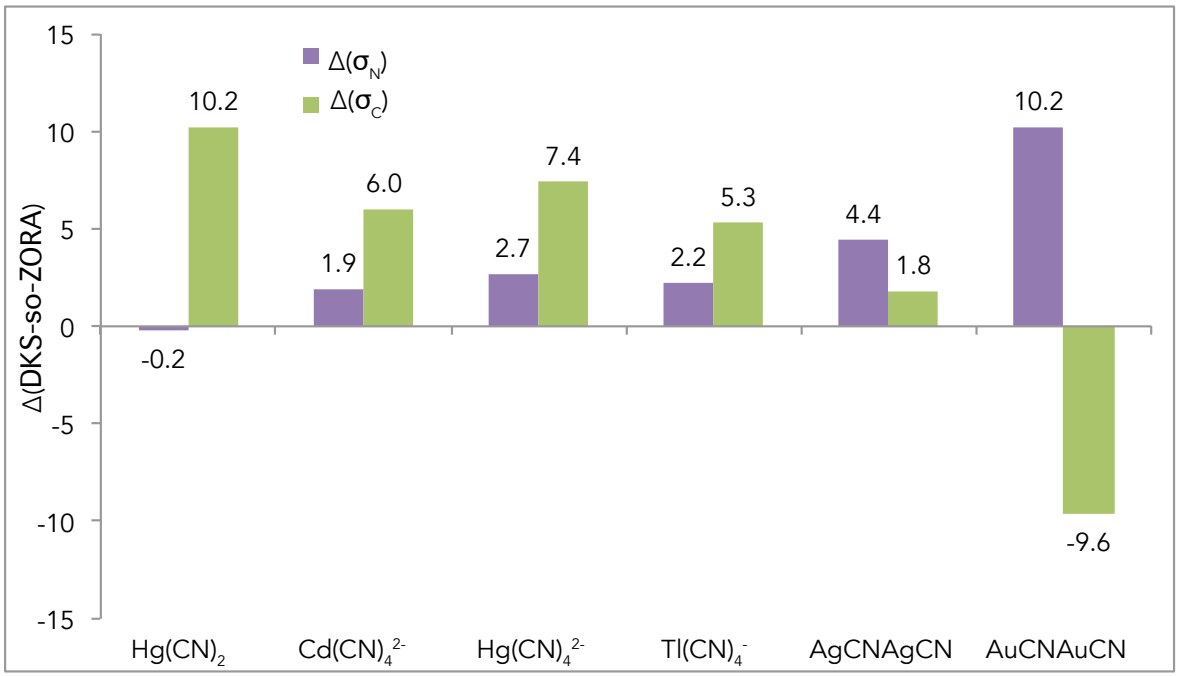

Figure 5.4: Differences between the chemical shift calculated with the DKS and the ZORA-DFT method

33% of the DKS result, respectively). For nitrogen chemical shifts the differences are smaller in comparison with the carbon chemical shifts (they do not exceed 4.5 ppm), and are particularly small for molecules where the nitrogen atom is not directly bonded to a heavy metal. Only for AuCNAuCN, the difference is larger (about 10 ppm) but, here, nitrogen is directly bonded to gold. All of this shows that the ZORA-DFT method underestimates the four-component Dirac results, but it may be a result of the basis set change (ADF employs Slater-type, whereas ReSpect Gauss-type basis sets).

The computations reported here have been performed in 2011. Inspired by the work of Autschbach from 2013 [174], I have decided to examine the influence of the hitherto neglected term from exchange-correlation response kernel (denoted here as fXC term) recently implemented in ADF2014. I have also used the unscaled ZORA form recommended by Autschbach for the NMR shielding constants (numerical investigations show that scaled ZORA leads to gauge dependence) and the correct form of the spin-orbit coupling term (up to the ADF2014 release there was a bug in the spin-orbit part of the calculated chemical shielding which caused the calculated chemical shielding to be gauge-dependent, see the manual of ADF [147]). The re-calculated chemical shifts are compared with the DKS results in Figure 5.5. The use of the newly proposed approach has reduced the difference twice for the carbon chemical shifts in AuCN. On

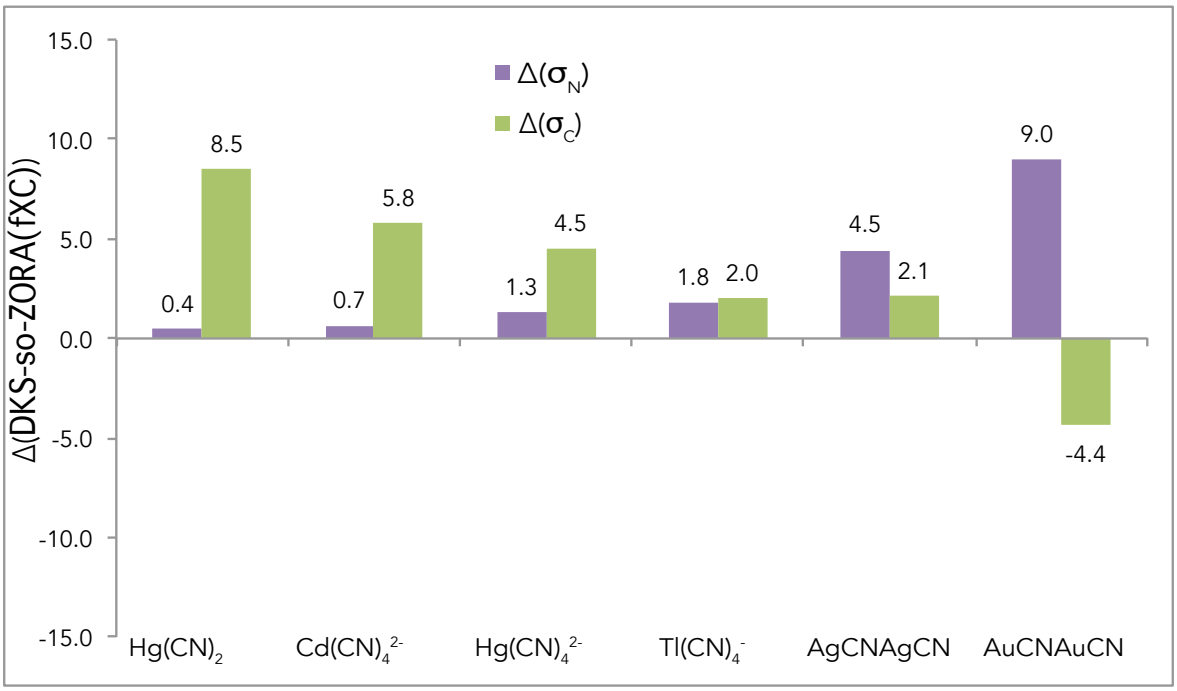

Figure 5.5: Differences between the chemical shift calculated by the DKS and ZORA-DFT method with the new approach (fXC/unscaled)

the other hand, for the nitrogen chemical shift in the same compound the improvement of the results is much smaller (about 1 ppm). It can be concluded that inclusion of the fXC term in the unscaled ZORA approach improves the agreement between the ZORA-DFT and the DKS results, but in many cases the differences remain sizeable.

5.2 The shielding constants of the carbon nuclei in organomercury compounds and halide derivatives

The calculations reported in this section have been carried out for the ^{13}C shielding constants in the selected organomercury compounds (CH_3HgCCH, PhHgCCH, $PhHgCH_3$, PhHgPh, PhHgCl, C_2H_5HgCl, $Hg(C_2H_5)_2$) and halogen derivatives of aliphatic (CH_3X, C_2H_5X, XCCH, X= Cl, Br, I) and aromatic (PhX, X= Cl, Br, I) compounds. For all discussed compounds the experimental chemical shifts are available.

As mentioned before, the relativistic effect for the shielding constants of light atoms is most pronounced for systems which can be described as having hybridization with strong s-character, especially for the nuclei which are immediate neighbours of heavy atoms. For that reason the systems containing carbon atoms of different hybridizations and in different positions with respect to a heavy atom (halogen or mercury) have been chosen. As the spin-orbit coupling cor-

rections to the shielding constants are quadratic response functions, the relativistic term should depend on the size of the energy gap in the molecular electronic structure. For that reason I have decided to investigate two classes of molecules (organomercury compounds and halide derivatives) which differ in electron configuration of the heavy atom which has primary influence on the size of the energy gap.

5.2.1 Estimation of the total relativistic term

The relativistic contributions for the series of organomercury and halogen derivatives compounds are show in Figure 5.6. Here only the ^{13}C shielding constants of the nuclei bonded to the heavy atom by one and two bonds will be shown. The results for meta and para position in the aryl derivatives will not be discussed because of small values of the relativistic terms.

An inspection of the results shows that the relativistic term significantly changes the value of the carbon shielding constants only for the carbon atoms directly bonded to a heavy atom (it is as much as 50 ppm for ICCH). In the case of the carbon atoms bonded by two bonds, the relativistic effects are much smaller (for the sp-hybridised carbon atoms it is less than 8 ppm). The relativistic term depends strongly on the hybridization of the carbon atom directly bonded with a heavy atom. For the series of halide derivatives, the relativistic contributions to the shielding constants of the sp^3- and sp^2-type carbon nuclei are of similar magnitude, whereas for the sp-type carbon atoms, the magnitude of the term is twice as large as that for sp^3- and sp^2-type carbon nuclei. For the organomercury compounds, the differences are much smaller but, what was expected, the relativistic term for the sp-type carbon is larger than for the sp^3-type carbon.

Figure 5.6 shows also the variation of the relativistic term in the series of halogen derivatives. The relativistic term for the iodine compounds is about 10 times larger than for the chlorine compounds.

Finally, it should be noted that, for the carbon in alpha/ipso position in the halide derivatives, the relativistic effects increase the carbon shielding whereas for the organomercury compounds they lead to deshielding of the carbon nuclei in the alpha position. For the beta/orto position, in most cases, the relativistic term increases the shielding of the carbon nuclei.

5.2.2 The scalar and the spin-orbit coupling term

A comparison of the scalar and spin-orbit contributions to the shielding constants in the series of compounds under study is shown in Figure 5.7. The strong dependence of the relativistic

Figure 5.6: Comparison of the relativistic contributions (calculated as a difference between the so-ZORA and the nonrelativistic results) to the shielding constants [ppm] of the carbon nuclei in alpha/ipso and beta/orto position in the selected organomercury compounds and halogen derivatives

term on the hybridisation of the carbon atom (discussed before) is mostly caused by the change of the spin-orbit term.

For the sp-hybridised carbon in the alpha position the spin-orbit coupling term (as estimated by comparison of the so-ZORA and the sc-ZORA results) affects the shielding by about 20–53 ppm for the iodine and organomercury compounds. The sign of the spin-orbit term depends on the type of the heavy nucleus: it is positive for the halide and negative for the mercury derivatives. The scalar terms (always negative for the sp-hybridised alpha atom) are much smaller in the series of halide derivatives (less than -5 ppm and in many cases negligible) whereas comparable with the spin-orbit coupling term in the series of organomercury compounds.

In the case of the monosubstituted benzenes, for the alpha shielding the spin-orbit terms are smaller than for the sp carbon atoms (between -8 ppm and -24 ppm) but still larger than the scalar terms.

Among the results for the sp^2 carbon atoms in the alpha position, the smallest spin-orbit coupling terms are observed for PhHgCl and PhCl. In the case of PhHgCl, it may be a conse-

quence of the electronegativity of the substituent bonded to mercury, since the strong dependence of the spin-orbit coupling term in the ^{13}C shielding on the substituent electronegativity (and related to its energy gap) has been observed before for CH_3HgX (X=CN,Cl,CH3,SiH3) systems [175].

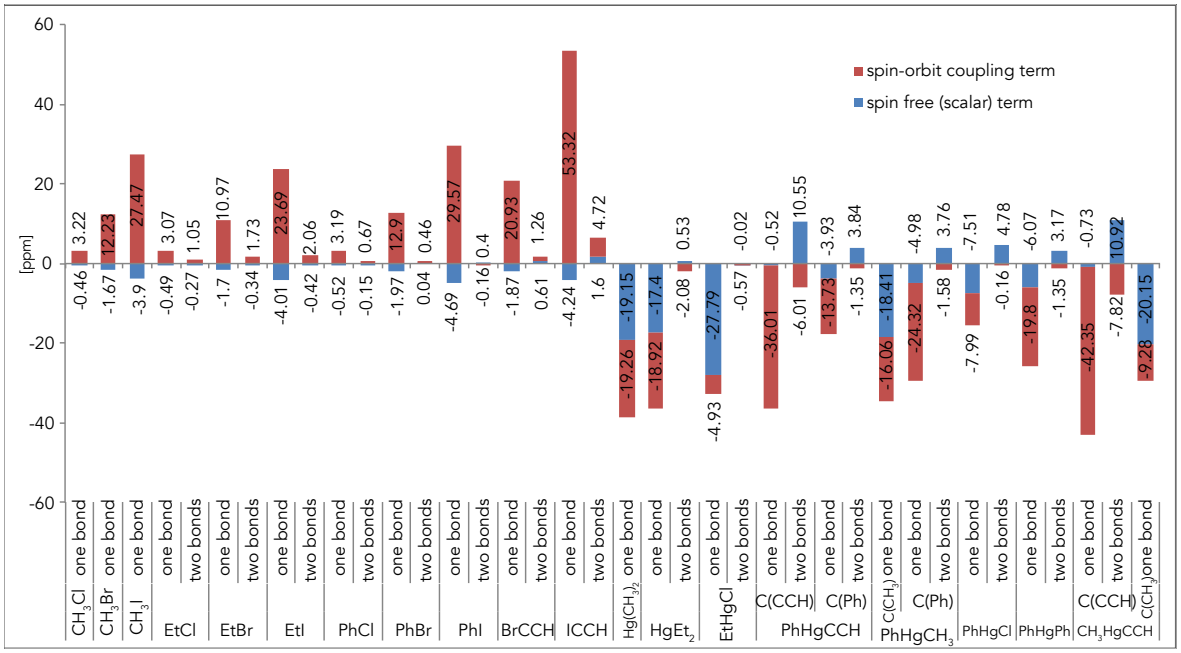

Figure 5.7: Comparison of the scalar and spin-orbit coupling term (calculated with ZORA approach) in the shielding constants [ppm] of the carbon atom in the alpha/ipso and the beta/orto position in the organomercury compounds and halide derivatives

For the compound containing the sp^3 carbon atoms, the spin-orbit coupling term is still substantial (except for C_2H_5HgCl) but, unlike for the sp and sp^2 carbon nuclei, the scalar terms are comparable or even larger than the spin-orbit terms and of the same sign. What was expected for C_2H_5HgCl, the spin-orbit coupling term is very small in comparison with the scalar one (see the discussion above for PhHgCl).

As in the previous investigations, focused on the transition metal cyanides, the change of the lowest singlet excitation energy after inclusion of the scalar term have been compared with the scalar contribution to paramagnetic term. Selection of the molecules in comparison has been limited to a series of halide derivatives extended by astatine compounds. The results shown as function of $(1/E^{nonrel}_{singlet} - 1/E^{sc-ZORA}_{singlet})$ are presented in Figure 5.8.

The linear dependence for each series of compounds (with different hybridization type of carbon atom) has been observed. It may suggest that the initial assumption that the main con-

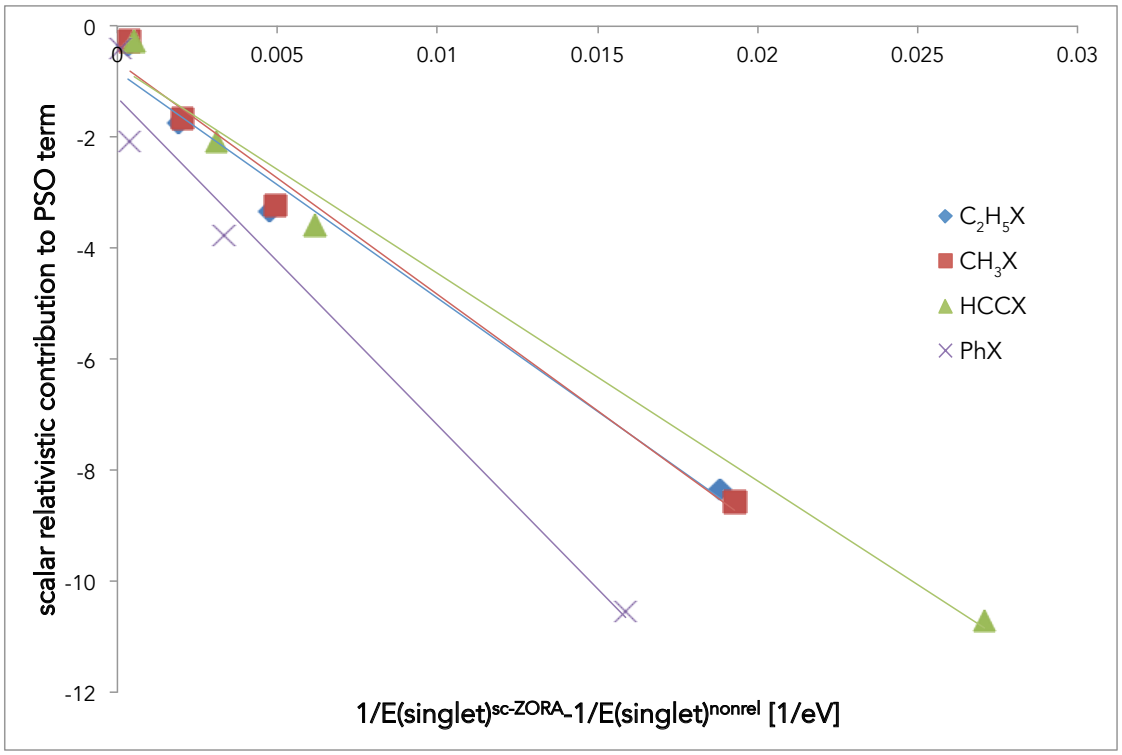

Figure 5.8: Comparison of the change of the first singlet excitation energy calculated as $1/E_{singlet}^{nonrel} - 1/E_{singlet}^{sc-ZORA}$ with the change of the paramagnetic term after inclusion of the scalar relativistic effects

tribution arises from the lowest singlet excitation is true. This can be also supported by the fact that the energy difference between first excitation energy (one or several quasi-degenerated energy states) and next excitation state is at least 0.3 eV (for heavier elements derivatives up to 1.5 eV). Inclusion of the scalar effects (at the sc-ZORA level) leads to an increase in absolute value of paramagnetic term and simultaneously to decrease in singlet-singlet excitation energy.

The increase of a paramagnetic term after inclusion of the scalar effects may be a result of increasing of either the numerator or decreasing of the denominator in sum-over states expansion (see equation 2.89). In order to investigate the behaviour of the numerator in the sum-over-states expansion, the numerator has been estimated by multiplication of the PSO term by the excitation energy. The relation between the change of the numerator and denominator (normalized to the numerator and denominator for chloride derivatives) is shown in Figure 5.9.

The numerator and denominator behave differently in each series of compounds. For the sp^3 carbon derivatives the scalar term is caused by both numerator and denominator change. For the sp carbon derivatives the denominator decreases much faster than numerator, and that increases the paramagnetic term. The PhX compounds can be treated as borderline case. The

numerator and denominator for lighter compounds behave like in compounds containing sp^3 carbon atoms, whereas in PhAt they behave rather like in HCCX compounds.

As expected, the increase of a heavy atom charge increases the scalar contribution to paramagnetic term which is mainly the result of decreasing value of the denominator in the sum-over-states expansion.

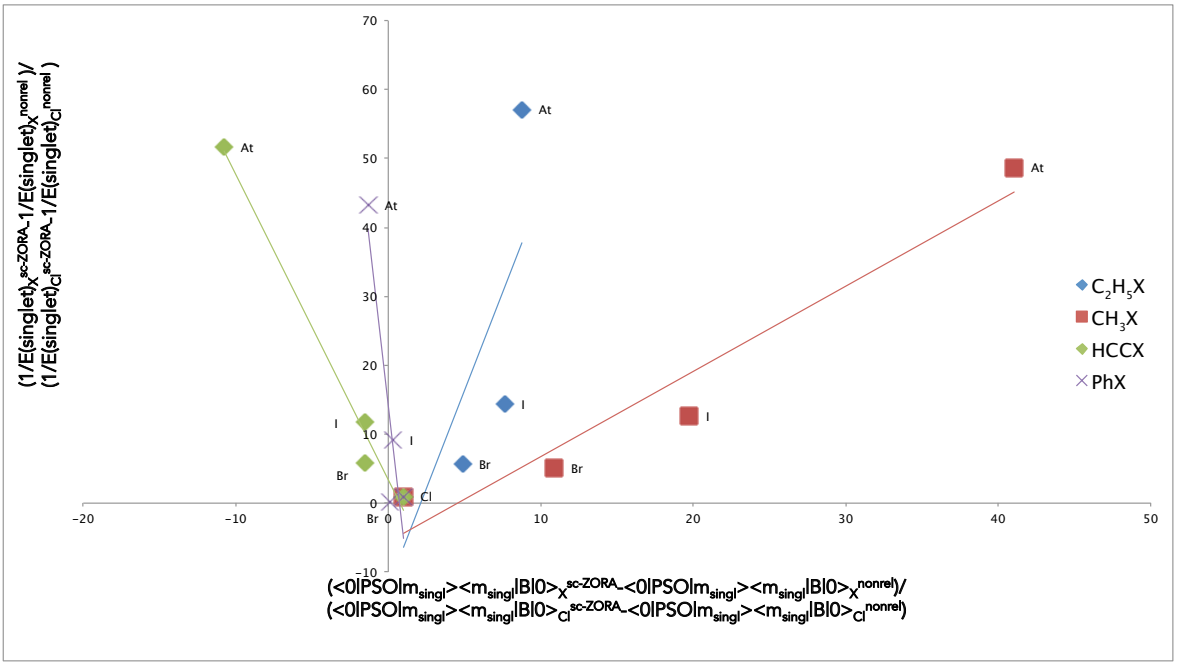

Figure 5.9: The relation between the change of the numerator and the denominator (normalized to the values for chloride derivatives) in paramagnetic term in the series of halide derivatives.

In the series of halide derivatives the contribution of the spin-orbit term in the shielding constants can be easily correlated with the inverse of the first singlet-triplet excitation energy (see Figure 5.10). The slope of the line shows that the transition moment (the numerator) depends on the hybridization type of the carbon atom (the largest for sp carbon and the smallest for sp^3 carbon compounds).

Unfortunately, the same dependence cannot be observed for organomercury compounds (see Figure 5.11). It may be a result of the fact that the change of the substituent bonded with the mercury atom changes not only the excitation energy but also influences transition moment. Another possible explanation is that the initial assumption (that the dominant contribution arises from the lowest excitation) is not fulfilled.

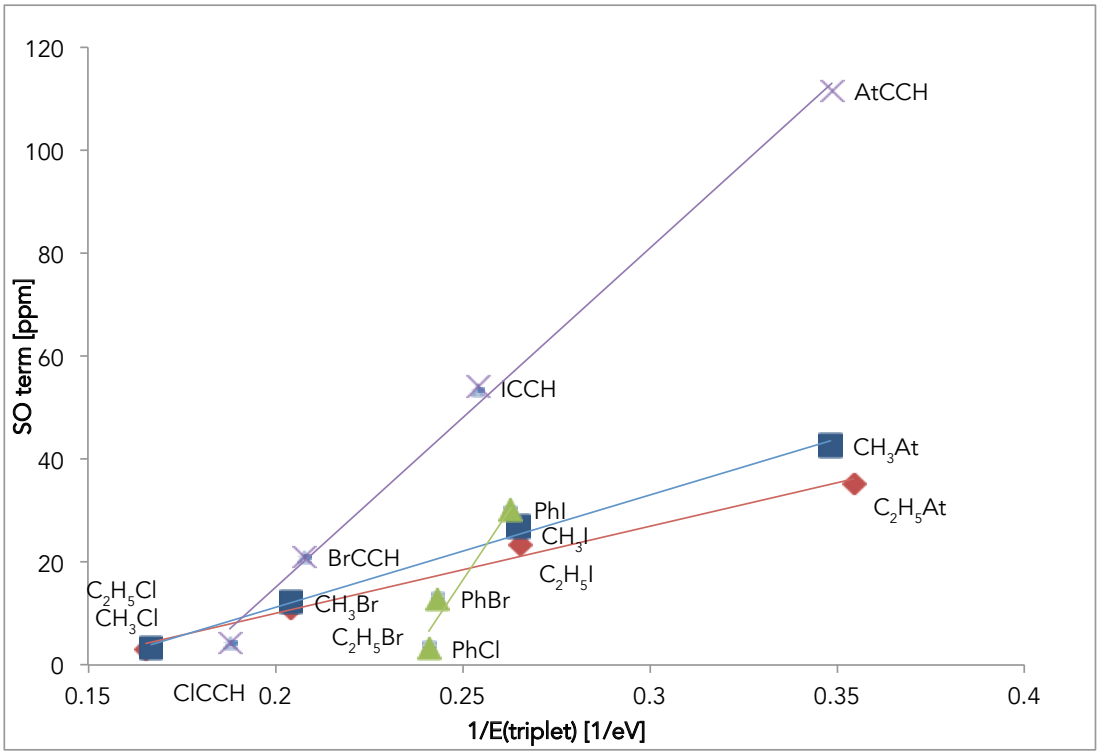

Figure 5.10: The relation between the spin-orbit contribution to the shielding constants and inverse of the first triplet excitation energy calculated at the so-ZORA level in the series of halogen derivatives

In the previous paragraphs the shielding constants for carbon in the alpha position with respect to the heavy atom have been discussed. The spin-orbit coupling contributions to the beta carbon shielding constants are much smaller than for the alpha carbon nuclei, amounting to about 8 ppm (in the absolute value). The scalar terms have the same sign as the spin-orbit terms for BrCCH and ICCH, but not for CH_3HgCCH and PhHgCCH. For the latter two molecules, the scalar terms are larger (in terms of the absolute values) than the spin-orbit coupling terms.

5.2.3 ZORA vs. DKS vs. experimental data

In this subsection the so-ZORA and DKS results are compared with the experimental data. Figure 5.12 shows differences between the experimental relative shielding constants (calculated for the benzene carbon nuclei as a reference) and those calculated with the so-ZORA and DKS approaches.

In most cases, the agreement with experimental data is usually slightly worse for the four-component calculations than for the ZORA results. Probably, it is a result of the cancellation of errors in the ZORA calculations. It can be a result of incorrect rendering of the fXC term

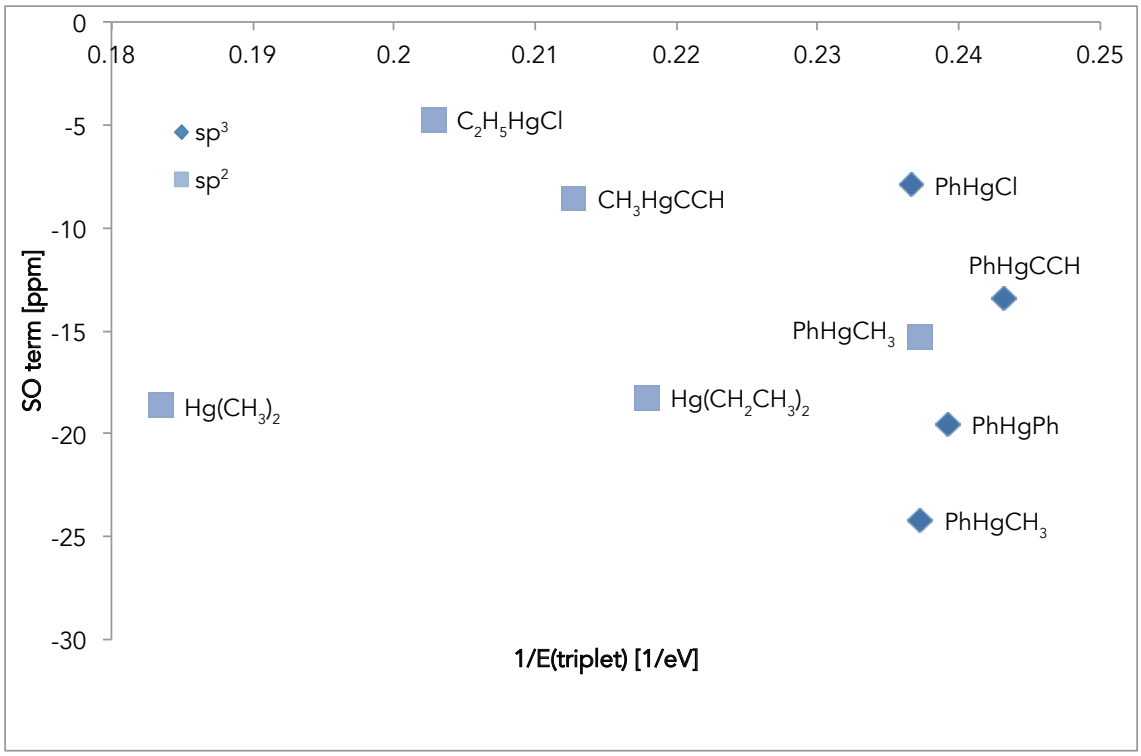

Figure 5.11: The relation between the spin-orbit term in the shielding constants and the inverse of the first triplet excitation energy calculated at the so-ZORA level in the series of organomercury compounds

(see the discussion of the transition metal cyanides) but on the other hand recalculation of the NMR parameters in the transition metal cyanides only slightly improves the agreement between the ZORA and DKS results. The largest differences between the ZORA and DKS results are observed for the organomercury compounds with sp and sp^2 carbons where ZORA seems to reproduce the experimental data slightly better. On the other hand, for the ipso nuclei in the PhX series, where again substantial differences between ZORA and experiment are observed, DKS leads to a better agreement with the experimental values.

For the molecules with sp^3 carbon containing mercury, the differences between the so-ZORA results and the experimental data vary from about -1 ppm for $Hg(C_2H_5)_2$ to about 8 ppm for $Hg(CH_3)_2$. The use of the DKS instead of the ZORA method reduces, in some cases, (e.g. $Hg(CH_3)_2$) the discrepancy with the experiment.

For the beta shielding constants in the organomercury compounds containing sp carbon atoms the differences between the experimental and the computational data can reach 10 ppm. Again, it is possible to conclude that so-ZORA seems to reproduce the experimental data slightly

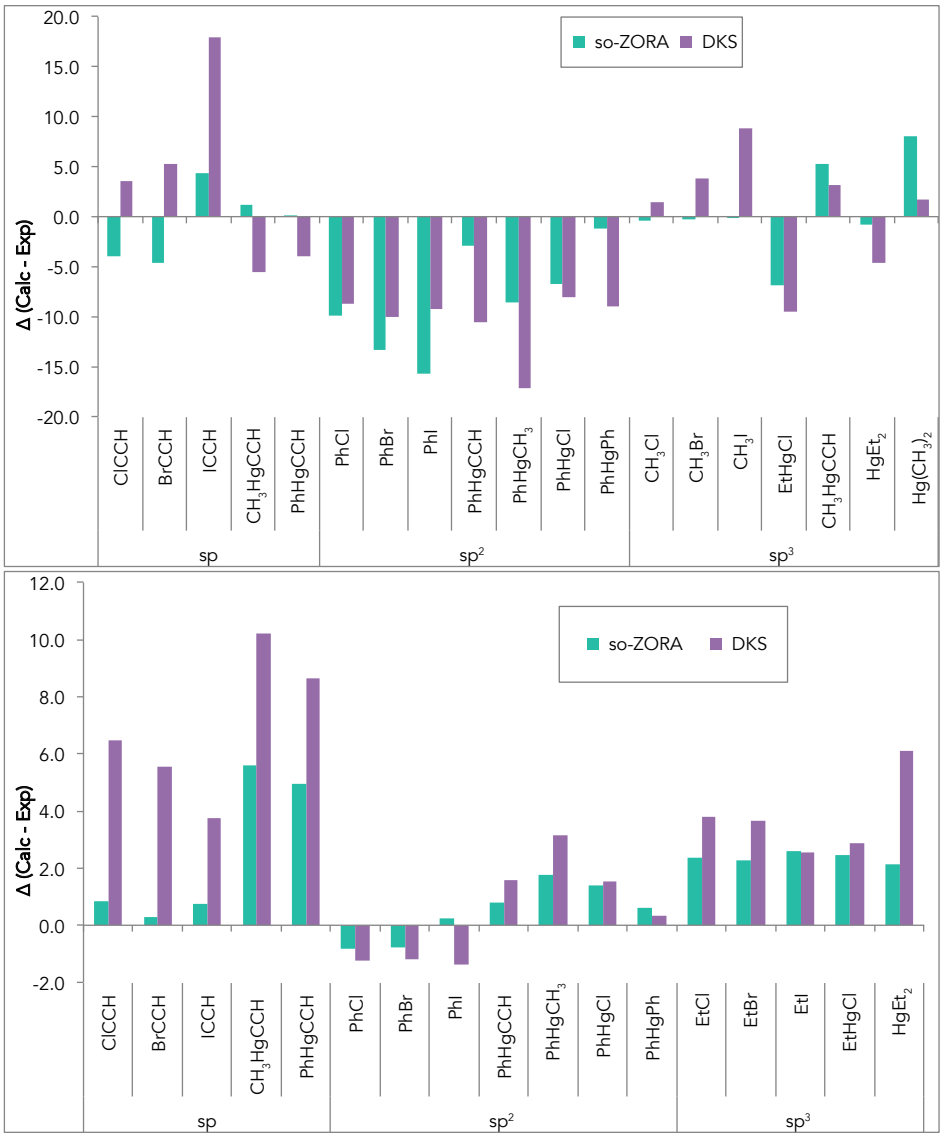

Figure 5.12: Comparison of the calculated and the experimental relative shielding constants [ppm] (both with benzene as a reference) for the carbon directly bonded to the heavy atom (upper figure) and separated from the heavy atom by two bonds (lower figure). All calculations have been performed using the so-ZORA and DKS methods

better than DKS. The same can be observed for sp^2 and sp^3 hybridization but here the differences are less than 3 ppm.

5.2.4 The influence of factors other than the relativistic effects on the quality of the results

Several other factors may affects the differences between the theoretical and the experimental results, namely the effect of choosing different exchange-correlation functionals and

the influence of the solvent effects and the vibrational effects. They may lead for example to the above mentioned error cancellation for ZORA in comparison with the experimental data. Some of these factors will be discussed in this subsection.

All the results discussed till now have been obtained using the PBE GGA functional because of the consistency with the DKS calculations, since hybrid functionals have not been available in the ReSpect program at the time of conducting research. I have carried out the so-ZORA calculations with the PBE0 hybrid functional to investigate how the inclusion of the exact exchange improves the agreement with experiment. The root-mean-square deviation (RMSD) between the theoretical and the experimental results (for the set of 53 relative shielding constants) is 4.54 ppm and 4.24 ppm for PBE and PBE0, respectively. Thus, it can be concluded that the choice of a GGA functional instead of hybrid one does not lead to large errors and should not change significantly the conclusions concerning the relativistic effects.

The results presented so far were calculated using a model neglecting any solvent effects, even though most of the experimental chemical shifts have been measured in solutions. The estimation of solvent effect have been performed at the so-ZORA level using COSMO model (both during the geometry optimization and in the calculation of the shielding constants). The RMSD for the computational results is 4.60 ppm and 5.00 ppm, for the isolated molecules and for the molecules in solution, respectively. Thus the continuum model does not lead to an improved agreement with the experiment, and using more elaborate (i.e. explicit) solvent models is too resource-consuming.

It is known [176] that vibrational effects for shielding constants can be sizeable. I have decided to perform calculation at nonrelativistic level because so far only for this level of theory the appropriate method is implemented [176]. Calculations have been performed for all systems containing halides and for selected organomercury compounds. In all cases inclusion of the vibrational term leads to deshielding of the carbon nuclei but in most cases it does not exceed -4.5 ppm. Atypically, a big vibrational term has been observed for four carbon shielding constants in the organomercury compounds (even -30 ppm). Test calculations of the shielding derivatives with respect to the bond lengths for CH_3I and $Hg(CH_3)_2$ at the so-ZORA level suggest that the vibrational term is close to being additive with the relativistic term for the halide derivatives, but probably non-additive for the series of organomercury compounds (which ex-

plains atypically big and probably not physical vibrational terms for the mercury compounds).

5.2.5 Reproduction of the scalar effects by a effective core potentials

The computationally cheapest method of accounting for the relativistic effects in *ab initio* calculations involves the use of effective core potentials (ECP). It is worthwhile to check to what extent effective core potential (pseudopotential) reproduces scalar relativistic effects on the ^{13}C relative shielding constants calculated with a more rigorous treatment (scalar ZORA). The comparison of the scalar terms obtained by these methods is presented in Figure 5.13. The comparison is limited to MWB60 and MDF60 pseudopotentials and to the mercury compounds because for this series the nonrelativistic ECPs (MHF60) are available. That gives a possibility to estimate the scalar relativistic terms in the shielding constants using ECPs (the use of a full atomic basis set in nonrelativistic calculations leads to a non-physical bias).

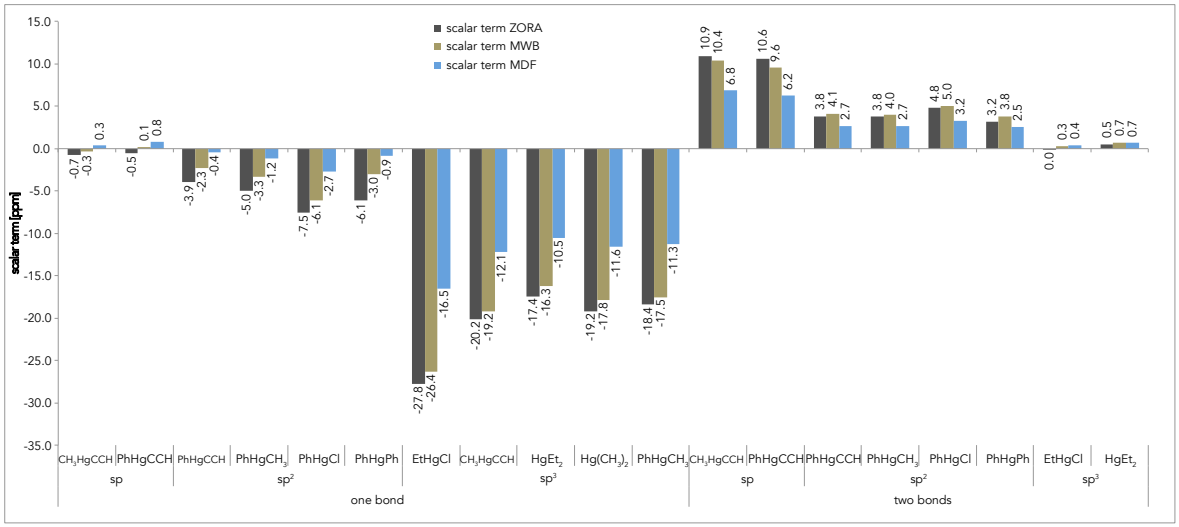

Figure 5.13: The estimation of scalar effects with the ZORA and ECP methods. The ZORA scalar term is calculated as a difference between the sc-ZORA result and the non-relativistic result obtained with the same basis set, while the ECP scalar term is calculated as a difference between the scalar relativistic pseudopotential results and the nonrelativistic pseudopotential results, with the same basis set for the light atoms

For the sp-type carbon atoms directly bonded with mercury the scalar terms are negligible, so the comparison is difficult. For the carbon atoms with the sp^2 hybridization they are more significant (especially for PhHgCl where the scalar term is about -7.5 ppm), and even larger

for the sp^3-types carbon atoms, so the discussion is mostly based on them. The effective core potential parametrized with respect to the Wood-Boring approximation to the Dirac equation (MWB60) reproduces the scalar term well (somewhat underestimating it) for this class of shieldings. On the other hand, MDF60 renders only from 18% (in the case of PhHgCCH) to 65% (in the case of the sp^3-type carbon compounds) of the MWB60 result.

For the relative shielding constants of the carbon atoms bonded to mercury with two bonds, the scalar effect decreases with the decreasing s-character of the carbon hybridization, unlike for the alpha-carbon atoms. MWB60 underestimates the sc-ZORA term for the sp hybridization (by about 0.5–1 ppm) and leads to a slight overestimation of the ZORA scalar term for sp^2. Similarly as for the alpha carbon shieldings, the MDF60 scalar terms are smaller than the MWB60 scalar terms.

All calculations here have been performed using the standard MDF60 implemented in the Gaussian package, but two types of MDF60 pseudopotentials are now available on the web page of Stuttgart research group [177] which differ with respect to the method of fitting. For that reason, additional calculations have been performed for selected molecules using a more recent version of MDF60. The obtained results are much closer to MWB60, thus, the observed difference is most likely a consequence of different fitting procedures employed to obtain the two ECPs.

In the case of the relative shielding constants of the carbon nuclei separated by three or four bonds from the heavy atom, the scalar terms are negligible (less than 1 ppm) and they will not be discussed any further.

Chapter 6

The influence of the heavy atom on the nuclear spin-spin coupling constants of light atoms

Despite the fact that the influence of the relativistic effects on the nuclear shielding constants has been extensively discussed in the literature, the parallel phenomenon on the nuclear spin-spin coupling constants of the light nuclei is almost unexplored. As mentioned in introduction there is a handful of papers dealing with the situation when a heavy atom mediates a geminal coupling between two light atoms [96, 97, 98, 99, 100, 101], but there are practically no studies concerning the situation where a heavy atom is not in the coupling path. For that reason the first stage of the research was focused on three types of the spin-spin coupling constants transmitted by one bond. The description of the results is organized as follows. First, the $^1J_{CN}$ coupling constants in the transition metal cyanides will be discussed. Next, the relativistic effects for the $^1J_{CC}$ and $^1J_{CH}$ coupling constants in organometallic (cadmium and mercury) compounds and heavy halide (iodine and astatine) derivatives will be investigated.

In the second stage of the research, a detailed investigation of the influence of the relativistic effects on the spin-spin coupling constants mediated by heavy atom has been performed. Here, the $^2J_{CC}$, $^3J_{CC}$, $^4J_{CC}$ coupling constants for a series of the p-block and 12th group heavy elements compounds will be discussed.

The results discussed in this chapter have been obtained at several levels of theory, starting from the nonrelativistic approach, through the one- and two-component ZORA-DFT, up to the DKS method. The proposed methodology, similar to the one used in the previous chapter, allows the evaluation of the relativistic effects and the estimation of the ratio of the spin-free and spin-dependent terms in the spin-spin coupling constants.

It should be stressed that experimental data for the discussed spin-spin coupling constants are not available. The comparison of the ZORA and DKS results, however, enables evaluating the accuracy of the ZORA method in reproduction of the relativistic effects.

6.1 The spin-spin coupling constants between the carbon and nitrogen nuclei in the transition metal cyanides

In this section the $^1J_{CN}$ coupling constants calculated for a series of the 11th, 12th group elements and thallium cyanides will be discussed. The values of the $^1J_{CN}$ constants at the non-relativistic and two-component ZORA level are shown in Figure 6.1.

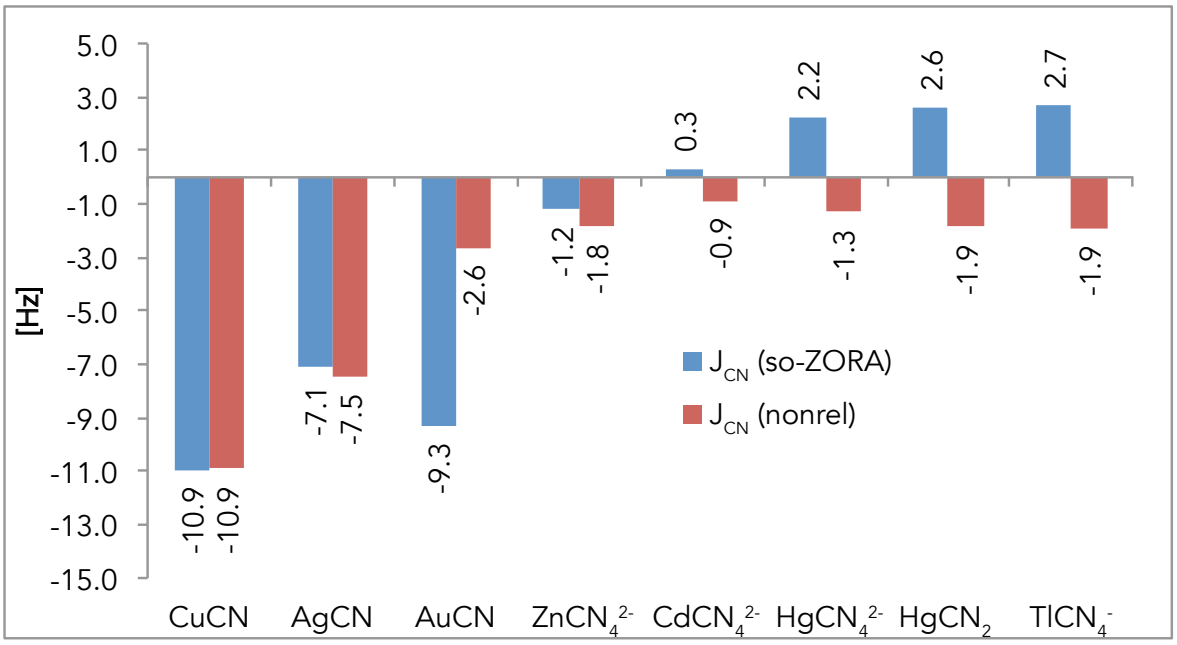

Figure 6.1: Comparison of the $^1J_{CN}$ results in the selected cyanides calculated with the nonrelativistic and spin-orbit coupling ZORA Hamiltonian

The highest absolute values (as large as -11 Hz) of the spin-spin coupling constants (calculated at so-ZORA level) are observed for the 11th group elements of the periodic table. For the 12th group and thallium compounds the values are much smaller (less than 3 Hz) but it should be kept in mind that here, in contrast to the molecules containing the 11th group elements, the nitrogen atom is directly bonded only to carbon nuclei in this series of compounds.

6.1.1 Estimation of the total relativistic term

Examination of the result presented in Figure 6.1 shows that the values of the $^1J_{CN}$ coupling constants calculated at the nonrelativistic level are always negative and in most cases (except for copper and silver compounds) do not exceed -2.6 Hz. Inclusion of the relativistic term changes significantly (up to 7 Hz) the values of $^1J_{CN}$ in the series of compounds with heavier elements (i.e. the 5th and 6th row of the periodic table) or even changes the sign of the coupling constant in the series of the 12th group elements and thallium compounds.

6.1.2 Importance of the scalar and the spin-orbit coupling term

The scalar and spin-orbit coupling corrections to the relativistic term in $^1J_{CN}$ are shown in Figure 6.2. In most cases the spin-orbit coupling contribution is small (less than 0.5 Hz) and

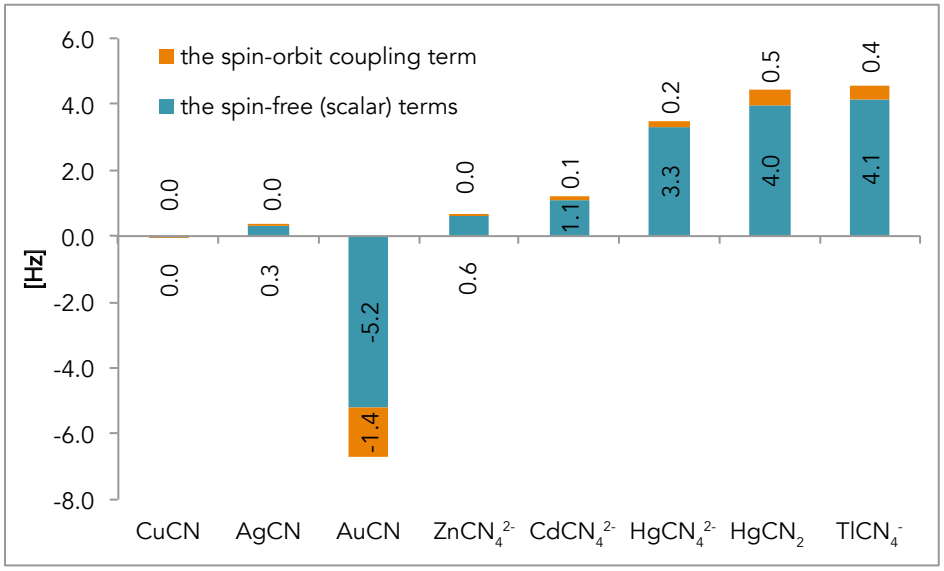

Figure 6.2: Comparison of the scalar relativistic and spin-orbit coupling contribution to $^1J_{CN}$ coupling constants, calculated with the nonrelativistic and spin-orbit coupling ZORA Hamiltonian, in selected cyanides

does not exceed 11% of the total relativistic term. Only for AuCN this contribution is slightly larger (-1.4 Hz which is 21% of the full relativistic term). To conclude, contrary to the case of the shielding constants, where the HALA effect is dominated by the spin-orbit coupling term, the influence of a heavy atom on the $^1J_{CN}$ spin-spin coupling constants in discussed compounds mainly depends on the spin-free (scalar) relativistic effects, at least for this series of compounds.

6.2 The carbon-carbon spin-spin coupling constants in organometallic compounds and halide derivatives

The preliminary findings for $^1J_{CN}$ inspired me to look more closely at the influence of a heavy atom on the one-bond spin-spin coupling constant of the nearby light nuclei. Additionally I have decided to investigate what factors determine the magnitude of the effect. For my investigations I chose derivatives of aliphatic hydrocarbons substituted with I, At, Cd and Hg, which allowed me to study both the one-bond carbon-carbon and one-bond proton-carbon (discussed in the next section) coupling constants. I have also investigated the influence of the nature of the heavy atom substituent and the carbon hybridization on the relativistic effect.

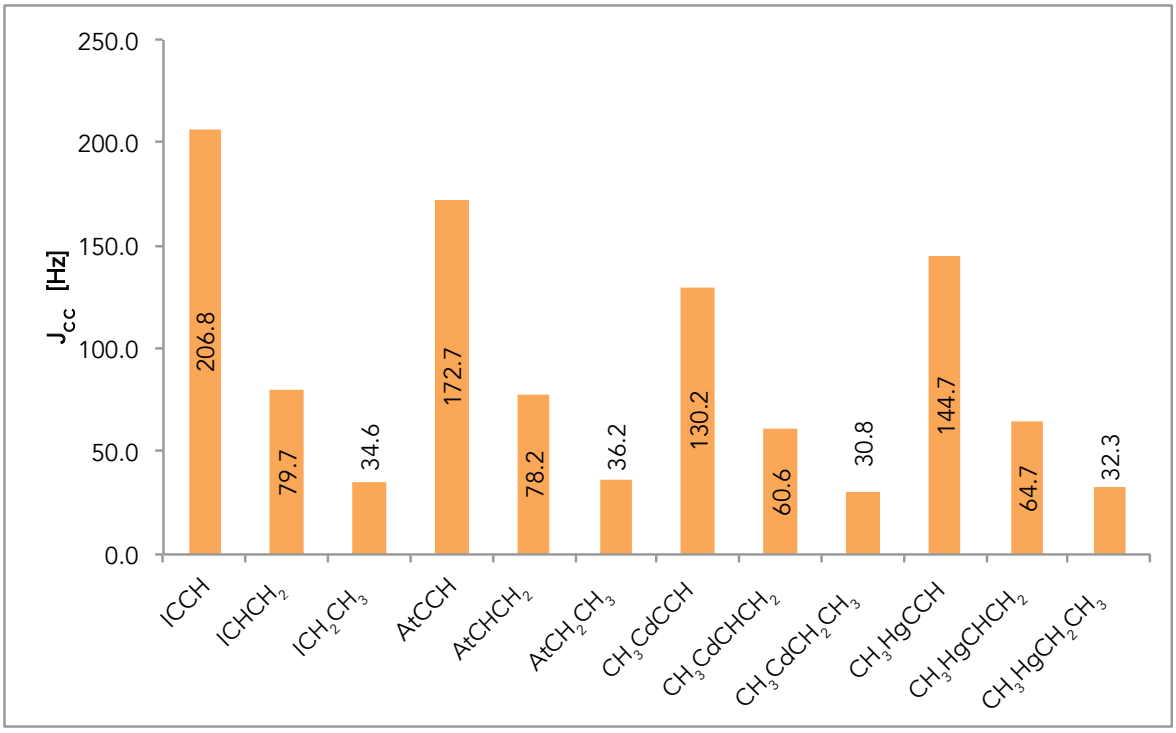

Figure 6.3: Comparison of the $^1J_{CC}$ results, calculated with the Dirac-Coulomb Hamiltonian, in the selected organometallic compounds and halogen derivatives

The DKS results for $^1J_{CC}$ are shown in Figure 6.3. As expected, the largest values of the spin-spin couplings are observed for the sp-type carbon atoms and the smallest for sp^3 carbon atoms. For most of the compounds, a change of the heavy atom charge in the same group does not change significantly the value of $^1J_{CC}$ (the difference is less than 6% of $^1J_{CC}$ in the heavier analogue). Only for the sp-type compounds the differences are bigger (for the 12th group of the periodic table it is about 10% and for the halide derivatives it can reach 20%).

6.2.1 Importance of the relativistic effects in the substituent effect

The overall substituent effect for the $^1J_{CC}$ spin-spin coupling constants under study has been estimated by comparison of the DKS results for the discussed compound and unsubstituted hydrocarbons (see Figure 6.4), whereas the relativistic contribution to the substituent effect have been evaluated using the nonrelativistic and DKS approach (see Figure 6.5).

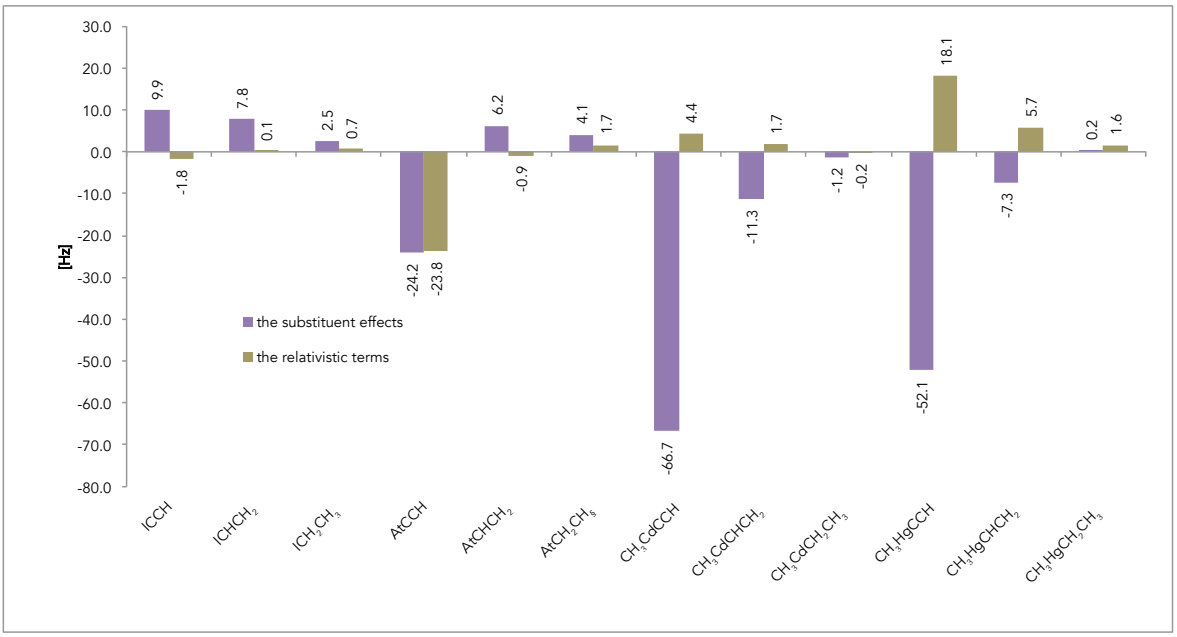

Figure 6.4: Importance of the relativistic contribution (calculated using DKS approach) in the substituent effect for $^1J_{CC}$ in the selected organometallic compounds and halogen derivatives

The inspection of the results shows that the relativistic effects, in comparison with the total substituent effect, are sizeable for the series of compounds containing the 6th row elements (mercury and astatine), but nearly negligible (10% or less) for the compounds containing 5th row elements. For the mercury compounds, the relativistic effects significantly lower the calculated substituent effect (the relativistic term is about 39% of the total substituent effect). It is also true for the cadmium derivatives, but in this case the relativistic effect is only about 10% of the total substituent effect.

In the case of AtCCH, the total substituent effect is dominated by the relativistic effect (the non-relativistic calculations lead to a very similar result as for HCCH). For the other astatine derivatives, the relativistic effect is smaller, but still significant in comparison with the substituent effect. For the iodine derivatives the relativistic effect on $^1J_{CC}$ is negligible (of the

order of magnitude of numerical accuracy) at least for the sp^2 and sp^3 carbon type derivatives (for ICCH, the relativistic effects lower the substituent effect by about 30%).

6.2.2 Influence of the carbon hybridization

The magnitude of the substituent and relativistic effects on the $^1J_{CC}$ spin-spin coupling constants depends strongly on the hybridization of carbon atoms (see Figure 6.4).

The largest relativistic effects are observed for the systems with the sp-type carbon atoms and the smallest effects (at least one order of magnitude smaller) for the systems with the sp^3-type carbon atoms. However, for the compounds containing the 12th group elements, the relative contribution of the relativistic effect to the substituent effect increases with decreasing s-type character of carbon atom.

6.2.3 Influence of the spin-orbit coupling

The importance of the relativistic spin-orbit contribution to the total substituent effect on the $^1J_{CC}$ spin-spin coupling constant depends strongly on the nature of the heavy atom substituent (see Figure 6.5). For halide derivatives, the scalar and spin-orbit coupling contributions are, as a rule, of similar magnitude. Only for $AtCHCH_2$ compound the scalar term dominates over the spin-orbit coupling contribution. In $ICHCH_2$ and ICH_2CH_3, the very small values of the relativistic effect are a result of mutual cancelling of the scalar and spin-orbit terms (each about 0.5 Hz, but of opposite signs). In the mercury and cadmium derivatives, most of the total relativistic effect comes from the scalar term, since the spin-orbit term contributes less than 10% to it. It can be concluded that the sizeable spin-orbit coupling term is observed for the molecules containing heavy atoms with strong p-character in the electron valence configuration

The spin-orbit coupling can change the pure FC+SD term, PSO term and also induces the cross term between the spin-dependent FC+SD terms, and the PSO term, denoted later as FC+SD/PSO (see the discussion in section 2.9). Table 6.1 compares the individual terms to the spin-orbit coupling term in AtCCH (where the spin-orbit contribution is the largest) and in CH_3HgCCH (where the spin-orbit contribution is negligible with respect to the scalar term). The results show that in the case of CH_3HgCCH, the FC+SD/PSO cross term is about 17% of the spin-orbit contribution (about -0.3 Hz), and approximately 15% of the spin-orbit contribution (about 2.4 Hz) in CH_3HgCCH. Despite the sizeable FC+SD/PSO cross term, inclusion of the spin-orbit coupling changes predominantly the pure FC term. This conclusion is in opposition

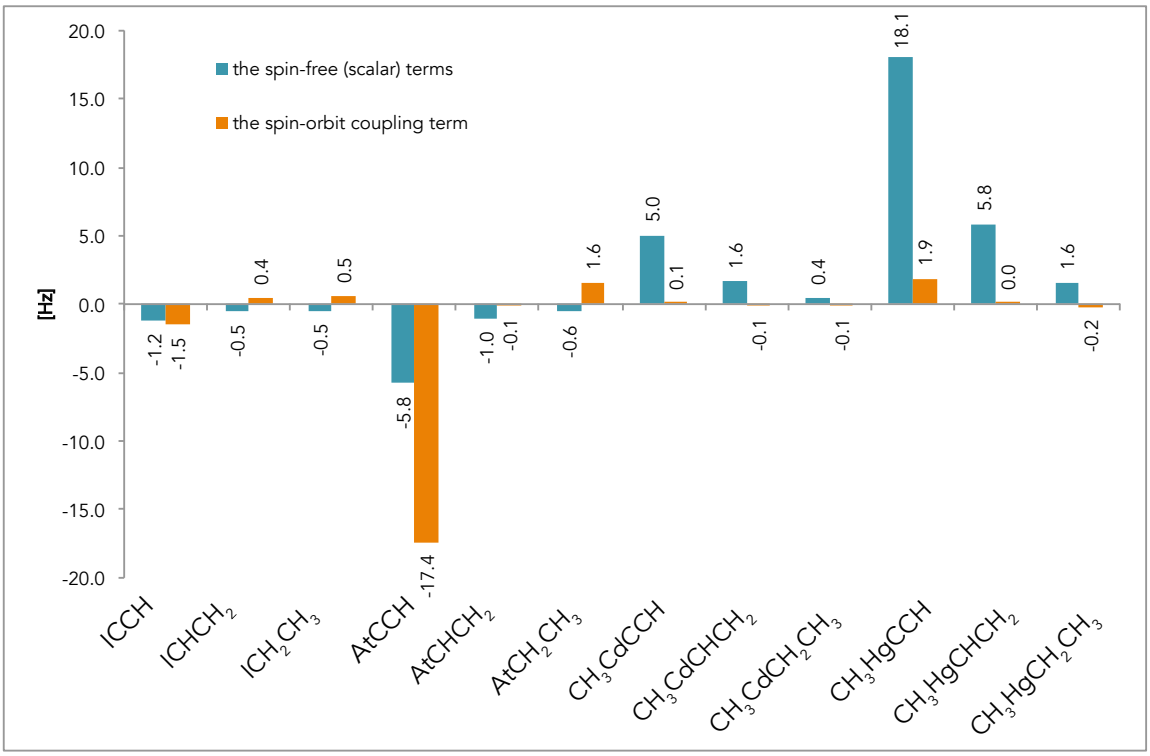

Figure 6.5: Comparison of the scalar and spin-orbit coupling contribution (calculated with the ZORA approach) to $^1J_{CC}$ in the selected organometallic compounds and halogen derivatives

Table 6.1: Comparison of the individual terms of $^1J_{CC}$ in AtCCH and CH_3HgCCH, obtained using the so-ZORA approach

	AtCCH [Hz]	CH_3HgCCH [Hz]
so term	-17.3	1.8
DSO	0.0	0.0
PSO	-0.8	0.1
FC	-16.9	1.9
SD	-2.0	0.2
FC+SD/PSO cross term	2.4	-0.3

to the results for the couplings of the heavy nuclei analyzed by Autschbach *et al.* [132] where the spin-orbit coupling term is dominated by the FC+SD/PSO cross term.

6.2.4 Comparison between so-ZORA and DKS results

In subsection 6.2.1, the $^1J_{CC}$ discussion is based on the results obtained at the DKS level of theory, but in subsection 6.2.3 the contributions to the relativistic effects have been estimated using an approximate ZORA method. It is worthwhile to check how well the calculations with the more approximate ZORA Hamiltonian reproduce the full Dirac-Coulomb Hamiltonian results.

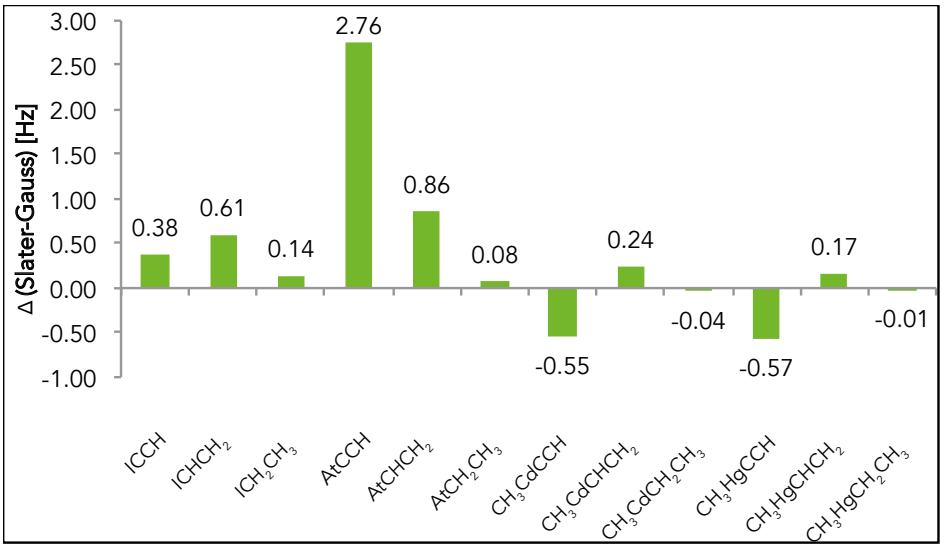

Figure 6.6: Comparison of the differences between $^1J_{CC}$ obtained with the Slater and the Gauss type basis set at the nonrelativistic level of theory

It should be stressed that the comparison of ZORA-DFT and Dirac-Kohn-Sham results is not straightforward, since, out of necessity, different basis sets are used (ADF employs the Slater orbital basis set, while in the DIRAC or Gaussian program the Gauss orbitals are used). To estimate the effect of basis set change the comparison of the results obtained using the Slater and Gauss orbitals with the non-relativistic Hamiltonians (calculated using the ADF and Dalton packages, respectively — see Figure 6.6) have been performed. Differences between the results obtained with these basis sets are in many cases small (less than 0.5 Hz) and negligible with respect to the values of the spin-spin coupling constants. Only in few cases the differences are larger (0.5–1.0 Hz and for AtCCH it is 2.8 Hz). Considering thus, the use of different basis sets should not influence substantially the comparison between the ZORA-DFT and DKS results, except when the relativistic effect is very small.

Comparison of the DKS and the so-ZORA results collected in Figure 6.7 shows that so-ZORA reproduces the DKS results very well. The differences are in most cases less than 1.0 Hz. The inclusion of the small spinor (in the DKS calculations) does not change significantly the cal-

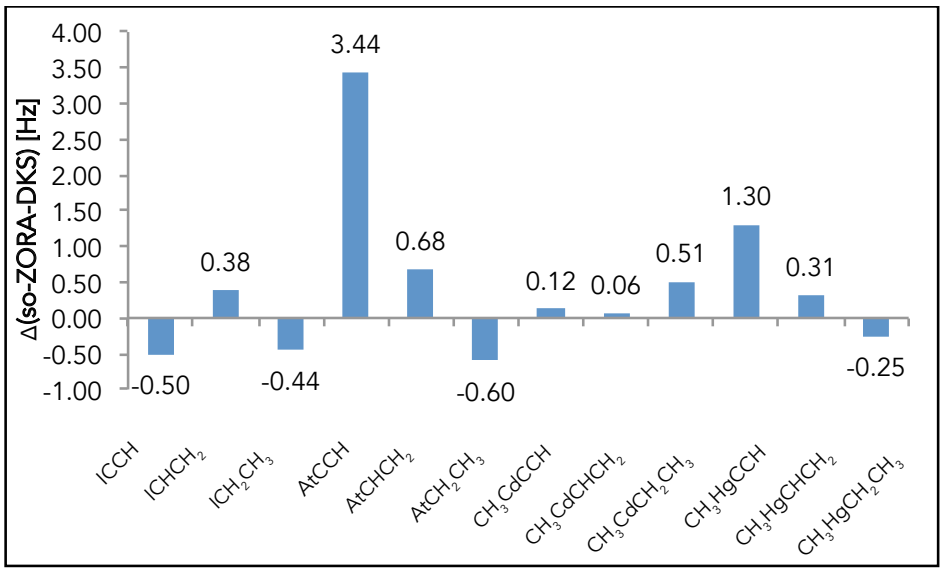

Figure 6.7: Comparison of the differences between the $^1J_{CC}$ coupling constants obtained using the so-ZORA and the DKS methods

culated $^1J_{CC}$ couplings in comparison with the two-component ZORA approximation. Only for CH_3HgCCH and AtCCH, Δ(so-ZORA-DKS) is slightly bigger (e.g. 3.4 Hz in the case of AtCCH) but, at least for AtCCH, a significant part of this difference can be attributed to the basis set change effect (in the case of AtCCH about 2.8 Hz, see above).

6.2.5 Comparison between the sc-ZORA and ECPs results

The differences between the $^1J_{CC}$ spin-spin coupling constants calculated using the scalar ECPs and scalar-only ZORA results are shown in Figure 6.8 and compared with the scalar ZORA term. Again, it should be pointed out that a different basis set has been used for the sc-ZORA and ECPs calculations.

Two types of ECPs have been investigated: Los Alamos ECPs (LANL2DZ) and a series of Stuttgart ECPs (MDF and MWB with the small and large core replacement, named sMDF or sMWB and lMDF or lMWB, respectively). Los Alamos ECPs (in this case LANL2DZ) do not reproduce the sc-ZORA results very well. The same is true for the lMDF and lMWB pseudopotentials, so it seems to be mainly a matter of replacing too many core electrons by the effective potential. On the other hand, the small-core ECPs (sMWB and sMDF) results are in excellent agreement with sc-ZORA results. In most cases, the differences are less than 1 Hz. Only for CH_3HgCCH a sizeable discrepancy (about 4 Hz) between the MWB60 and the MDF60 results has been observed. For that reason, additional calculations with a more recent version

		LANL2DZ-(sc-ZORA) [Hz]	lMDF-(sc-ZORA) [Hz]	sMDF-(sc-ZORA) [Hz]	sMDF(new)-(sc-ZORA) [Hz]	lMWB-(sc-ZORA) [Hz]	sMWB-(sc-ZORA) [Hz]	scalar term(sc-ZORA)
I	ICCH	2.22	1.75	-0.15		2.92		-1.16
	$ICHCH_2$	-0.23	-0.27	-0.41		-0.20		-0.54
	ICH_2CH_3	-0.04	-0.09	0.02		-0.07		-0.47
At	AtCCH		4.41	0.75		2.99		-5.78
	$AtCHCH_2$		0.00	-0.35		-0.24		-1.04
	$AtCH_2CH_3$		-0.12	-0.01		-0.11		-0.57
Cd	CH_3CdCCH	-8.90		1.16		-9.82	1.26	5.02
	$CH_3CdCHCH_2$	-2.74		-0.04		91.05	0.01	1.64
	$CH_3CdCH_2CH_3$	-0.69		0.07		-0.64	0.10	0.40
Hg	CH_3HgCCH	-16.24		-3.61	-0.09	-13.60	0.07	18.11
	$CH_3HgCHCH_2$	-4.12		-1.83	-0.43	-3.98	-0.38	5.84
	$CH_3HgCH_2CH_3$	-1.05		-0.43	-0.09	-0.93	-0.05	1.57

Figure 6.8: Comparison of $^1J_{CC}$ calculated with different types of effective core potentials on heavy atoms and pcJ-2 basis set on C and H, using the PBE0 functional.

of MDF60[178] (denoted as sMDF(new) in Figure 6.8) were performed. The obtained results are much closer to the MWB60 results. It suggests that the observed difference is most likely a consequence of different fitting procedures employed to obtain the two ECPs.

6.3 The carbon-proton spin-spin coupling constants in the organometallic compounds and halide derivatives

The reported values of the $^1J_{CH}$ spin-spin coupling constants are shown in Paper III. Two types of the $^1J_{CH}$ coupling constants will be discussed in the section: the $^1J_{CH}$ coupling constants of the carbon nuclei directly bonded to the heavy atom ($^1J_{C_\alpha H}$) and the $^1J_{CH}$ coupling constants involving the carbon nuclei in beta position with respect to the heavy atom ($^1J_{C_\beta H}$). Additionally, for the coupling constants involving carbon in beta position, the coupled proton in the $RCHCH_2$ systems can be either in *cis* or in *trans* position with respect to the heavy atom, whereas for the RCH_2CH_3 systems, the dihedral angle between the heavy atom-alpha carbon

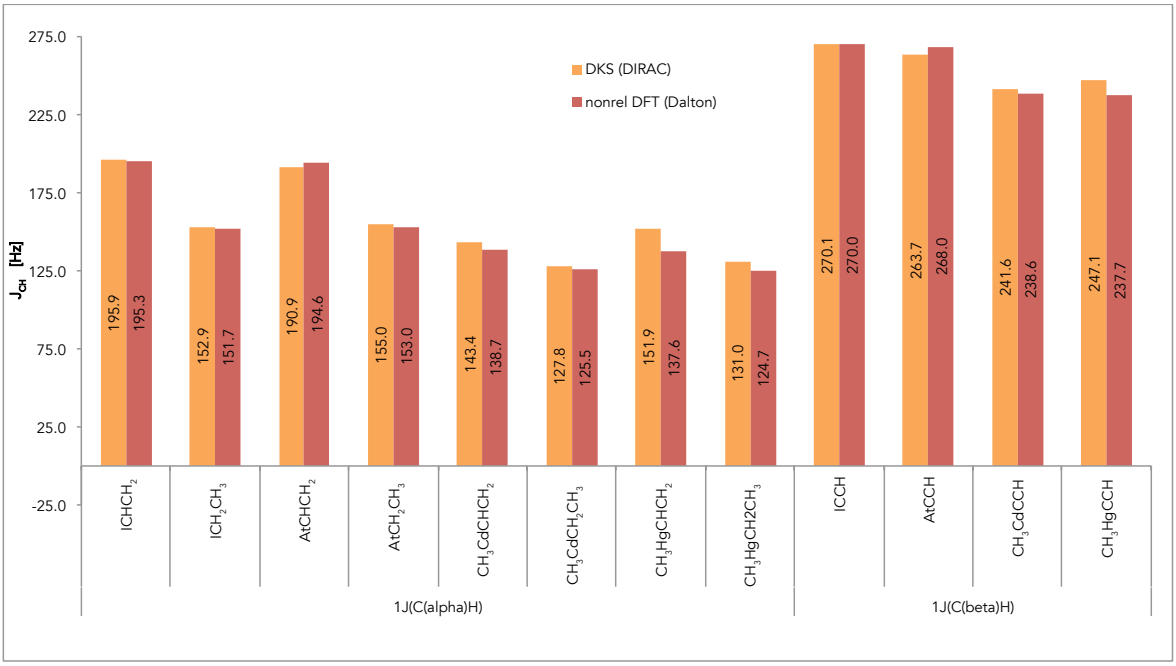

Figure 6.9: Comparison of the results for the selected $^1J_{CH}$ coupling constants, calculated with the Dirac-Coulomb and nonrelativistic Hamiltonians, in organometallic compounds and halogen derivatives

and hydrogen-beta carbon may play a role. The influence of these factors will be discussed in this section.

Comparison of the selected $^1J_{CH}$ coupling constants calculated with the DKS and nonrelativistic Hamiltonian with the same basis set is shown in Figure 6.9. The relativistic effects (calculated as a difference between the nonrelativistic and the DKS results) on the $^1J_{CH}$ coupling constants in iodine-substituted hydrocarbons are 1 Hz or less (even when carbon is in the α position) which is negligible with respect to the total value of the spin-spin coupling constant. For the cadmium compounds, the relativistic effects are larger (even 5 Hz) but still small in comparison with the results for the organomercury compounds. Because of all that only the 6th row derivatives will be discussed in the following sections.

The biggest values of the $^1J_{CH}$ coupling constants are observed for $^1J_{C_\beta H}$ in the $-$CCH compounds and the smallest for $^1J_{CH}$ involving sp^3 carbon atoms (see Figure 6.10). For the astatine derivatives, as a rule, the $^1J_{C_\alpha H}$ coupling constants are larger than the $^1J_{C_\beta H_{cis}}$ or $^1J_{C_\beta H_{trans}}$ coupling constants. The coupling constants involving hydrogen atom in the *cis* position are in all cases larger than the coupling constants involving hydrogen atom in the *trans* position. A similar situation can be observed for the sp^3 compounds. When the dihedral angle

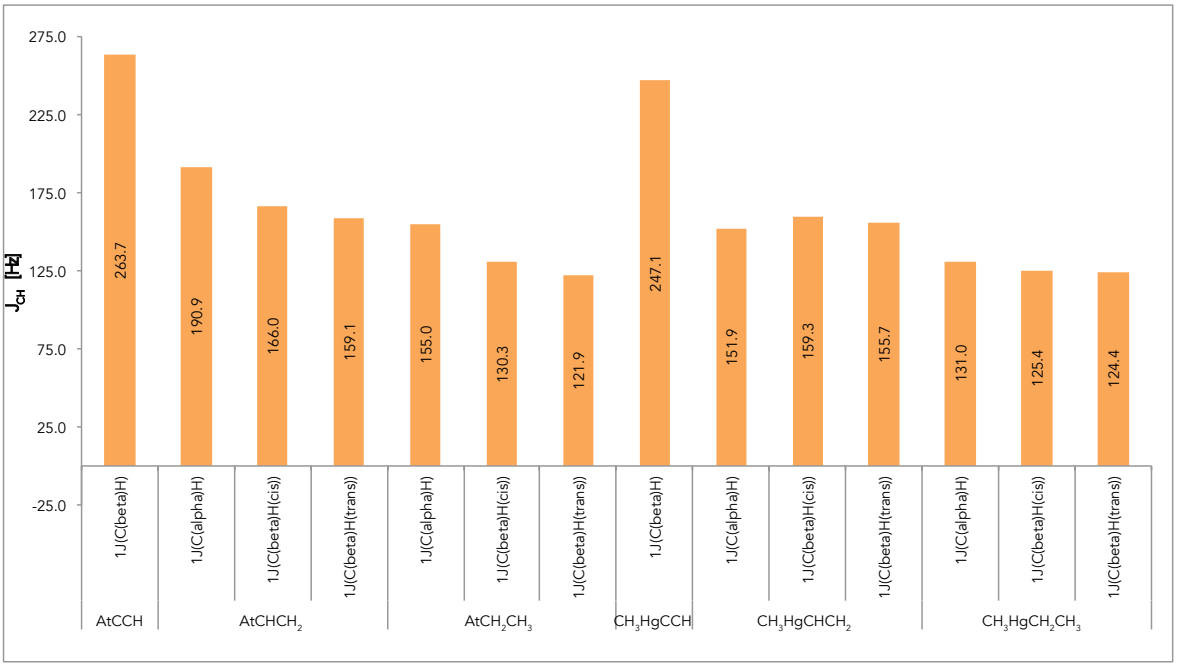

Figure 6.10: Comparison of the $^1J_{CH}$ coupling constants calculated with the Dirac-Coulomb Hamiltonians in mercury and astatine derivatives

between the heavy atom and the coupled atom is 0–90° in the -CH_2CH_3 derivatives, the coupling constant is larger than the coupling constant obtained for the dihedral angle equal 180°.

6.3.1 Importance of the total relativistic effects in comparison with the substituent effect

The relativistic effects sizeable with respect to the substituent effect (see Figure 6.11) can be observed for the $^1J_{CH}$ coupling constants in astatine-substituted hydrocarbons, containing sp and sp^2 carbon atoms. In case of AtCCH the relativistic effect is about -5 Hz and dominates the substituent effect but still its magnitude is small with respect to the total value of the $^1J_{CH}$ coupling constants (less than 2% of the total coupling constant). For the organomercury compounds, in all cases the relativistic contribution to $^1J_{CH}$ constitutes a majority of the substituent effect and is non-negligible with respect to the total value of the $^1J_{CH}$ coupling constants — the relativistic effect exceeds 15 Hz which is about 10% of the total coupling constants.

As a rule, the relativistic effect becomes smaller with the distance of the coupled nuclei from the heavy atom. For the $^1J_{C_\alpha H}$ coupling constants, the relativistic effect is 14.6 Hz (for $CH_3HgCHCH_2$), whereas the $^1J_{C_\beta H}$ coupling constants, it is 9.3 Hz (for CH_3HgCCH). Interestingly, the relativistic calculations lead in these cases to a much smaller substituent effect than

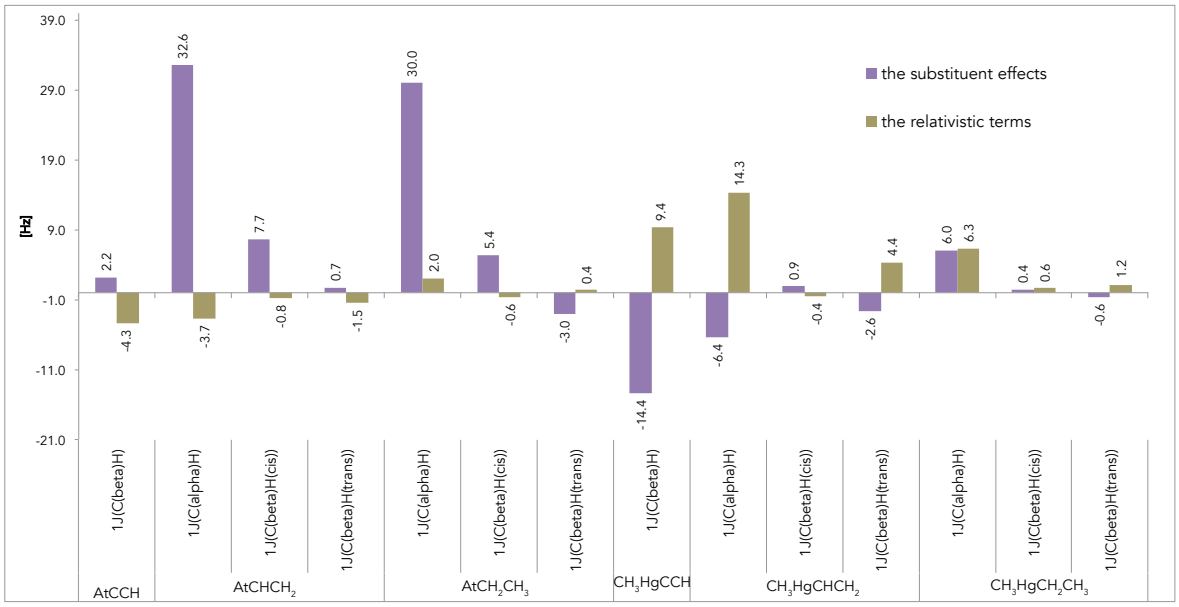

Figure 6.11: Comparison of the substituent effect and the relativistic term, calculated using the DKS approach, in $^1J_{CC}$ in the selected organometallic compounds and halogen derivatives

the non-relativistic ones.

6.3.2 Influence of the carbon hybridization

The type of the carbon hybridization again influences the magnitude of the relativistic effects. In the case of the $^1J_{C_\alpha H}$ coupling constants, larger relativistic effects are observed for the systems with the sp^2 hybridization than for the systems with the sp^3 hybridization (15.3 Hz and 6.6 Hz for $CH_3HgCHCH_2$ and $CH_3HgCH_2CH_3$, respectively).

The relativistic contribution to $^1J_{C_\beta H}$ depends not only on the carbon hybridization, but exhibits a variation with the heavy atom-carbon-carbon-hydrogen dihedral angle. As a rule, the coupling of the proton in the *trans* position is more affected by the relativistic effects. Only for $AtCH_2CH_3$ compound a reverse trend is observed.

6.3.3 Influence of the spin-orbit coupling

A comparison of the so-ZORA and the sc-ZORA results (see Figure 6.12) shows that the spin-orbit coupling effect is, as a rule, a dominating term in the relativistic contribution for astatine derivatives and is negligible in comparison to the scalar term for organomercury compounds. The biggest spin-orbit coupling effects are observed for astatine compounds with the sp and sp^2 carbon atoms (for $^1J_{C_\alpha H}$ in $AtCHCH_2$ it is about -4.9 Hz and for $^1J_{C_\beta H}$ in AtCCH

it is about -4.7 Hz), whereas the scalar term is negligible in these compounds (less than 0.5 Hz). Finally, it should be noted that for the astatine derivatives with sp^3 hybridization, the spin-orbit coupling term is much smaller than for the derivatives with sp^2 and sp carbon (less than 0.7 Hz).

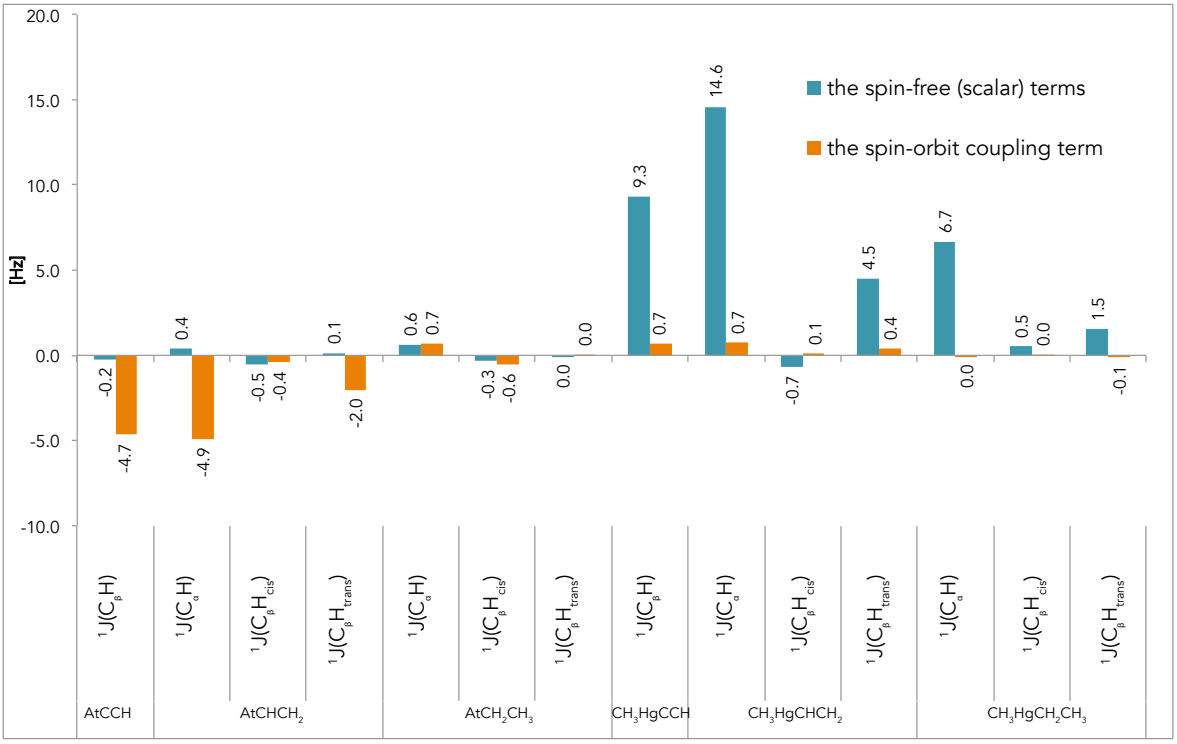

Figure 6.12: Comparison of the spin-free (scalar) and the spin dependent (spin-orbit coupling) term to the $^1J_{CH}$ coupling constants in the organomercury compounds and the astatine derivatives calculated with the one- and two-component ZORA Hamiltonian

6.3.4 Comparison between so-ZORA and DKS results

Like for the $^1J_{CC}$ coupling constants, the basis set change effects contaminating the comparison between the DKS and the so-ZORA results have been estimated using two types of basis set with nonrelativistic Hamiltonian (see Figure 6.13). For the organomercury compounds, in most cases the differences are smaller than 1 Hz. For the astatine derivatives the differences are a bit larger (0.6–2.4 Hz) but still small with respect to the relativistic effects.

Results collected in Figure 6.14 confirm that the two-component ZORA approximation reproduces the four-component DKS results very well for this series of the spin-spin coupling constants. In most cases, the differences between so-ZORA DFT and DKS are less than 1.0 Hz. The biggest difference between so-ZORA DFT and DKS (about 1.6 Hz) is observed for $^1J_{C_\alpha H}$

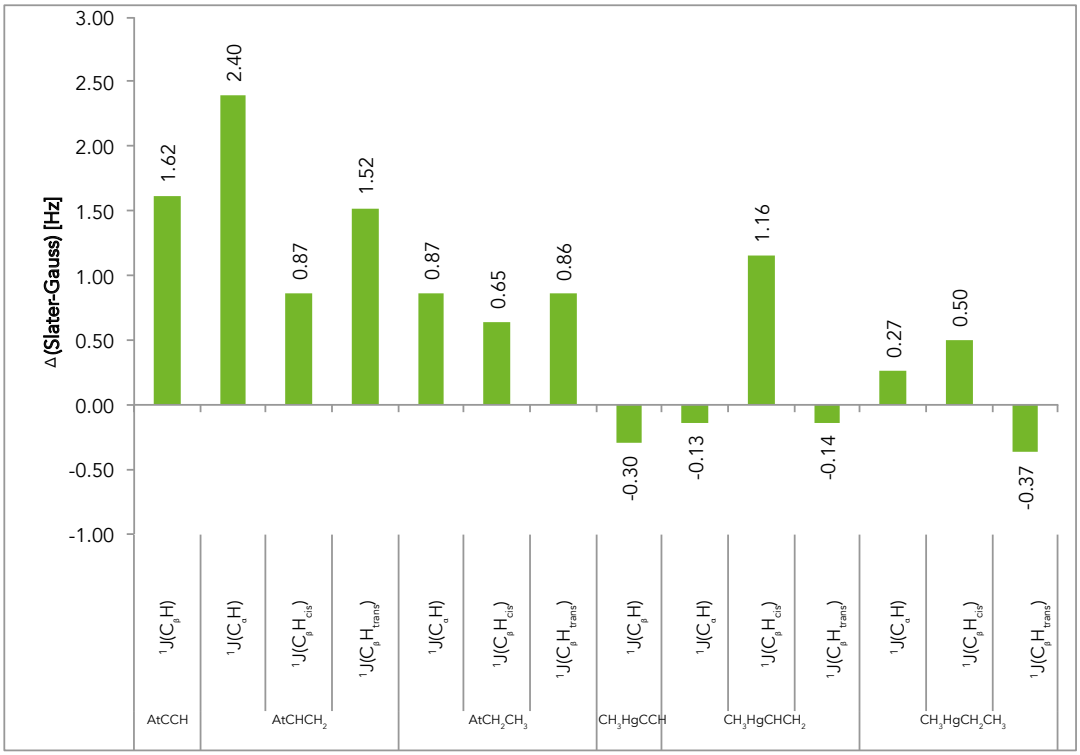

Figure 6.13: Comparison of the differences between the $^1J_{CH}$ coupling constants obtained with the Slater and Gauss type basis set calculated at the nonrelativistic level of theory

in $AtCHCH_2$, but it seems to originate from different basis sets used (see above — the difference for $^1J_{C_\alpha H}$ in $AtCHCH_2$ is 2.4 Hz). Thus, I can conclude that so-ZORA DFT is very efficient in rendering the HALA effects not only for $^1J_{CC}$ but also the $^1J_{CH}$ coupling constants.

6.3.5 Comparison between the sc-ZORA and ECPs results

The investigations discussed above have shown that the contribution of the scalar term to the total relativistic effect on the $^1J_{CH}$ spin-spin coupling constant depends strongly on the nature of the heavy atom. It is negligible for the 17th group of the periodic table, whereas it is dominant for organometallic compounds. As a consequence of this and because the discussed ECPs can render only the scalar contribution to spin-spin coupling constants (spin-orbit coupling term is neglected), only the results for the organometallic (cadmium and mercury) compounds will be discussed in this paragraph.

The differences between the $^1J_{CH}$ spin-spin coupling constants calculated using the scalar ECPs and scalar-only ZORA results are shown in Figure 6.15 and compared with the scalar

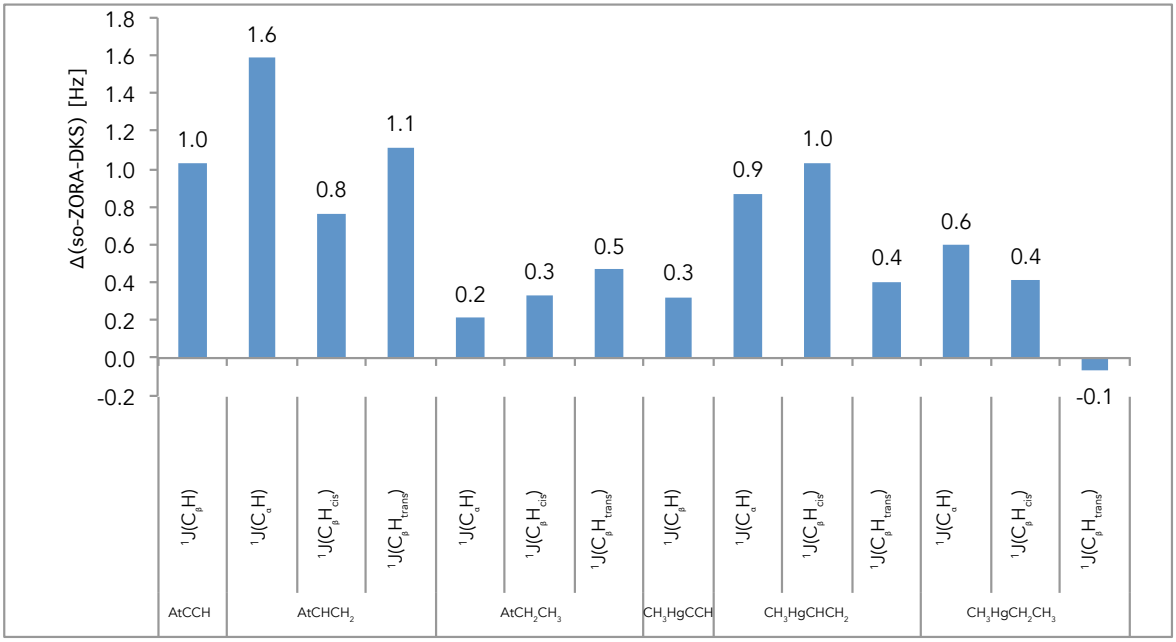

Figure 6.14: Comparison of the differences between the results obtained with the so-ZORA and the DKS method

			LANL2DZ-(sc-ZORA) [Hz]	sMDF-(sc-ZORA) [Hz]	sMDF(new)-(sc-ZORA) [Hz]	lMWB-(sc-ZORA) [Hz]	sMWB-(sc-ZORA) [Hz]	scalar term(sc-ZORA) [Hz]
Cd	CH_3CdCCH	$^1J_{C(\beta)H}$	-4.98	-0.74		-5.58	-0.67	2.89
	$CH_3CdCHCH_2$	$^1J_{C(\alpha)H}$	-6.65	-0.33		-7.61	-0.06	4.70
		$^1J_{C(\beta)H(cis)}$	-1.11	-1.10		-1.28	-1.02	0.04
		$^1J_{C(\beta)H(trans)}$	-2.16	-0.78		-2.76	-0.73	1.34
	$CH_3CdCHCH_2$	$^1J_{C(\alpha)H}$	-2.73	-0.59		-3.12	-0.29	2.77
		$^1J_{C(\beta)H(cis)}$	-0.81	-0.52		-0.99	-0.46	0.25
		$^1J_{C(\beta)H(trans)}$	-1.04	-0.81		-1.39	-0.77	0.87
Hg	CH_3HgCCH	$^1J_{C(\beta)H}$	-6.24	-2.34	-0.26	-6.53	-0.23	9.32
	$CH_3HgCHCH_2$	$^1J_{C(\alpha)H}$	-9.04	-4.78	-1.39	-9.44	-1.08	14.60
		$^1J_{C(\beta)H(cis)}$	-1.09	-0.83	-1.25	-1.20	-1.20	-0.66
		$^1J_{C(\beta)H(trans)}$	-2.48	-1.74	-0.66	-2.76	-0.61	4.52
	$CH_3HgCH_2CH_3$	$^1J_{C(\alpha)H}$	-3.31	-2.79	-1.25	-3.99	-0.93	6.95
		$^1J_{C(\beta)H(cis)}$	-1.09	-0.73	-0.70	-1.25	-0.68	0.52
		$^1J_{C(\beta)H(trans)}$	-0.55	-0.58	-0.30	-0.63	-0.25	1.52

Figure 6.15: Comparison of $^1J_{CC}$ calculated with different types of effective core potentials on heavy atoms and pcJ-2 basis set on C and H, using the PBE0 functional

ZORA term. The observations are similar as for the $^1J_{CC}$ coupling constants. The ECPs in general seem suitable for the purpose, and the best results are obtained when small-core ECPs

are employed. Among small-core ECPs, MWB appears to perform slightly better than MDF, but the differences are small.

6.4 The carbon-carbon coupling constants mediated by a heavy atom

In the previous section, the importance of the relativistic contribution to the $^1J_{CC}$ and $^1J_{CH}$ coupling constants in the vicinity of a heavy atom has been discussed. Here, I will extend these investigations to the carbon-carbon coupling constants through two, three and four bonds, mediated by heavy metal atom (Cd, In, Sn, Sb, Te, Hg, Tl, Pb, Bi and Po). The heavy atoms under study have been selected to cover a wide range of electron configurations (see Table 6.2 and Figure 6.16). Additionally, this selection allows for an investigation of the influence of the heavy nucleus charge on the HALA effect. In this research, a methodology similar to the previously employed has been used. The relativistic effects have been calculated using the DKS and nonrelativistic approach, whereas the role of the scalar and spin-orbit coupling term has been estimated using the ZORA approach. Additionally, the performance of the ECPs in reproduction of the relativistic effects for this class of coupling constants has been investigated.

Cd	In	Sn	Sb	Te
[Kr] $4d^{10}$ $5s^2$	[Kr] $4d^{10}$ $5s^2$ $5p^1$	[Kr] $4d^{10}$ $5s^2$ $5p^2$	[Kr] $4d^{10}$ $5s^2$ $5p^3$	[Kr] $4d^{10}$ $5s^2$ $5p^4$
Hg	Tl	Pb	Bi	Po
[Xe] $4f^{14}$ $5d^{10}$ $6s^2$	[Xe] $4f^{14}$ $5d^{10}$ $6s^2$ $6p^1$	[Xe] $4f^{14}$ $5d^{10}$ $6s^2$ $6p^2$	[Xe] $4f^{14}$ $5d^{10}$ $6s^2$ $6p^3$	[Xe] $4f^{14}$ $5d^{10}$ $6s^2$ $6p^4$

Table 6.2: Electron configuration of the selected heavy atoms

6.4.1 Influence of the electron configuration and the charge of the heavy atom

The $^2J_{CC}$ coupling constants in the series of molecules containing the -CCH substituents calculated using the Schrödinger and Dirac-Coulomb Hamiltonians are compared in Figure 6.17.

The absolute value of the geminal spin-spin coupling constant changes significantly with the electron configuration of the heavy atom. The inspection of the results shows that in most cases the biggest spin-spin coupling constants are observed for the 12th group of the periodic table and the smallest for systems containing the 15th group elements (the absolute value of coupling

I have investigated how the $^2J_{CC}$ couplings in the discussed compounds correlate with the C-Me-C bond angle. The results show a quasi-linear relationship between the absolute value of the spin-spin coupling constant and the C-Me-C angle for 6th row of the periodic table (see Figure 6.18), which suggests that much of the variation of the $^2J_{CC}$ coupling constants in the series of 6th row elements compounds can be rationalized in that way.

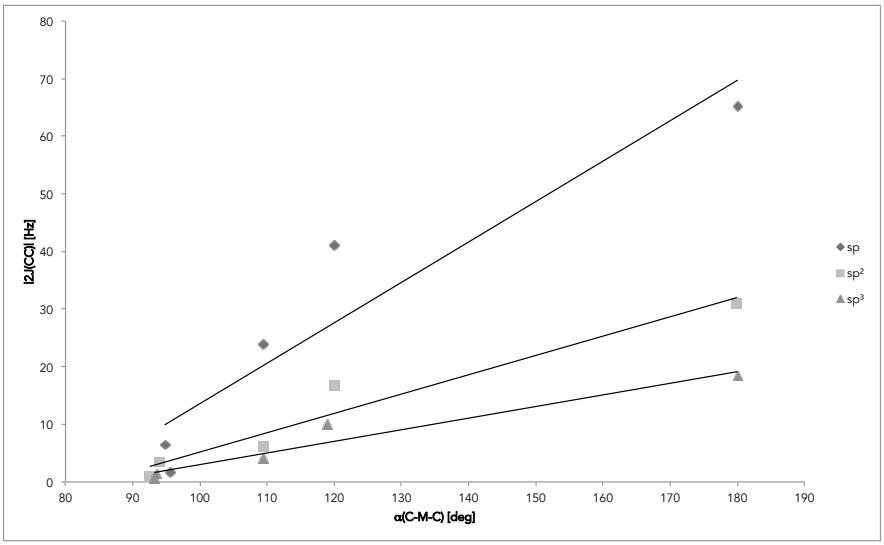

Figure 6.18: Correlation of $^2J_{CC}$ coupling constants calculated at the so-ZORA level with the plane angle in the systems containing the 6th row elements

The $^2J_{CC}$ coupling in the 5th row compounds are, as a rule, smaller than in the 6th row analogues. A comparison of the relativistic and non-relativistic results shows that it is purely a relativistic effect: the non-relativistic results for the same group of the periodic table are almost the same (only for cadmium and mercury compound a slightly bigger difference is observed).

6.4.2 Importance of the relativistic term and the influence of the carbon hybridization

The $^2J_{CC}$ couplings in the 5th row compounds are smaller than in the 6th row analogues, since for the 5th row of the periodic table, the relativistic effects in most cases do not exceed 26% of the total spin-spin coupling constant, whereas for the 6th row they can dominate the

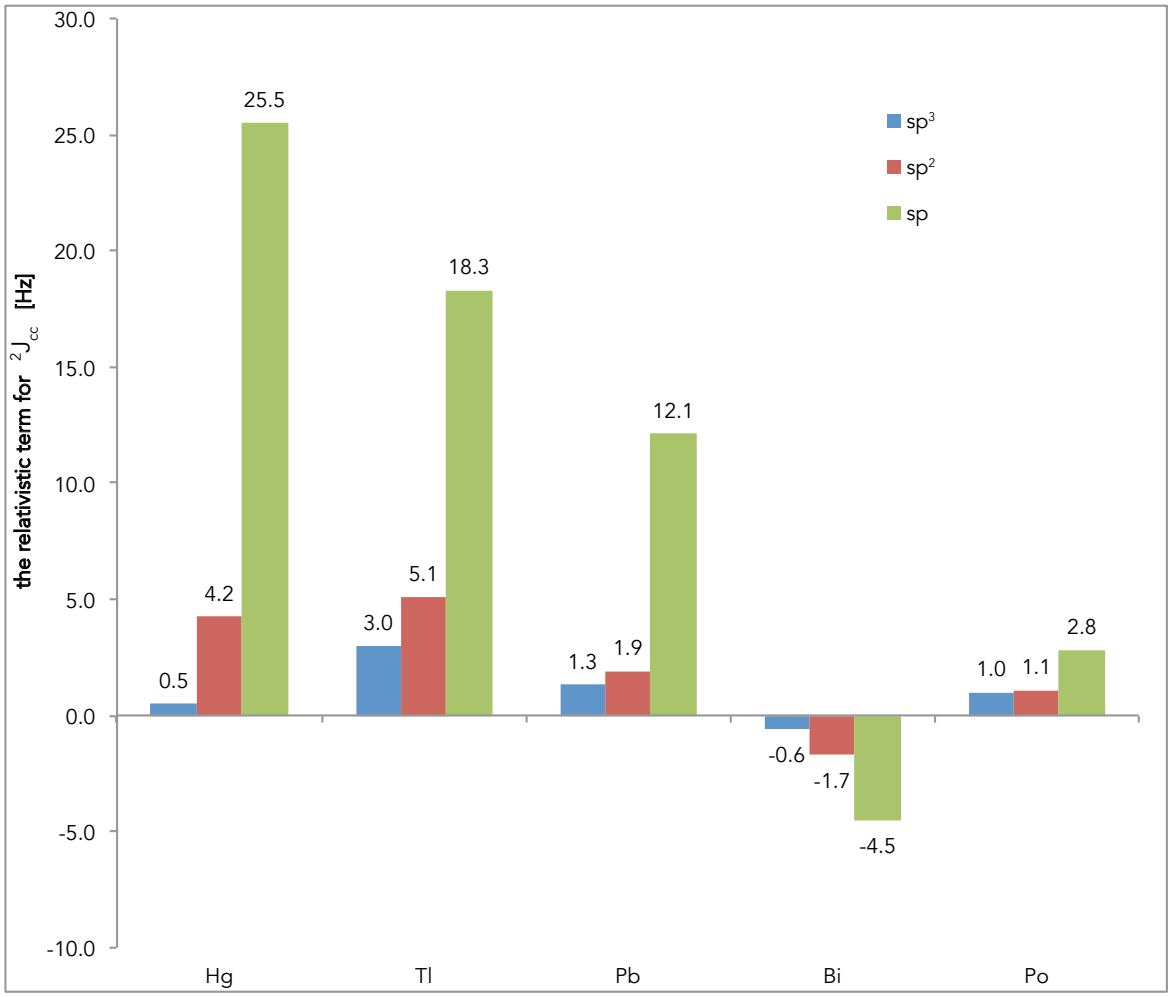

Figure 6.19: Comparison of the relativistic terms, calculated at the DKS level of theory, in the $^2J_{CC}$ coupling constants for $M(CCH)_n$ where M are the 6th row heavy elements

value of the $^2J_{CC}$ coupling. For that reason, in further studies I will discuss only the results for the 6th row elements.

Comparison of the relativistic terms for $^2J_{CC}$ for compounds with different carbon hybridization are show in Figure 6.19. For the 6th row elements (except for polonium), the relativistic effects can exceed 80% (for $Bi(CCH)_3$) of the total spin-spin coupling constant (see Figure 6.20), which leads to a significant increase of the coupling constant. For polonium compounds, the relativistic terms dominate the spin-spin coupling constants (for $Po(CCH)_2$ it is four times larger than the value of spin-spin coupling constant calculated at DKS level).

The largest relativistic terms are observed, as a rule, for the systems with the sp hybridization of carbon atom and the smallest effects are observed for the systems with the sp^3 hybridization.

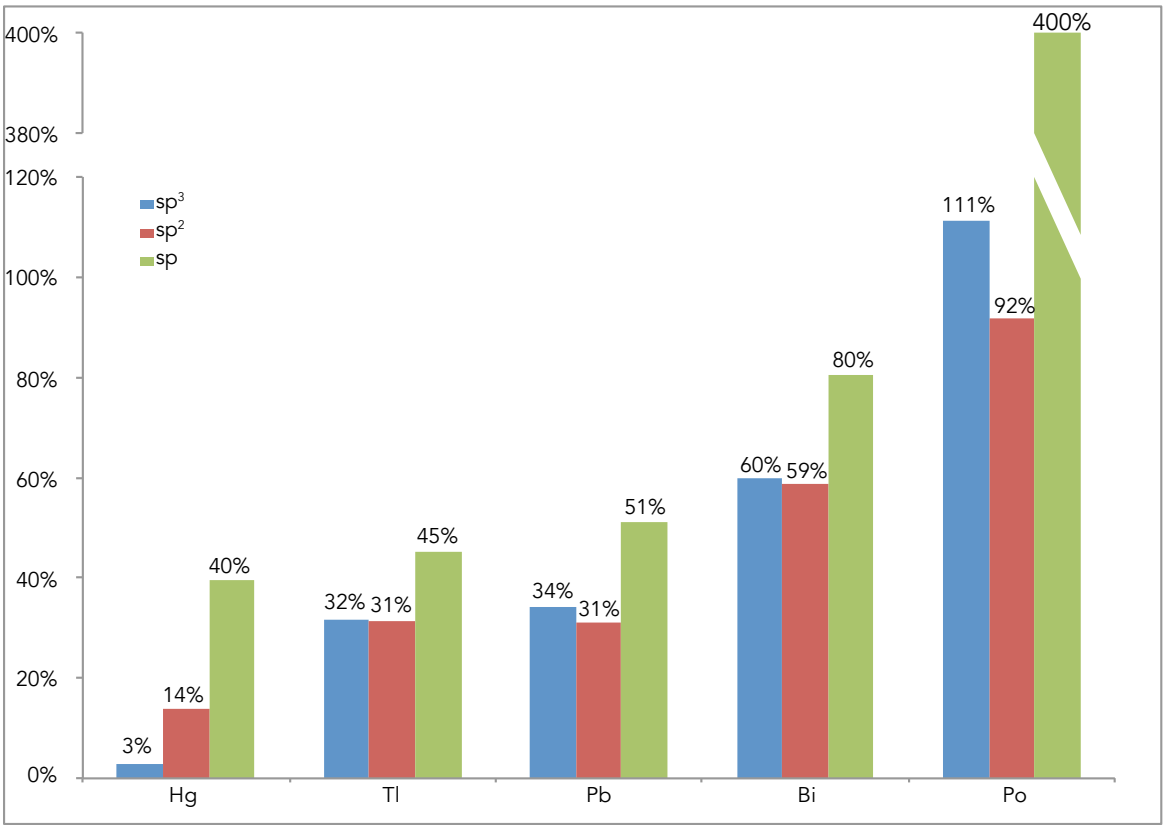

Figure 6.20: Comparison of the percentage contribution, calculated at the DKS level of theory, to the $^2J_{CC}$ coupling constants for $M(CCH)_n$, where M are the 6th row heavy elements

For p-block elements, the relativistic contributions in the sp^3 and sp^2 systems are comparable to each other and are about 2-35% (see Figure 6.20) of the relativistic contribution for the systems containing sp-type carbon.

6.4.3 Importance of the scalar and the spin-orbit coupling terms

The comparison of the spin-free (scalar) terms and the spin-orbit coupling terms for the series of $M(CCH)_n$ compounds containing the 6th row elements is shown in Figure 6.21. In most cases, the scalar terms and the spin-orbit coupling have opposite signs but the ratio between the spin-orbit coupling and the scalar terms depends strongly on the electron configuration of the metal atom.

For mercury compounds the spin-orbit coupling contribution is about 15% of the scalar term. In the case of the compound containing p-block elements, this term is much smaller (3-10%) but, surprisingly, in the case of the polonium compounds, the spin-orbit coupling dominates the scalar term (the spin-orbit coupling term is 30% larger than the scalar term). The size

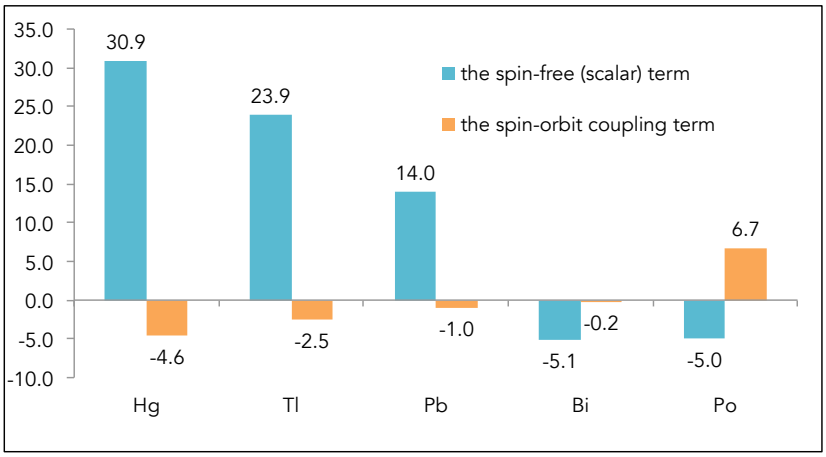

Figure 6.21: Comparison of the scalar relativistic contribution and the spin-orbit coupling term using the sc-ZORA and the so-ZORA approaches, in the $^{2}J_{CC}$ coupling constants for $M(CCH)_n$ where M are the 6th row heavy elements

and relative ratio of scalar term and the spin-orbit coupling terms depends strongly also on the hybridization of carbon atoms. It should be stressed that although the spin-orbit coupling term is the smallest for sp^3 derivatives, its impact on the relativistic term is the largest (in the case of polonium derivatives, the spin-orbit coupling is about 2.5 times larger than scalar term — see Figure 6.22). This shows that the spin-orbit coupling term is less sensitive to the change of hybridization type than the scalar term.

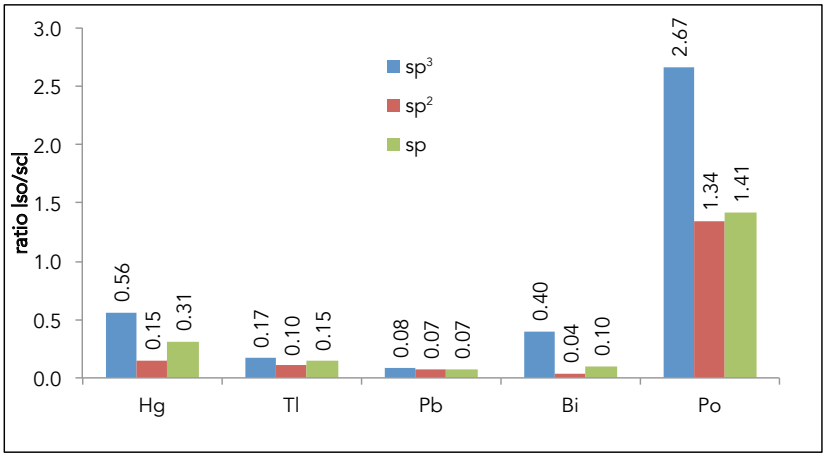

Figure 6.22: Comparison of the ratio between the scalar contribution and the spin-orbit coupling term in the $^{2}J_{CC}$ coupling constants for the 6th row element compounds differing in hybridization type of the carbon atoms

Previous research has shown that for the $^{1}J_{CC}$ coupling constant the spin-orbit coupling term is dominated by the change of the pure Fermi contact term. In this part of the research, I

have also checked the relation between the change of the pure FC+SD term and the FC+SD/PSO cross term. I have therefore compared (Table 6.3) the individual terms of $^2J_{CC}$ for the tellurium and polonium compounds, where the spin-orbit coupling contribution is the largest. The results show that the spin-orbit coupling changes the pure FC+SD term (denoted as the FC+SD change) and induces a sizeable FC+SD/PSO cross term, whereas the change of the SO (PSO+DSPO) term is negligible (less than 0.01 Hz).

Table 6.3: Comparison of the spin-orbit coupling contributions to FC+SD, SO(PSO+DSO) terms and FC+SD/PSO cross term in $^2J_{CC}$ coupling constants

	$^2J_{CC}$			
	FC+SD	SO	FC+SD/PSO	SO sum
$Te(CCH)_2$	0.14	0.00	0.80	0.94
$Te(CHCH_2)_2$	0.04	0.00	0.51	0.54
$Te(CH_3)_2$	-0.06	0.00	0.55	0.49
$Po(CCH)_2$	3.77	0.00	2.89	6.67
$Po(CHCH_2)_2$	0.97	0.09	1.39	2.44
Po(CH3)2	0.40	-0.04	1.32	1.68

The sum-over-states expressions for the spin-orbit coupling terms suggest their dependence on the inverse of the lowest singlet-triplet excitation energy, assuming the dominant contribution arises from this excitation (this effect has been investigated several times in series of shielding constants — see for example [92]). For that reason the HOMO-LUMO triplet excitation energies (at two-component ZORA level) have been compared with spin-orbit coupling contributions to $^2J_{CC}$. The results (shown as a function of an inverse of the triplet excitation energy) are shown in Figure 6.23 (the spin-orbit coupling contributions to the FC+SD term) and Figure 6.24 (the FC+SD/PSO cross term induced by spin-orbit coupling). Some correlation in both cases is observed but in many cases quite big deviations from the trend are noted, like for example in $Hg(CCH)_2$, where the spin-orbit contribution is much larger than expected on the basis of its HOMO-LUMO triplet excitation. It may be a result of the value of the transition moment (the numerator in the sum-over-states expansion) in the molecule larger than the values of transition moments in the remaining ones in the series. The detailed analysis of the elements of the sum-over-states has shown that the large effect of spin-orbit coupling for polo-

nium compounds is connected with the low-energy HOMO-LUMO triplet transition involving the p electrons of the central atom.

The scalar relativistic effects influence predominantly the Fermi contact term whereas the changes of other terms are negligible (less than 1%). The relative scalar effect on the Fermi contact term correlates to some extent with the change of electron density on the carbon nucleus, as shown in Figure 6.25. The correlation is not perfect (the result for $Bi(CCH)_3$ stands out) but it should be stressed that the actual dependence of the FC term is on the perturbed electron density, not on the static one.

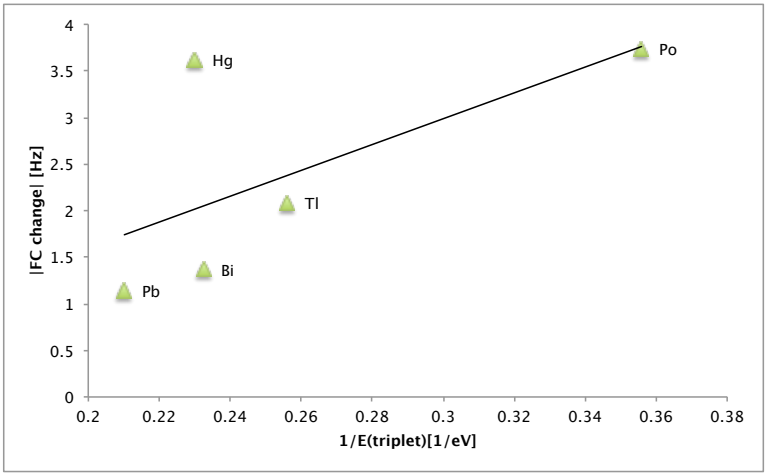

Figure 6.23: The correlation of the spin-orbit coupling contributions to the FC term in $^2J_{CC}$ for the $M(CCH)_n$ series with the singlet-triplet HOMO-LUMO excitation energy

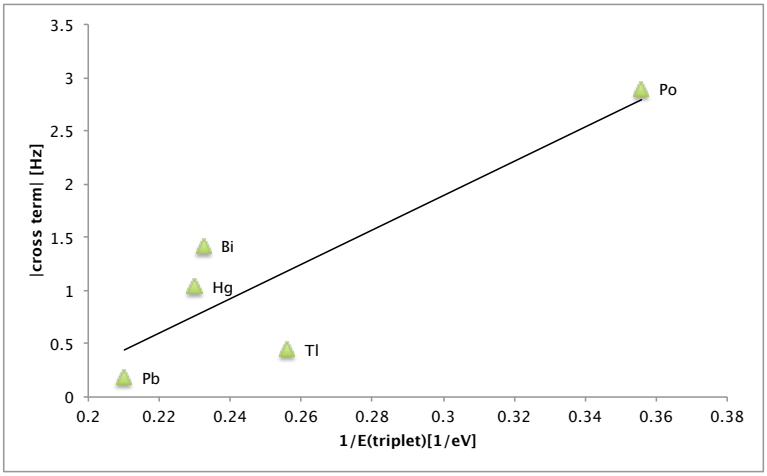

Figure 6.24: The correlation of the FC+SD/PSO cross term contribution to $^2J_{CC}$ for the $Me(CCH)_n$ series with the singlet-triplet HOMO-LUMO excitation energy.

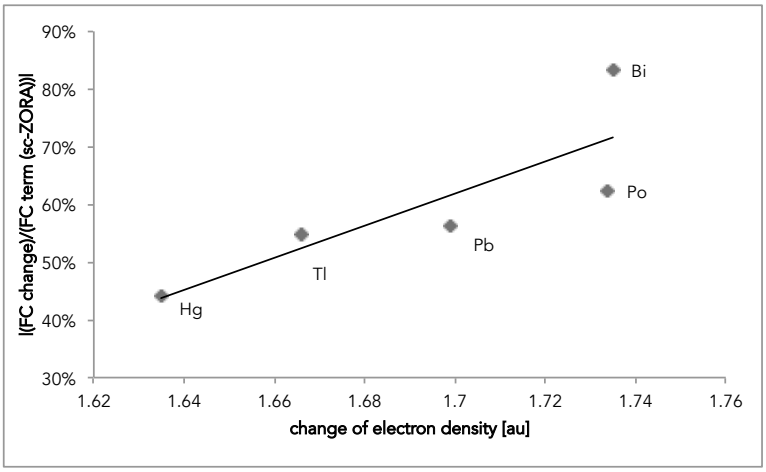

Figure 6.25: The correlation of the scalar relativistic effect on the FC contribution to $^2J_{CC}$ (shown as a percentage of the total value of the scalar FC term) for the $Me(CCH)_n$ series with the change of electron density on the carbon nucleus induced by the scalar relativistic effects.

6.4.4 Comparison between so-ZORA and DKS results

The inspection of the differences between so-ZORA and DKS results (Δ(so-ZORA-DKS)) collected in Figure 6.26 leads to the conclusion that for this class of compounds so-ZORA reproduces the DKS results very well.

Explicit inclusion of the small spinor during the calculation does not change significantly the calculated $^2J_{CC}$ couplings in comparison with the two-component ZORA approximation. In most cases, the differences between the Slater-type and Gauss-type basis set results (Δ(so-ZORA-DKS)) are less than 1.0 Hz, and seem to be caused mostly by the change of the basis set (see the discussion above for $^1J_{CC}$ coupling constants) rather than the picture change effects. To confirm these hypothesis I have calculated also Δ(Slater-Gauss) obtained at the nonrelativistic level (see Paper IV). The comparison shows that while the results obtained with the Gauss-type basis set systematically overestimate the results obtained with the Slater-type basis set, in most cases the absolute values of Δ(Slater-Gauss) do not exceed 1 Hz. Only for the -CCH derivatives, the differences are larger (1.2–3.9 Hz for mercury, thallium and lead compounds),

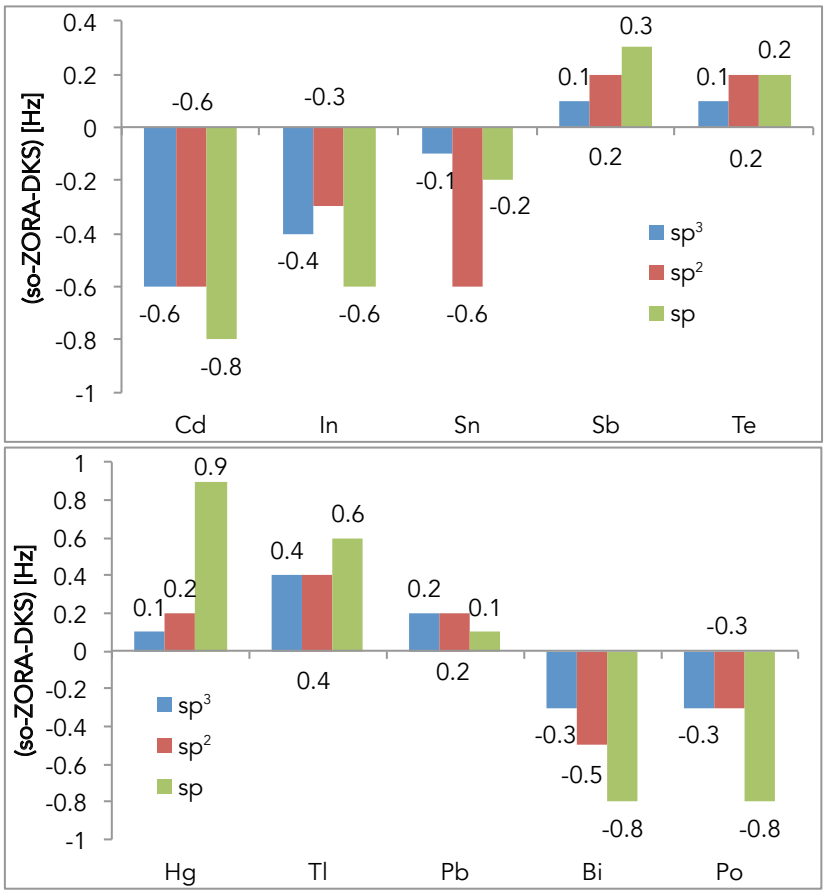

Figure 6.26: The differences between the so-ZORA and the DKS results for the $^2J_{CC}$ coupling constants for $M(CCH)_n$ where M are the 5th (upper diagram) and 6th (lower diagram) row heavy element atoms

but they are still only about 10% of the relativistic term calculated at the ZORA level.

6.4.5 Comparison between the sc-ZORA and ECPs results

As in the previous research, the differences between the $^2J_{CC}$ spin-spin coupling constants calculated using the scalar ECPs and the scalar-only ZORA results have been investigated (Figure 6.27).

Again LANL2DZ does not reproduce the sc-ZORA results very well, overestimating the scalar term twice or more. The same is observed for large-core MDF and MWB pseudopotentials. In contrast, the small-core MWB results are usually in excellent agreement with sc-ZORA. As before, MDF60 performs very poorly for organomercury compounds but after applying new

		LANL2DZ-(sc-ZORA) [Hz]	IMDF-(sc-ZORA) [Hz]	sMDF-(sc-ZORA) [Hz]	sMDF(new)-(sc-ZORA) [Hz]	IMWB-(sc-ZORA) [Hz]	sMWB-(sc-ZORA) [Hz]	scalar term(sc-ZORA)
Cd	$Cd(CCH)_2$	-0.33		0.77		-14.11	0.48	10.40
	$Cd(CHCH_2)_2$	4.83		0.34		-2.39	0.15	4.08
	$CdMe_2$	5.05		0.18		0.37	0.02	1.94
In	$In(CCH)_3$	-3.86		0.31		-2.96	1.19	5.97
	$In(CHCH_2)_3$	-0.65		0.09		-0.49	-0.12	2.04
	$InMe_3$	-0.26		-0.12		-0.20	-0.31	1.04
Sn	$Sn(CCH)_4$	-1.22	-0.92	0.43		-0.95		3.21
	$Sn(CHCH_2)_4$	-0.06	-0.06	0.19		-0.01		0.68
	$SnMe_4$	0.00	-0.04	0.12		0.04		0.34
Sb	$Sb(CCH)_3$	1.23	1.06	-0.14		0.38		-1.40
	$Sb(CHCH_2)_3$	0.56	0.51	-0.01		0.24		-0.61
	$SbMe_3$	0.49	0.46	0.10		0.28		-0.38
Te	$Te(CCH)_2$	0.99	0.55	-0.62		0.01		-1.59
	$Te(CHCH_2)_2$	0.48	0.35	-0.02		0.23		-0.60
	$TeMe_2$	0.36	0.30	0.02		0.27		-0.29
Hg	$Hg(CCH)_2$	3.46		-13.94	-1.11	-12.25	-1.91	30.96
	$Hg(CHCH_2)_2$	10.19		-4.50	0.10	1.46	-0.43	9.57
	$HgMe_2$	9.11		-2.26	0.31	3.88	-0.10	4.07
Tl	$Tl(CCH)_3$	-1.66		-1.53		-6.71	-1.19	23.89
	$Tl(CHCH_2)_3$	1.43		-0.42		-1.22	-0.46	7.53
	$TlMe_3$	1.33		-0.31		-0.56	-0.39	3.61
Pb	$Pb(CCH)_4$	-1.44	-2.86	-0.52		-3.74		14.00
	$Pb(CHCH_2)_4$	-0.14	-0.40	-0.09		-0.93		2.67
	$PbMe_4$	-0.14	-0.36	-0.05		-0.55		1.27
Bi	$Bi(CCH)_3$	1.26	3.44	0.57		-0.09		-5.08
	$Bi(CHCH_2)_3$	0.54	1.84	0.25		0.13		-1.96
	$BiMe_3$	0.45	0.89	0.26		0.27		-1.03
Po	$Po(CCH)_2$		0.88	-0.48		0.33		-5.01
	$Po(CHCH_2)_2$		0.44	0.07		0.27		-1.69
	$PoMe_2$		0.32	0.08		0.27		-0.68

Figure 6.27: Comparison of $^2J_{CC}$ coupling constants calculated with different types of effective core potentials on heavy atoms and the pcJ-2 basis set on C and H, using the PBE functional

version of this ECP (denoted as sMDF(new)) good agreement with the sc-ZORA results is observed.

6.4.6 Coupling constants by three and four bonds

Comparison of the $^3J_{CC}$ and $^4J_{CC}$ coupling constants (calculated using DKS method) with the $^2J_{CC}$ coupling is shown in Figure 6.28.

As expected, the number of bonds changes significantly the value of the total spin-spin coupling constant. As a rule, the couplings transmitted by two bonds are the largest and by four bonds are the smallest. The relativistic contribution to the total spin-spin coupling does not

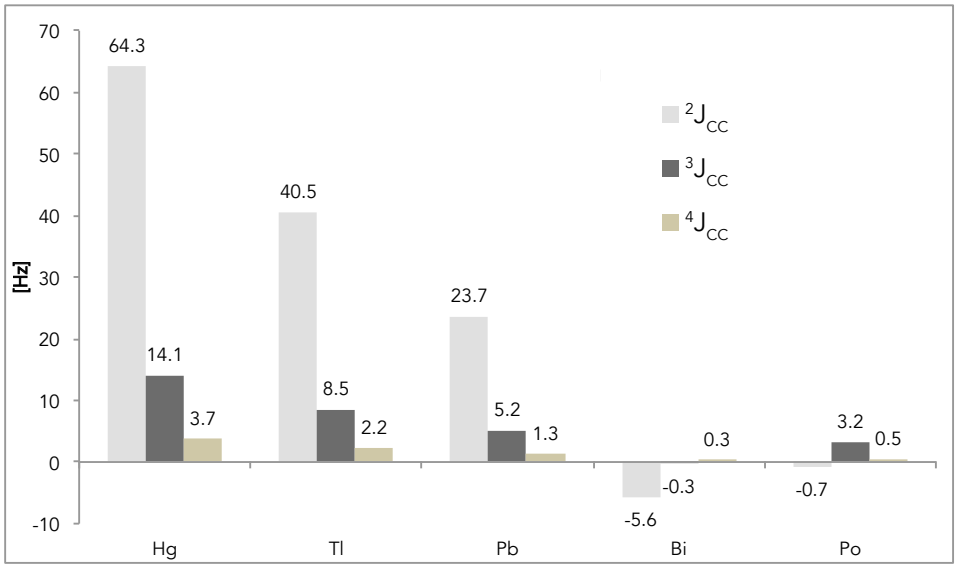

Figure 6.28: Comparison of the values of the $^{2}J_{CC}$, $^{3}J_{CC}$, $^{4}J_{CC}$ coupling constants, calculated at the DKS level of theory, for M(CCH)n where M are the 6th row heavy elements

change significantly (see Figure 6.29). Regardless of the number of the bonds participating in coupling path, the relativistic percentage contributions to the coupling constants, for most cases, are between 33% and 62%. Only for bismuth and polonium compound, in several cases, the relativistic term dominates the full spin-spin coupling constant (it is even 6.5 times larger than value of spin-spin coupling) but it should be kept in mind that in these cases very small values are discussed (and very sensitive to the computational protocol).

The importance of the spin-orbit coupling term

Finally, the ratio between the scalar term and the spin orbit coupling in the series of the $^{2}J_{CC}$, $^{3}J_{CC}$ and $^{4}J_{CC}$ coupling constants has been compared (see Figure 6.30). The results show that the importance of the spin-orbit coupling term in the relativistic contribution becomes larger for $^{3}J_{CC}$ and in particular for the $^{4}J_{CC}$ coupling constants. In other words, the scalar term decreases faster than the spin-orbit coupling term when the number of bonds participating in the coupling path increases.

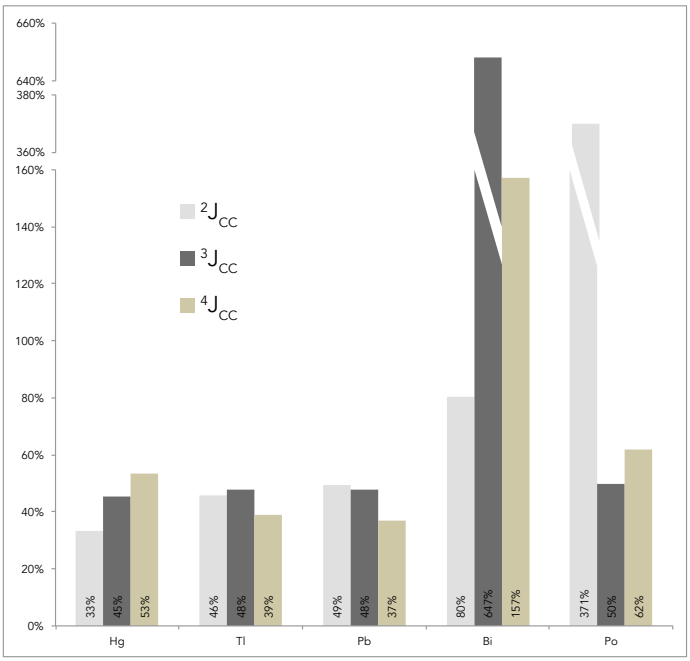

Figure 6.29: Comparison of the percentage contribution of the relativistic term to the $^2J_{CC}$, $^3J_{CC}$, $^4J_{CC}$ coupling constants, calculated at the DKS level of theory, for $M(CCH)_n$ where M are the 6th row heavy elements.

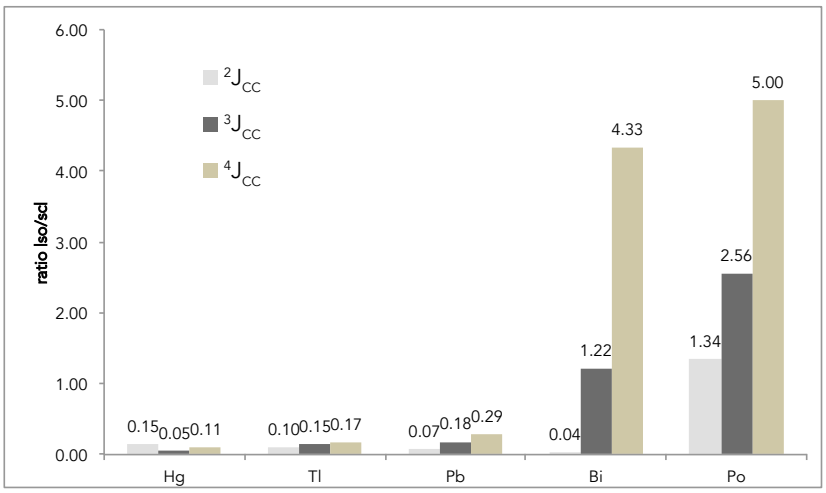

Figure 6.30: Comparison of the ratios between the spin-orbit coupling term and the scalar contribution to the relativistic effects of the $^2J_{CC}$ coupling constants, calculated using the sc-ZORA and so-ZORA approach, for $M(CCH)_n$ where M are the 6th row heavy elements

Chapter 7

Summary

The application part of the thesis consists of two chapters. The first one (Chapter 5) is focused on the HALA effects on the shielding constants. It includes reinvestigation of the ^{13}C shielding constants in halide derivatives, carried out to estimate the performance of the newly developed implementations of the density functional theory with relativistic Hamiltonians. Next, the HALA effects in the organomercury compounds and transition metal cyanides have been investigated to gain knowledge on the relativistic effects on the light atom shielding constants in a wide range of compounds containing heavy atoms. The second chapter (Chapter 6) focuses on the description of the influence of a heavy atom on the nuclear spin-spin coupling constants of light atoms, since this effect is almost unexploited in the literature. In both cases efforts have been made to rationalize the observed effects by correlating them with structural parameters.

All NMR parameters in the thesis have been calculated by means of the density functional theory for a wide range of compounds containing heavy elements (11th, 12th group and p-block elements). The applied methods range, in order of reduced complexity, from Dirac-Kohn-Sham method (DFT with four-component Dirac-Coulomb Hamiltonian), through DFT with two- and one-component ZORA Hamiltonians, to DFT employing the scalar relativistic effective core potentials with the non-relativistic Hamiltonian.

The most important detailed observations can be summarized as follows.

7.1 The influence of a heavy atom on the shielding constants of the light atoms

The results reported in Chapter 5 show that the magnitude of the relativistic effects on carbon shielding constants depends on several factors. The most important ones seem to be the position of light nucleus with respect to the heavy atom, the charge of the heavy nucleus, and the electronic structure of the carbon atom (described here as carbon hybridization).

The position of the light nucleus The largest relativistic effects are observed for the nuclei directly bonded with a heavy nucleus (they amount to 50 ppm for iodine derivatives). In general (with the exception of the nitrogen shieldings in transition metal cyanides), the relativistic terms for beta position with respect to the heavy nucleus are smaller (they do not exceed 23 ppm) than for alpha position.

The hybridization of the light atom The largest relativistic contributions have been observed for the sp-type carbon atoms and the smallest for the sp^2 carbon atoms. Slightly larger contributions found for the sp^3 carbons than for the sp^2 carbons may be a result of the fact that in discussion of the influence of the sp and sp^3 hybridization on the shielding constants, non-aromatic compounds have been taken into account, whereas in the case of sp^2 series only benzene derivatives have been discussed in this thesis.

The ratio between the scalar and spin-orbit coupling contributions In the series of halide derivatives and selected transition metal cyanides, the relativistic effects on shielding constants of the alpha carbon nuclei are dominated by the spin-orbit coupling term. The relation between hybridization of the light atom under study and the spin-orbit coupling contribution, postulated earlier by other authors on the basis of perturbative calculations, have been confirmed by two-component calculations of the spin-orbit coupling contribution.

In the series of the organomercury compounds and transition metal cyanides, the ratio between the scalar and spin-orbit coupling terms depends on the position and hybridization of the light atom under study. In the series of the alpha carbon shielding constants, the spin-orbit coupling term is larger than the scalar term for the compounds containing the sp-type carbon atoms, but it has similar magnitude to the scalar term in the series of compounds containing sp^3-type carbon atoms. For the beta carbon nuclei as a rule the scalar terms are of the same order

of magnitude as the spin-orbit contribution, whereas for the beta nitrogen nuclei in transition metal cyanides, the scalar relativistic term is larger than the spin-orbit coupling contribution.

The charge of the heavy nucleus As expected, the relativistic contributions to the shielding constant of the alpha carbon nuclei depend strongly on the charge of the heavy nucleus. The largest relativistic effects are observed for the derivatives of the 6th row elements. Detailed investigation has shown that the magnitude of the scalar relativistic contribution to shielding constants (dominated by a change of the paramagnetic term) in a series of halide derivatives can be correlated with the lowest singlet excitation energy. It may suggest (at least for the compounds containing sp^3 carbon atoms) that the observed increase of the scalar term with increase of the charge of a heavy atom is mainly a result of a change of the excitation energy in a series. A similar correlation have been observed between the triplet HOMO-LUMO excitation energy and the spin-orbit contribution to shielding constants. It suggests that the sizeable spin-orbit contribution for the heaviest compounds may be a result of a decreasing energy gap between the ground state and the lowest-lying triplet excited state.

Methodological aspects of inclusion of the relativistic effects For the transition metal cyanides so-ZORA underestimates the chemical shifts calculated using DKS methodology but it is probably mainly the result of methodological inconsistency in basis sets selection for so-ZORA (Slater-type basis sets) and DKS (Gauss-type basis sets) computations. In the series of halide and mercury derivatives so-ZORA usually reproduces the experimental results much better than the DKS method, which suggests some kind of error cancellation for so-ZORA computations.

The scalar terms calculated with MWB ECP agree well with the scalar ZORA results. Because of the scalar-only character of the employed ECP methods, they lead to good agreement with the experimental data only for these carbon chemical shifts where the spin-orbit term is small.

7.2 The influence of the heavy atom on the spin-spin coupling constants of the light nuclei

Chapter 6 summarizes the results of the calculations of the one-bond and multi-bond spin-spin coupling constants, the latter with a heavy atom in the coupling path. The magnitude of the relativistic effects differs significantly for these two cases. For the coupling constants transmitted by one bond the relativistic effects do not exceed 40% of coupling value, whereas for the couplings transmitted by the heavy nuclei the relativistic effect can dominate the value of the coupling constant. Several other factors which may influence the magnitude of the relativistic effect on spin-spin coupling constants have been discussed in this chapter: the charge of the heavy nucleus, the position of the light nuclei with respect to the heavy nucleus and finally the type of the carbon atom hybridization.

The charge of the heavy nucleus The results have shown that when heavy nucleus is outside the coupling path the relativistic effects are relatively important (with respect to the value of the coupling constant or the total substituent effect) only for the compounds of the 6th row elements. It is not necessarily true for the $^{n}J_{CC}$ (n=2,3,4) coupling constants with the heavy nucleus in the coupling path. In such cases the relativistic contribution can be sizeable, even for compounds containing the 5th row elements. It is worthwhile to mention that the comparison of the results obtained with the relativistic and non-relativistic Hamiltonians shows that the difference between the $^{n}J_{CC}$ coupling constants in the analogous compounds of the 5th and 6th row elements is in many cases a purely relativistic effect: the non-relativistic values for the appropriate analogues are almost the same.

The position of the light nuclei with respect to a heavy nucleus Predictably, the relativistic contribution to the $^{1}J_{CH}$ coupling constants is larger (in percentage) for couplings involving the carbon nucleus in the alpha position with respect to the heavy nucleus than for the couplings involving the beta carbon nucleus. In contrast to this, in a series of the $^{n}J_{CC}$ (n=2,3,4) coupling constants transmitted by a heavy nucleus, the percentage relativistic contribution remains almost unchanged with increasing number of bonds in the coupling path.

The hybridization of the light atom The magnitude of the relativistic contribution to all coupling constants discussed in the thesis depends strongly on the hybridization of the carbon

atom involved in the coupling. The largest relativistic contributions are observed as a rule for the sp-type carbon atoms, and the smallest ones for the sp^3 carbon atoms.

The ratio between the scalar and spin-orbit coupling contributions The scalar term dominates the total relativistic contribution to the coupling constants in the transition metal and selected p-block derivatives. This conclusion is in good agreement with previous findings of other researchers concerning the influence of the relativistic effects on the nuclear spin-spin coupling constants calculated for other compounds. Only for the compounds containing the 16th and 17th group elements the spin-orbit coupling term becomes sizeable, in isolated cases even larger than the scalar relativistic contribution to the $^1J_{CC}$ and $^2J_{CC}$ coupling constants.

The spin-orbit contribution to $^2J_{CC}$ coupling constants in a series of 6th row compounds can be correlated with the lowest triplet excitation energy. This may explain a surprisingly large spin-orbit contribution for the 16th and 17th group compounds, since for example for polonium derivatives the low-energy HOMO-LUMO triplet transition, involving the p electrons of the central atom have been observed.

The investigations of the compounds with sizeable spin-orbit contribution to $^2J_{CC}$ coupling constants have shown that the spin-orbit coupling not only induces the FC+SD/PSO cross term but in many cases changes also the magnitude of the pure Fermi contact term.

Methodological aspects of inclusion of the relativistic effects A comparison of the $^nJ_{CC}$ (n=1,2,3,4) coupling constants obtained by means of different methods of inclusion of the relativistic effects indicates that so-ZORA-DFT reproduces the DKS results very well. The performance of the ECPs depends on the magnitude of the scalar term in the relativistic contribution, since the ECPs discussed in the thesis incorporate only the scalar relativistic effects, but when the scalar term is the dominant relativistic contribution, properly selected ECPs reproduce correctly the results obtained with more rigorous relativistic methods.

7.3 General conclusions

The research discussed in the thesis gives insight into the influence of the relativistic effects on the shielding constants of the nuclei in the vicinity of a heavy atom and on the spin-spin coupling constants of light nuclei in a wide range of compounds containing a heavy atom. The results suggest that the discussion of the HALA effect should be extended to spin-spin coupling

constants of light nuclei. Based on the preliminary research of other authors, sizeable effects on the coupling constants, where a heavy nucleus is in the coupling path, were expected. My research has confirmed these expectations for a wide range of compounds. It also has been shown for the first time that sizeable relativistic effects on the one-bond coupling constants are observed when a heavy atom is in the vicinity of the coupled light nuclei.

In the thesis not only the magnitude of the HALA effect on NMR properties has been estimated but also the efforts have been made to rationalize the observed effects by correlating them with structural parameters. The physical reasons of the HALA effect, for selected properties, has been also discussed. In previous research the leading role of the spin-orbit coupling term in the HALA effect on shieldings has been emphasized, whereas my work shows that the scalar relativistic terms should also be taken into account. It has also been found that although the influence of the HALA effect on the spin-spin coupling constants is dominated by the scalar relativistic term, the spin-orbit coupling contribution should be taken into account in certain cases as well (for the compounds containing heavy atoms with a large number of p valence electrons).

Comparison of the methods of inclusion of the relativistic effects has shown that the two-component ZORA-DFT approach very efficiently reproduces much more rigorous DKS results (at least for chemical shifts and spin-spin coupling constants). The ECPs approach may also be used, but only when the scalar relativistic term dominates the relativistic contribution.

Comparison of the computational results with the experiment has shown that although the relativistic effects play an important role in the discussed properties, the other effects should be taken into account. In particular, vibrational effects should be described at a sufficient level of theory. So far, the vibrational effects have been calculated using nonrelativistic approach but the preliminary research shows that the vibrational and relativistic effects are interrelated. It suggests that a proper methodology should be implemented using the relativistic or pseudorelativistic Hamiltonians.

Bibliography

[1] J. Vaara, J. Jokisaari, R. E. Wasylishen, and D. L. Bryce. *Prog. Nucl. Magn. Reson. Spectrosc.*, 41:233 – 304, 2002.

[2] R. H. Contreras, V. Barone, J. C. Facelli, and J. E. Peralta. Advances in theoretical and physical aspects of spin-spin coupling constants. In G. Webb, editor, *Annual Reports on NMR Spectroscopy*, volume 51, page 167. Academic Press, 2003.

[3] T. Helgaker, M. Jaszuński, and M. Pecul. *Prog. Nucl. Magn. Reson. Spectrosc.*, 53(4):249–268, 2008.

[4] L. B. Krivdin and R. H. Contreras. Recent advances in theoretical calculations of indirect spin-spin coupling constants. In G. Webb, editor, *Annual Reports on NMR Spectroscopy*, volume 61, page 133. Academic Press, 2007.

[5] T. Helgaker, M. Jaszuński, and K. Ruud. *Chem. Rev.*, 99:293–352, 1999.

[6] M. Kaupp, M. Bühl, and V. G. Malkin. *Calculation of NMR and EPR parameters. Theory and applications.* Wiley–VCH, Weinheim, 2004.

[7] M. S. Vallarta and N. Rosen. *Phys. Rev.*, 41:708–712, 1932.

[8] J. R. Yates, C. J. Pickard, M. C. Payne, and F. Mauri. *J. Chem. Phys*, 118(13):5746–5753, 2003.

[9] T. F. G. Green and J. R. Yates. *J. Chem. Phys*, 140(23):–, 2014.

[10] P. Manninen, K. Ruud, P. Lantto, and J. Vaara. *J. Chem. Phys.*, 122(11):114107, 2005.

[11] P. Manninen, K. Ruud, P. Lantto, and J. Vaara. *J. Chem. Phys.*, 124(14):149901, 2006.

[12] P. Manninen, P. Lantto, J. Vaara, and K. Ruud. *J. Chem. Phys.*, 119(5):2623–2637, 2003.

[13] M. Hanni, P. Lantto, M. Iliaš, H. J. A. Jensen, and J. Vaara. *J. Chem. Phys.*, 127(16):164313, 2007.

[14] J. Vaara, P. Manninen, and P. Lantto. Perturbational and ECP Calculation of Relativistic Effects in NMR Shielding and Spin–Spin Coupling. In M. Kaupp, M. Bühl, and V. G. Malkin, editors, *Calculation of NMR and EPR parameters. Theory and applications*, page 209. Wiley–VCH, Weinheim, 2004.

[15] J. Roukala, A. F. Maldonado, J. Vaara, G. A. Aucar, and P. Lantto. *Phys. Chem. Chem. Phys.*, 13:21016–21025, 2011.

[16] P. Salek, T. Helgaker, and T. Saue. *Chem. Phys.*, 311:187–201, 2005.

[17] N. Gaston, P. Schwerdtfeger, T. Saue, and P. Norman. *J. Chem. Phys.*, 124:044304, 2006.

[18] A. Devarajan, A. Gaenko, and J. Autschbach. *J. Chem. Phys.*, 130(19):194102, 2009.

[19] C. Thierfelder, B. Assadollahzadeh, P. Schwerdtfeger, S. Schaefer, and R. Schaefer. *Phys. Rev. A*, 78(5):052506, 2008.

[20] S. Villaume, T. Saue, and P. Norman. *J. Chem. Phys.*, 133:064105, 2010.

[21] J. Henriksson, T. Saue, and P. Norman. *J. Chem. Phys.*, 128:024105, 2008.

[22] R. Bast, T. Saue, J. Henriksson, and P. Norman. *J. Chem. Phys.*, 130:024109, 2009.

[23] R. Bast, K. Ruud, A. Rizzo, and T. Helgaker. *Theor. Chem. Acc.*, 129:685–699, 2011.

[24] P. Hrobárik, M. Repiskỳ, S. Komorovskỳ, V. Hrobáriková, and M. Kaupp. *Theor. Chem. Acc.*, 129(3-5):715–725, 2011.

[25] S. Komorovskỳ, M. Repiskỳ, O. L. Malkina, V. G. Malkin, I. Malkin, and M. Kaupp. *J. Chem. Phys*, 124(8):084108, 2006.

[26] J. Autschbach, S. Patchkovskii, and B. Pritchard. *J. Chem. Theory Comput.*, 7(7):2175–2188, 2011.

[27] C. Thierfelder, P. Schwerdtfeger, and T. Saue. *Phys. Rev. A*, 76:034502, 2007.

[28] M. Srebro and J. Autschbach. *J. Phys. Chem. Lett.*, 3(5):576–581, 2012.

[29] F. Aquino, N. Govind, and J. Autschbach. *J. Chem. Theory Comput.*, 6(9):2669–2686, 2010.

[30] J. Vaara, K. Ruud, and O. Vahtras. *J. Comput. Chem.*, 20:1314, 1999.

[31] J. I. Melo, M. C. Ruiz de Azúa, J. E. Peralta, and G. E. Scuseria. *J. Chem. Phys.*, 123:204112, 2005.

[32] V. G. Malkin, O. L. Malkina, and D. R. Salahub. *Chem. Phys. Lett.*, 221:91, 1994.

[33] O. L. Malkina, D. R. Salahub, and V. G. Malkin. *J. Chem. Phys.*, 105:8793, 1996.

[34] M. Hricovini, O. L. Malkina, F. Bizik, L. T. Nagy, and V. G. Malkin. *J. Phys. Chem. A*, 101:9756, 1997.

[35] R. M. Dickson and T. Ziegler. *J. Phys. Chem.*, 100:5286, 1996.

[36] V. Sychrovský, J. Gräfenstein, and D. Cremer. *J. Chem. Phys.*, 113:3530, 2000.

[37] T. Helgaker, M. Watson, and N. C. Handy. *J. Chem. Phys.*, 113:9402, 2000.

[38] S. A. Perera, H. Sekino, and R. J. Bartlett. *J. Chem. Phys.*, 101:2186, 1994.

[39] J. F. Stanton and J. Gauss. *Int. Rev. Phys. Chem.*, 19:61, 2000.

[40] A. A. Auer and J. Gauss. *J. Chem. Phys.*, 115:1619, 2001.

[41] O. Vahtras, H. Ågren, P. Jørgensen, H. J. A. Jensen, S. B. Padkjær, and T. Helgaker. *J. Chem. Phys.*, 96:6120, 1992.

[42] J. Autschbach and T. Ziegler. *J. Chem. Phys.*, 113:936, 2000.

[43] J. Autschbach and T. Ziegler. *J. Chem. Phys.*, 113:9410, 2000.

[44] M. Filatov and D. Cremer. *J. Chem. Phys.*, 120:11407, 2004.

[45] J. Autschbach, C. D. Igna, and T. Ziegler. *J. Am. Chem. Soc.*, 125(4):1028–1032, 2003.

[46] J. Autschbach and T. Ziegler. *J. Am. Chem. Soc.*, 123(22):5320–5324, 2001.

[47] J. Autschbach and T. Ziegler. *J. Am. Chem. Soc.*, 123:3341, 2001.

[48] J. Autschbach, A. M. Kantola, and J. Jokisaari. *J. Phys. Chem. A*, 111:5343, 2007.

[49] A. Bagno and M. Bonchio. *Magn. Reson. Chem.*, 42:S79, 2004.

[50] G. Schreckenbach and T. Ziegler. *J. Phys. Chem.*, 99:606, 1995.

[51] R. Fukuda, M. Hada, and H. Nakatsuji. *J. Chem. Phys.*, 118:1015, 2003.

[52] R. Fukuda, M. Hada, and H. Nakatsuji. *J. Chem. Phys.*, 118:1027, 2003.

[53] S. K. Wolff, T. Ziegler, E. van Lenthe, and E. J. Baerends. *J. Chem. Phys.*, 110:7689, 1999.

[54] J. Autschbach and T. Ziegler. In D. M. Grant and R. K. Harris, editors, *Encyclopedia of Nuclear Magnetic Resonance*, volume 9, page 306. John Wiley & Sons, 2003.

[55] J. Autschbach. Calculation of Heavy-Nucleus Chemical Shifts. Relativistic All-Electron Methods. In M. Kaupp, M. Bühl, and V. G. Malkin, editors, *Calculation of NMR and EPR parameters. Theory and applications*, page 227. Wiley–VCH, Weinheim, 2004.

[56] A. Rodriguez-Fortea, P. Alemany, and T. Ziegler. *J. Phys. Chem. A*, 103(41):8288–8294, 1999.

[57] T. Gilbert and T. Ziegler. *J. Phys. Chem. A*, 103(37):7535–7543, 1999.

[58] G. Schreckenbach, S. Wolff, and T. Ziegler. *J. Phys. Chem. A*, 104(35):8244–8255, 2000.

[59] G. Schreckenbach. *Inorg. Chem.*, 41(25):6560–6572, 2002.

[60] W. Nakanishi, S. Hayashi, Y. Katsura, and M. Hada. *J. Phys. Chem. A*, 115(31):8721–8730, 2011.

[61] A. Wodyński, M. Repiskỳ, and M. Pecul. *J. Chem. Phys*, 137(1):014311, 2012.

[62] V. Arcisauskaite, J. I. Melo, L. Hemmingsen, and S. P. A. Sauer. *J. Chem. Phys.*, 135(4):044306, 2011.

[63] J. Autschbach. *Theor. Chem. Acc.*, 112(1):52–57, 2004.

[64] T. Enevoldsen, L. Visscher, T. Saue, H. J. A. Jensen, and J. Oddershede. *J. Chem. Phys.*, 112(8):3493–3498, 2000.

[65] S. S. Gomez, R. H. Romero, and G. A. Aucar. *J. Chem. Phys.*, 117(17):7942–7946, 2002.

[66] A. Antušek, M. Pecul, and J. Sadlej. *Chem. Phys. Lett.*, 427(4-6):281–288, 2006.

[67] M. Hada. *Chem. Phys. Lett.*, 310(3-4):342–346, 1999.

[68] L. Visscher, T. Enevoldsen, T. Saue, H. J. A. Jensen, and J. Oddershede. *J. Comput. Chem.*, 20(12):1262–1273, 1999.

[69] M. Hada. *Chem. Phys. Lett.*, 321(5-6):452–458, 2000.

[70] S. S. Gomez, R. H. Romero, and G. A. Aucar. *J. Chem. Phys.*, 117(17):7942, 2002.

[71] M. Repiský, S. Komorovský, O. L. Malkina, and V. G. Malkin. *Chem. Phys.*, 356:236–242, 2009.

[72] M. Olejniczak, R. Bast, T. Saue, and M. Pecul. *J. Chem. Phys.*, 136(1):014108, 2012.

[73] F. London. *J. Phys. Radium*, 8(10):397–409, 1937.

[74] S. Komorovský, M. Repiský, O. Malkina, V. G. Malkin, I. M. Ondík, and M. Kaupp. *J. Chem. Phys.*, 128(10):104101–104115, 2008.

[75] S. Komorovský, M. Repiský, O. L. Malkina, and V. G. Malkin. *J. Chem. Phys.*, 132(15):154101, 2010.

[76] A. Antušek, M. Jaszuński, and M. Olejniczak. *Comp. and Theor. Chem.*, 970:54–60, 2011.

[77] P. Lantto, K. Jackowski, W. Makulski, M. Olejniczak, and M. Jaszuński. *J. Phys. Chem. A*, 115:10617–10623, 2011.

[78] T. B. Demissie, M. Jaszuński, E. Malkin, S. Komorovskỳ, and K. Ruud. *Mol. Phys.*, (ahead-of-print):1–9, 2015.

[79] M. Jaszuński, T. B. Demissie, and K. Ruud. *J. Phys. Chem. A*, 118(40):9588–9595, 2014.

[80] K. Ruud, T. B. Demissie, and M. Jaszuński. *J. Chem. Phys*, 140(19):194308, 2014.

[81] E. Malkin, S. Komorovsky, M. Repisky, T. B. Demissie, and K. Ruud. *J. Phys. Chem. Lett.*, 4(3):459–463, 2013.

[82] T. B. Demissie, M. Repisky, S. Komorovsky, J. Isaksson, J. S. Svendsen, H. Dodziuk, and K. Ruud. *J. Phys. Org. Chem.*, 26(8):679–687, 2013.

[83] P. Pyykkö, A. Görling, and N. Rösch. *Mol. Phys.*, 61:195, 1987.

[84] N. Nakagawa, S. Sinada, and S. Obinata. *The 6th NMR Symposium, Kyoto*, page 8, 1967.

[85] Y. Nomura, Y. Takeuchi, and N. Nakagawa. *Tetrahedron Lett.*, 10(8):639 – 642, 1969.

[86] I. Morishima, K. Endo, and T. Yonezawa. *J. Chem. Phys*, 59(6):3356–3364, 1973.

[87] M. Volodicheva and T. Rebane. *Theor. Exp. Chem.*, 14(4):348–354, 1979.

[88] A. Cheremisin and P. Schastnev. *J. Magn. Reson. (1969)*, 40(3):459 – 468, 1980.

[89] M. Kaupp, O. L. Malkin, and V. G. Malkin. *Chem. Phys. Lett.*, 265(1–2):55 – 59, 1997.

[90] M. Kaupp, O. L. Malkina, V. G. Malkin, and P. Pyykkö. *Chem. Eur. J.*, 4(1):118–126, 1998.

[91] S. K. Wolff and T. Ziegler. *J. Chem. Phys*, 109(3):895–905, 1998.

[92] M. Kaupp and O. L. Malkina. *J. Chem. Phys*, 108(9):3648–3659, 1998.

[93] M. Hyvarinen, J. Vaara, A. Goldammer, B. Kutzky, K. Hegetschweiler, M. Kaupp, and M. Straka. *J. Am. Chem. Soc.*, 131(33):11909–11918, 2009.

[94] A. C. Neto, L. C. Ducati, R. Rittner, C. F. Tormena, R. H. Contreras, and G. Frenking. *J. Chem. Theory Comput.*, 5(9):2222–2228, 2009.

[95] J. Vícha, M. Straka, M. L. Munzarová, and R. Marek. *J. Chem. Theory Comput.*, 10(4):1489–1499, 2014.

[96] A. Bagno and G. Saielli. *J. Am. Chem. Soc.*, 129:11360–11361, 2007.

[97] M. Olejniczak and M. Pecul. *ChemPhysChem*, 10:1247–1259, 2009.

[98] M. Kauch and M. Pecul. *ChemPhysChem*, 13:1332–1338, 2012.

[99] S. Kirpekar, H. Jensen, and J. Oddershede. *Theor. Chim. Acta*, 95(1-2):35–47, 1997.

[100] J. Vaara, K. Ruud, and O. Vahtras. *J. Comput. Chem.*, 20(12):1314–1327, 1999.

[101] A. Gryff-Keller, A. Kraska-Dziadecka, S. Molchanov, and A. Wodyński. *J. Phys. Chem. A*, 116(43):10615–10620, 2012.

[102] L. Piela. *Ideas of quantum chemistry*. Elsevier, 2013.

[103] M. Reiher and A. Wolf. *Relativistic quantum chemistry: the fundamental theory of molecular science*. John Wiley & Sons, 2009.

[104] U. Kaldor and S. Wilson. *Theoretical chemistry and physics of heavy and superheavy elements*, volume 11. Springer Science & Business Media, 2003.

[105] *Relativistic Computation of NMR Shieldings and Spin-Spin Coupling Constants in eMagRes.* John Wiley and Sons, Ltd, 2007.

[106] F. Jensen. *Introduction to computational chemistry.* John Wiley & Sons, 2013.

[107] K. Faegri Jr et al. *Introduction to relativistic quantum chemistry.* Oxford University Press, 2007.

[108] A. Rudziński, M. Puchalski, and K. Pachucki. *arXiv preprint arXiv:0904.4153*, 2009.

[109] V. Yerokhin, K. Pachucki, Z. Harman, and C. Keitel. *Phys. Rev. Lett.*, 107(4):043004, 2011.

[110] V. A. Yerokhin, K. Pachucki, Z. Harman, and C. H. Keitel. *Phys. Rev. A*, 85:022512, 2012.

[111] L. L. Foldy and S. A. Wouthuysen. *Phys. Rev.*, 78:29–36, 1950.

[112] M. Douglas and N. M. Kroll. *Annals of Physics*, 82(1):89 – 155, 1974.

[113] B. A. Hess. *Phys. Rev. A*, 32:756–763, 1985.

[114] B. A. Hess. *Phys. Rev. A*, 33:3742–3748, 1986.

[115] B. A. Hess, R. J. Buenker, and P. Chandra. *Int. J. Quantum Chem.*, 29(4):737–753, 1986.

[116] C. Chang, M. Pelissier, and P. Durand. *Phys. Scr.*, 34(5):394, 1986.

[117] J.-L. Heully, I. Lindgren, E. Lindroth, S. Lundqvist, and A.-M. Martensson-Pendrill. *J. Phys. B*, 19(18):2799, 1986.

[118] D. Figgen, G. Rauhut, M. Dolg, and H. Stoll. *Chem. Phys.*, 311(1):227–244, 2005.

[119] B. Metz, H. Stoll, and M. Dolg. *J. Chem. Phys*, 113(7):2563, 2000.

[120] K. A. Peterson, D. Figgen, E. Goll, H. Stoll, and M. Dolg. *J. Chem. Phys.*, 119(21):11113–11123, 2003.

[121] H. Stoll, B. Metz, and M. Dolg. *J. Comput. Chem.*, 23(8):767–778, 2002.

[122] D. Andrae, U. Häussermann, M. Dolg, H. Stoll, and H. Preuss. *Theor. Chim. Acta*, 77(2):123–141, 1990.

[123] T. Leininger, A. Nicklass, H. Stoll, M. Dolg, and P. Schwerdtfeger. *J. Chem. Phys*, 105(3):1052, 1996.

[124] F. Schautz, H.-J. Flad, and M. Dolg. *Theor. Chem. Acc.*, 99(4):231–240, 1998.

[125] A. Bergner, M. Dolg, W. Küchle, H. Stoll, and H. Preuß. *Mol. Phys.*, 80(6):1431–1441, 1993.

[126] U. Häussermann, M. Dolg, H. Stoll, H. Preuss, P. Schwerdtfeger, and R. Pitzer. *Mol. Phys.*, 78(5):1211–1224, 1993.

[127] D. Andrae, U. Häussermann, M. Dolg, H. Stoll, and H. Preuss. *Theor. Chim. Acta*, 77(2):123–141, 1990.

[128] T. Leininger, A. Berning, A. Nicklass, H. Stoll, H.-J. Werner, and H.-J. Flad. *Chem. Phys.*, 217(1):19 – 27, 1997.

[129] W. Küchle, M. Dolg, H. Stoll, and H. Preuss. *Mol. Phys.*, 74(6):1245–1263, 1991.

[130] P. J. Hay and W. R. Wadt. *J. Chem. Phys.*, 82(1):270–283, 1985.

[131] W. R. Wadt and P. J. Hay. *J. Chem. Phys.*, 82(1):284–298, 1985.

[132] J. Autschbach and T. Ziegler. *J. Chem. Phys.*, 113(21):9410–9418, 2000.

[133] J. Leszczynski. *Handbook of computational chemistry*, volume 2. Springer Science & Business Media, 2011.

[134] M. Jaszuński, A. Rizzo, and K. Ruud. *Electric, magnetic and optical properties and their ab initio calculation in the DALTON program, url: http://folk.uio.no/michalj/*.

[135] A. D. Becke. *Phys. Rev. A*, 38(6):3098–3100, 1988.

[136] J. P. Perdew. *Phys. Rev. B*, 33(12):8822–8824, 1986.

[137] J. P. Perdew, K. Burke, and M. Ernzerhof. *Phys. Rev. Lett.*, 77:3865–3868, 1996.

[138] J. P. Perdew, K. Burke, and M. Ernzerhof. *Phys. Rev. Lett.*, 78:1396–1396, 1997.

[139] P. J. Stephens, F. J. Devlin, C. F. Chabalowski, and M. J. Frisch. *J. Phys. Chem.*, 98(45):11623–11627, 1994.

[140] V. Vetere, C. Adamo, and P. Maldivi. *Chem. Phys. Lett.*, 325(1-3):99 – 105, 2000.

[141] T. Saue and T. Helgaker. *J. Comput. Chem.*, 23(8):814–823, 2002.

[142] D. L. Bryce and R. E. Wasylishen. *Inorg. Chem.*, 41(16):4131–4138, 2002.

[143] P. M. Aguiar and S. Kroeker. *Phys. Chem. Chem. Phys.*, 11(5):834–840, 2009.

[144] K. J. Harris and R. E. Wasylishen. *Inorg. Chem.*, 48(5):2316–2332, 2009.

[145] C. Fonseca Guerra, J. G. Snijders, G. te Velde, and E. J. Baerends. *Theor. Chem. Acc.*, 99(6):391–403, 1998.

[146] G. te Velde, F. M. Bickelhaupt, E. J. Baerends, C. Fonseca Guerra, S. J. A. van Gisbergen, J. G. Snijders, and T. Ziegler. *J. Comput. Chem.*, 22(9):931–967, 2001.

[147] ADF2010, SCM, Theoretical Chemistry, Vrije Universiteit, Amsterdam, The Netherlands, http://www.scm.com.

[148] S. Vosko, L. Wilk, and M. Nusair. *Can. J. Phys.*, 58(8):1200–1211, 1980.

[149] C. C. Pye and T. Ziegler. *Theor. Chem. Acc.*, 101(6):396–408, 1999.

[150] A. Klamt and G. Schüürmann. *J. Chem. Soc., Perkin Trans. 2*, pages 799–805, 1993.

[151] A. Klamt. *J. Phys. Chem.*, 99(7):2224–2235, 1995.

[152] A. Klamt and V. Jonas. *J. Chem. Phys.*, 105(22):9972–9981, 1996.

[153] ReSpect program, version 3.1.0 (2011), writen by V. G. Malkin, O. L. Malkina, M. Repiský, S. Komorovský, I. Malkin, E. Malkin, A. V. Arbuznikov, M. Kaupp and K. Ruud.

[154] J. P. Perdew, K. Burke, and M. Ernzerhof. *Phys. Rev. Lett.*, 77(18):3865–3868, 1996.

[155] F. Jensen. *J. Chem. Phys.*, 115(20):9113, 2001.

[156] F. Jensen. *J. Chem. Phys.*, 116(8):3502, 2002.

[157] K. G. Dyall. *Theor. Chem. Acc.*, 112(5-6):403–409, 2004.

[158] DIRAC, a relativistic ab initio electronic structure program, Release DIRAC11 (2011), written by R. Bast, H. J. Aa. Jensen, T. Saue, and L. Visscher, with contributions from V. Bakken, K. G. Dyall, S. Dubillard, U. Ekström, E. Eliav, T. Enevoldsen, T. Fleig, O. Fossgaard, A. S. P. Gomes, T. Helgaker, J. K. Lærdahl, J. Henriksson, M. Iliaš, Ch. R. Jacob, S. Knecht, C. V. Larsen, H. S. Nataraj, P. Norman, M. Olejniczak, J. Olsen, J. K. Pedersen, M. Pernpointner, K. Ruud, P. Sałek, B. Schimmelpfennig, J. Sikkema, A. J. Thorvaldsen, J. Thyssen, J. van Stralen, S. Villaume, O. Visser, T. Winther, and S. Yamamoto (see http://dirac.chem.vu.nl).

[159] T. Saue. Dirac-kohn-sham calculations of nuclear spin-spin coupling constants. Personal communication.

[160] C. Adamo and V. Barone. *J. Chem. Phys.*, 110(13):6158–6170, 1999.

[161] P. F. Provasi, G. A. Aucar, and S. P. A. Sauer. *J. Chem. Phys.*, 115(3):1324, 2001.

[162] A. Křístková, S. Komorovsky, M. Repisky, V. G. Malkin, and O. L. Malkina. *J. Chem. Phys*, 142(11):114102, 2015.

[163] F. Jensen. *J. Chem. Theory Comput.*, 2(5):1360–1369, 2006.

[164] J. Autschbach. *J. Chem. Phys.*, 129(9):094105, 2008.

[165] M. J. Frisch, G. W. Trucks, H. B. Schlegel, G. E. Scuseria, M. A. Robb, J. R. Cheeseman, J. A. Montgomery, Jr., T. Vreven, K. N. Kudin, J. C. Burant, J. M. Millam, S. S. Iyengar, J. Tomasi, V. Barone, B. Mennucci, M. Cossi, G. Scalmani, N. Rega, G. A. Petersson, H. Nakatsuji, M. Hada, M. Ehara, K. Toyota, R. Fukuda, J. Hasegawa, M. Ishida, T. Nakajima, Y. Honda, O. Kitao, H. Nakai, M. Klene, X. Li, J. E. Knox, H. P. Hratchian, J. B. Cross, V. Bakken, C. Adamo, J. Jaramillo, R. Gomperts, R. E. Stratmann, O. Yazyev, A. J. Austin, R. Cammi, C. Pomelli, J. W. Ochterski, P. Y. Ayala, K. Morokuma, G. A. Voth, P. Salvador, J. J. Dannenberg, V. G. Zakrzewski, S. Dapprich, A. D. Daniels, M. C. Strain, O. Farkas, D. K. Malick, A. D. Rabuck, K. Raghavachari, J. B. Foresman, J. V. Ortiz, Q. Cui, A. G. Baboul, S. Clifford, J. Cioslowski, B. B. Stefanov, G. Liu, A. Liashenko, P. Piskorz, I. Komaromi, R. L. Martin, D. J. Fox, T. Keith, M. A. Al-Laham, C. Y. Peng, A. Nanayakkara, M. Challacombe, P. M. W. Gill, B. Johnson, W. Chen, M. W. Wong, C. Gonzalez, and J. A. Pople. Gaussian 03, Revision C.02. Gaussian, Inc., Wallingford, CT, 2004.

[166] Gaussian 09 Revision C.01, Gaussian Inc. Wallingford CT 2009, M. J. Frisch, G. W. Trucks, H. B. Schlegel, G. E. Scuseria, M. A. Robb, J. R. Cheeseman, G. Scalmani, V. Barone, B. Mennucci, G. A. Petersson, H. Nakatsuji, M. Caricato, X. Li, H. P. Hratchian, A. F. Izmaylov, J. Bloino, G. Zheng, J. L. Sonnenberg, M. Hada, M. Ehara, K. Toyota, R. Fukuda, J. Hasegawa, M. Ishida, T. Nakajima, Y. Honda, O. Kitao, H. Nakai, T. Vreven, Montgomery, Jr., J. A., J. E. Peralta, F. Ogliaro, M. Bearpark, J. J. Heyd, E. Brothers, K. N. Kudin, V. N. Staroverov, R. Kobayashi, J. Norm„ K. Raghavachari, A. Rendell, J. C. Burant, S. S. Iyengar, J. Tomasi, M. Cossi, N. Rega, J. M. Millam, M. Klene, J. E. Knox, J. B. Cross, V. Bakken, C. Adamo, J. Jaramillo, R. Gomperts, R. E. Stratmann, O. Yazyev, A. J. Austin, R. Cammi, C. Pomelli, J. W. Ochterski, R. L. Martin, K. Morokuma, V. G. Zakrzewski, G. A. Voth, P. Salvador, J. J. Dannenberg, S. Dapprich, A. D. Daniels, Ö. Farkas, J. B. Foresman, J. V. Ortiz, J. Cioslowski and D. J. Fox.

[167] U. Häussermann. Unpublished Report, 1988.

[168] Dalton2011, a molecular electronic structure program (2011), http://www.daltonprogram.org.

[169] J. Cukras and J. Sadlej. *Phys. Chem. Chem. Phys.*, 13(34):15455–15467, 2011.

[170] G. Wu, S. Kroeker, and R. Wasylishen. *Inorg. Chem.*, 34(6):1595–1598, 1995.

[171] S. Kroeker, R. E. Wasylishen, and J. V. Hanna. *J. Am. Chem. Soc.*, 121(7):1582–1590, 1999.

[172] S. Molchanov and A. Gryff-Keller. *Magn. Reson. Chem.*, 41(10):788–793, 2003.

[173] M. Kaupp. Relativistic Effects on NMR Chemical Shifts. In P. Schwerdtfeger, editor, *Relativistic Electronic Structure Theory. Part 2. Applications*, page 552. Elsevier, Amsterdam, 2004.

[174] J. Autschbach. *Mol. Phys.*, 111(16-17):2544–2554, 2013.

[175] M. Kaupp and O. L. Malkina. *J. Chem. Phys.*, 108(9):3648–3659, 1998.

[176] K. Ruud, P.-O. Astrand, and P. R. Taylor. *J. Chem. Phys.*, 112(6):2668–2683, 2000.

[177] *url: http://www.tc.uni-koeln.de/PP/index.en.html.*

[178] D. Figgen, G. Rauhut, M. Dolg, and H. Stoll. *Chem. Phys.*, 311(1):227–244, 2005.

[179] M. Pecul, M. Jaszuński, and J. Sadlej. *Chem. Phys. Lett.*, 305(1–2):139 – 146, 1999.

All papers by the author

1. **Wodyński A.**, Pecul M., Malkin O. (2015): *The relativistic effects on the carbon-carbon coupling constants mediated by a heavy atom*, in preparation

2. **Wodyński A.**, Kraska-Dziadecka A., Kubica D., Gryff-Keller A. (2015): *Interpretation of the longitudinal ^{13}C nuclear spin relaxation and chemical shift data for five bromo-azaheterocycles supported by the non-relativistic and relativistic DFT calculations* In: The Journal of Physical Chemistry A, 119, 517-524

3. Narbutt J., **Wodyński A.**, Pecul M. (2015): *On the selectivity of diglycolamide (TODGA) and bis-triazine-bipyridine (BTBP) ligands in actinide/lanthanide complexation and solvent extraction separation — a theoretical approach.* In: Dalton Transactions. 44, 2657-2666

4. Bernatowicz P., Kubica D., Ociepa M., **Wodyński A.**, Gryff-Keller A. (2014): *Scalar Relaxation of the Second Kind. A Potential Source of Information on the Dynamics of Molecular Movements. 4. Molecules with Collinear C-H and C-Br Bonds.* In: The Journal of Physical Chemistry A, 118 (23), 4063-4070

5. Kubica D., **Wodyński A.**, Kraska-Dziadecka A., Gryff-Keller A. (2014): *Scalar relaxation of the second kind — a potential source of information on the dynamics of molecular movements. 3. A ^{13}C Nuclear Spin Relaxation Study of $CBrX_3$ (X = Cl, CH_3, Br) Molecules.* In: The Journal of Physical Chemistry A 2014, 118 (16), 2995-3003

6. Molchanov S., **Wodyński A.**, Gryff-Keller A. (2014): *Scalar relaxation of the second kind — a potential source of information on the dynamics of molecular movements. 2. A unique carbon-bromine spin system.* In: The Journal of Physical Chemistry A 2014, 118 (1), 128-133

7. **Wodyński A.**, Pecul M. (2014): *The influence of a presence of a heavy atom on the spin-spin coupling constants between two light nuclei in organometallic compounds and halogen derivatives.* In: The Journal of Chemical Physics 2014, 140 (2), 024319

8. **Wodyński A.**, Gryff-Keller A., Pecul M. (2013): *The influence of a presence of a heavy atom on* ^{13}C *shielding constants in organomercury compounds and halogen derivatives.* In: Journal of Chemical Theory and Computation 2013, 9 (4), 1909-1917

9. Gryff-Keller A., Kraska-Dziadecka A., Molchanov S., **Wodyński A.** (2013): *Shielding and Indirect Spin-Spin Coupling Tensors in the Presence of a Heavy Atom: An Experimental and Theoretical Study of bis(phenylethynyl)mercury.* In: The Journal of Physical Chemistry A 2013, 116 (43), 10615-10620

10. **Wodyński A.**, Repiský M.,Pecul M. (2012): *A comparison of two-component and four-component approaches for calculations of spin-spin coupling constants and NMR shielding constants of transition metal cyanides.* In: The Journal of Chemical Physics 2012, 137, 014311

11. Pecul M., Urbańczyk M., **Wodyński A.**, Jaszuński M. *DFT calculations of* ^{31}P *spin-spin coupling constants and chemical shift in dioxaphosphorinanes.* In: Magnetic Resonance in Chemistry 2011, 49 (7), 399-404

Paper I

A comparison of two-component and four-component approaches for calculations of spin-spin coupling constants and NMR shielding constants of transition metal cyanides

Artur Wodyński,[1] Michal Repiský,[2] and Magdalena Pecul[1,a)]
[1]*Faculty of Chemistry, University of Warsaw, Pasteura 1, 02-093 Warszawa, Poland*
[2]*Centre for Theoretical and Computational Chemistry, Department of Chemistry, University of Tromsø, N-9037 Tromsø, Norway*

(Received 13 March 2012; accepted 11 June 2012; published online 5 July 2012)

Relativistic density functional theory (DFT) calculations of nuclear spin-spin coupling constants and shielding constants have been performed for selected transition metal (11th and 12th group of periodic table) and thallium cyanides. The calculations have been carried out using zeroth-order regular approximation (ZORA) Hamiltonian and four-component Dirac-Kohn-Sham (DKS) theory with different nonrelativistic exchange-correlation functionals. Two recent approaches for representing the magnetic balance (MB) between the large and small components of four-component spinors, namely, mDKS-RMB and sMB, have been employed for shielding tensor calculations and their results have been compared. Relativistic effects have also been analysed in terms of scalar and spin-orbit contributions at the two-component level of theory, including discussion of heavy-atom-on-light-atom effects for $^1J_{CN}$, σ_C, and σ_N. The results for molecules containing metals from 4th row of periodic table show that relativistic effects for them are small (especially for spin-spin coupling constants). The biggest effects are observed for the 6th row where nonrelativistic theory reproduces only about 50%–70% of the two-component ZORA results for $^1J_{MeC}$ and about 75% for heavy metal shielding constants. It is important to employ a full Dirac picture for calculations of heavy metal shielding constants, since ZORA reproduces only 75%–90% of the DKS results. Smaller discrepancies between ZORA-DFT and DKS are observed for nuclear spin-spin coupling constants. No significant differences are observed between the results obtained using mDKS-RMB and sMB approaches for magnetic balance in four-component calculations of the shielding constants. © *2012 American Institute of Physics*. [http://dx.doi.org/10.1063/1.4730944]

I. INTRODUCTION

The nuclear shielding constants and spin-spin coupling constants, main parameters of the nuclear magnetic resonance (NMR) spectra, constitute an important source of structural information. Quantum chemical calculations of the NMR parameters of molecules containing light atoms (up to the second row of periodic table) are nowadays a standard research tool (see, for example, reviews of Refs. 1–6), and are frequently performed even by non-specialists. However, this is not the case for molecules containing heavy atoms, where the standard computational methods based on the Schrödinger equation are not sufficient and the relativistic effects are of paramount importance. The relativistic effects tend to be particularly pronounced for nuclear shielding constants and spin-spin coupling constants of heavy nuclei, since these properties (in particular, the spin-spin coupling constant) are related to the atomic core region, where the electron velocities are the largest. However, it is well known that the presence of a heavy atom affects also the NMR parameters of neighbouring light nuclei,[7,8] a phenomenon which is known as heavy-atom-on-light-atom (HALA) effect. Thus, to calculate NMR parameters of molecules containing heavy atoms one needs to resort to relativistic methods.

Computationally cheapest methods of accounting for relativistic effects in *ab initio* calculations are effective core potentials (ECPs) parametrized for the purpose. However, their usefulness in calculations of NMR parameters (particularly of heavy nuclei) is limited since ECPs by definition do not allow for accurate modelling of electron density in the core region. There are reports in the literature of the calculations of relativistic effects on the shielding constants by means of perturbational theory based on the Breit-Pauli Hamiltonian and nonrelativistic wave function (from the group of Vaara,[9–12] see also Refs. 13 and 14 for specialized reviews). Unfortunately, these methods cannot be generally applied to calculation of spin-spin coupling constants, since some terms diverge upon basis set expansion,[13] or for shielding constants of sixth row nuclei (including 1/2-spin nuclei such as ^{199}Hg or ^{205}Tl, important in NMR spectroscopy), since there the nonrelativistic wave function does not provide a good expansion point to the perturbation theory. In this situation, the use of a relativistic Hamiltonian, either four-component or two-component one, in *ab initio* calculations is the only solution.

Implementation of relativistic Hamiltonians for calculations of NMR parameters is not a trivial task, since the calculations of nuclear shielding constants and spin-spin coupling

a)Author to whom correspondence should be addressed. Electronic mail: mpecul@chem.uw.edu.pl.

constants are associated with several obstacles. For nuclear shielding constants one of the the most important concerns is ensuring the gauge invariance (independence of the calculated results on the gauge origin chosen for the vector potential) when a finite basis set is employed, while in the case of the spin-spin coupling constants accounting for electron correlation is the most important concern. It has been shown several times at the nonrelativistic level (see, for example, Ref. 3 for a review) that the Hartree-Fock method often produces completely spurious results for spin-spin coupling constants. This remains true also for relativistic calculations, although in this case the body of numerical evidence is much smaller (a comparison of correlated and Hartree-Fock relativistic results can be found, for example, in Refs. 15 and 16). Moreover, the time to calculate the spin-spin coupling constants rises significantly with the system size, since a set of response equations has to be solved individually for each magnetic nucleus. The high computational demands along with the importance of including the electron correlation have hampered the relativistic calculations of spin-spin coupling constants until the advent of density functional theory (DFT).[17–22] Although there exist implementations of electron-correlated methods for the calculation of nuclear spin-spin coupling constants at the nonrelativistic level (such as coupled cluster[23–26] or multiconfigurational self consistent field method[27]), simultaneous inclusion of the relativistic effects and electron correlation is currently possible only via density functional theory.

Several different Hamiltonians have been used in two-component relativistic calculations of NMR properties, such as the zeroth-order regular approximation (ZORA (Refs. 28 and 29)), the infinite-order regular approximation with modified metric[30] or Douglas-Kroll-Hess (DKH (Ref. 16)) Hamiltonians. Currently, the most popular two-component approach is ZORA-DFT implementation which has been successfully applied to several molecular systems involving transition metals, including, for instance J_{PtPt},[31] J_{PtTl},[32] J_{PtC},[32] J_{TlC},[32] Hg couplings,[33,34] and Ru couplings.[35] In case of NMR shielding constants, both ZORA (Ref. 36) and Douglas-Kroll-Hess[37] methods have been used, for example, for HX where X = Cl, Br, I (ZORA-DFT (Refs. 38 and 39) and DKH2-HF (Ref. 40)) and for the series of HgX_2 and HgMeX where X = Cl, Br, I and Me = CH_3 (Refs. 36 and 40). ZORA-DFT has also been used, for example, for ^{183}W,[41] ^{207}Pb,[41] ^{199}Hg,[36] ^{195}Pt,[42] ^{235}U,[43,44] and ^{77}Se[45] shielding constants, see also Ref. 46 for a review.

The four-component calculations of spin-spin coupling constants have been carried out so far mainly at the uncorrelated four-component Dirac-Hartree-Fock level of theory (without accounting for the Breit interaction). This approach has been examined for several systems, for example, XH_4 (X = C, Si, Ge, Sn, Pb) and $Pb(CH3)_3H$,[47] XH_3 (X = N, P, As, Sb, Bi) and XH_2 (X = O, S, Se, Te, Po),[48] and XF_n (n = 2, 4, 6).[49] However, the lack of electron correlation tends to lead to less than satisfactory results. Recently, density functional methods have been implemented at the four-component level[50,51] and the initial results are promising. The same approaches as for the spin-spin coupling constant have been applied for four-component calculations of chemical shifts. Dirac-Hartree-Fock level of theory has been used, for example, for the shielding constants in HX (X = Cl, Br, I),[52,53] H_2Y(Y = O, S, Se, Te),[54] and H_3Y (Y = N, P, As, Sb, Bi).[48] Four-component Dirac-Kohn-Sham density functional theory with London atomic orbitals (LAOs) (Ref. 55) has been recently implemented for the shielding constants[56–58] and has been used for HgL_2 (L = Cl, Br, I, CH_3)[59] and several other small molecules.[60–62]

We have decided to study the relativistic effects in a series of closed-shell transition metal compounds for which experimental data are available and selected transition metal cyanides as model systems. The choice of cyanides has been motivated by the possibility to consider the relativistic effects not only on the coupling constants and shielding constants of heavy metal nuclei but also on the coupling constant between light nuclei in vicinity of the metal atom ($^1J_{CN}$) and light nuclei (^{15}N, ^{13}C) shielding constants. There have been several experimental papers on NMR properties of these compounds ($Hg(CN)_2$,[63] $Zn(CN)_4^{2-}$,[64] $Cd(CN)_4^{2-}$,[64] $Hg(CN)_4^{2-}$;[64] $Tl(CN)_4^-$;[65] CuCN,[66] and AgCN (Ref. 67)), but so far no systematic theoretical study has been conducted. As far as we know there are ZORA results reported only for $^1J_{HgC}$ in $Hg(CN)_2$ and $Hg(CN)_4^{2-}$[68,69] and $^1J_{AgC}$ in AgCN.[67]

In this paper we present two-component (ZORA-DFT) results for spin-spin coupling constants and nuclear shielding constants of cyanides containing transition metals of 11th and 12th group of periodic table and thallium. Four-component DFT calculations of spin-spin coupling constants for $Hg(CN)_2$ and shielding constants for selected compounds have also been carried out. The four-component calculations of NMR shielding constants have been performed using different ways of handling the balance between small and large components: that of Olejniczak *et al.*,[58] numerically equivalent to unrestricted kinetic balance and that of Komorovský *et al.*,[57] which employs explicit magnetic balance. The results have been compared for $Hg(CN)_2$. Additionally, the performance of selected GGA and hybrid exchange-correlation functionals in relativistic calculations of NMR parameters is examined. As far as we know, this is the first face-to-face comparison of two- and four-component Hamiltonians for the calculations of NMR shielding constants and spin-spin coupling constants at the DFT level.

II. COMPUTATIONAL DETAILS

The geometric parameters of the cyanides under study have been obtained in a twofold way. AgCN, CuCN, AuCN in crystals exist as "infinite" linear chains, so for these compounds the experimental chain structures X–C–N–X–C–N (X = Ag, Cu, Au) have been used, obtained in diffraction experiments.[67,70,71] For other cyanides, the DFT geometry optimization has been carried out using Amsterdam density functional (ADF) package[72–74] (version 2009 and 2010), scalar ZORA Hamiltonian,[28,29] VWN (Ref. 75) + Becke88 (Ref. 76), and Perdew86 (Ref. 77) nonlocal gradient corrections (BVP86) as exchange-correlation functional and Slater-type TZ2P basis sets. The innermost atomic shells, namely, 1*s* of carbon and nitrogen, 1*s*–2*p* of zinc, 1*s*–3*d* of cadmium, and 1*s*–4*d* of mercury and thallium, have been

approximated by the frozen core densities. Test calculations with ZORA spin-orbit coupling operator have not lead to any visible improvement of geometry optimization results.

Two-component ZORA calculations of NMR properties have been carried out using two GGA functionals (BVP86 (Refs. 75–77) and KT2 (Ref. 78)) and two hybrid functionals (B3LYP (Ref. 79) and PBE0 (Ref. 80)). For BVP86, KT2, and B3LYP functionals in case of spin-spin coupling constants calculations the ADF program uses VWN functional to determine first-order perturbed MOs, but for PBE0 calculation first-order potential of the hybrid PBE0 functional is used. In the case of shielding constants scaled-ZORA variant default in ADF has been used.

We have used standard Slater basis sets available in ADF (Ref. 74) program: TZP (triple-ζ with one polarization function), TZ2P (triple-ζ with two polarization functions), and jcpl[81] basis sets. Differences between TZP and TZ2P are generally negligible. Comparison of the results obtained using jcpl and TZP basis sets shows bigger differences on the spin-spin coupling constants, but the jcpl basis set is available only for a small selection of discussed heavy metals. Unless otherwise stated, for consistency we will only discuss the results obtained with TZP basis set.

The four-component calculation of shielding constants for molecules containing heavy metals from 5th and 6th rows have been performed with the mDKS-RMB-GIAO module of the RESPECT program (version 3.1.0),[82] employing different nonrelativistic exchange-correlation (XC) functionals: LSDA, BP86, PBE. On light atoms (nitrogen and carbon), the uncontracted pc-2 Gaussian basis set of Jensen[83,84] has been attached, while triple-ζ Dyall's[85] basis set has been used for silver, cadmium, gold, mercury, and thallium atoms. The calculations have been further speeded up by the density fitting technique employing complementary auxiliary basis sets. In order to test the performance of hybrid functionals (not available in RESPECT of the version 3.1.0) as well as to compare two recent four-component DFT approaches for the calculation of NMR shielding constants, we performed calculations for $Hg(CN)_2$ with a local version of the DIRAC program.[86] The main difference between these two approaches is the treatment of balance between large and small components of molecular spinors in the presence of an external magnetic field as a perturbation: an explicit restricted magnetic balance[57,87] (RMB) is invoked at the integral level in RESPECT, while DIRAC combines a unrestricted kinetic balance *ansatz* and LAOs in the simple magnetic balance (sMB) approach.[58]

The four-component calculations of spin-spin coupling constants for $Hg(CN)_2$ have been carried out with Gaussian basis sets, using augmented version of triple-ζ Dunning basis set modified for spin-spin coupling constants calculations (aug-cc-pVTZ-J[88]) for nitrogen and carbon, and triple-ζ Dyall[85] basis set for mercury. BP86, B3LYP, and PBE0 functionals have been used. In the four-component calculations of spin-spin coupling constants no magnetic balance has been employed: the large and small components of the wave function have been connected by unrestricted kinetic balance, as implemented in DIRAC.[86]

Four-component calculations have been carried out using Gaussian charge distribution nuclear model (for both the SCF step and the perturbation operator), while two-component ZORA calculations have been performed with point-nuclear model, unless otherwise noted.

III. RESULTS AND DISCUSSION

We will now discuss the calculated spin-spin coupling constants and NMR shielding constants in transition metal cyanides. For each property under study we will first compare the relative weights of scalar and spin-orbit relativistic terms and performance of different exchange-correlation functionals. Afterwards, more physical aspects such as trends in the given group of periodic table will be considered. This discussion will be based mostly on the ZORA DFT results (denoted so-ZORA for the calculations including spin-orbit effects and sc-ZORA for the scalar-only calculations). The four-component results for selected molecules will be presented at the end of this section.

A. Spin-spin coupling constants

1. The $^1J_{MeC}$ spin-spin coupling constant

The ZORA and nonrelativistic results for $^1J_{MeC}$ are tabulated in Table I. Predictably, for the $^1J_{MeC}$ coupling of lighter

TABLE I. Comparison of $^1J_{MeC}$ (Hz) calculated using nonrelativistic and ZORA approaches (left side of the table) and different functionals (right side of the table) with experiment.

	B3LYP/TZP			so-ZORA/TZP				
Molecule	Nonrel	sc-ZORA	so-ZORA	BVP86	B3LYP	PBE0	KT2	Expt.
$Hg(CN)_2$	1742	2439	2362	1807	2362	2354	1691	3140 (Ref. 63)
$Zn(CN)_4^{2-}$	82	83	83	70	83	78	63	88 (Ref. 64)
$Cd(CN)_4^{2-}$	− 478	− 614	− 606	− 498	− 606	− 578	− 448	(−)[a] 575 (Ref. 64)
$Hg(CN)_4^{2-}$	796	1578	1522	1159	1522	1469	1054	1540 (Ref. 64)
$Tl(CN)_4^{-}$	2944	4768	4548	2731	4548	4430	2376	5440 (Ref. 65)
CuCNCuCN	809	809	809	729	809	764	672	725 ± 20 (Ref. 66)
AgCNAgCN	− 254	− 317	− 315	− 273	− 315	− 303	− 252	(−)[a] 297 ± 15 (Ref. 67)
AuCNAuCN	147	227	220	185	220	217	176	...

[a]The minus sign has not been determined in experiment.

metal nuclei the difference between relativistic and nonrelativistic results is small, and it increases with the charge of the metal nucleus. In the 12th group of periodic table the nonrelativistic calculations reproduce 99% of relativistic (spin-orbit) result for $Zn(CN)_4^{2-}$, 78% for $Cd(CN)_4^{2-}$, and only 53% for $Hg(CN)_4^{-2}$. For $Hg(CN)_2$ and $Tl(CN)_4^-$ the percentage is similar: the nonrelativistic calculations reproduce about 73% and 65% of the so-ZORA result, respectively. In the 11th group of periodic table we observe the same trend: the ratio of nonrelativistic to relativistic result is 100%, 81%, and 67% for CuCN, AgCN, and AuCN, respectively.

The difference between scalar and spin-orbit level of theory for $^1J_{MeC}$ of 4th row metals atoms is negligible (less than 1 Hz for Zn and Cu), probably because the relativistic contribution to spin-spin coupling constant is generally small. For heavier metals it is bigger and sc-ZORA results are slightly overestimated in comparison with so-ZORA. The spin-orbit coupling term is, for example, about 77 Hz lower for Hg in $Hg(CN)_2$, that is, 13% of the relativistic contribution (difference between spin-orbit and nonrelativistic result). For 11th group couplings the differences are even smaller: from less than 1 Hz for CuCN to 7 Hz for AuCN (again, it is about 10% of the relativistic contribution). For $Tl(CN)_4^-$ we observe the biggest spin-orbit effect of about 220 Hz (14% of relativistic contribution), again of the opposite sign than the scalar effects. It has been known[69] that for some thallium complexes the spin-orbit effect is more significant than for the other systems, and our results confirm this tendency.

Table I contains also the $^1J_{MeC}$ coupling constants in transition metal cyanides obtained with different exchange-correlation functionals. Hybrid functionals (B3LYP and PBE0) lead generally to good agreement with the experimental data, while the BVP86 values seem underestimated. Another non-hybrid functional, KT2, leads to even smaller values than BVP86, reproducing only 69%–75% of B3LYP result. For $Tl(CN)_4^-$ the tendency is the same, but the difference is bigger: BVP86 reproduces only 60% of the B3LYP result, and KT2 only 52% of the B3LYP result.

For the $^1J_{MeC}$ coupling constants in cyanides of metals from the 11th group of periodic table the B3LYP hybrid functional still produces the highest values, but in this case they are slightly overestimated in comparison with experiment (about 10%–15%). The BVP86 and PBE0 values are smaller, and for them we observe the best agreement with experiment in the case of CuCN (for AuCN there are no experimental data). KT2 reproduces 92%–95% of the BVP86 result (80%–83% of the B3LYP result).

Several factors should be taken into account in the comparison of the calculated NMR parameters and their experimental values. First, our model neglects environmental effects, while the experimental values for $Hg(CN)_2$ have been measured in DMSO,[63] for $Tl(CN)_4^-$ in aqueous solution,[65] and for all $Me(CN)_4^{2-}$ in solid state.[64] We have used a crude two-molecules "chain" model for 11th group cyanides, which is another source of error. Second, the experimental error bars are in some cases unknown, which in particular for the smaller couplings makes the comparison difficult.

TABLE II. The individual contributions to $^1K_{MeC}$ [10^{19} kg $m^{-2}s^{-2}A^{-2}$] (where Me = Zn, Cd, Hg, Cu, Ag, Au, Tl) calculated at the so-ZORA/B3LYP/TZP level.

Molecule	$^1K_{MeC}$	K^{DSO}	K^{PSO}	K^{FC+SD}
$Hg(CN)_2$	4315.8	0.1	− 18.4	4334.1
$Zn(CN)_4^{2-}$	435.8	0.2	− 0.6	436.2
$Cd(CN)_4^{2-}$	901.3	0.1	− 9.9	911.1
$Hg(CN)_4^{2-}$	2780.9	0.1	− 109.7	2890.5
$Tl(CN)_4^-$	2565.1	0.2	− 157.3	2722.2
CuCNCuCN	1007.6	0.2	− 0.5	1007.9
AgCNAgCN	2233.6	0.1	− 4.2	2237.7
AuCNAuCN	4127.7	0.1	− 75.0	4202.6

a. Comparison between reduced coupling constant in different cyanides. We have compared the changes of reduced $^1K_{MeC}$ with the increasing nucleus charge in the same group of periodic table. The comparison, together with individual contributions to the coupling constants, is displayed in Table II.

The Fermi contact + spin-dipole contribution is dominant for these couplings, while the diamagnetic contribution is negligible. The reduced coupling constant $^1K_{MeC}$ increases in the 12th group of periodic table, despite increasing bond length between heavy nuclei and carbon: it is twice as big for cadmium as for zinc, even though the bond length between metal and carbon is about 0.2 Å longer for cadmium. The bond lengths are similar for cadmium and mercury cyanides (HgC bond is shorter by 0.01 Å) but $^1K_{HgC}$ is about three times larger than $^1K_{CdC}$.

In the 11th group of periodic table we observe the same tendency. The reduced spin-spin coupling constant of gold is two times bigger than that of silver in spite of the same bond length between metal and carbon. $^1K_{AgC}$ is two times bigger than $^1K_{CuC}$, even though the metal–carbon bond is 0.18 Å longer for silver.

A comparison can also be made between mercury and thallium cyanides, which have a similar geometric structure and equal number of electrons. The reduced $^1K_{MeC}$ coupling constants are similar (compare the relevant rows of Table II). A difference of 216 10^{19}kg $m^{-2}s^{-2}A^{-2}$ is probably caused by the bond length variation: about 0.08 Å between R(TlC) and R(HgC) (R(TlC) is shorter).

2. The $^2J_{MeN}$ and $^1J_{MeN}$ spin-spin coupling constants

Although there are less experimental data for nitrogen coupling constants than for the $^1J_{MeC}$ coupling constant in cyanides, we have decided to investigate also $^2J_{MeN}$ and (for chain structures of CuCN, AgCN, and AuCN) $^1J_{MeN}$. The relativistic and nonrelativistic results for $^2J_{MeN}$ and $^1J_{MeN}$ are tabulated in Table III.

For $^2J_{MeN}$ the comparison of nonrelativistic and relativistic (scalar and spin-orbit) results leads to the same observations as in the case of $^1J_{MeC}$. For the nuclei of 4th and 5th row of periodic table the differences between nonrelativistic, scalar, and spin-orbit results are negligible (from 0.1 Hz to 2 Hz). The relativistic contributions dominate for cyanides of the 6th row metals, especially for $Hg(CN)_2$, where

TABLE III. Comparison of $^2J_{\mathrm{MeN}}$ and $^1J_{\mathrm{MeN}}$ (Hz) calculated using nonrelativistic and ZORA approaches (left side of the table) and different functionals at the so-ZORA level (right side of the table) with experiment.

	B3LYP/TZP			so-ZORA/TZP				
Molecule	Nonrel	sc-ZORA	so-ZORA	BVP86	B3LYP	PBE0	KT2	Expt.
$Hg(CN)_2$	− 62.6	− 18.4	− 37.3	− 6.6	− 37.3	− 46.3	3.2	(−)[a] 101 (Ref. 63)
$Zn(CN)_4^{2-}$	− 2.5	− 2.4	− 2.3	− 2.0	− 2.3	− 2.6	− 1.5	…
$Cd(CN)_4^{2-}$	13.1	11.8	11.8	8.9	11.8	14.0	6.1	…
$Hg(CN)_4^{2-}$	− 23.4	− 5.2	− 5.3	6.9	− 5.3	− 11.2	13.2	29.0 ± 2.0 (Ref. 93)
$Tl(CN)_4^-$	− 25.4	171.1	157.2	225.4	157.2	132.4	235.9	…
CuCNCuCN	− 32.9	− 30.9	− 31.4	− 25.7	− 31.4	− 35.0	− 21.4	…
AgCNAgCN	10.2	10.7	11.1	9.0	11.1	12.5	7.4	…
AuCNAuCN	− 7.5	− 5.5	− 7.5	− 10.2	− 7.5	− 8.3	− 10.5	…
CuCNCuCN	− 170.2	− 162.6	− 162.2	− 156.9	− 162.2	− 159.7	− 147.3	−250 ± 15 (Ref. 66)
AgCNAgCN	58.6	67.9	67.4	60.2	67.4	68.0	56.1	…
AuCNAuCN	− 68.1	− 87.0	− 83.6	− 76.8	− 83.6	− 85.9	− 75.1	…

[a]The minus sign has not been determined in experiment.

nonrelativistic result overweighs the relativistic one (spin-orbit) by 168%, and scalar relativistic and spin-orbit effects act in the opposite directions (the sc-ZORA result is only 49% of the so-ZORA result). In contrast to that the difference between scalar and spin-orbit result for $^2J_{\mathrm{MeN}}$ in $Hg(CN)_4^{2-}$ is small (about 0.1 Hz) but nonrelativistic result is about five times larger than the so-ZORA value. For $^2J_{\mathrm{MeN}}$ in $Tl(CN)_4^-$ the nonrelativistic result has an opposite sign to the relativistic values (both scalar and including spin-orbit coupling), and the difference between sc-ZORA and so-ZORA result is 13.9 Hz (it is 8% of the total relativistic contribution). For $^2J_{\mathrm{MeN}}$ in AuCN the scalar relativistic effects and spin-orbit coupling act again in the opposite directions, and the outcome is that the nonrelativistic result is in good agreement with the so-ZORA value, while sc-ZORA reproduces only 73% of the total relativistic value. We stress again that $^2J_{\mathrm{MeN}}$ calculated for the 11th group may not be in good agreement with the experiment data because of the use of a two-molecules "chain" model in which one of the coupled nuclei of $^2J_{\mathrm{MeN}}$ is a terminal one, which is a crude approximation of the actual structure.

For the 11th group we have also calculated $^1J_{\mathrm{MeN}}$ in a "chain" model described above. For CuCN the difference between the nonrelativistic and spin-orbit result is rather small (8 Hz, which constitutes 5% of the total relativistic result). The spin-orbit effects are negligible for molecules containing copper and silver. For molecule containing gold the difference between scalar and total relativistic result is bigger (about 3.4 Hz, that is 22% of the full relativistic contribution). For AgCN and AuCN the nonrelativistic results reproduce 87% and 81% of the total relativistic values, respectively.

A comparison of the $^2J_{\mathrm{MeN}}$ and $^1J_{\mathrm{MeN}}$ spin-spin coupling constants as calculated with different exchange-correlation functionals is also shown in Table III. For all molecules except $Tl(CN)_4^-$ the B3LYP values are smaller than the PBE0 ones (47–90%), while for $^2J_{\mathrm{TlN}}$ in $Tl(CN)_4^-$ PBE0 reproduces 84% of the B3LYP result. For mercury cyanides the sign of this coupling constant (not known from NMR experiment) changes with the choice of an exchange-correlation functional.

a. Comparison of the reduced coupling constant between different cyanides. Table IV contains the values of the reduced $^1K_{\mathrm{MeN}}$ and $^2K_{\mathrm{MeN}}$ coupling constants for the 12th and 11th group of periodic table together with the individual contributions to them. For $^2K_{\mathrm{MeN}}$ in the 12th group of periodic table the magnitude of the reduced coupling constant changes in a non-monotonic fashion with the metal charge: the absolute value increases when going from the Zn to Cd compound but decreases for the Hg compound. The paramagnetic spin-orbit and Fermi contact with spin-dipole contributions are dominant, and the PSO contribution increases with the charge of the heavy nucleus. Diamagnetic spin-orbit contributions are negligible. For 11th group cyanides we observe similar tendencies but the magnitude of reduced coupling constant increases in monotonic fashion with the heavy nucleus charge and the PSO term is smaller in comparison with the FC + SD term.

For $^1K_{\mathrm{MeN}}$ in the 11th group of periodic table both DSO and PSO terms are negligible, and the coupling is dominated by the FC + SD contribution. The magnitude of reduced coupling constant increases with the charge of heavy nucleus (the

TABLE IV. The individual contributions to $^2K_{\mathrm{MeN}}$ and $^1K_{\mathrm{MeN}}$ (10^{19} kg $m^{-2}s^{-2}A^{-2}$), where Me = Zn, Cd, Hg, Cu, Ag, Au, Tl calculated at the so-ZORA/B3LYP/TZP level.

	K_{MeN}	K^{DSO}	K^{PSO}	$K^{\mathrm{FC+SD}}$
$Hg(CN)_2$	169.3	− 0.1	131.1	38.3
$Zn(CN)_4^{2-}$	30.6	− 0.1	12.1	18.6
$Cd(CN)_4^{2-}$	43.6	− 0.1	17.4	26.3
$Hg(CN)_4^{2-}$	24.2	− 0.1	35.6	− 11.3
$Tl(CN)_4^-$	− 219.9	− 0.1	41.0	− 260.8
CuCNCuCN	97.1	− 0.2	12.9	84.4
AgCNAgCN	194.5	− 0.1	22.2	172.4
AuCNAuCN	349.2	− 0.1	74.3	275.0
CuCNCuCN	501.2	0.2	0.0	501.0
AgCNAgCN	1183.9	0.2	5.2	1178.5
AuCNAuCN	3881.1	0.2	20.4	3860.5

TABLE V. Comparison of $^1J_{CN}$ (Hz) calculated using nonrelativistic and ZORA approaches (left side of the table) and different functionals at the so-ZORA level (right side of the table).

	B3LYP/TZP			so-ZORA/TZP			
Molecule	Nonrel	sc-ZORA	so-ZORA	BVP86	B3LYP	PBE0	KT2
$Hg(CN)_2$	−15.8	−13.2	−12.8	−2.8	−12.8	−15.3	0.6
$Zn(CN)_4^{2-}$	−13.9	−13.4	−13.3	−6.2	−13.3	−14.6	−2.7
$Cd(CN)_4^{2-}$	−12.9	−12.0	−11.9	−4.6	−11.9	−13.2	−1.3
$Hg(CN)_4^{2-}$	−13.4	−10.8	−10.6	−2.8	−10.6	−11.9	0.4
$Tl(CN)_4^{-}$	−14.4	−10.8	−10.4	−1.5	−10.4	−12.1	1.6
CuCNCuCN	−21.5	−21.5	−21.5	−13.8	−21.5	−22.8	−8.7
AgCNAgCN	−17.8	−18.3	−18.2	−9.8	−18.2	−19.3	−5.6
AuCNAuCN	−12.6	−22.8	−23.8	−8.9	−23.8	−24.9	−2.7

biggest difference is observed between silver and gold couplings: $^1K_{AuN}$ is about 3 times larger than $^1K_{AgN}$).

3. The $^1J_{CN}$ spin-spin coupling constant

Table V contains the $^1J_{CN}$ spin-spin coupling constant calculated for transition metal cyanides under investigation. Even though the heavy atom is not in the coupling path, the coupling is visibly affected by the HALA effect. The relativistic effects are relatively small for 4rd and 5th row metal cyanides (less than 5% of the total value), but they are sizeable for the cyanides containing the heaviest metals: for thallium compound the difference between nonrelativistic and so-ZORA value is 4 Hz (38%), for mercury compounds it is 23% and 26% and for AuCN it is 47%. It is worth noting that the HALA effect for $^1J_{CN}$ is mostly (≈90%) caused by the scalar relativistic effects.

The values of the $^1J_{CN}$ spin-spin coupling constant obtained with different exchange-correlation functionals are also shown in Table V. The main difference is between hybrid and non-hybrid functionals: while the PBE0 and B3LYP results are similar, BVP86 reproduces only 48% of the B3LYP result for zinc compound and only 21% for $Hg(CN)_2$. It is also worth noting that KT2 renders the sign opposite to the other functionals for the heaviest metals (mercury and thallium). This is not specific for relativistic Hamiltonians, since equally strong dependence of the calculated $^1J_{CN}$ coupling on the employed exchange correlation functional has been observed in nonrelativistic calculations for HCN (where PBE0 renders 17.1 Hz and KT2 5.1 Hz) and CN^- (7.6 Hz and 1.2 Hz, respectively). A similar tendency (very large differences between the results of calculations with hybrid and non-hybrid functionals) has been observed before for $^1J_{CO}$ in CO and $^1J_{NN}$ in N_2.[3]

a. Comparison of $^1J_{CN}$ between different cyanides. The $^1J_{CN}$ coupling constant varies considerably with the metal substituent, even though the calculated CN bond lengths are practically the same for all systems under study (in the 12th group of periodic table). The variation of $^1J_{CN}$ can be therefore related to purely electronic effects and to the variation in the bond lengths between heavy atom and carbon (about 0.2 Å between zinc and mercury compound).

TABLE VI. Comparison of four-component results for the spin-spin coupling constants (Hz) in $Hg(CN)_2$ obtained using aug-cc-pVTZ-J (C,N) and dyall.v3z (Hg) basis sets and different exchange-correlation functionals.

Functional	$^1J_{HgC}$	$^2J_{HgN}$	$^1J_{CN}$
B3LYP	2481	−62.2	−6.9
PBE0	2476	−66.5	−6.1
BP86	1964	−21.3	2.9
KT2	1973	4.6	3.9
ZORA (B3LYP/TZP)	2362	−37.3	−12.8

In the 11th group the value of $^1J_{CN}$ is much larger than for the other cyanides under study, probably because of the effect of alternating triple bonds in a chain structure. It changes in a non-monotonic fashion with the metal nucleus charge: the absolute value of $^1J_{CN}$ decreases when going from Cu to Ag (like in the 12th group), but increases for Au. The carbon-nitrogen bond length difference between copper and silver compound is small (0.01 Å) but between silver and gold it is much bigger (0.05 Å). The geometry is probably the reason why $^1J_{CN}$ changes in non-monotonic fashion: silver cyanide has the shortest R(CN) bond length and the largest R(MeN) bond length.

4. Four-component calculations of the spin-spin coupling constants

In order to gain a further insight into the relativistic effects on the NMR parameters of transition metal cyanides, we have performed four-component DFT calculations for $Hg(CN)_2$, the smallest molecule with heavy nucleus from the set under study. The results are displayed in Table VI. The difference between $^1J_{HgC}$ calculated in four-component calculations and "best" (closest to the experiment) ZORA B3LYP/jcpl result of 2731 Hz is about 250 Hz, and the ZORA value is closer to the experiment. However, for $^2J_{HgN}$ four-component calculation leads to the result closer to experiment than ZORA: −62.2 Hz vs −47.6 Hz, while the experimental result is (−)101 Hz (Ref. 63) (the minus sign comes from the calculations). In principle, the four-component calculations should be more accurate, but it should be taken into account when making a comparison with experiment that our calculations completely neglect environmental effects which may be of the opposite sign than the relativistic effects not included in ZORA calculations (environmental effects for $Hg(CN)_2$ are discussed, for example, in Refs. 33 and 89). The largest difference (in relative terms) between ZORA and four-component results is observed for $^1J_{CN}$. Unfortunately, we do not have in this case experimental data for comparison.

The comparison of ZORA and Dirac-Kohn-Sham results is not straightforward, since, out of necessity, different basis sets have been used (ADF employs Slater orbital basis set, while in DIRAC Gauss orbitals are used). Therefore, in order to check whether the difference between ZORA and DKS result is not a result of a deficiency of the employed Gaussian basis set, we have carried out also investigation of basis set effects for $Hg(CN)_2$. Using double-ζ Dyall basis set for mercury and double-ζ Dunning basis set for light atoms produces the result for $^1J_{HgC}$ which differs only by 90 Hz

TABLE VII. Comparison of point-nucleus model and finite-nucleus model in ZORA with two types of basis sets and B3LYP functional for the spin-spin coupling constants in $Hg(CN)_2$ (in Hz).

	TZP		jcpl	
	Point-nucleus	Finite-nucleus	Point-nucleus	Finite-nucleus
$^1J_{MeC}$	2362	2335	2731	2497
$^2J_{MeN}$	− 37.3	− 37.6	− 47.6	− 47.2
$^1J_{CN}$	− 12.8	− 12.8	− 3.1	− 2.9

from the triple-ζ one, while reducing the computation time threefold. We have also performed calculations with Dyall basis set with additional even-tempered Gaussian functions: four *s* functions and four *p* functions. We have received practically the same result as for the original basis set (1 Hz difference). Therefore, it does not seem probable that deficiencies of a Gaussian basis set are a main cause of the discrepancy between the ZORA and four-component results.

Another factor which may influence the calculated spin-spin coupling constants is the nucleus model. The presented four-component results have been obtained with the Gaussian charge distribution, while for the results obtained in ADF point-nucleus model has been used. A detailed investigation of this issue is beyond the scope of this paper, but a limited comparison (for $Hg(CN)_2$ only) is shown in Table VII. As expected,[90] the difference between point-nucleus model and finite-nucleus model depends on the employed basis set, and it is much larger if a basis set with tight exponents is used (in this case jcpl). It is rewarding that the use of the jcpl basis set together with finite-nucleus model in ADF still leads to good agreement with the four-component Dirac result (better than for point-nucleus model with TZP basis set). We can also conclude that it would not make much sense to use finite-nucleus model in conjunction with the TZP basis set (as mentioned above, jcpl is not available for some of the elements of interest, so for consistency we decided to use TZP).

The variation of the spin-spin coupling constants in $Hg(CN)_2$ with the choice of different exchange-correlation functional is similar for Dirac-Kohn-Sham and ZORA calculations (compare Table VI with Tables I, III, and V). The changes in magnitude of the $^1J_{MeC}$ coupling constant calculated using the DKS approach with different functionals mirror that of the ZORA results. Like for ZORA, the geminal $^2J_{MeN}$ coupling constant calculated using KT2 has the opposite sign than the PBE0 and B3LYP results, and the BP86 result is much lower than the others in absolute value. For $^1J_{CN}$ we also observe a similar tendency in the two-component and four-component calculations: non-hybrid functionals lead to an opposite sign in comparison with hybrid functionals.

B. Shielding constants

Now we shall discuss the NMR shielding constants calculated for the cyanides under investigation. Similarly, as in the case of spin-spin coupling constants, ZORA results are going to be discussed first, and then we will proceed to discuss the four-component results.

TABLE VIII. Comparison of σ_{Me} (ppm) calculated using nonrelativistic and ZORA approaches (left side of the table) and different functionals at the so-ZORA level (right side of the table).

	B3LYP/TZP			so-ZORA/TZP			
Molecule	Nonrel	sc-ZORA	so-ZORA	BVP86	B3LYP	PBE0	KT2
$Hg(CN)_2$	7353	7116	9980	9805	9980	10 060	9916
$Zn(CN)_4^{2-}$	1501	1443	1538	1443	1538	1564	1507
$Cd(CN)_4^{2-}$	3303	3160	3618	3516	3618	3652	3602
$Hg(CN)_4^{2-}$	6715	6109	8932	8623	8932	9010	8734
$Tl(CN)_4^-$	6755	6407	9457	9173	9457	9532	9318
CuCN**Cu**CN	1168	1102	1220	991	1220	1276	1020
AgCN**Ag**CN	3383	3271	3750	3640	3750	3808	3712
AuCN**Au**CN	6643	6042	8954	8670	8954	9080	8634

1. Metal shielding constant

The σ_{Me} isotropic shielding constants calculated using ZORA and nonrelativistic approaches are shown in Table VIII. The scalar effects on the shielding constants of heavy metal nuclei are on the average somewhat smaller than for the spin-spin coupling constants in the same systems. The scalar effects work in the opposite direction (leading to deshielding) in comparison with spin-orbit coupling effects, but the latter are much larger, especially for the heaviest nuclei. Because of this, while in the 12th group of periodic table the nonrelativistic results for zinc and cadmium shielding are in good agreement with relativistic ones (the difference is only 3% and 9% for zinc and cadmium, respectively), the difference is much bigger for mercury shielding in $Hg(CN)_4^{2-}$ and $Hg(CN)_2$: about 25%–26%. For the 11th group of periodic table the tendency is similar: the relativistic effects on σ_{Me} are about 4%–10% for lighter metals and about 25% for gold.

The choice of a functional has a smaller effect on the calculated σ_{Me} than on the spin-spin coupling constants. For molecules containing zinc, cadmium, mercury, and thallium the non-hybrid functional BVP86 systematically underestimates the shielding constant calculated using B3LYP hybrid functional, while PBE0 somewhat overestimates it. The KT2 results are, as a rule, between the BVP86 and B3LYP results (only for AuCN the KT2 result is slightly smaller than BVP86 result), and are in good agreement (95%–99%) with the B3LYP results for lighter metal nuclei (except for CuCN where the KT2 result is only 83% of the B3LYP result).

When analysing the trends in σ_{Me} in cyanides of the same group of periodic table we observe that in the 12th group the value of the heavy atom shielding constant is rising from zinc to mercury, and this is caused mainly by the growing magnitude of diamagnetic contribution connected with electronic density (the difference of the diamagnetic term between zinc and mercury compound is about 7100 ppm and of the paramagnetic term about 2700 ppm). The same tendency can be observed in the 11th group of periodic table.

2. Carbon and nitrogen shielding constant

It is also instructive to examine the HALA effects on the light atom shielding constants, tabulated in Table IX. For 4th

TABLE IX. Comparison of σ_N and σ_C (ppm) calculated using nonrelativistic and ZORA approaches.

	σ_N			σ_C		
Molecule	Nonrel	sc-ZORA	so-ZORA	Nonrel	sc-ZORA	so-ZORA
$Hg(CN)_2$	− 111.7	− 88.9	− 89.1	59.6	64.2	40.1
$Zn(CN)_4^{2-}$	− 46.0	− 45.1	− 44.1	34.0	34.1	33.8
$Cd(CN)_4^{2-}$	− 53.4	− 51.1	− 50.4	36.2	36.8	33.7
$Hg(CN)_4^{2-}$	− 57.9	− 47.5	− 47.8	36.7	39.1	28.5
$Tl(CN)_4^-$	− 91.6	− 74.6	− 75.2	53.8	55.2	41.0
Cu**CN**CuCN	− 16.0	− 16.7	− 15.8	53.1	54.6	55.6
Ag**CN**AgCN	− 9.2	− 4.8	− 8.6	50.3	54.4	53.4
Au**CN**AuCN	− 24.4	− 7.9	− 23.1	43.1	67.2	78.4

and 5th row of periodic table the relativistic effects for carbon and nitrogen are small (less than 7% of the total value). However, for the 6th row they are much bigger: from about 20%–25% for σ_N and about 30% for σ_C in $Me(CN)_4^{n-}$ anions to 48% and 45% for σ_C in $Hg(CN)_2$ and AuCNAuCN, respectively. Interestingly, for the 12th group of periodic table the relativistic effect leads to ^{13}C deshielding and for the 11th group to increased shielding of carbon. Another important observation is that the HALA effect in the 12th group for σ_C is mostly caused by spin-orbit effects and for σ_N by scalar effects. It is known[91] that for systems containing orbitals with larger *s*-character spin-orbit couplings effects are important, but this is apparently not necessarily true for shieldings of nuclei which are not in the immediate neighbourhood of the heavy atom. The relativistic effects influence mostly the paramagnetic terms for both σ_N and σ_C.

3. Four-component calculations of the shielding constants

Finally, we present the results of the four-component calculations of the shielding constants. Two sets of calculations have been carried out, one using the magnetic balance approach (available in RESPECT) and one using the "simple" kinetic balance approach numerically equivalent to unrestricted kinetic balance (available in DIRAC). The second set of calculations has been performed for $Hg(CN)_2$ only, using different exchange-correlation functionals.

TABLE XI. Comparison of four-component results for nuclear shieldings constants (ppm) in $Hg(CN)_2$ obtained using DIRAC program (upc-2 and dyall.v3z basis set) and RESPECT program (upc-2 and dyall.v3z basis set).

	Functional	σ_{Hg} (ppm)	σ_C (ppm)	σ_N (ppm)
DIRAC	B3LYP	12 570	27.7	−93.3
DIRAC	PBE0	12 657	31.4	−92.3
DIRAC	BP86	12 355	34.3	−80.4
RESPECT	BP86	12 494	34.5	−79.5

The results for the first set of four-component calculations are compared with the shielding constants calculated using ZORA Hamiltonian in Table X. As far as the heavy atom shielding is concerned, ZORA reproduces about 90% of the four-component results for 5th row of periodic table, while for 6th row of periodic table it reproduces only 75%–79% of four-component results. ZORA (including spin-orbit coupling) therefore systematically underestimates the relativistic effect on the heavy atom shielding constant.

Table X exhibits also the calculated carbon and nitrogen shielding constants, so the HALA effect calculated using Dirac-Kohn-Sham and ZORA approach can be compared. For all light atoms (except carbon in compound containing gold) inclusion of the four-component term leads to deshielding of light atoms. The differences are quite big especially for ^{13}C shielding constants: for σ_C in mercury cyanide the ZORA-DKS difference is about 40%–43% and for thallium cyanide about 23% of the DKS result. As expected, for cadmium cyanide the difference is smaller (about 32%) than in $Hg(CN)_4^{2-}$ because cadmium is lighter than mercury. For the 11th group of periodic table for compound containing silver we observe similar tendency as in the 12th group, but for gold compound the tendency is opposite: including four-component terms leads to increasing shielding (which is probably connected with large spin-orbit coupling effect in this compound). For nitrogen in case of the 12th group of periodic table and for thallium compound the ZORA-DKS differences are small (5%–16%), probably because nitrogen is farther than carbon from the heavy atom. For the 11th group of periodic table the ZORA-DKS differences on σ_N are much bigger, since nitrogen is bonded there with heavy atom. For σ_N in silver cyanide the DKS result has the opposite sign than ZORA and for gold cyanide the DKS-ZORA difference

TABLE X. Comparison of σ_{Me}, σ_N, and σ_C (ppm) calculated with PBE functional using nonrelativistic, so-ZORA, and DKS approach (ADF and RESPECT calculations, respectively). TZP basis set has been used for the nonrelativistic and ZORA calculation. upc-2 for carbon and nitrogen and dyall.v3z for heavy metal have been used for the DKS calculations.

	σ_{Me}			σ_N			σ_C		
	Nonrel	ZORA	DKS	Nonrel	ZORA	DKS	Nonrel	ZORA	DKS
$Hg(CN)_2$	7297	9812	12 464	− 100.9	− 76.4	− 80.8	65.6	48.4	34.4
$Cd(CN)_4^{2-}$	3229	3527	3927	− 45.4	− 42.0	− 48.5	42.9	40.8	31.0
$Hg(CN)_4^{2-}$	6576	8635	11 463	− 50.1	− 38.4	− 45.7	43.7	37.0	25.8
$Tl(CN)_4^-$	6662	9195	11 895	− 82.4	− 63.7	− 70.5	59.6	48.3	39.1
Ag**CNAg**CN	3327	3631	4017	0.9	1.5	− 7.4	59.8	63.6	57.9
Au**CNAu**CN	6497	8631	11 194	− 10.5	− 13.2	− 27.9	57.7	95.5	101.3

TABLE XII. Comparison of chemical shifts δ_{Hg}, δ_N, and δ_C (ppm) shifted with HCN reference in case of δ_N and δ_C and $Hg(CN)_4^{2-}$ as reference in case of δ_{Hg}. All results have been calculated with PBE functional using nonrelativistic, so-ZORA, and DKS approach (ADF and RESPECT calculations, respectively). TZP basis set has been used for nonrelativistic, ZORA calculation and upc-2 for carbon and nitrogen and dyall.v3z basis sets for heavy metal for DKS calculations.

	δ_{Me}			δ_N			δ_C		
	Nonrel	ZORA	DKS	Nonrel	ZORA	DKS	Nonrel	ZORA	DKS
$Hg(CN)_2$	−726	−1187	−1013	61.1	37.5	37.3	10.2	27.6	37.8
$Cd(CN)_4^{2-}$	…	…	…	5.6	3.1	5.0	33.0	35.3	41.3
$Hg(CN)_4^{2-}$	…	…	…	10.3	− 0.4	2.3	32.1	39.1	46.5
$Tl(CN)_4^-$	…	…	…	42.6	24.8	27.0	16.2	27.8	33.1
Ag**CNAg**CN	…	…	…	− 40.7	− 40.4	− 36.0	16.0	12.5	14.3
Au**CNAu**CN	…	…	…	− 29.3	− 25.7	− 15.5	18.1	− 19.5	− 29.1

is about 50% of the DKS result. We should stress however that this comparison is not consistent because we use not only other types of Hamiltonian but also different basis sets (Slater type orbitals for ZORA and Gauss type orbitals for DKS) and the ZORA-DKS differences are affected by this fact.

Hybrid functionals are not available at present in RESPECT program, therefore for completeness we have decided to perform four-component calculations of shielding constants for $Hg(CN)_2$ using DIRAC program with B3LYP, PBE0 hybrid, and BP86 non-hybrid functionals. The results are shown in Table XI. For mercury shielding the difference between BP86 and B3LYP is small (about 2% of B3LYP result), but for lighter atoms differences are much bigger (about 24% for σ_N and about 14% for σ_C). A similar tendency has been observed in ZORA results: the difference between BVP86 and B3LYP is 15% for σ_N and about 20% for σ_C.

A comparison can be made between RESPECT and DIRAC results obtained using the same BP86 functional (compare two last lines in Table XI). We should stress that this comparison is not consistent, since the employed basis set is different even for the large component (in case of RESPECT calculation additional auxiliary basis sets are used) and different treatments of magnetic balance affect the small component. Even so, the results for RESPECT and DIRAC are close to each other (the differences are about 1%).

Large differences between ZORA and four-component results should at least partially cancel out if chemical shifts instead of absolute shielding constants are compared. For this reason we have converted the calculated shieldings into chemical shifts (see Table XII). In the case of carbon and nitrogen chemical shifts the carbon and nitrogen nuclei in HCN molecule have been used as a reference. In the case of heavy atom only chemical shift of mercury nucleus has been calculated (using shielding constant of mercury in $Hg(CN)_4^{2-}$ as a reference), since finding suitable references for the other heavy nuclei is problematic.

The differences between chemical shifts calculated using ZORA and DKS methods are smaller than that for shielding constants, but still non-negligible. In the case of chemical shift of mercury ZORA calculation leads to overestimation of the DKS result by about 17%. In the case of carbon chemical shifts for molecules containing 5th row metals the differences between ZORA and DKS are from 2 ppm to 6 ppm (i.e., about 13%–15% of the DKS result). For molecules containing 6th row metals differences are from 5 to 8 ppm in case of $Hg(CN)_4^{2-}$ and $Tl(CN)_4^-$ (about 16% of DKS result) and about 10 ppm for $Hg(CN)_2$ and AuCNAuCN (about 27% and 33% of DKS result, respectively). In case of nitrogen chemical shifts differences are smaller in comparison with carbon chemical shifts (they do not exceed 4.5 ppm), especially for molecules where nitrogen is not directly bonded with heavy metal. Only for AuCNAuCN difference is bigger (about 10 ppm) but this is probably caused by nitrogen being directly bonded with gold for this molecule.

In the case of shielding constants, the finite-nucleus model is implemented in ADF in SCF step only. Test ZORA calculation with finite-nucleus in the SCF step for Hg shielding in $Hg(CN)_2$ shows that the difference between the two approaches is negligible when TZP basis set is used (9788 ppm for Gaussian charge distribution and 9805 for point nuclear model in BVP86 calculations, i.e., about 0.2% difference). Thus, this effect has not been investigated any further.

IV. SUMMARY AND CONCLUSIONS

Relativistic DFT calculations of nuclear spin-spin coupling constants and shielding constants have been performed for selected transition metal (11th and 12th group of periodic table) and thallium cyanides. The properties have been computed using ZORA Hamiltonian and four-component DKS Hamiltonian with different XC functionals. Two recent approaches for representing the MB between the large and small components of four-component spinors, namely, mDKS-RMB and sMB, have been employed and the results of shielding tensor calculations have been compared. Relativistic effects have been also analysed in terms of scalar and spin-orbit contributions at the two-component level of theory, including discussion of HALA effects for $^1J_{CN}$, σ_C, and σ_N. The main conclusions can be summarized as follows.

The results for molecules containing metals from 4th row of periodic table show that the relativistic effects for them are, as expected, small (especially for spin-spin coupling

constants). The biggest effects have been observed for 6th row where nonrelativistic theory reproduces the two-component ZORA results by only about 50%–70% for $^1J_{MeC}$ and about 75% for heavy metal shielding constants. The total relativistic effect for the shielding constants is usually an interplay of scalar and spin-orbit effects (not always of the same sign), with the SO contribution dominant for heavy nuclei and light nuclei in their immediate neighbourhood. Scalar effects are dominant for the $^1J_{MeC}$ coupling constant, but spin-orbit coupling is significant for $^2J_{MeN}$ (and $^1J_{MeN}$ in chain structures). Interestingly, the HALA effect on $^1J_{CN}$ seems to originate mostly from the scalar relativistic effects, unlike the HALA effect on the ^{13}C and ^{15}N shielding constants. Large influence of spin-orbit coupling on the latter is probably connected with large *s*-character of the CN bond in cyanides.

The comparison of ZORA and four-component calculations for $^1J_{HgC}$ and $^2J_{HgN}$ in $Hg(CN)_2$ indicates that ZORA performs very well for heavy metal spin-spin coupling constants. The small variation between ZORA and four-component results is as expected from the analysis of accuracy of hyperfine integrals in ZORA.[92] As far as the heavy atom shielding is concerned, ZORA reproduces about 89%–90% of the four-component results for 5th row of periodic table, while for 6th row of periodic table it reproduces only 75%–78% of the four-component results. ZORA (including spin-orbit coupling) therefore systematically underestimates the relativistic effect on the heavy atom shielding constant. In the case of ^{13}C and ^{15}N shielding constants, the performance of ZORA with respect to four-component calculations depends on the position of the light atom with respect to the heavy atom: the discrepancies are large for shielding constants of nuclei which are immediate neighbours of heavy atom, but much smaller for other nuclei (which is probably a consequence of different role of spin-orbit coupling in these situations). As expected, the ZORA-DKS differences are smaller for chemical shifts than for the shielding constants.

The shielding constants calculated by means of four-component DFT using two approaches for representing the MB between the large and small components of four-component spinors (mDKS-RMB implemented in RESPECT and sMB implemented in DIRAC) are comparable: the discrepancies do not exceed 1%, even though different basis sets are used.

The calculated spin-spin coupling constants are very sensitive to the choice of exchange-correlation functional (in some cases even the sign of the calculated coupling constant depends on the functional chosen). Hybrid functionals B3LYP and PBE0 lead in most cases to the higher values of the spin-spin coupling constants than GGA functionals and better agreement with experiment, while KT2 (designed for the shielding constants) fails for the spin-spin coupling constants. The variation of the calculated shielding constants with the choice of exchange-correlation functional is somewhat smaller than for the calculated spin-spin coupling constants, and the trends are the same independently on the chosen Hamiltonian. For the heavy metal shielding constants hybrid functionals produce the highest values.

ACKNOWLEDGMENTS

This work has received support from the Polish Ministry of Science and Higher Education via Grant No. N N204 148565, and from the Wrocław Centre for Networking and Supercomputing through a grant of computer time. MPD/2010/4 project, realized within the MPD programme of Foundation for Polish Science, cofinanced from European Union, Regional Development Fund, is acknowledged for a fellowship to A. Wodyński. The project has been carried out with the use of CePT infrastructure financed by the European Union—the European Regional Development Fund within the Operational Programme "Innovative economy" for 2007–2013. The COST-CMTS Action CM1002 COnvergent Distributed Environment for Computational Spectroscopy (CODECS) and the support granted by Iceland, Liechtenstein, and Norway by means of cofinancing from the European Economic Area Financial Mechanism and the Norwegian Financial Mechanism as part of the Scholarship and Training Fund are also acknowledged.

[1] J. Vaara, J. Jokisaari, R. E. Wasylishen, and D. L. Bryce, Prog. Nucl. Magn. Reson. Spectrosc. **41**, 233 (2002).
[2] R. H. Contreras, V. Barone, J. C. Facelli, and J. E. Peralta, in *Annual Reports on NMR Spectroscopy* (Academic, 2003), Vol. 51, p. 167.
[3] T. Helgaker, M. Jaszuński, and M. Pecul, Prog. Nucl. Magn. Reson. Spectrosc. **53**, 249 (2008).
[4] L. B. Krivdin, and R. H. Contreras, in *Annual Reports on NMR Spectroscopy*, edited by G. Webb (Academic, 2007), Vol. 61, p. 133.
[5] T. Helgaker, M. Jaszuński, and K. Ruud, Chem. Rev. **99**, 293 (1999).
[6] M. Kaupp, M. Bühl, and V. G. Malkin, *Calculation of NMR and EPR parameters: Theory and Applications* (Wiley-VCH, Weinheim, 2004).
[7] P. Pyykkö, A. Görling, and N. Rösch, Mol. Phys. **61**, 195 (1987).
[8] M. Kaupp, O. L. Malkina, V. G. Malkin, and P. Pyykkö, Chem.-Eur. J. **4**, 118 (1998).
[9] P. Manninen, K. Ruud, P. Lantto, and J. Vaara, J. Chem. Phys. **122**, 114107 (2005).
[10] P. Manninen, K. Ruud, P. Lantto, and J. Vaara, J. Chem. Phys. **124**, 149901 (2006).
[11] P. Manninen, P. Lantto, J. Vaara, and K. Ruud, J. Chem. Phys. **119**, 2623 (2003).
[12] M. Hanni, P. Lantto, M. Iliaš, H. J. A. Jensen, and J. Vaara, J. Chem. Phys. **127**, 164313 (2007).
[13] J. Vaara, P. Manninen, and P. Lantto, in *Calculation of NMR and EPR Parameters: Theory and Applications*, edited by M. Kaupp, M. Bühl, and V. G. Malkin (Wiley-VCH, Weinheim, 2004), p. 209.
[14] J. Roukala, A. F. Maldonado, J. Vaara, G. A. Aucar, and P. Lantto, Phys. Chem. Chem. Phys. **13**, 21016 (2011).
[15] J. Vaara, K. Ruud, and O. Vahtras, J. Comput. Chem. **20**, 1314 (1999).
[16] J. I. Melo, M. C. Ruiz de Azúa, J. E. Peralta, and G. E. Scuseria, J. Chem. Phys. **123**, 204112 (2005).
[17] V. G. Malkin, O. L. Malkina, and D. R. Salahub, Chem. Phys. Lett. **221**, 91 (1994).
[18] O. L. Malkina, D. R. Salahub, and V. G. Malkin, J. Chem. Phys. **105**, 8793 (1996).
[19] M. Hricovini, O. L. Malkina, F. Bizik, L. T. Nagy, and V. G. Malkin, J. Phys. Chem. A **101**, 9756 (1997).
[20] R. M. Dickson and T. Ziegler, J. Phys. Chem. **100**, 5286 (1996).
[21] V. Sychrovský, J. Gräfenstein, and D. Cremer, J. Chem. Phys. **113**, 3530 (2000).
[22] T. Helgaker, M. Watson, and N. C. Handy, J. Chem. Phys. **113**, 9402 (2000).
[23] S. A. Perera, H. Sekino, and R. J. Bartlett, J. Chem. Phys. **101**, 2186 (1994).
[24] J. F. Stanton and J. Gauss, Int. Rev. Phys. Chem. **19**, 61 (2000).
[25] A. A. Auer and J. Gauss, J. Chem. Phys. **115**, 1619 (2001).
[26] A. A. Auer, J. Gauss, and M. Pecul, Chem. Phys. Lett. **368**, 172 (2003).
[27] O. Vahtras, H. Ågren, P. Jørgensen, H. J. A. Jensen, S. B. Padkjær, and T. Helgaker, J. Chem. Phys. **96**, 6120 (1992).

[28]J. Autschbach and T. Ziegler, J. Chem. Phys. **113**, 936 (2000).
[29]J. Autschbach and T. Ziegler, J. Chem. Phys. **113**, 9410 (2000).
[30]M. Filatov and D. Cremer, J. Chem. Phys. **120**, 11407 (2004).
[31]J. Autschbach, C. D. Igna, and T. Ziegler, J. Am. Chem. Soc. **125**, 1028 (2003).
[32]J. Autschbach and T. Ziegler, J. Am. Chem. Soc. **123**, 5320 (2001).
[33]J. Autschbach and T. Ziegler, J. Am. Chem. Soc. **123**, 3341 (2001).
[34]J. Autschbach, A. M. Kantola, and J. Jokisaari, J. Phys. Chem. A **111**, 5343 (2007).
[35]A. Bagno and M. Bonchio, Magn. Reson. Chem. **42**, S79 (2004).
[36]S. K. Wolff, T. Ziegler, E. van Lenthe, and E. J. Baerends, J. Chem. Phys. **110**, 7689 (1999).
[37]R. Fukuda, M. Hada, and H. Nakatsuji, J. Chem. Phys. **118**, 1015 (2003).
[38]J. Autschbach and T. Ziegler, in *Encyclopedia of Nuclear Magnetic Resonance*, edited by D. M. Grant, and R. K. Harris (Wiley, 2003), Vol. 9, p. 306.
[39]J. Autschbach, in *Calculation of NMR and EPR Parameters: Theory and Applications*, edited by M. Kaupp, M. Bühl, and V. G. Malkin (Wiley-VCH, Weinheim, 2004), p. 227.
[40]R. Fukuda, M. Hada, and H. Nakatsuji, J. Chem. Phys. **118**, 1027 (2003).
[41]A. Rodriguez-Fortea, P. Alemany, and T. Ziegler, J. Phys. Chem. A **103**, 8288 (1999).
[42]T. Gilbert and T. Ziegler, J. Phys. Chem. A **103**, 7535 (1999).
[43]G. Schreckenbach, S. Wolff, and T. Ziegler, J. Phys. Chem. A **104**, 8244 (2000).
[44]G. Schreckenbach, Inorg. Chem. **41**, 6560 (2002).
[45]W. Nakanishi, S. Hayashi, Y. Katsura, and M. Hada, J. Phys. Chem. A **115**, 8721 (2011).
[46]J. Autschbach and S. Zheng, Annu. Rep. NMR Spectros. **67**, 1 (2009).
[47]T. Enevoldsen, L. Visscher, T. Saue, H. J. A. Jensen, and J. Oddershede, J. Chem. Phys. **112**, 3493 (2000).
[48]S. S. Gomez, R. H. Romero, and G. A. Aucar, J. Chem. Phys. **117**, 7942 (2002).
[49]A. Antusek, M. Pecul, and J. Sadlej, Chem. Phys. Lett. **427**, 281 (2006).
[50]M. Repiský, S. Komorovský, O. L. Malkina, and V. G. Malkin, Chem. Phys. **356**, 236 (2009).
[51]R. Bast and T. Saue, private communication (2011).
[52]L. Visscher, T. Enevoldsen, T. Saue, H. J. A. Jensen, and J. Oddershede, J. Comput. Chem. **20**, 1262 (1999).
[53]M. Hada, Chem. Phys. Lett. **310**, 342 (1999).
[54]M. Hada, Chem. Phys. Lett. **321**, 452 (2000).
[55]F. London, J. Phys. Radium **8**, 397 (1937).
[56]L. Cheng, Y. Xiao, and W. Liu, J. Chem. Phys. **131**, 244113 (2009).
[57]S. Komorovský, M. Repiský, O. L. Malkina, V. G. Malkin, I. M. Ondík, and M. Kaupp, J. Chem. Phys. **128**, 104101 (2008).
[58]M. Olejniczak, R. Bast, T. Saue, and M. Pecul, J. Chem. Phys. **136**, 014108 (2012).
[59]V. Arcisauskaite, J. I. Melo, L. Hemmingsen, and S. P. A. Sauer, J. Chem. Phys. **135**, 044306 (2011).
[60]W. Liu, L. Cheng, and D. Peng, J. Chem. Phys. **126**, 214101 (2007).
[61]A. Antusek, M. Jaszuński, and M. Olejniczak, Comput. Theor. Chem. **970**, 54 (2011).
[62]P. Lantto, K. Jackowski, W. Makulski, M. Olejniczak, and M. Jaszuński, J. Phys. Chem. A **115**, 10617 (2011).
[63]S. Molchanov and A. Gryff-Keller, Magn. Reson. Chem. **41**, 788 (2003).
[64]G. Wu, S. Kroeker, and R. Wasylishen, Inorg. Chem. **34**, 1595 (1995).
[65]K. E. Berg, J. Blixt, and J. Glaser, Inorg. Chem. **35**, 7074 (1996).
[66]S. Kroeker, R. E. Wasylishen, and J. V. Hanna, J. Am. Chem. Soc. **121**, 1582 (1999).
[67]D. L. Bryce and R. E. Wasylishen, Inorg. Chem. **41**, 4131 (2002).
[68]J. Autschbach and T. Ziegler, J. Chem. Phys. **113**, 936 (2000).
[69]S. Moncho and J. Autschbach, J. Chem. Theory Comput. **6**, 223 (2010).
[70]P. M. Aguiar and S. Kroeker, Phys. Chem. Chem. Phys. **11**, 834 (2009).
[71]K. J. Harris and R. E. Wasylishen, Inorg. Chem. **48**, 2316 (2009).
[72]C. Fonseca Guerra, J. G. Snijders, G. te Velde, and E. J. Baerends, Theor. Chem. Acc. **99**, 391 (1998).
[73]G. te Velde, F. M. Bickelhaupt, E. J. Baerends, C. Fonseca Guerra, S. J. A. van Gisbergen, J. G. Snijders, and T. Ziegler, J. Comput. Chem. **22**, 931 (2001).
[74]ADF2010, SCM, *Theoretical Chemistry* (Vrije Universiteit, Amsterdam, The Netherlands, 2010), see http://www.scm.com.
[75]S. Vosko, L. Wilk, and M. Nusair, Can. J. Phys. **58**, 1200 (1980).
[76]A. D. Becke, Phys. Rev. A **38**, 3098 (1988).
[77]J. P. Perdew, Phys. Rev. B **33**, 8822 (1986).
[78]T. W. Keal and D. J. Tozer, J. Chem. Phys. **119**, 3015 (2003).
[79]P. J. Stephens, F. J. Devlin, C. F. Chabalowski, and M. J. Frisch, J. Phys. Chem. **98**, 11623 (1994).
[80]V. Vetere, C. Adamo, and P. Maldivi, Chem. Phys. Lett. **325**, 99 (2000).
[81]J. Autschbach, J. Chem. Phys. **129**, 094105 (2008).
[82]RESPECT program, version 3.1.0 (2011), written by V. G. Malkin, O. L. Malkina, M. Repiský, S. Komorovský, I. Malkin, E. Malkin, A. V. Arbuznikov, M. Kaupp, and K. Ruud.
[83]F. Jensen, J. Chem. Phys. **115**, 9113 (2001).
[84]F. Jensen, J. Chem. Phys. **116**, 3502 (2002).
[85]K. G. Dyall, Theor. Chem. Acc. **112**, 403 (2004).
[86]R. Bast, H. J. Aa. Jensen, and T. Saue, plbibsc-dirac, a relativistic *ab initio* electronic structure program, release DIRAC11, 2011, see http://dirac.chem.vu.nl.
[87]S. Komorovský, M. Repiský, O. L. Malkina, and V. G. Malkin, J. Chem. Phys. **132**, 154101 (2010).
[88]P. F. Provasi, G. A. Aucar, and S. P. A. Sauer, J. Chem. Phys. **115**, 1324 (2001).
[89]S. Zheng and J. Autschbach, Chem.-Eur. J. **17**, 161 (2011).
[90]J. Autschbach, ChemPhysChem **10**, 2274 (2009).
[91]M. Kaupp, in *Relativistic Electronic Structure Theory. Part 2. Applications*, edited by P. Schwerdtfeger (Elsevier, Amsterdam, 2004), p. 552.
[92]J. Autschbach, Theor. Chem. Acc. **112**, 52 (2004).
[93]G. Wu and R. E. Wasylishen, J. Phys. Chem. **97**, 7863 (1993).

Paper II

JCTC Journal of Chemical Theory and Computation

Article

pubs.acs.org/JCTC

The Influence of a Presence of a Heavy Atom on ^{13}C Shielding Constants in Organomercury Compounds and Halogen Derivatives

Artur Wodyński,[†] Adam Gryff-Keller,[‡] and Magdalena Pecul*[,†]

[†]Faculty of Chemistry, University of Warsaw, Pasteura 1, 02-093 Warszawa, Poland

[‡]Faculty of Chemistry, Warsaw University of Technology, Noakowskiego 3, 00-664 Warszawa, Poland

Supporting Information

ABSTRACT: ^{13}C nuclear magnetic resonance shielding constants have been calculated by means of density functional theory (DFT) for several organomercury compounds and halogen derivatives of aliphatic and aromatic compounds. Relativistic effects have been included through the four-component Dirac–Kohn–Sham (DKS) method, two-component Zeroth Order Regular Approximation (ZORA) DFT, and DFT with scalar effective core potentials (ECPs). The relative shieldings have been analyzed in terms of the position of carbon atoms with respect to the heavy atom and their hybridization. The results have been compared with the experimental values, some newly measured and some found in the literature. The main aim of the calculations has been to evaluate the magnitude of heavy atom effects on the ^{13}C shielding constants and to check what are the relative contributions of scalar relativistic effects and spin–orbit coupling. Another object has been to compare the DKS and ZORA results and to check how the approximate method of accounting for the heavy-atom-on-light-atom (HALA) relativistic effect by means of scalar effective core potentials on heavy atoms performs in comparison with the more rigorous two- and four-component treatment.

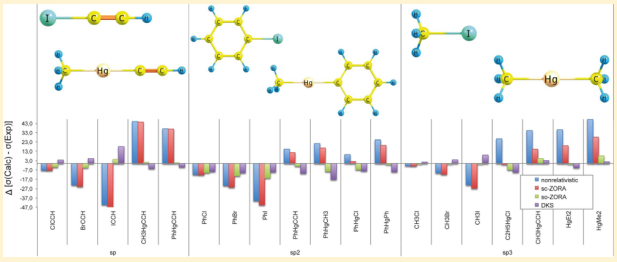

1. INTRODUCTION

Nuclear magnetic resonance (NMR) shielding constants (and related to them chemical shifts) are among the most important spectroscopic parameters used in chemistry and biology, as they provide valuable insight into the electronic structure of systems under study.[1] The basic (nonrelativistic) theory for these parameters was formulated in a series of landmark papers in the 1950s by Ramsey,[2−5] and nowadays nonrelativistic *ab initio* calculations of these properties are a routine task. However, NMR shielding constants exhibit strong relativistic effects: first, they are magnetic properties and therefore inherently relativistic phenomena,[6] and second, the associated property operators probe the electron density in the core region, where relativistic effects tend to be the most pronounced. As a consequence, relativistic effects affect not only the shielding constants of heavy nuclei (like ^{129}Xe, ^{183}W, ^{195}Pt, or ^{199}Hg) but also of light nuclei (^{1}H, ^{13}C, ^{15}N) in proximity of heavy atoms. The latter phenomenon manifests itself as a so-called heavy-atom-on-light-atom (HALA) effect.[7]

The relativistic effects can be divided into scalar (spin-free) and spin–orbit coupling effects. Both contribute, to different degrees, to the HALA effects on the chemical shifts, but the factors on which their relative magnitude depends are not fully investigated. A systematic study of this problem has been carried out for chemical shifts of the carbon nuclei in the α position to the heavy atom.[8] However, very approximate methods have been used to account for the relativistic effects, since implementations of two- and four-component relativistic Hamiltonians for the shielding constants were not available at the time. Nowadays, the situation has changed, and therefore we decided to revisit the subject and carry out a systematic study of scalar and spin–orbit contributions to the HALA effect on carbon chemical shifts using the density functional approach with the two-component Zeroth Order Regular Approximation (ZORA) Hamiltonian. The calculated chemical shifts are compared with experimental results and the results obtained with the four-component Dirac–Coulomb Hamiltonian.

Our other aim is to check how the most widespread (and the most approximate) method of accounting for relativistic effects—through the use of relativistic effective core potentials (ECPs)—performs in comparison to explicitly relativistic methods. This is motivated by the fact that scalar effective core potentials are commonly used nowadays in calculations of the shielding constants of light nuclei (proton, carbon, nitrogen) in the proximity of the heavy atoms, especially in organometallic compounds,[9−12] allowing one to perform calculations of NMR spectra for sizable systems containing fourth and fifth row elements, but they have never been optimized for calculations of the shielding constants (or magnetic properties in general), and their use is based on the assumption of a similar performance to that for the energy. ECPs have been constructed by fitting their form to match the numerical relativistic orbitals[13,14] or to reproduce the spectral

Received: October 24, 2012
Published: March 14, 2013

properties obtained by all-electron calculations.[15−17] Furthermore, most applications of ECPs (including the one used in the present work) pose some problems with gauge invariance.[18] The numbers of ECP calculations will be compared with scalar ZORA results, since ECPs parametrized to include the spin−orbit coupling effects,[19]as far as we know, have never been implemented for the calculations of the shielding constants.

The molecules under study are selected organomercury compounds (CH_3HgCCH, PhHgCCH, $PhHgCH_3$, PhHgPh, PhHgCl, C_2H_5HgCl, $Hg(C_2H_5)_2$) and halogen derivatives of aliphatic (CH_3X, C_2H_5X, XCCH, X = Cl, Br, I) and aromatic (PhX, X = Cl, Br, I) compounds. It is known that for systems which can be described as having hybridization with a strong s character, the spin−orbit coupling effects are important, especially for nuclei which are immediate neighbors of the heavy atoms.[20−22] Therefore, the chosen systems contain carbon atoms of different hybridizations and in different positions with respect to the heavy atom (halogen or mercury).

The paper is organized as follows. After the description of experimental and computational details, we discuss the calculated heavy atom on light atom (HALA) effects on the ^{13}C relative shielding constants, comparing the results obtained when modeling the relativistic effects using DKS and ZORA Hamiltonians (the latter with the two-component term including the spin−orbit effects and in one-component form without the spin−orbit effects) with experimental results. Next, we examine the performance of ECPs, comparing the scalar relativistic term as received from the ECP calculations with the scalar term from the ZORA calculations. The results are discussed in order of increasing number of bonds between the carbon nucleus and the heavy atom. After the discussion of relativistic effects, some other factors which may influence the comparison with experimental results are discussed, i.e., solvents effects as estimated by means of conductor-like screening model (COSMO), vibrational effects, and the effects of using different exchange-correlation functionals. Finally, a summary and main conclusions are presented.

2. EXPERIMENTAL AND COMPUTATIONAL DETAILS

2.1. NMR Experimental Details. The ^{13}C chemical shift data for halogenobenzenes have been taken from the free-access database,[23] whereas the data for aliphatic halides,[24,25] CH_3HgCCH,[26] $PhHgCH3$,[27] PhHgCl,[27] $Hg(CH_3)_2$,[28] $Hg(C_2H_5)_2$,[28] and C_2H_5HgCl[28] have been found in the indicated literature sources. The ^{13}C NMR chemical shifts for PhHgCCH and PhHgPh have been measured as part of this work.

Commercially available phenylmercury chloride and diphenylmercury (Aldrich) have been used in measurements and synthesis without purification. Ethynylphenylmercury (PhHgCCH) has been synthesized from phenylmercury chloride and acetylene using the literature procedure.[26]

Approximately 0.1 M solutions for NMR measurements have been prepared directly in 5 mm outer-diameter NMR tubes by weighing an appropriate amount of solute and dissolving it in 0.6 mL of $CDCl_3$. All measurements have been performed at the temperature stabilized at 25 °C using a 500 MHz VNMRS spectrometer working at B_0 = 11.7 T. The ^{13}C chemical shifts have been referenced to the carbon signal of the solvent assuming $\sigma(CDCl_3)$ = 77.0 ppm. The 1D ^{13}C NMR spectra as well as 2D ^{1}H-detected ^{13}C NMR spectra have been acquired using the standard spectrometer software and parameter sets. Each time, the number of scans has been adjusted to obtain $S/N > 5$ for the weakest signal in the recorded spectrum.

2.2. Computational Details. *Geometry.* The geometric parameters of the isolated molecules under study have been obtained by means of geometry optimization carried out using ZORA DFT[29] (spin−orbit coupling included, called so-ZORA through the paper) as implemented in the ADF[30] program with the ADF version of the BP86 exchange-correlation functional (composed of VWN[31]+Becke88[32] and Perdew86[33] functionals) and the TZ2P basis set. Frozen core included 1s for carbon, 1s to 4d for mercury, 1s to 2p for chlorine, 1s to 3d for bromine, and 1s to 4p for iodine. Test calculations for PhHgCCH by means of scalar-only ZORA show the variation of the bond lengths in comparison to the spin−orbit ZORA of about 0.005 Å for $R(HgC_\alpha)$ and 0.001 Å for $R(C_{ipso}C_{orto})$ and $R(C_{orto}C_{meta})$; therefore for consistency we have decided to perform all geometry optimization including spin−orbit coupling. The same geometry parameters (obtained by spin−orbit ZORA calculation) have been used for all calculations (DKS, ZORA, ECP) of shielding constants in order to separate the effects of using different computational models on the molecular geometry and the shielding constants.

Another set of geometry parameters (used for estimating solvent effects) has been obtained using the same electron structure model as above and the conductor-like screening model (COSMO[34−37]). Dielectric constants of 4.8 and 46.7 have been employed to describe $CHCl_3$ and DMSO, respectively, and the cavity has been built from the default van der Waals radii.

DKS Calculations of the Shielding Constants. The four-component Dirac−Kohn−Sham calculations of the shielding constants have been carried out using the implementation available in the ReSpect program (version 3.1.0).[38] Restricted magnetic balance has been ensured by transformation of the Dirac Hamiltonian,[39,40] and gauge invariant atomic orbitals (GIAOs) have been employed. The generalized gradient approximation (GGA) functional of Perdew, Burke, and Ernzerhof (PBE[41]); triple-ζ uncontracted pc-2 Gaussian basis set of Jensen[42,43] for carbon, hydrogen, and chlorine; and Dyall's[44] triple-ζ for mercury, bromine, and iodine basis set have been used. The calculated shielding constants (obtained using DKS and other employed methods) have been converted into relative shielding constants using benzene as a reference ($\Delta_{rel}\sigma = \sigma - \sigma_{benzene}$).

ZORA Calculations of the Shielding Constants. The NMR shielding constants have been calculated using DFT as implemented in the ADF program at the spin−orbit, scalar ZORA (scaled-ZORA variant, called sc-ZORA through the paper) and nonrelativistic levels, with a standard PBE and Perdew, Burke, and Ernzerhof functional with Adamo and Barone's HF exchange contribution (PBE0).[45] We have used the standard Slater basis set available in the ADF[30] program: TZP (triple-ζ with one polarization function) with GIAOs. In one set of calculations, the conductor-like screening model (COSMO) with the same set of parameters as for geometry optimization has been applied to include solvent effects.

ECP Calculations of the Shielding Constants. The effective core potential results have been obtained using the Gaussian 03 program.[46] We have used the PBE functional and the upc-2 basis set for carbon and hydrogen and two effective core potentials, MWB60[16] and MDF60[17] (the standard version available in Gaussian program, coming with the (8s8p7d)/[6s6p4d] valence basis set), for mercury. Additionally, we have performed calculations with nonrelativistic MHF60[47] ECP to

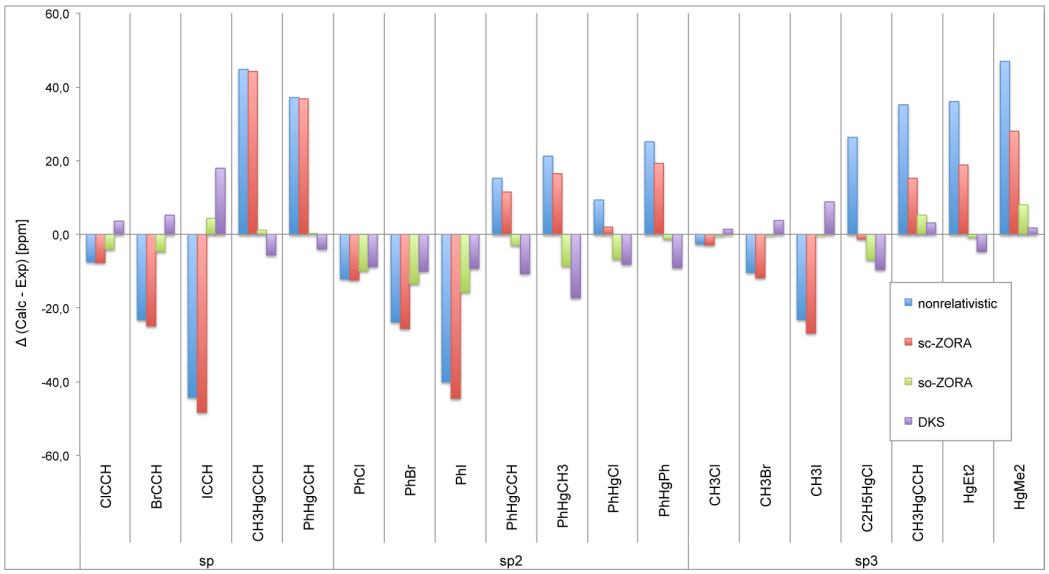

Figure 1. A comparison of the calculated relative shielding constants [ppm] for carbon directly bonded with the heavy atom with the experimental data (differences between experimental and calculated data; both with benzene as a reference) for nonrelativistic DFT, sc-ZORA, so-ZORA, and DKS.

estimate scalar relativistic effects as rendered by the relativistic ECPs.

Calculations of Vibrational Corrections of the Shielding Constants. The vibrational corrections have been obtained using the Dalton 2011[48] program at the nonrelativistic level. We have used the PBE functional and the upc-2 basis set for carbon, hydrogen, and chlorine and the dyall.v3z basis set for bromine, iodine, and mercury. The calculations have been performed at a temperature of 300 K, using a geometry step of 0.05 Å for numerical differentiation.

3. RESULTS

3.1. Performance of Different Methods of Modeling the HALA Effect. In this subsection, we will discuss how the relative ^{13}C shieldings (with benzene as a reference) obtained by means of DKS and ZORA-DFT compare with the experimental data. No environmental or vibrational effects are included in this set of calculations. The relevant numerical values can be found in the Supporting Information (Tables S1–S6).

3.1.1. The Relative Shielding Constants of the Carbon Nuclei Directly Bonded with the Heavy Atom. The comparison of the ^{13}C relative shielding constants calculated using various computational methods with the experimental results is shown in Figure 1, where deviations from the experimental results are displayed for each method and each compound under study. Inspection of these results shows that in most cases so-ZORA reproduces the experimental results very well. The agreement is good for carbons with the sp hybridization in the systems containing mercury and for the sp^3 hybridization for the series of CH_3X where X = Cl, Br, I. A poorer agreement is observed for the phenyl ipso position in $PhHgCH_3$, PhHgCl, $Hg(CH_3)_2$, and the PhX (X = Cl, Br, I) series, where the so-ZORA relative shieldings are smaller than the experimental ones.

Interestingly, the agreement with experimental results is usually slightly worse for the four-component calculations than for ZORA. As a rule, it appears as if DKS overestimated the relativistic effects. Apparently, there is a cancellation of errors in the ZORA calculations of relative shielding constants of ^{13}C nuclei in immediate proximity of a heavy atom. It is particularly noticeable for sp and sp^2 hybridization (for systems containing mercury). However, for the PhX series where there are substantial differences between ZORA and experimental results, DKS leads to a somewhat better agreement with experimental results.

The magnitude of the spin–orbit effect (as estimated by comparison of the so-ZORA and sc-ZORA results) and consequently the performance of scalar ZORA in comparison with experimental results depends strongly on carbon hybridization. The spin–orbit coupling affects the shieldings of the sp-hybridized α carbons by as much as 20–52 ppm (the sign of the spin–orbit term depends on type of the heavy nucleus: it is positive for halides and negative for mercury). The scalar terms (negative in this case) are smaller: for example, for systems containing carbon with sp hybridization, the scalar terms are less (in terms of the absolute values) than −4 ppm (the biggest one is found for ICCH), and in many cases they are negligible in comparison with the spin–orbit term.

For carbon nuclei with the sp^2 hybridization directly bonded to the heavy atoms (occupying the ipso position in the benzene ring in the systems under study), large differences between the experimental relative shielding constants and the sc-ZORA results are observed again. This is particularly striking in the case of halogen derivatives, especially PhI, where the difference amounts to about 50 ppm. This is again a result of the fact that the scalar effects are small (in most cases at most about −5 ppm) in comparison with the spin–orbit term. On the other hand, even inclusion of the spin–orbit term at the ZORA level of theory only partially improves the agreement with experimental results (still, a difference of about 15.7 ppm is observed for PhI), so apparently the relativistic effects are not described fully by ZORA. As already mentioned, in the case of PhI, the use of DKS improves further the agreement with experimental results (the difference between DKS and experimental data is about 9.2 ppm). Inclusion of solvent

dx.doi.org/10.1021/ct300921f | J. Chem. Theory Comput. 2013, 9, 1909–1917

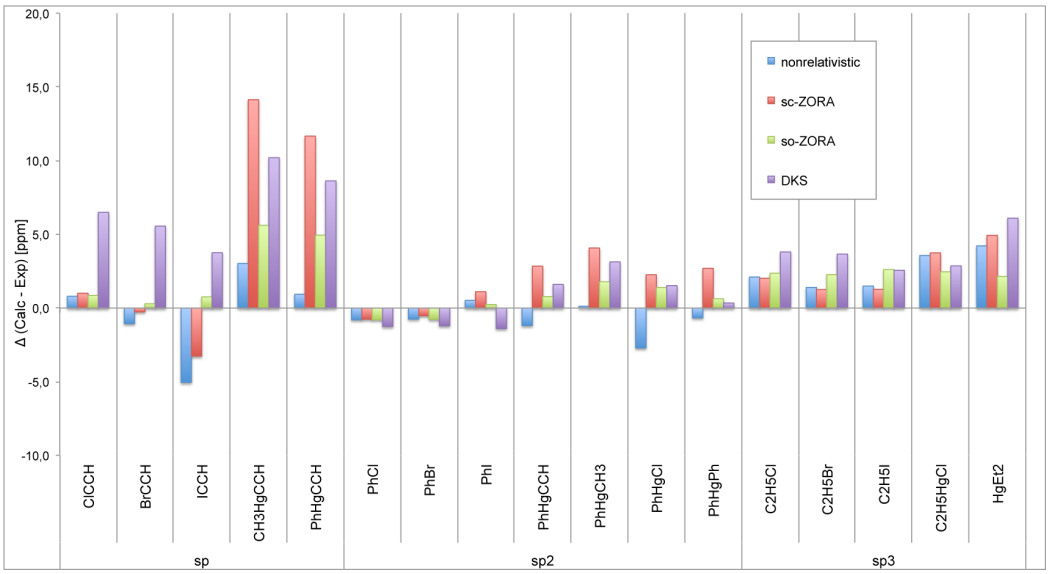

Figure 2. A comparison of the calculated relative shielding constants [ppm] for carbon bonded with the heavy atom with two bonds with the experimental data (differences between experimental and calculated data; both with benzene as a reference) for nonrelativistic DFT, sc-ZORA, so-ZORA, and DKS.

effects additionally improves agreement with experimental results, but the effects are rather small (0.8 ppm for PhI, see Table S7).

For monosubstituted benzenes containing mercury, the spin−orbit terms are smaller (between −8.7 ppm and −25.0 ppm) but still larger than the scalar terms (inclusion of only the scalar terms improves very little the agreement of the computational results with the experimental ones). In this case, the so-ZORA relative shieldings are smaller than the experimental ones, and this tendency is even more pronounced for the DKS results.

Among the results for the sp^2 carbons in the α position, the smallest differences between the DKS, so-ZORA, and sc-ZORA results are observed for PhHgCl and PhCl. It is due to small values of the SO terms. In the case of PhHgCl, it may be a consequence of electronegativity of the substituent bounded with mercury, since strong dependence of the SO term in ^{13}C shielding on the substituent electronegativity has been observed before for CH3HgX (X = CN, Cl, CH_3, SiH_3) systems[10] in perturbational calculations carried out on top of the nonrelativistic electron density. In the case of PhCl, a small value of the SO term is due to the small nuclear charge of Cl, as discussed for example by Vaara et al.[8]

Now, the relative shielding constants of the carbon nuclei with sp^3 hybridization will be discussed. We do not include in this section the results for $PhHgCH_3$, because no experimental data are available (the computed results will be used in the discussion of scalar terms in next subsection) and omit the series of C_2H_5X (X = Cl, Br, I) because the trends are similar to those for the CH_3X series.

For the molecules of this class containing mercury, the relativistic effects (as calculated using ZORA) span the range of about 40 ppm, and the differences between so-ZORA results and the experimental data vary from about −1 ppm for $Hg(C_2H_5)_2$ to about 8 ppm for $Hg(CH_3)_2$. In this series of compounds, the use of DKS instead of ZORA reduces in some cases (e.g., $Hg(CH_3)_2$) the discrepancy with experimental results. The spin−orbit term for C_2H_5HgCl is very small in comparison with the scalar one, similarly to that for another molecule under study containing the HgCl moiety, PhHgCl (see above). The differences between HALA effects calculated using sc-ZORA and so-ZORA (i.e., the spin−orbit coupling effects) are substantial (except for C_2H_5HgCl), but unlike for sp and sp^2 carbon nuclei, the scalar terms are comparable or even bigger than the spin−orbit terms and of the same sign.

For the CH_3X series, the trends are similar to those for PhX, but the relativistic effects are generally smaller. The biggest spin−orbit term is observed, as expected, for CH_3I (about 26 ppm), and it has an opposite sign to the scalar term.

3.1.2. The Relative Shielding Constants of the Carbon Nuclei in β Position to the Heavy Atom. The differences between the experimental and calculated relative shielding constants of carbon nuclei separated by two bonds from the heavy atom are shown in Figure 2. As expected, the relativistic effects are smaller than for carbon in the α position to the heavy atom (here, they reach about 6 ppm). Again, a marked difference in the magnitude of the spin−orbit effect (and therefore in the performance of different computational methods) can be observed for the carbon nuclei of different hybridizations.

For carbon atoms in β positions with the sp hybridization, the results computed using different methods vary significantly (the differences can reach 9 ppm), although, because of smaller relativistic effects, they are much less scattered in comparison with the shieldings of the sp carbons directly bonded with the heavy atoms. Again, so-ZORA seems to perform slightly better than DKS. The SO terms, as calculated using ZORA, are much smaller for the β carbon nuclei than for the α carbon nuclei, amounting to about 8 ppm (in the absolute value). The scalar terms have the same sign as the spin−orbit terms for BrCCH and ICCH but not for CH_3HgCCH and PhHgCCH. For the latter two molecules, the scalar terms are larger (in terms of absolute values) than the SO ones, so the variation of the performance of the different computational methods originates partially from different rendering of the scalar terms.

dx.doi.org/10.1021/ct300921f | J. Chem. Theory Comput. 2013, 9, 1909−1917

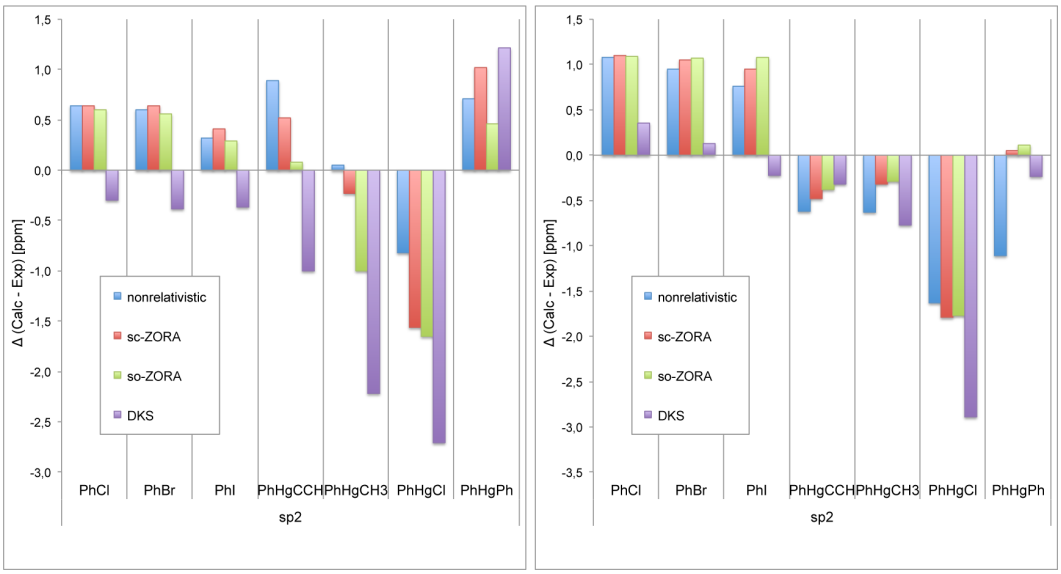

Figure 3. A comparison of the calculated relative shielding constants [ppm] for carbon bonded with the heavy atom with three or four bonds with the experimental data (differences between experimental and calculated data; both with benzene as a reference) for nonrelativistic DFT, sc-ZORA, so-ZORA, and DKS.

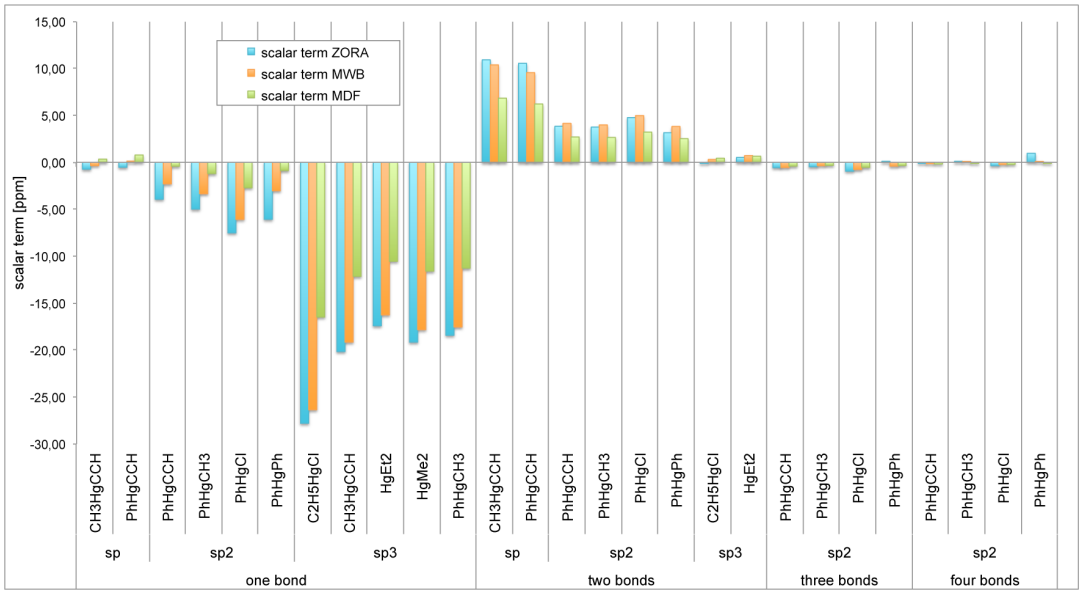

Figure 4. A comparison of the scalar effects calculated with the ZORA method and ECP methods.

In the case of the carbon atoms with the sp^2 hybridization in the benzene ring (separated by two bonds from the heavy atom, therefore in orto position to it), the relativistic effects do not exceed 4.1 ppm (for molecules containing mercury), and they are negligible for halide derivatives. Generally, DKS seems to perform worse than so-ZORA, but the differences are less than 1.7 ppm.

For the carbon atoms with the sp^3 hybridization in the β position, the discrepancies between the so-ZORA results and experimental results do not exceed 3 ppm. (Inclusion of the solvent effects by means of COSMO leads to slightly larger differences of 4−4.5 ppm.) The DKS method again works worse than so-ZORA, especially for $Hg(C_2H_5)_2$. For C_2H_5HgCl, the relativistic effects are relatively small (especially the scalar contribution). Generally, the SO term dominates over the scalar one, and they have opposite signs.

3.1.3. The Relative Shielding Constants of the Carbon Nuclei Separated from the Heavy Atom by Three or Four Bonds. The carbon atoms separated from the heavy nuclei by three or four bonds in the molecules under study are all in the phenyl ring (in the meta or para position), and thus all have the sp^2 hybridization. For relative shielding constants of the carbon nuclei in the meta positions, the HALA effects are small, not exceeding −1 ppm, as shown in Figure 3. For all meta carbon nuclei, the scalar terms are on the same order of magnitude as the spin−orbit terms or even bigger (as in the case of PhHgCl), and in the case of molecules containing mercury (except PhHgPh) the scalar and SO terms have the same signs (for the

dx.doi.org/10.1021/ct300921f | J. Chem. Theory Comput. 2013, 9, 1909−1917

series of PhX, they have opposite signs, but in this case, the relativistic terms are negligible, i.e., between 0 ppm and −0.2 ppm). In most cases, using DKS leads to underestimation of the experimental results (only for PhHgPh the opposite trend is observed), and the results are, on average, in worse agreement with experimental results than the so-ZORA results.

In the case of the relative shielding constants of the carbon nuclei in the para position, the observations are similar as for the meta position (except that for the para carbon nuclei, the spin−orbit term is negligible in comparison with the scalar term), and again for PhHgCl we observe a relatively large difference between so-ZORA or DKS and the experimental result (about 1.8 ppm for so-ZORA). The relativistic effects are very small, so no reliable conclusions about the performance of different methods in rendering them can be drawn.

3.1.4. Reproduction of the Scalar Effects by the Effective Core Potentials. In this subsection, we will discuss how the effective core potentials reproduce the scalar relativistic effects on the ^{13}C relative shielding constants in comparison with a more rigorous treatment by means of ZORA. (At the DKS level, we have at present no means to divide the total relativistic effect into scalar and spin−orbit contributions.) The ZORA scalar term is calculated as a difference between the sc-ZORA result and the nonrelativistic result obtained with the same basis set. It should be taken into account that the comparison is affected by different basis sets employed: Slater orbitals in ZORA and Gaussian orbitals in ECP calculations. The comparison is limited to MWB60 and MDF60 because, for this series, nonrelativistic ECP (MHF60) is available for Hg, allowing one to calculate the scalar relativistic term as a difference between the results obtained with the relativistic and nonrelativistic ECPs. Only the systems containing mercury are considered, since for halogen atoms MHF60 is not available and the usage of a full atomic basis on halogens leads to a nonphysical bias.

The comparison of the scalar relativistic effects on the relative carbon shielding constants calculated using different approaches is shown in Figure 4. In the case of carbon bonded directly to mercury, the scalar effect (always negative) changes significantly with decreasing s character of the carbon hybridization. For carbon with the sp hybridization, the scalar terms are generally negligible (between 0 ppm and −1 ppm). For carbon with sp^2 hybridization, they are more significant (especially for PhHgCl where the scalar term is about −7.5 ppm). The effective core potential parametrized with respect to the scalar two-component approximation to the Dirac equation (MWB60) reproduces the sc-ZORA term well for this class of shieldings, but MDF60 renders only from 18% (in the case of PhHgCCH) to 44% (in the case of PhHgCl) of the MWB60 result. For the relative shielding constants of the carbon nuclei with the sp^3 hybridization, the scalar effects are the biggest among all discussed systems (for C_2H_5HgCl, the scalar term is as large as −28 ppm), and generally MWB60 reproduces the sc-ZORA results quite well (although all MWB60 results are underestimated in comparison with sc-ZORA ones). Again, a substantial difference between the MWB60 and MDF60 scalar terms is observed (MDF60 reproduces about 63−65% of the MWB60 term). We have performed additional calculations for selected molecules with a more recent version of MDF60[19] and obtained results much closer to MWB60; thus the observed difference is most likely a consequence of different fitting procedures employed to obtain the two ECPs.

In the case of the relative shielding constants of the carbon atoms bonded with mercury with two bonds, the scalar effect decreases with decreasing s character of the carbon hybridization, unlike for the carbon α atoms. The largest scalar terms (about 11 ppm) are observed for the sp hybridization, smaller (3−5 ppm) for the sp^2 hybridization, and smaller still (less than 1 ppm) for the sp^3 hybridization. For the sp hybridization, MWB60 underestimates the sc-ZORA term, but not significantly (by about 0.5−1 ppm), and for sp^2 it leads to a slight overestimation of the ZORA scalar term. Almost all scalar terms for the carbon atoms in the β position have positive signs. Similarly as for the α carbon shieldings, the MDF60 scalar terms are smaller than the MWB60 scalar terms (from 65 to 67%).

In the case of the relative shieldings of the carbon nuclei separated by three or four bonds from the heavy atom, the scalar terms are negligible (less than 1 ppm), and they will not be discussed any further.

3.2. The Influence of the Factors Other than the Relativistic Effects on the Quality of the Results. In the previous subsection, we focused on how different methods of accounting for the relativistic effects perform for the carbon shielding constants. In this subsection, we will discuss briefly other factors which may cause a difference between theoretical and experimental results, namely the effect of choosing different exchange-correlation functionals, solvents effects (as estimated by means of the COSMO model), and vibrational effects.

3.2.1. Comparison of Hybrid and Nonhybrid Functionals. All results discussed so far have been obtained using the PBE GGA functional. This has been done to ensure consistency with the DKS calculations, since hybrid functionals are not available yet in the ReSpect program. To check whether including exact exchange improves the agreement with experimental results, we have carried out so-ZORA calculations with the PBE0 hybrid functional. The root-mean-square deviation (RMSD) between theoretical and experimental results is 4.54 ppm and 4.24 ppm for PBE and PBE0, respectively, for the set of 53 relative shielding constants under study (see Tables S9 and S10 in the Supporting Information). The biggest differences between PBE and PBE0 are observed for the shieldings of the carbons directly bonded with the heavy atoms (between 0.3 ppm and 10.5 ppm, but in most cases more than 3.5 ppm). Thus, we can conclude that the inclusion of the hybrid component (going from PBE to PBE0) should not influence materially the conclusions concerning the relativistic effects.

3.2.2. Estimation of Solvent Effects. The results presented so far did not include solvent effects, even though most of the experimental chemical shifts have been measured in solutions. We have decided therefore to estimate solvent effects at the so-ZORA level using the COSMO model (both during geometry optimization and calculation of shielding constants). For most of the systems under study, they do not exceed ±1.5 ppm (see Tables S7 and S8 in the SI). The largest solvent effects are predicted for C_2H_5I (about −4.2 ppm) and for $PhHgCH_3$ and PhHgCCH (about 3.9 ppm and 3.0 ppm, respectively). RMSD for the computational results obtained for the isolated molecules is 4.60 ppm, and for molecules in solution modeled by means of COSMO, it is 5.00 ppm, so actually the calculations without accounting for the environmental effects lead to better agreement with the experimental data. The continuum model does not seem to be a suitable tool for the purpose, and using more elaborate solvent models is at present beyond our means.

3.2.3. Estimation of Vibrational Effects. The vibrational effects can be sizable for shielding constants,[49] and it is worthwhile to check how large they are in comparison with the relativistic effects. The calculations have been performed at the nonrelativistic level because, so far, only for this level of theory is the appropriate methodology implemented.[49] Calculations have been performed for all systems containing halides and for selected organomercury compounds.

Inclusion of a vibrational term leads to deshielding of carbon nuclei, for halides not exceeding −4.5 ppm (except for β carbon in the C_2H_5X series where they are about −7 ppm). Large vibrational effects have been predicted for four shielding constants in organomercury compounds (about −22 ppm for $Hg(CH_3)_2$, about −17 ppm and −20 ppm for the α and β positions, respectively, in PhHgCCH, and 15−30 ppm for the α position in $Hg(C_2H_5)_2$). However, it should be stressed that a comparison of the relativistic (so-ZORA) and nonrelativistic results of test calculations for CH_3I and $Hg(CH_3)_2$ with deformed geometry indicates that while for halide derivatives the vibrational term is nearly additive with the relativistic term, this is not the case for organomercury compounds. Numerical derivatives of ^{13}C shielding with respect to the bond length (calculated with the displacement of 0.01 Å) are similar for the so-ZORA and Schrödinger Hamiltonians in the case of CH_3I (for R_{IC} displacement, it is −109.5 ppm/Å and −112.5 ppm/Å and for R_{CH} displacement, −44.0 ppm/Å and −60.5 ppm/Å for the so-ZORA and Schrödinger Hamiltonians, respectively), but for $Hg(CH_3)_2$ they differ significantly (for R_{HgC} displacement it is 0.5 ppm/Å and −5.5 ppm/Å and for R_{CH} displacement, 3 ppm/Å and 1.5 ppm/Å for the so-ZORA and Schrödinger Hamiltonians, respectively).

To conclude, in most cases, the vibrational terms should not influence materially the conclusions concerning the relativistic effects, especially for the relative shielding constants where the vibrational correction for the compound under study should partially cancel out with that for benzene (about −3.2 ppm). For organomercury systems, the vibrational terms calculated at the nonrelativistic level are large, but the comparison of the bond length shielding derivatives calculated at relativistic and nonrelativistic levels indicates that they are not reliable. Calculation of the vibrational effects at the relativistic level is our future goal.

4. SUMMARY AND CONCLUSIONS

The ^{13}C nuclear magnetic resonance relative shielding constants have been calculated by means of density functional theory (DFT) for several organomercury compounds and halogen derivatives of aliphatic and aromatic compounds. The relativistic effects have been included through the four-component Dirac−Kohn−Sham (DKS) method, two-component Zeroth Order Regular Approximation (ZORA) DFT, and scalar effective core potentials (ECPs). The relative shielding constants have been analyzed in terms of the carbon hybridization and the position of carbon atoms with respect to the heavy atom. The results have been compared with the experimental values, some measured for the first time in this work and some found in the literature. The main conclusions can be summarized as follows.

The magnitude of relativistic effects on carbon chemical shifts depends strongly on the position of the carbon nucleus with respect to the heavy nucleus, the charge of the heavy nucleus, and type of carbon hybridization. The biggest relativistic contributions to chemical shifts are observed for the carbon nuclei directly bonded with the heavy atoms (they amount to 50 ppm). For the carbon nuclei in the β position, the relativistic terms do not exceed 6 ppm and are below 1.3 ppm for carbon nuclei separated from the heavy nucleus by three or four bounds. Predictably, the relativistic contributions for the carbon nuclei directly bonded with halide depend strongly on the charge of the halide nucleus (they range from about 2 ppm for the systems containing chlorine to about 25 ppm for systems containing iodine for carbon with the sp^2 and sp^3 hybridization, and from 4 ppm to about 49 ppm for carbon with the sp hybridization).

Relativistic contributions tend to be the biggest for the carbon nucleus with the sp hybridization (even about 50 ppm for α carbons). In the case of a carbon atom directly bonded with the heavy nucleus, the relativistic contribution is the smallest (up to about 30 ppm) for the sp^2 hybridization and up to about 40 ppm for sp^3. For the β position, the relativistic contributions for the sp^2 carbon nucleus are of the same order of magnitude as for the carbon with the sp^3 hybridization—i.e., less than 2 ppm (only for PhHgCl is the relativistic contribution slightly bigger, about 4 ppm).

The relativistic contributions calculated at the ZORA level have been split into the scalar and spin−orbit terms. In the case of ^{13}C atoms with the sp and sp^2 hybridization bonded directly to the heavy nuclei, the scalar term is small in comparison with the spin−orbit coupling term, but for sp^3 it is comparable with the spin−orbit coupling term (for the systems containing mercury). For carbon in the β position, the scalar terms are of the same order of magnitude as the spin−orbit coupling terms. In most cases, the scalar terms have the opposite sign to the spin−orbit terms for the systems containing halides (only for carbon with the sp hybridization in the β position the opposite trend is observed), and for the systems containing mercury they have the same sign. An atypically small spin−orbit term has been observed for the systems containing the HgCl moiety.

Three methods of including relativistic effects at several levels of theory have been examined. Inspection of the results shows that so-ZORA usually reproduces the experimental results very well, in most cases better than DKS, so it appears as if DKS overestimated the relativistic effects. However, for a few cases (especially for carbon in the α position in PhX) in which so-ZORA does not perform satisfactorily, DKS leads to a better agreement with the experimental data. These observations are confirmed by statistical analysis (see Table 1) for the shieldings of carbon in the α position, where the relativistic effects are the largest. The slope values confirm that the DKS method overestimates the experimental data (by about 10%) and that

Table 1. Statistical Analysis of the Calculated Relative Shielding Constants for Carbon Directly Bonded with the Heavy Atom against the Experimental Data

	slope	RMSD [ppm]	R^2
nonrel	0.87	27.61	0.811
sc-ZORA	0.84	24.71	0.847
so-ZORA	1.03	6.69	0.993
so-ZORA[a]	1.02	5.30	0.995
DKS	1.10	8.15	0.995
DKS[b]	1.08	6.50	0.997
MWB	0.83	26.52	0.822

[a]Excluded results for PhBr and PhI. [b]Excluded results for ICCH and PhHgCH3.

dx.doi.org/10.1021/ct300921f | J. Chem. Theory Comput. 2013, 9, 1909−1917

so-ZORA performs much better in this respect (it overestimates experimental results only by about 2%). The correlation between the calculated and the experimental data is very high for so-ZORA and DKS results. RMSD for DKS is slightly bigger (about 8.15 ppm) than for so-ZORA (6.69 ppm), showing a poorer agreement of the DKS results with experimental data, which is only partially improved by exclusion of the results differing more than 2*RMSD (6.50 ppm).

The scalar terms calculated with MWB ECP agree well with the scalar ZORA results, whereas MDF underestimates these terms. Because of the scalar-only character of the employed ECP methods, they lead to good agreement with the experimental data only for carbon, where the spin−orbit term is very small; otherwise there is scarcely any improvement over the nonrelativistic calculations (compare the RMSD and R^2 parameters in Table 1).

The solvent effects on the chemical shifts as obtained using COSMO are usually small: for most of the systems under study, they do not exceed ±1.5 ppm, and they are never bigger than 3−4 ppm. The choice of a nonhybrid functional PBE instead of hybrid functional PBE0 does not lead to large errors and should not influence materially the conclusions concerning the relativistic effects. Vibrational effects seem small for halide derivatives. They may be sizable for organomercury compounds, but our preliminary tests indicate that they should be evaluated by means of a relativistic method, which is at present outside our means.

■ ASSOCIATED CONTENT

Supporting Information

Calculated ^{13}C shielding constant of benzene (Table S1), relative shielding constants used for the graphs exhibited in the paper (Tables S2−S6), relative shielding constants calculated with and without accounting for solvent effect (Tables S7 and S8), relative shielding constants calculated with PBE and PBE0 functionals (Tables S9 and S10), and vibrational corrections at the nonrelativistic level (Tables S11 and S12). This information is available free of charge via the Internet at http://pubs.acs.org/.

■ AUTHOR INFORMATION

Corresponding Author

*E-mail: mpecul@chem.uw.edu.pl.

Notes

The authors declare no competing financial interest.

■ ACKNOWLEDGMENTS

This work has received support from the Polish Ministry of Science and Higher Education via the No. N N204 148565 grant and from the Wrocław Centre for Networking and Supercomputing through a grant of computer time. MPD/2010/4 project, realized within the MPD programme of Foundation for Polish Science, cofinanced from European Union, Regional Development Fund, is acknowledged for a fellowship to A.W. The project has been carried out with the use of CePT infrastructure financed by the European Union—the European Regional Development Fund within the Operational Programme "Innovative economy" for 2007−2013.

■ REFERENCES

(1) Kaupp, M.; Bühl, M.; Malkin, V. G. *Calculation of NMR and EPR Parameters. Theory and Applications*; Wiley−VCH: Weinheim, Germany, 2004.
(2) Ramsey, N. F. *Phys. Rev.* **1950**, *77*, 567−567.
(3) Ramsey, N. F. *Phys. Rev.* **1950**, *78*, 699−703.
(4) Ramsey, N. F. *Phys. Rev.* **1951**, *83*, 540−541.
(5) Ramsey, N. F. *Phys. Rev.* **1952**, *86*, 243−246.
(6) Saue, T. *Adv. Quantum Chem.* **2005**, *48*, 383−405.
(7) Pyykkö, P.; Görling, A.; Rösch, N. *Mol. Phys.* **1987**, *61*, 195.
(8) Vaara, J.; Malkina, O. L.; Stoll, H.; Malkin, V. G.; Kaupp, M. *J. Chem. Phys.* **2001**, *114*, 61−71.
(9) Kaupp, M.; Malkin, V. G.; Malkina, O. L.; Salahub, D. R. *Chem. Phys. Lett.* **1995**, *235*, 382−388.
(10) Kaupp, M.; Malkina, O. L. *J. Chem. Phys.* **1998**, *108*, 3648−3659.
(11) Berger, S.; Bock, W.; Frenking, G.; Jonas, V.; Mueller, F. *J. Am. Chem. Soc.* **1995**, *117*, 3820−3829.
(12) Kaupp, M. *Chem.—Eur. J.* **1996**, *2*, 348−358.
(13) Hay, P. J.; Wadt, W. R. *J. Chem. Phys.* **1985**, *82*, 270−283.
(14) Wadt, W. R.; Hay, P. J. *J. Chem. Phys.* **1985**, *82*, 284−298.
(15) Bergner, A.; Dolg, M.; Küchle, W.; Stoll, H.; Preuß, H. *Mol. Phys.* **1993**, *80*, 1431−1441.
(16) Andrae, D.; Häussermann, U.; Dolg, M.; Stoll, H.; Preuss, H. *Theor. Chim. Acta* **1990**, *77*, 123−141.
(17) Häussermann, U.; Dolg, M.; Stoll, H.; Preuss, H.; Schwerdtfeger, P.; Pitzer, R. *Mol. Phys.* **1993**, *78*, 1211−1224.
(18) van Wüllen, C. *J. Chem. Phys.* **2012**, *136*, 114110.
(19) Figgen, D.; Rauhut, G.; Dolg, M.; Stoll, H. *Chem. Phys.* **2005**, *311*, 227−244.
(20) Kaupp, M. *Relativistic Electronic Structure Theory. Part 2. Applications*; Elsevier: Amsterdam, 2004; p 552.
(21) Kaupp, M.; Malkina, O. L.; Malkin, V. G.; Pyykkö, P. *Chem.—Eur. J.* **1998**, *4*, 118−126.
(22) Wodyński, A.; Repiský, M.; Pecul, M. *J. Chem. Phys.* **2012**, *137*, 014311.
(23) SDBSWeb, National Institute of Advanced Industrial Science and Technology. http://riodb01.ibase.aist.go.jp/sdbs/.
(24) Wiberg, K. B.; Pratt, W. E.; Bailey, W. F. *J. Org. Chem.* **1980**, *45*, 4936−4947.
(25) Jackowski, K.; Gryff-Keller, A.; Sas, W.; Szczeciński, P. *Pol. J. Chem.* **1996**, *70*, 221−230.
(26) Sebald, A.; Wrackmeyer, B. *Spectrochim. Acta, Part A* **1982**, *38*, 163−173.
(27) Michel, E.; Perie, J.; Lattes, A. *J. Organomet. Chem.* **1981**, *204*, 1−12.
(28) Browning, J.; Goggin, P. L.; Goodfellow, R. J.; Hurst, N. W.; Mallinson, L. G.; Murray, M. *J. Chem. Soc., Dalton Trans.* **1978**, 872−876.
(29) Versluis, L.; Ziegler, T. *J. Chem. Phys.* **1988**, *88*, 322−328.
(30) *ADF2010*; SCM, Theoretical Chemistry, Vrije Universiteit: Amsterdam, The Netherlands. http://www.scm.com.
(31) Vosko, S.; Wilk, L.; Nusair, M. *Can. J. Phys.* **1980**, *58*, 1200−1211.
(32) Becke, A. D. *Phys. Rev. A* **1988**, *38*, 3098−3100.
(33) Perdew, J. P. *Phys. Rev. B* **1986**, *33*, 8822−8824. Erratum: Perdew, J. P. *Phys. Rev. B* **1986**, *34*, 7406.
(34) Pye, C. C.; Ziegler, T. *Theor. Chem. Acc.* **1999**, *101*, 396−408.
(35) Klamt, A.; Schüürmann, G. *J. Chem. Soc., Perkin Trans. 2* **1993**, 799−805.
(36) Klamt, A. *J. Phys. Chem.* **1995**, *99*, 2224−2235.
(37) Klamt, A.; Jonas, V. *J. Chem. Phys.* **1996**, *105*, 9972−9981.
(38) Malkin, V. G.; Malkina, O. L.; M. Repiský, S. Komorovský, Malkin, I.; Malkin, E.; Arbuznikov, A. V.; Kaupp, M.; Ruud, K. *ReSpect program*, version 3.1.0; 2011.
(39) Komorovský, S.; Repiský, M.; Malkina, O.; Malkin, V. G.; Ondk, I. M.; Kaupp, M. *J. Chem. Phys.* **2008**, *128*, 104101−104115.
(40) Komorovský, S.; Repisky, M.; Malkina, O. L.; Malkin, V. G. *J. Chem. Phys.* **2010**, *132*, 154101.

(41) Perdew, J. P.; Burke, K.; Ernzerhof, M. *Phys. Rev. Lett.* **1996**, *77*, 3865−3868.
(42) Jensen, F. *J. Chem. Phys.* **2001**, *115*, 9113−9125.
(43) Jensen, F. *J. Chem. Phys.* **2002**, *116*, 3502−3502.
(44) Dyall, K. G. *Theor. Chem. Acc.* **2004**, *112*, 403−409.
(45) Adamo, C.; Barone, V. *J. Chem. Phys.* **1999**, *110*, 6158−6170.
(46) Frisch, M. J. et al. *Gaussian 03*, revision C.02; Gaussian, Inc.: Wallingford, CT, 2004.
(47) Häussermann, U. Unpublished report, 1988.
(48) Dalton2011, a molecular electronic structure program (2011). http://www.daltonprogram.org.
(49) Ruud, K.; Astrand, P.-O.; Taylor, P. R. *J. Chem. Phys.* **2000**, *112*, 2668−2683.

Paper III

The influence of a presence of a heavy atom on the spin-spin coupling constants between two light nuclei in organometallic compounds and halogen derivatives

Artur Wodyński and Magdalena Pecul

Citation: The Journal of Chemical Physics **140**, 024319 (2014); doi: 10.1063/1.4858466
View online: http://dx.doi.org/10.1063/1.4858466
View Table of Contents: http://scitation.aip.org/content/aip/journal/jcp/140/2?ver=pdfcov
Published by the AIP Publishing

THE JOURNAL OF CHEMICAL PHYSICS **140**, 024319 (2014)

The influence of a presence of a heavy atom on the spin-spin coupling constants between two light nuclei in organometallic compounds and halogen derivatives

Artur Wodyński and Magdalena Pecul[a)]
Faculty of Chemistry, University of Warsaw, Pasteura 1, 02-093 Warszawa, Poland

(Received 6 October 2013; accepted 13 December 2013; published online 14 January 2014)

The $^1J_{CC}$ and $^1J_{CH}$ spin-spin coupling constants have been calculated by means of density functional theory (DFT) for a set of derivatives of aliphatic hydrocarbons substituted with I, At, Cd, and Hg in order to evaluate the substituent and relativistic effects for these properties. The main goal was to estimate HALA (heavy-atom-on-light-atom) effects on spin-spin coupling constants and to explore the factors which may influence the HALA effect on these properties, including the nature of the heavy atom substituent and carbon hybridization. The methods applied range, in order of reduced complexity, from Dirac-Kohn-Sham method (density functional theory with four-component Dirac-Coulomb Hamiltonian), through DFT with two- and one-component Zeroth Order Regular Approximation (ZORA) Hamiltonians, to scalar non-relativistic effective core potentials with the non-relativistic Hamiltonian. Thus, we are able to compare the performance of ZORA-DFT and Dirac-Kohn-Sham methods for modelling of the HALA effects on the spin-spin coupling constants. © *2014 AIP Publishing LLC*. [http://dx.doi.org/10.1063/1.4858466]

I. INTRODUCTION

In the last two decades great progress has been made in methodology of relativistic quantum chemical calculations and in development of computer codes for this purpose. The importance of the relativistic effects is getting widely recognized in the scientific community and more and more molecular properties are being calculated using relativistic Hamiltonians. Developments in perturbational density functional theory (DFT) allowed for simultaneous inclusion of the relativistic and electron correlation effects for a variety of molecular properties for fairly large systems. Four- and two-components Hamiltonians are applied within the framework of density functional theory for calculations of such properties as linear molecular polarizabilities,[1–5] non-linear molecular polarizabilities and other high-order optical properties,[6–8] nuclear shielding constants,[9–15] and indirect spin-spin coupling constants.[16–20] The nuclear shielding constants and the spin-spin coupling constants of heavy nuclei are of special interest in this respect, since they depend on electron density in the vicinity of the nucleus, and it has been recognized early on[21] that electron velocities (and consequently the relativistic effects) are the largest in this region.

The presence of a heavy nucleus in a molecule affects not only the Nuclear Magnetic Resonance (NMR) properties of the heavy nucleus in question, but influences also the shielding constants and indirect spin-spin coupling constants of the nearby light nuclei. This phenomenon is called, after Pyykkö *et al.*,[22] the heavy-atom-on-light-atom (HALA) effect. While the relativistic effects on the shielding constants (or related to them chemical shifts) of light nuclei neighbouring heavy atoms are relatively well investigated in the literature[23–30] (although mainly for proton and carbon shielding constants in halogen derivatives, much less is known about metalorganic compounds), the parallel phenomenon occurring for the nuclear spin-spin coupling constants is almost unexplored. There is a handful of papers dealing with the situation when a heavy atom mediates the geminal coupling between two light nuclei,[31–35] and there seems to be a consensus that in this case the total relativistic effect is usually dominated by the scalar effects (unlike the HALA effect on the shielding constants, for which spin-orbit coupling plays a crucial role). There are, however, very few investigations concerning the situation where the heavy atom is not in the coupling path. One of those is our study on heavy metal cyanides,[29] where we have shown that the relativistic effect on the $^1J_{CN}$ spin-spin coupling constant may exceed 20% (for mercury cyanide) or even 40% (for gold cyanide) of the total value of the coupling. These findings inspired us to look more closely at the influence of the presence of heavy atom on the one-bond spin-spin coupling constant of the nearby light nuclei, and to investigate what factors determine the magnitude of the effect and whether the dominant role of the scalar relativistic effects is a general rule.

The systems under study are derivatives of aliphatic hydrocarbons substituted with I, At, Cd, and Hg. This choice allowed us to study both one-bond carbon-carbon and one-bond proton-carbon coupling constants and to explore the factors which may influence the HALA effect on these properties: the nature of the heavy atom substituent and carbon hybridization. These factors have been found important for carbon chemical shifts.[30,36] The calculations are carried out using density functional theory with the zeroth-order regular approximation (ZORA) Hamiltonian (with the spin-orbit term included), as implemented by Autschbach for the spin-spin

a)Author to whom correspondence should be addressed. Electronic mail: mpecul@chem.uw.edu.pl

coupling constants,[16,17] with the four-component Dirac-Coulomb Hamiltonian (as implemented recently by Saue),[37] and with the non-relativistic Hamiltonian combined with scalar effective core potentials (ECPs), since our secondary aim is to compare the performance of DFT with scalar ECPs, ZORA-DFT, and Dirac-Kohn-Sham (DKS) methods for modelling of the HALA effects on the spin-spin coupling constants.

The paper is organized as follows. After the description of the computational methods, we discuss the calculated $^1J_{CC}$ and $^1J_{CH}$ coupling constants, for each considering first the influence of the heavy atom charge and carbon hybridization on the HALA effect, and then moving to the methodological issues, comparing the results of calculations with ZORA, Dirac-Coulomb, and Schrödinger Hamiltonians, the latter both with relativistic ECPs and all-electron basis set. Finally, the results are summarized and main conclusions are presented.

II. COMPUTATIONAL DETAILS

A. Geometry optimization

The geometric parameters of the isolated molecules under study have been obtained by means of geometry optimization carried out using DFT with the zeroth-order regular approximation Hamiltonian[38] (the spin-orbit coupling term included) as implemented in the ADF[39] program with VWN[40]+Becke88[41] and Perdew86[42] exchange-correlation functional (the functional is denoted as BP86 in ADF, but actually differs from the functional usually indicated by this acronym by using VWN instead of the local correlation PZ81 functional[43]) and the TZ2P basis set. The same geometry parameters (obtained by means of spin-orbit ZORA calculation) have been used for all (DKS, ZORA, ECP) calculations of the spin-spin coupling constants in order to separate the effects of a different computational model on the molecular geometry and the spin-spin coupling constants.

B. DKS calculations of the spin-spin coupling constants

The four-component DKS calculations of the spin-spin coupling constants have been carried out with a local version of the DIRAC program,[44] including the recent developments by Saue.[37] The large and small components of the wave function have been connected by unrestricted kinetic balance, as implemented in DIRAC.[44] The Perdew, Burke, and Ernzerhof functional with Adamo and Barone's HF exchange contribution (PBE0)[45] has been used together with the uncontracted triple-ζ basis set with additional tight functions (aug-cc-pVTZ-J[46]) for carbon and hydrogen, and uncontracted triple-ζ Dyall's basis set (dyall.v3z[47]) for mercury, cadmium, iodine, and astatine. All calculations have been performed with the Gaussian charge distribution model, as default in DIRAC.

C. ZORA calculations of the spin-spin coupling constants

The ZORA results have been obtained using the DFT as implemented in the ADF program, employing the PBE0 hybrid functional. (First-order potential of the hybrid PBE0 functional have been used during the calculations of the spin-spin coupling constants.) The results obtained with both one-component scalar ZORA Hamiltonian (denoted as sc-ZORA) and with two-component spin-orbit ZORA Hamiltonian (denoted so-ZORA) will be presented. We have used triple-ζ Slater basis set with additional tight functions (jcpl[48]) for hydrogen, carbon, mercury, and iodine and the TZ2P (triple-ζ+2 polarization functions basis set) for cadmium and astatine. All calculations have been performed with the Gaussian charge distribution model.

D. ECP calculations of the spin-spin coupling constants

The effective core potential results have been obtained using the Gaussian 09[49] program. We have employed the PBE0 functional, the aug-cc-pVTZ-J basis set for carbon and hydrogen, and several effective core potentials for the heavy elements: LANL2DZ for iodine,[50] cadmium,[51] and mercury,[51] MWB28 for cadmium,[52] MWB46 for cadmium[53] and iodine,[54] MWB60 for mercury,[52] MWB78 for astatine[55] and mercury,[55] MDF28 for cadmium[56] and iodine,[57] MDF46 for iodine,[58] MDF60 for astatine[57] and mercury,[59] and MDF78 for astatine.[58]

E. Non-relativistic calculation of the spin-spin coupling constants

Two sets of non-relativistic calculations of the spin-spin coupling constants have been performed. The first set has been carried out using DFT as implemented in the ADF program with the PBE0 functional. We have used the triple-ζ Slater jcpl basis set available in the ADF program for hydrogen, carbon, mercury, and iodine and TZ2P for cadmium and astatine. The second set of calculations has been performed using DFT as implemented in Dalton 2011[60] program. The PBE0 functional, the Gauss-type uncontracted aug-cc-pVTZ-J basis set for carbon and hydrogen, and the uncontracted dyall.v3z basis set[47] for mercury, cadmium, iodine, and astatine have been used. This allows us to estimate the effect of using different basis sets in ADF and DIRAC calculations.

III. RESULTS AND DISCUSSION

Below, we are going to discuss the influence of the presence of a heavy atom on the spin-spin coupling constants between two light nuclei (first $^1J_{CC}$, then $^1J_{CH}$). For each coupling constant, we first consider the influence of various factors (the charge of the heavy nucleus, the carbon hybridization, the relative magnitude of the scalar and spin-orbit terms), and then compare the ZORA-DFT and DKS results and discuss the performance of the ECPs in rendering the scalar relativistic effects (Secs. III A 2 and III B 2, respectively). All results discussed in Subsections III A 1 and III B 1 have been obtained with the ADF package using the ZORA or non-relativistic Hamiltonians. Additional calculations, reported in Secs. III A 2 and III B 2, have been performed with

TABLE I. The $^1J_{CC}$ coupling constants calculated with the PBE0 functional using different Hamiltonians. Jcpl basis sets (TZ2P for cadmium and astatine) have been used for nonrelativistic, sc-ZORA, and so-ZORA calculations, aug-cc-pVTZ-J basis set for carbon and hydrogen, and dyall.v3z basis set for cadmium, mercury, iodine, astatine for DKS calculations. The relativistic term has been calculated as difference between so-ZORA and nonrelativistic results.

	Nonrelativistic (Hz)	sc-ZORA (Hz)	so-ZORA (Hz)	Relativistic term (Hz)	DKS (Hz)	Substituent effect (Hz)
ICCH	208.9	207.7	206.3	− 2.6	206.8	9.0
$ICHCH_2$	80.2	79.7	80.1	− 0.1	79.7	8.1
ICH_2CH_3	34.0	33.6	34.1	0.1	34.6	1.8
AtCCH	199.3	193.5	176.2	− 23.1	172.7	− 21.1
$AtCHCH_2$	80.0	78.9	78.9	− 1.1	78.2	6.8
$AtCH_2CH_3$	34.6	34.0	35.6	1.0	36.2	3.3
CH_3CdCCH	125.2	130.2	130.3	5.1	130.2	− 67.0
$CH_3CdCHCH_2$	59.2	60.8	60.7	1.5	60.6	− 11.4
$CH_3CdCH_2CH_3$	31.0	31.4	31.3	0.3	30.8	− 1.0
CH_3HgCCH	126.0	144.1	146.0	20.0	144.7	− 51.2
$CH_3HgCHCH_2$	59.1	64.9	64.9	5.9	64.7	− 7.1
$CH_3HgCH_2CH_3$	30.6	32.1	32.0	1.4	32.3	− 0.3
HCCH	197.2	197.3	197.3	...	...	...
CH_2CH_2	72.2	72.1	72.0	...	...	...
CH_3CH_3	32.4	32.3	32.3	...	...	...

the Dirac-Coulomb Hamiltonian and Schrödinger Hamiltonian combined with scalar relativistic ECPs.

A. $^1J_{CC}$ coupling constants

The $^1J_{CC}$ coupling constants calculated using the Schrödinger, ZORA and Dirac-Coulomb Hamiltonians are shown in Table I. Table I contains also the "relativistic effect," calculated as a difference between the so-ZORA and non-relativistic results, and the "substituent effect," calculated as a difference between the so-ZORA result for the compound under study and the corresponding unsubstituted aliphatic hydrocarbon.

1. General considerations

a. Influence of the charge of the heavy nucleus. The relativistic effects for the $^1J_{CC}$ spin-spin coupling constants under study are sizable for substituents from the 6th row of periodic table (for mercury and astatine compounds) in comparison with the total substituent effects, but nearly negligible (10% or less) for the 5th row compounds. In the case of mercury compounds, taking into account the relativistic effects significantly lower the calculated substituent effects. The same can be observed for cadmium derivatives, but in this case the relativistic effect is only about 10% of the total substituent effect. For iodine derivatives the relativistic effect on $^1J_{CC}$ is negligible (of the order of magnitude of numerical accuracy), with the exception of ICCH, where it lowers the calculated substituent effect by about 30%. In the case of AtCCH, the total substituent effect is actually dominated by the relativistic effect (the non-relativistic calculations lead to a very similar result as for HCCH). For other astatine derivatives, the relativistic effect is smaller, but still quite significant in comparison with the substituent effect. (Of the same sign for $AtCH_2CH_3$, of the opposite sign for $AtCHCH_2$.)

The magnitude of the relativistic effect changes strongly with carbon hybridization (as discussed in more detail below), but the trends in these changes are very similar in both series of structural analogs. The ratio between the relativistic effects for astatine derivative and its iodine analog is always about 11, and about 4 for mercury derivative and its cadmium analog.

b. Influence of the carbon hybridization. The magnitude of the substituent and relativistic effects on the $^1J_{CC}$ spin-spin coupling constants depends strongly on the hybridization of carbon atoms. The largest effects are observed for the systems with the *sp* hybridization and the smallest (at least one order of magnitude smaller) effects for the systems with the sp^3 hybridization (except for halides, where the relativistic effects for the sp^2 and sp^3 hybridization are of comparable magnitude). It is however worth noting that for the compounds containing the 12th group elements the relative contribution of the relativistic effect to the substituent effect actually increases when going from the *sp* to sp^3 hybridization, since the substituent effect decreases to a larger extent than the relativistic effect.

c. Influence of the spin-orbit coupling. The ratio of the scalar and spin-orbit contributions to the total relativistic effect on the $^1J_{CC}$ spin-spin coupling constant depends strongly on the nature of the heavy atom substituent. For halides both contributions are, as a rule, of similar magnitude, except for $AtCHCH_2$, where the scalar term dominates. Very small values of the relativistic effect on $^1J_{CC}$ in $ICHCH_2$ and ICH_2CH_3 result from mutual cancelling of the scalar and spin-orbit term, each about 0.5 Hz, but with the opposite signs. In mercury and cadmium derivatives, nearly the total relativistic effect comes from the scalar term, since the spin-orbit term contributes less than 10% to it (except for $CH_3CdCH_2CH_3$, but here the relativistic effect is very small). Larger role of spin-orbit coupling in the molecular properties of halides seems a general rule, connected with p-character of the heavy atom.

TABLE II. Comparison of the individual terms of $^1J_{CC}$ in AtCCH and CH_3HgCCH, obtained using nonrelativistic, sc-ZORA, and so-ZORA Hamiltonians.

	AtCCH (Hz)	CH_3HgCCH (Hz)
Nonrelativistic (ADF)	199.3	126.1
DSO	0.2	0.3
PSO	10.4	4.4
FC	176.2	111.3
SD	12.4	10.1
sc-ZORA	193.5	144.2
DSO	0.2	0.3
PSO	11.1	5.8
FC	169.7	127.5
SD	12.5	10.6
so-ZORA	176.2	146.0
DSO	0.2	0.3
PSO	10.3	5.9
FC	152.8	129.4
SD	10.5	10.8
FC+SD/PSO cross term	2.4	−0.3

Inspired by the work of Autschbach *et al.*,[17] we decided to examine the influence of the spin-orbit coupling on the individual terms of the spin-spin coupling constant. In the two-component computation, there exists a cross term between the spin-dependent Fermi contact (FC) and spin-dipole (SD) terms, and the paramagnetic spin-orbital (PSO) term, denoted later as FC+SD/PSO. In most cases the spin-orbit contribution to spin-spin coupling is dominated by this term. We have therefore compared (Table II) the individual terms of $^1J_{CC}$ in AtCCH (where the spin-orbit contribution is the largest) and in CH_3HgCCH, where the spin-orbit contribution is negligible with respect to the scalar term. The results show that in the case of CH_3HgCCH the FC+SD/PSO cross term is about 17% of the spin-orbit contribution (about −0.3 Hz), and approximately 15% of the spin-orbit contribution (about 2.4 Hz) in AtCCH. Therefore, unlike for the couplings of heavy nuclei analyzed by Autschbach *et al.*,[17] the FC+SD/PSO cross term is sizeable for $^1J_{CC}$, but does not dominate the spin-orbit contribution. Inclusion of the spin-orbit coupling changes predominantly the pure FC term.

2. Comparison of different computational methods

In this paragraph we compare the one-component and two-component ZORA results with the results of other available computational methods including the relativistic effects: four-component all-electron Dirac-Kohn-Sham method and effective core potentials. It should be stressed that comparison of ZORA and Dirac-Kohn-Sham results or ZORA and ECP results is not straightforward, since, out of necessity, different basis sets are used (ADF employs Slater orbital basis set, while in DIRAC or Gaussian program Gauss orbitals are used). For that reason we have also performed comparison of the results obtained using the Slater and Gauss orbitals with the non-relativistic Hamiltonians. Very good agreement between the results obtained with the jcpl (Slater type) basis set and the aug-cc-pVTZ-J/dyall.v3z (Gauss type) has been observed (see Ref. 61 for the data in Table 1). In most cases the results differ less than 0.5 Hz (for several cases the difference is between 0.5 and 1.0 Hz). Only for AtCCH a significantly larger difference is observed (about 2.8 Hz). Considering this, the use of different basis sets should not influence materially the comparison between the ZORA-DFT and DKS results, except when the relativistic effect is very small.

a. Comparison between so-ZORA and DKS. Inspection of the results in Table I leads to the conclusion that so-ZORA reproduces the DKS results very well. Explicit inclusion of small spinor during the calculation does not change significantly the calculated $^1J_{CC}$ couplings in comparison with two-component ZORA approximation: in most cases the differences are less than 1 Hz, and seems to be caused mostly by the change of the basis set (see above) rather than the picture change effects. Only for the systems with the heaviest metallic substituents and *sp*-hybridized carbon nuclei (i.e., CH_3HgCCH and AtCCH) the ZORA-DFT—DKS difference is slightly bigger (e.g., 3.4 Hz in the case of AtCCH) but a significant part of this change can be again attributed to the basis set effect (about 2.8 Hz, see above).

b. Comparison between sc-ZORA and ECPs methods. The $^1J_{CC}$ spin-spin coupling constants calculated using scalar ECPs are compared in Table III with the one-component scalar-only ZORA results. Again, it should be pointed out that a different basis set has been used for sc-ZORA and ECP calculations. Two types of ECPs have been investigated: Los Alamos ECPs (LANL2DZ) and series of Stuttgart ECPs (MDF and MWB with small and big core replacement). LANL2DZ does not reproduce the sc-ZORA results very well, and actually it does not offer any consistent improvement over the non-relativistic calculations. The same is true of the large-core MDF and MWB pseudopotentials, so it seems to be mainly a matter of replacing too many core electrons by the effective potential. The small-core MWB results are in excellent agreement with sc-ZORA. A slightly worse agreement is observed for small-core MDF results, but they are still a big improvement over the non-relativistic calculations, and the differences between the MWB60 and MDF60 results are usually very small.

One of a very few cases when a sizeable discrepancy (about 4 Hz) between the MWB60 and MDF60 results is observed is $^1J_{CC}$ in CH_3HgCCH. We have performed additional calculations with a more recent version of MDF60[56] (denoted in Table III as MDF60(new)) and obtained results much closer to MWB60; thus the observed difference is most likely a consequence of different fitting procedures employed to obtain the two ECPs.

B. $^1J_{CH}$ coupling constants

$^1J_{CH}$ coupling constants in the systems under study are of two types, as far as the placement of the coupled nuclei with respect to the heavy atom is concerned. First we are going to discuss the $^1J_{CH}$ coupling constants of the carbon nuclei directly bound with the heavy atom ($^1J_{C_\alpha H}$), and later the $^1J_{CH}$ coupling constants involving the carbon nuclei in beta

TABLE III. Comparison of $^1J_{CC}$ calculated with different types of effective core potentials on heavy atoms and aug-cc-pVTZ-J basis set on C and H, using PBE0 functional.

	LANL2DZ (Hz)	MDF Large[a] (Hz)	MDF Small[b] (Hz)	MDF60 New[c] (Hz)	MWB Large[a] (Hz)	MWB Small[b] (Hz)	sc-ZORA (Hz)
ICCH	210.0	209.5	207.6	...	210.7	...	207.7
$ICHCH_2$	79.5	79.4	79.3	...	79.5	...	79.7
ICH_2CH_3	33.5	33.5	33.6	...	33.5	...	33.6
AtCCH	...	197.9	194.3	...	196.5	...	193.5
$AtCHCH_2$	...	78.9	78.6	...	78.7	...	78.9
$AtCH_2CH_3$	...	33.9	34.0	...	33.9	...	34.0
CH_3CdCCH	121.3	...	131.4	...	120.4	131.5	130.2
$CH_3CdCHCH_2$	58.0	...	60.7	...	151.8	60.8	60.8
$CH_3CdCH_2CH_3$	30.7	...	31.4	...	30.7	31.5	31.4
CH_3HgCCH	128.0	...	140.6	144.1	130.6	144.3	144.2
$CH_3HgCHCH_2$	60.8	...	63.1	64.5	60.9	64.6	64.9
$CH_3HgCH_2CH_3$	31.1	...	31.8	32.1	31.3	32.1	32.2

[a]Large-core pseudopotential.
[b]Small-core pseudopotential.
[c]Small-core pseudopotential (60 core electrons replaced by a pseudopotential in Hg) reparametrized.[56]

position with respect to the heavy atom. In the latter case, for the system of the $RCHCH_2$ type, the coupled proton can be either in *cis* or in *trans* position with respect to the heavy atom, and for the RCH_2CH_3 systems the dihedral angle between the heavy atom–alpha carbon and hydrogen–beta carbon may play a role, so these factors will be discussed. The computational results are presented in Table IV.

1. General considerations

a. Influence of the charge of the heavy nucleus. The relativistic effects on the $^1J_{CH}$ coupling constants in iodine-substituted hydrocarbons are 1 Hz or less (even when carbon is in the α position with respect to the heavy atom). Somewhat larger effects (but still rather smaller than those resulting from other changes in computational protocol, e.g., the use of a different basis set) can be observed for astatine-substituted analogs. The only case when the relativistic effect on $^1J_{CH}$ constitutes a majority of the substituent effect (apart from $CH_3CdCH_2CH_3$, where the substituent effect is very small) takes place in organomercury compounds—there the relativistic effect can even exceed 10 Hz. The ratio between the relativistic effect for $^1J_{C_\alpha H}$ in organomercury compound and its cadmium analog is about 3 (similarly as for $^1J_{CC}$), and a similar regularity can be observed for the $^1J_{C_\beta H}$ couplings (but not for iodine/astatine analogs). Not surprisingly, the relativistic effect weakens with the distance of the coupled nuclei from the heavy atom: it is much larger for $^1J_{C_\alpha H}$ than for $^1J_{C_\beta H}$. In the case of $^1J_{C_\beta H}$ for cadmium compound with sp^2 and sp^3 carbon hybridization the relativistic contributions do not exceed 1.4 Hz, and for iodine compounds they are even smaller (about 0.4 Hz). The biggest contribution for $^1J_{C_\beta H}$ coupling constants is observed for CH_3HgCCH, where the relativistic term is 10.0 Hz. Interestingly, the relativistic calculations lead in this case to much smaller substituent effect than the non-relativistic ones.

b. Influence of the carbon hybridization and molecular geometry. Similarly as for $^1J_{CC}$, carbon hybridization influences the magnitude of the relativistic effects on $^1J_{C_\alpha H}$. They are bigger for the systems with the sp^2 hybridization than for the systems with the sp^3 hybridization (compare 15.3 Hz for $CH_3HgCHCH_2$ and 6.6 Hz for $CH_3HgCH_2CH_3$). Only for iodine derivatives a reverse trend is observed but in this case the relativistic terms are small (less than 0.7% of the total spin-spin coupling constant) and therefore sensitive to numerical noise. In the case of 12th group of periodic table and astatine compounds the ratio between the relativistic effects for the analogous systems with sp^2 and sp^3 hybridization is about 2–2.5.

The relativistic effects on $^1J_{C_\beta H}$ are visibly affected by the heavy atom–carbon–carbon-hydrogen dihedral angle. When *cis* and *trans* configurations of cadmium and mercury derivatives are compared, always the coupling of the proton in the *trans* position is more affected by the relativistic effects (and exhibits larger variation with carbon hybridization). This is not necessarily true for iodine and astatine derivatives, but, as mentioned above, the relativistic effects are usually negligibly small there.

c. Influence of the spin-orbit coupling. A comparison of the so-ZORA and sc-ZORA results shows that the spin-orbit coupling effect is as a rule negligible in comparison with the scalar term for all types of $^1J_{CH}$, except for astatine derivatives. For $^1J_{C_\alpha H}$ in $AtCHCH_2$ the spin-orbit coupling term is about −4.9 Hz (the scalar term is only 0.4 Hz), while for $^1J_{C_\beta H}$ in AtCCH it is about −4.7 Hz (to be compared with the scalar term of 0.2 Hz) and for $^1J_{C_\beta H_{trans}}$ in $AtCHCH_2$ it is about −2.0 Hz (the scalar term 0.1 Hz). It is noticeable that for astatine derivatives with sp^3 hybridization the spin-orbit coupling term is much smaller than for derivatives with sp^2 and *sp* carbon.

2. Comparison of different computational approaches

a. Comparison between so-ZORA and DKS. Inspection of the results (see Table IV) for all $^1J_{CH}$ confirms that the two-component ZORA approximation reproduces the

TABLE IV. $^1J_{CH}$ calculated with PBE0 functional at different levels of theory. The Jcpl basis sets (TZ2P for cadmium and astatine) have been used for nonrelativistic, sc-ZORA, and so-ZORA calculations, aug-cc-pVTZ-J basis set for carbon and hydrogen, and dyall.v3z basis set for cadmium, mercury, iodine, astatine for DKS calculations. The relativistic term has been calculated as a difference between so-ZORA and nonrelativistic results.

		Nonrelativistic (Hz)	sc-ZORA (Hz)	so-ZORA (Hz)	Relativistic term (Hz)	DKS (Hz)	Substituent effect (Hz)
$^1J_{C_\alpha H}$	$ICHCH_2$	196.1	197.2	197.0	0.9	195.9	37.9
	ICH_2CH_3	151.9	152.5	153.0	1.1	152.9	27.8
	$AtCHCH_2$	197.0	197.4	192.5	−4.5	190.9	33.4
	$AtCH_2CH_3$	153.8	154.5	155.2	1.3	155.0	30.0
	$CH_3CdCHCH_2$	139.0	143.8	143.7	4.7	143.4	−15.4
	$CH_3CdCH_2CH_3$	126.0	128.3	128.2	2.2	127.8	2.9
	$CH_3HgCHCH_2$	137.5	152.1	152.8	15.3	151.9	−6.3
	$CH_3HgCH_2CH_3$	125.0	131.6	131.6	6.6	131.0	6.4
$^1J_{C_\beta H_{cis}}$	$ICHCH_2$	167.9	167.7	167.6	−0.3	166.8	8.5
	ICH_2CH_3	131.6	131.5	131.4	−0.2	131.1	6.2
	$AtCHCH_2$	167.7	167.2	166.8	−0.9	166.0	7.7
	$AtCH_2CH_3$	131.6	131.2	130.7	−0.9	130.3	5.4
	$CH_3CdCHCH_2$	159.0	159.1	159.1	0.0	158.2	−0.1
	$CH_3CdCH_2CH_3$	124.7	125.0	124.9	0.2	124.7	−0.3
	$CH_3HgCHCH_2$	160.9	160.3	160.3	−0.6	159.3	1.2
	$CH_3HgCH_2CH_3$	125.3	125.8	125.8	0.5	125.4	0.6
$^1J_{C_\beta H_{trans}}$	$ICHCH_2$	161.7	162.4	161.9	0.2	160.9	2.8
	ICH_2CH_3	122.2	122.6	122.6	0.4	122.2	−2.6
	$AtCHCH_2$	162.1	162.2	160.2	−1.9	159.1	1.0
	$AtCH_2CH_3$	122.4	122.4	122.4	0.0	121.9	−2.8
	$CH_3CdCHCH_2$	153.3	154.6	154.6	1.4	153.9	−4.5
	$CH_3CdCH_2CH_3$	124.1	124.5	124.5	0.4	124.3	−0.8
	$CH_3HgCHCH_2$	151.2	155.8	156.1	4.9	155.7	−3.0
	$CH_3HgCH_2CH_3$	122.9	124.4	124.3	1.5	124.4	−0.9
$^1J_{C_\beta H}$	ICCH	270.7	271.6	271.1	0.4	270.1	8.7
	AtCCH	269.6	269.4	264.7	−4.9	263.7	2.3
	CH_3CdCCH	239.7	242.6	242.6	2.9	241.6	−19.8
	CH_3HgCCH	237.4	246.8	247.4	10.0	247.1	−14.9
$^1J_{C_\alpha H}$ $-CH_3$	CH_3CdCCH	129.7	132.1	132.0	2.3	131.3	6.2
	CH_3HgCCH	128.1	135.0	134.9	6.8	133.9	9.1
$^1J_{CH}$	CHCH	262.2	262.4	262.4	...	...	...
	CH_2CH_2	159.1	159.2	159.1	...	...	...
	CH_3CH_3	125.2	125.3	125.2	...	...	...
	CH_4	125.7	125.8	125.8	...	...	...

four-component DKS results very well, especially when the fact that two different basis sets (Slater- and Gauss-type) are used is taken into account. The biggest difference between so-ZORA/DFT and DKS (about 1.6 Hz) is observed for $^1J_{C_\alpha H}$ in $AtCHCH_2$, but it seems to originate from different basis sets used (compare the non-relativistic results obtained with the Slater- and Gauss-type basis sets tabulated in Table 2 in the supplementary material[61]). For the other $^1J_{CH}$ spin-spin coupling constants the differences between so-ZORA/DFT and DKS are in most cases less than 1.0 Hz and also seem to come mostly from using different basis sets. Thus, we conclude that so-ZORA/DFT is very efficient in rendering HALA effects on the $^1J_{CH}$ coupling constants. In fact, in most cases (apart from astatine derivatives), using one-component scalar ZORA is sufficient.

b. Comparison between sc-ZORA and ECPs methods. The $^1J_{CH}$ coupling constants calculated using different scalar relativistic effective core potentials are compared with the sc-ZORA results in Table 3 in the supplementary material.[61] The observations are similar as for the $^1J_{CC}$ coupling constants. ECPs in general seem suitable for the purpose, and the best results are obtained when small-core ECPs are employed. Among small-core ECPs, MWB appears to perform slightly better than MDF, but the differences are small.

IV. SUMMARY AND CONCLUSIONS

The $^1J_{CC}$ and $^1J_{CH}$ spin-spin coupling constants have been calculated by means of density functional theory for a set of derivatives of aliphatic hydrocarbons substituted with I, At, Cd, and Hg in order to evaluate the substituent and relativistic effects for these properties. The methods applied range, in order of reduced complexity, from Dirac-Kohn-Sham method (density functional theory with four-component Dirac-Coulomb Hamiltonian), through DFT with two- and one-component zeroth order regular approximation Hamiltonians, to scalar non-relativistic effective core potentials with

the non-relativistic Hamiltonian. The most important observations can be summarized as follows.

The relativistic effects on the spin-spin coupling constants under study are at most about 25 Hz (for $^1J_{CC}$ in organomercury compounds), and constitute up to 30% of the substituent effect (defined as a difference between the value of the coupling in the compound under study and the corresponding hydrocarbon). Predictably, they vary with the charge of the heavy nucleus. For $^1J_{CC}$, the ratio between relativistic effects for astatine derivative and its iodine analog is always about 11, and for mercury derivative and its cadmium analog about 4. The ratio between the relativistic effect for $^1J_{C_\alpha H}$ in organomercury compound and its cadmium analog is about 3 and a similar regularity can be observed for the $^1J_{C_\beta H}$ couplings (but not for the iodine/astatine analogs).

The magnitude of the relativistic effects on the $^1J_{CC}$ and $^1J_{CH}$ coupling constants depends very much on carbon hybridization. For both couplings the largest effects are observed for the *sp* hybridization. As expected, the relativistic effects are larger for $^1J_{C_\alpha H}$ than for $^1J_{C_\beta H}$, although even for the latter they can be non-negligible (10 Hz for CH_3HgCCH). $^1J_{C_\beta H}$ are larger when the proton is in the *trans* position to the heavy substituent than when it is in a *cis* position.

A comparison of the results obtained by means of different methods of including the relativistic effects indicates that ZORA-DFT (with the spin-orbit term included) reproduces the DKS results very well. The scalar contributions dominate the total relativistic effect on $^1J_{CC}$ and $^1J_{CH}$ in mercury and cadmium derivatives, while for $^1J_{CC}$ and $^1J_{CH}$ in halides scalar and spin-orbit effects contribute to a similar degree. The performance of scalar ECPs depends, obviously, on the relative weight of the scalar and relativistic effects, but when the former are dominant, ECPs reproduce correctly the results obtained with more elaborate relativistic method, provided the outer core electrons on the heavy atom are accounted for explicitly ("small core" types of ECPs).

ACKNOWLEDGMENTS

This work has received support from the Polish National Science Centre via the Grant No. N N204 148565, and from the Wrocław Centre for Networking and Supercomputing through a grant of computer time. MPD/2010/4 project, realized within the MPD programme of Foundation for Polish Science, cofinanced from European Union, Regional Development Fund, is acknowledged for a fellowship to A. Wodyński. The project has been carried out with the use of CePT infrastructure financed by the European Union - the European Regional Development Fund within the Operational Programme "Innovative economy" for 2007-2013.

[1] P. Salek, T. Helgaker, and T. Saue, Chem. Phys. **311**, 187 (2005).
[2] N. Gaston, P. Schwerdtfeger, T. Saue, and P. Norman, J. Chem. Phys. **124**, 044304 (2006).
[3] A. Devarajan, A. Gaenko, and J. Autschbach, J. Chem. Phys. **130**, 194102 (2009).
[4] C. Thierfelder, B. Assadollahzadeh, P. Schwerdtfeger, S. Schaefer, and R. Schaefer, Phys. Rev. A **78**, 052506 (2008).
[5] S. Villaume, T. Saue, and P. Norman, J. Chem. Phys. **133**, 064105 (2010).
[6] J. Henriksson, T. Saue, and P. Norman, J. Chem. Phys. **128**, 024105 (2008).
[7] R. Bast, T. Saue, J. Henriksson, and P. Norman, J. Chem. Phys. **130**, 024109 (2009).
[8] R. Bast, K. Ruud, A. Rizzo, and T. Helgaker, Theor. Chem. Acc. **129**, 685 (2011).
[9] S. Wolff, T. Ziegler, E. van Lenthe, and E. Baerends, J. Chem. Phys. **110**, 7689 (1999).
[10] Y. Xiao, D. Peng, and W. Liu, J. Chem. Phys. **126**, 081101 (2007).
[11] L. Cheng, Y. Xiao, and W. Liu, J. Chem. Phys. **130**, 144102 (2009); **131**, 019902 (2009) (erratum).
[12] J. Seino and M. Hada, J. Chem. Phys. **132**, 174105 (2010).
[13] S. Komorovský, M. Repiský, O. L. Malkina, V. G. Malkin, I. M. Ondík, and M. Kaupp, J. Chem. Phys. **128**, 104101 (2008).
[14] S. Komorovský, M. Repiský, O. L. Malkina, and V. G. Malkin, J. Chem. Phys. **132**, 154101 (2010).
[15] M. Olejniczak, R. Bast, T. Saue, and M. Pecul, J. Chem. Phys. **136**, 014108 (2012).
[16] J. Autschbach and T. Ziegler, J. Chem. Phys. **113**, 936 (2000).
[17] J. Autschbach and T. Ziegler, J. Chem. Phys. **113**, 9410 (2000).
[18] M. Filatov and D. Cremer, J. Chem. Phys. **120**, 11407 (2004).
[19] J. I. Melo, M. C. Ruiz de Azúa, J. E. Peralta, and G. E. Scuseria, J. Chem. Phys. **123**, 204112 (2005).
[20] M. Repiský, S. Komorovský, O. L. Malkina, and V. G. Malkin, Chem. Phys. **356**, 236 (2009).
[21] M. S. Vallarta and N. Rosen, Phys. Rev. **41**, 708 (1932).
[22] P. Pyykkö, A. Görling, and N. Rösch, Mol. Phys. **61**, 195 (1987).
[23] M. Kaupp, V. G. Malkin, O. L. Malkina, and D. R. Salahub, Chem. Phys. Lett. **235**, 382 (1995).
[24] M. Kaupp and O. L. Malkina, J. Chem. Phys. **108**, 3648 (1998).
[25] S. Berger, W. Bock, G. Frenking, V. Jonas, and F. Mueller, J. Am. Chem. Soc. **117**, 3820 (1995).
[26] M. Kaupp, Chem. Eur. J. **2**, 348 (1996).
[27] M. Kaupp, in *Relativistic Electronic Structure Theory. Part 2. Applications*, edited by P. Schwerdtfeger (Elsevier, Amsterdam, 2004), p. 552.
[28] M. Kaupp, O. L. Malkina, V. G. Malkin, and P. Pyykkö, Chem. Eur. J. **4**, 118 (1998).
[29] A. Wodyński, M. Repiský, and M. Pecul, J. Chem. Phys. **137**, 014311 (2012).
[30] A. Wodyński, A. Gryff-Keller, and M. Pecul, J. Chem. Theory Comput. **9**, 1909 (2013).
[31] A. Bagno and G. Saielli, J. Am. Chem. Soc. **129**, 11360 (2007).
[32] M. Olejniczak and M. Pecul, ChemPhysChem **10**, 1247 (2009).
[33] M. Kauch and M. Pecul, ChemPhysChem **13**, 1332 (2012).
[34] S. Kirpekar, H. Jensen, and J. Oddershede, Theor. Chim. Acta **95**, 35 (1997).
[35] J. Vaara, K. Ruud, and O. Vahtras, J. Comput. Chem. **20**, 1314 (1999).
[36] J. Vaara, O. L. Malkina, H. Stoll, V. G. Malkin, and M. Kaupp, J. Chem. Phys. **114**, 61 (2001).
[37] T. Saue, "Dirac-Kohn-Sham calculations of nuclear spin-spin coupling constants," personal communication (2013).
[38] L. Versluis and T. Ziegler, J. Chem. Phys. **88**, 322 (1988).
[39] ADF2010, SCM, Theoretical Chemistry, Vrije Universiteit, Amsterdam, The Netherlands, see http://www.scm.com.
[40] S. Vosko, L. Wilk, and M. Nusair, Can. J. Phys. **58**, 1200 (1980).
[41] A. D. Becke, Phys. Rev. A **38**, 3098 (1988).
[42] J. P. Perdew, Phys. Rev. B **33**, 8822 (1986).
[43] J. P. Perdew and A. Zunger, Phys. Rev. B **23**, 5048 (1981).
[44] DIRAC, a relativistic *ab initio* electronic structure program, Release DIRAC11, 2011, written by R. Bast, H. J. Aa. Jensen, T. Saue, and L. Visscher, with contributions from V. Bakken, K. G. Dyall, S. Dubillard, U. Ekström, E. Eliav, T. Enevoldsen, T. Fleig, O. Fossgaard, A. S. P. Gomes, T. Helgaker, J. K. Lærdahl, J. Henriksson, M. Iliaš, Ch. R. Jacob, S. Knecht, C. V. Larsen, H. S. Nataraj, P. Norman, M. Olejniczak, J. Olsen, J. K. Pedersen, M. Pernpointner, K. Ruud, P. Sałek, B. Schimmelpfennig, J. Sikkema, A. J. Thorvaldsen, J. Thyssen, J. van Stralen, S. Villaume, O. Visser, T. Winther, and S. Yamamoto, see http://dirac.chem.vu.nl.
[45] C. Adamo and V. Barone, J. Chem. Phys. **110**, 6158 (1999).
[46] P. F. Provasi, G. A. Aucar, and S. P. A. Sauer, J. Chem. Phys. **115**, 1324 (2001).
[47] K. G. Dyall, Theor. Chem. Acc. **112**, 403 (2004).
[48] J. Autschbach, J. Chem. Phys. **129**, 094105 (2008).
[49] M. J. Frisch, G. W. Trucks, H. B. Schlegel *et al.*, Gaussian 09, Revision C.01, Gaussian Inc., Wallingford, CT, 2009.
[50] W. R. Wadt and P. J. Hay, J. Chem. Phys. **82**, 284 (1985).
[51] P. J. Hay and W. R. Wadt, J. Chem. Phys. **82**, 270 (1985).

[52]D. Andrae, U. Häussermann, M. Dolg, H. Stoll, and H. Preuss, Theor. Chim. Acta **77**, 123 (1990).
[53]F. Schautz, H.-J. Flad, and M. Dolg, Theor. Chem. Acc. **99**, 231 (1998).
[54]A. Bergner, M. Dolg, W. Küchle, H. Stoll, and H. Preuß, Mol. Phys. **80**, 1431 (1993).
[55]W. Küchle, M. Dolg, H. Stoll, and H. Preuss, Mol. Phys. **74**, 1245 (1991).
[56]D. Figgen, G. Rauhut, M. Dolg, and H. Stoll, Chem. Phys. **311**, 227 (2005).
[57]K. A. Peterson, D. Figgen, E. Goll, H. Stoll, and M. Dolg, J. Chem. Phys. **119**, 11113 (2003).
[58]H. Stoll, B. Metz, and M. Dolg, J. Comput. Chem. **23**, 767 (2002).
[59]U. Häussermann, M. Dolg, H. Stoll, H. Preuss, P. Schwerdtfeger, and R. Pitzer, Mol. Phys. **78**, 1211 (1993).
[60]Dalton2011, a molecular electronic structure program, 2011, see http://www.daltonprogram.org.
[61]See supplementary material at http://dx.doi.org/10.1063/1.4858466 for comparison of the carbon-carbon (Table 1) and carbon-proton (Table 2) coupling constants calculated at non-relativistic level with Slater-type and Gauss-type basis sets; comparison of the carbon-proton coupling constants calculated with different types of effective core potentials (Table 3).

Paper IV

The relativistic effects on the carbon-carbon coupling constants mediated by a heavy atom

Artur Wodyński,[1] Olga Malkin,[2] and Magdalena Pecul [a)1]

[1)] *Faculty of Chemistry, University of Warsaw, Pasteura 1, 02-093 Warszawa, Poland*

[2)] *Institute of Inorganic Chemistry, Slovak Academy of Sciences, Dubravska cesta 9, SK-84536 Bratislava, Slovak Republic;*
Department of Inorganic Chemistry, Faculty of Natural Sciences, Comenius University, SK-84215 Bratislava, Slovakia

The $^{2}J_{CC}$, $^{3}J_{CC}$, and $^{4}J_{CC}$ spin-spin coupling constants in the systems with a heavy atom (Cd, In, Sn, Sb, Te, Hg, Tl, Pb, Bi and Po) in the coupling path have been calculated by means of density functional theory. The main goal was to estimate the relativistic effects on spin-spin coupling constants and to explore the factors which may influence them, including the nature of the heavy atom and carbon hybridization. The methods applied range, in order of reduced complexity, from the Dirac-Kohn-Sham (DKS) method (density functional theory with four-component Dirac-Coulomb Hamiltonian), through DFT with two- and one-component Zeroth Order Regular Approximation (ZORA) Hamiltonians, to scalar effective core potentials (ECPs) with the non-relativistic Hamiltonian. The use of DKS and ZORA methods leads to very similar results, and small-core ECPs of the MDF and MWB variety reproduce correctly the scalar relativistic effects. Scalar relativistic effects usually are larger than the spin-orbits coupling effects. The latter tend to influence the most the coupling constants of the sp^3-hybridized carbon atoms, and in compounds of the p-block heavy atoms.

[a)] Corresponding author, mpecul@chem.uw.edu.pl

I. INTRODUCTION

Prediction of spectroscopic parameters of metalorganic compounds containing transition or rare earth elements presents unique challenges. Such calculations require going beyond the conventional approaches of quantum chemistry, based on the Schrödinger equation, and employing instead methods capable of including relativistic effects. It is particularly vital for Nuclear Magnetic Resonance (NMR) parameters such as nuclear shielding constants (or chemical shifts) and nuclear spin-spin coupling constants, since these properties depend to a large extent on the electron density in immediate proximity of the nucleus, where the electron velocities (and consequently the relativistic effects) are the largest. However, it turns out that relativity affects not only the NMR parameters of heavy nuclei, but also of the nearby light nuclei, the phenomenon known as heavy-atom-on-light-atom (HALA) effect[1].

The HALA effect for the shielding constants is relatively well investigated in the literature[2–10]. It has been found that it is usually dominated by the spin-orbit coupling, at least when the light nucleus in question is directly bonded to the heavy atom[11–15]. Less is known about the parallel phenomenon occurring for the nuclear spin-spin coupling constants. It seems in this case scalar relativistic effects tend to be dominant[8,11–13], although the ratio between them and spin-orbit effects seems to depend on several factors, among them the nature of the heavy atom substituent and the type of its bond with the light nucleus. In the case of one-bond carbon-carbon coupling constants, strong correlation between the HALA effect and carbon hybridization can be observed, as shown in the previous work by the authors[10]. In this contribution, we extent these investigations to the carbon-carbon coupling constants through two, three and four bonds, where the heavy atom is in the coupling path.

We present the results of the calculation of the carbon-carbon coupling constants carried out for a series of systems with a heavy metal atom (Cd, In, Sn, Sb, Te, Hg, Tl, Pb, Bi and Po) mediating the coupling. For most of them no experimental data exist, and obtaining them would be difficult. They have been selected instead to cover a wide range of electron configurations of the heavy atom and hybridization of the carbon atom, and to allow for investigation of the influence of the charge of the heavy nucleus on the HALA effect. The applied computational methods range from the relativistic effective core potentials applied with non-relativistic Hamiltonians, through calculations with relativis-

tic one-component (scalar zeroth-order perturbational theory, ZORA) and two-component (spin-orbit zeroth order regular approximation ZORA) Hamiltonians, to Dirac-Kohn-Sham calculations (with four-component Dirac-Coulomb Hamiltonian).

Our secondary aim is to compare the DKS results obtained using density fitting procedure in evaluation of matrix elements of the exchange-correlation kernel (which considerably speeds up the calculations)[16] *and conventional computational procedure.*

II. COMPUTATIONAL DETAILS

A. Geometry optimization

The geometric parameters of the isolated molecules under study have been obtained by means of geometry optimization carried out using DFT with the zeroth-order regular approximation Hamiltonian [17] (the spin-orbit coupling included) as implemented in the ADF[18] program with VWN[19]+Becke88[20] and Perdew86[21] exchange-correlation functional (the functional is denoted as BP86 in ADF, but actually differs from the functional usually indicated by this acronym by using VWN instead of the local correlation PZ81 functional[22]) and the TZ2P basis set. Optimization of the structural parameters was followed by a frequency check to ensure that the obtained stationary points are true minima on the potential energy surface.

The same geometry parameters (obtained by means of spin-orbit ZORA calculation) have been used for all (DKS, ZORA, ECP) calculations of the spin-spin coupling constants in order to separate the effects of a different computational model on the molecular geometry and the spin-spin coupling constants.

B. DKS calculations of the spin-spin coupling constants

The four-component Dirac-Kohn-Sham (DKS) calculations of the spin-spin coupling constants have been carried out with the ReSpect program, including the recent modifications by Křístkováa *et al*[16]. The large and small components of the wave function have been connected by explicit magnetic balance approach of Komorovský *et al*[23]. The Perdew, Burke and Ernzerhof functional (PBE)[24] has been used together with the uncontracted triple-ζ Jensen basis set with additional tight functions (upcJ-2) for carbon and hydrogen, and

uncontracted triple-ζ Dyall's basis set (dyall.v3z[25]) for cadmium, indium, tin, antimony, tellurium, mercury, thallium, lead, bismuth and polonium. Density fitting procedure with upc-2 auxiliary basis set has been applied for one set of the results. The calculations have been performed with the Gaussian charge distribution model and the finite model to describe the nuclear magnetic moment.

C. ZORA-DFT calculations of the spin-spin coupling constants

The ZORA-DFT results have been obtained using DFT as implemented in the ADF program[18] **Cytujemy tylko program czy autorow modulow?**, employing the PBE functional. (First-order potential of the PBE functional have been used during the calculations of the spin-spin coupling constants.) The results obtained with both one-component scalar ZORA Hamiltonian (denoted as sc-ZORA) and with two-component spin-orbit ZORA Hamiltonian (denoted so-ZORA) will be presented. We have used triple-ζ Slater basis set with additional tight functions (jcpl[26]) for hydrogen, carbon, mercury, thallium, lead and the TZ2P (triple-ζ+2 polarization functions basis set) for cadmium, indium, tin, antimony, tellurium, bismuth and polonium. The calculations have been performed with the Gaussian charge distribution model. Other options have been set as default in ADF.

D. ECP calculations of the spin-spin coupling constants

The effective core potential results have been obtained using the Gaussian 09[27] program. We have employed the PBE functional, the pcJ-2 basis set for carbon and hydrogen, and several effective core potentials for the heavy elements: LANL2DZ[28] for cadmium, indium, tin, antimony, tellurium, mercury, tallium, lead and bismuth; MDF28[29–31] for cadmium, indium, antimony and tellurium; MWB28[32,33] for cadmium and indium; MWB46[34,35] for cadmium, indium, tin, antimony, tellurium; MDF60 [29–31,36] for mercury, tallium, lead, bismuth and polonium; MWB60[37,38] for mercury and tallium; MWB78[39] for mercury, tallium, lead, bismuth and pollonium; MDF78[30,40] for lead, bimsuth and polonium.

E. Non-relativistic calculation of the spin-spin coupling constants

Two sets of non-relativistic calculations of the spin-spin coupling constants have been performed. The first set has been carried out using DFT as implemented in the ADF program with the PBE functional and the same basis set as used for ZORA calculations. The second set of calculations has been performed using DFT as implemented in the Dalton 2011[41] program, also with the PBE functional, and the same basis set as used for DKS calculations. This allows us to estimate the effect of using different basis sets in ZORA (ADF) and DKS (ReSpect) calculations.

III. RESULTS AND DISCUSSION

The calculated $^2J_{CC}$,$^3J_{CC}$ and $^4J_{CC}$ coupling constants are shown in Table I, II and III, respectively. For the compounds where the couplings differ because of broken symmetry (i.e. those with the sp^2 carbon) the arthmetic averages are shown.

A. $^2J_{CC}$ coupling constants

1. Influence of the type of the heavy atom

a. Influence of the electron configuration of the heavy atom The $^2J_{CC}$ coupling constants calculated using the Schrödinger, ZORA and Dirac-Coulomb Hamiltonians are shown in Table I. Predictably, the absolute value of geminal spin-spin coupling constant changes significantly with the electron configuration of the heavy atom through which it is transmitted. Inspection of the results shows that in most cases the biggest (in terms of their absolute values) spin-spin coupling constants are observed for the 12th group of the periodic table and the smallest for systems containing elements from the 16th group of the periodic table. It is worth noting that, unlike geminal couplings transmitted through single-bonded carbon atom, most of the calculated $^2J_{CC}$ couplings are positive (even when evaluated at the non-relativistic level). The negative sign occurs only for the couplings in the 15th and 16th group compounds.

b. Influence of the charge of the heavy nucleus The $^2J_{CC}$ coupling constants vary significantly when the compounds containing metal atoms from the same group of periodic

table are compared. A comparison of the relativistic and non-relativistic results shows that this is purely a relativistic effect: the non-relativistic results for example for cadmium and mercury compounds are almost the same. The $^2J_{CC}$ coupling in the 5th row compounds are smaller than in the 6th row analogs, since for the 5th row of periodic table the relativistic effects do not exceed 26% of the total spin-spin coupling constant (with the exception of $Sb(CCH)_3$ and $Te(CH_3)_3$ where the relative effects are bigger, but only because the total spin-spin coupling constant are small). For the 6th row of periodic table the relativistic effects are even as much as 83% (for $Bi(CCH)_3$) of the total spin-spin coupling constant, leading to significant increase of the coupling. The ratio between relativistic contributions (calculated as percentage of the relativistic term in the total value of spin-spin coupling constant) for 5th row elements and 6th row elements in the same group of periodic table is about 2.0-2.5 (with deviations for some molecules containing the metals of the 12th and 15th group).

c. Correlation with geometry parameters It is known that geminal coupling constants depend strongly on bond angle (see for example Ref.[42]). Consequently, we have investigated how the $^2J_{CC}$ couplings in the compounds under study correlate with the C-Me-C bond angle. A quasi-linear relationship between the absolute value of the spin-spin coupling constant (computed with the so-ZORA Hamiltonian) and the C-Me-C angle was observed for 5th and 6th row of periodic table (see Figure 2 and 3). Apparently, much of the variation of the metal-transmitted $^2J_{CC}$ with the electron configuration of the metal can be rationalized in this way.

2. Influence of the carbon hybridization

The magnitude of the relativistic term on the $^2J_{CC}$ spin-spin coupling constants depends strongly on the hybridization of carbon atoms. Similarly as it has been observed for the $^1J_{CC}$ coupling constants[10] the largest relativistic effects are observed for the systems with the sp hybridization and the smallest effects (at least five time smaller) for the systems with the sp^3 hybridization. The size of the relativistic contribution for systems containing the sp^3-type carbon atom is about 7-61% of the size of relativistic contributions for the systems containing the sp-type carbon atom.

3. The spin-orbit coupling and scalar terms

Relativistic effects can be divided into those originating from the spin-orbit coupling (spin-dependent terms) and the spin-free, or scalar terms. For the discussed properties the scalar terms as a rule dominate and the spin-orbit coupling contributions have an opposite sign to it. However, the ratio between them depends strongly on the charge of the metal nucleus, the metal electron configuration, and the hybridization type of carbon atom.

The spin-orbit coupling term in $^2J_{CC}$ is much bigger for the 6th row elements derivatives than for the 5th row elements derivatives, and in some cases prevails over the scalar term. It varies strongly with the electron configuration of the metal atom. For mercury compounds the spin-orbit coupling term is about 56% of the scalar term (for $Hg(CH_3)_2$), for thallium and lead compounds it does not exceed 17%, for bismuth compounds this term is slightly bigger (about 40%), and finally for polonium compounds the spin-orbit coupling dominates over the scalar term (for $Po(CH_3)_2$ the spin-orbit coupling term is 2.5 times bigger than the scalar term). Similar variation can be observed for the 5th row compounds: the spin-orbit coupling term for cadmium, indium and tin compounds is about 3-10% of the scalar term, while for antimony and tellurium compounds it can be even about 84% of the scalar term.

The ratio between the spin-orbit coupling and the scalar terms depends strongly on carbon hybridization. Smallest impact of the spin-orbit coupling term is observed for systems with the -CCH substituent and the largest for systems with the $-CH_3$ substituent.

Inspired by the work of Autschbach *et al*[43] and our previous research on $^1J_{CC}$ in systems containing heavy atoms[10], in order to rationalize the observed trends we decided to examine the influence of the spin-orbit coupling on the individual terms of the spin-spin coupling constant. At the two-component level there exists a cross term between the spin-dependent FC+SD terms, and the PSO term, denoted later as FC+SD/PSO (for one-component calculations this term is zero, since there is no coupling between triplet and singlet operators). In most cases, the spin-orbit contribution to spin-spin coupling is dominated by this cross term for the coupling constants between heavy nuclei[43], whereas for the coupling constants between light atoms ($^1J_{CC}$ and $^1J_{CH}$) spin-orbit coupling term is dominated by change of pure Fermi contact term[10]. We have therefore compared (Table IV) the individual terms of $^2J_{CC}$ for tellurium and polonium compounds, where the spin-orbit coupling contribution is the largest. The results show that the spin-orbit coupling changes the pure FC+SD term

(denoted later as FC+SD change) and induces a sizeable FC+SD/PSO cross term, whereas the change of the SO (PSO+DSO) term is negligible (less than 0.01 Hz).

The sum-over-states expressions for the spin-orbit coupling terms suggest their linear dependence on the inverse of the lowest singlet-triplet excitation energy, assuming the dominant contribution arises from this excitation.[44]. To verify this, the relevant HOMO-LUMO triplet excitation energies have been computed using two-component ZORA approach and compared with spin-orbit coupling contributions to $^2J_{\mathrm{CC}}$. The results (shown as a function of an inverse of the triplet excitation energy) are shown in Figure 5 (the spin-orbit coupling contributions to the FC+SD term) and Figure 6 (the FC+SD/PSO cross term). For both spin-orbit terms there is some correlation, but a rather crude one. In particular, the spin-orbit contribution to the Fermi contact term in $Hg(CCH)_2$ is much larger than its HOMO-LUMO triplet excitation energy would indicate, which can be ascribed to the large value of the transition moment (numerator in the sum-over-states expansion). The large effect of spin-orbit coupling for pollonium compounds is connected with the low-energy HOMO-LUMO triplet transition involving the p electrons of the central atom.

The scalar relativitic effects influence predominantly the Fermi contact term. The changes of other terms (i.e. paramagnetic spin-orbit, diamagnetic spin-orbit and spin-dipole term) are negligible (less than 1%). The relative scalar effect on the Fermi contact term correlates to some extent with the change of electron density on carbon nucleus induced by the scalar effects, as shown in Figure 4. The correlation is not perfect: the result for $Bi(CCH)_3$ stands apart, and the dependence for the $Me(CHCH_2)_n$ and $Me(CH_3)_n$ series is much less clear-cut than for $Me(CCH)_n$, but it should be kept in mind that the actual dependence of the FC term is on perturbed electron density on the nucleus, not on the static one.

4. Comparison of different computational methods

In this subsection we compare the one-component and two-component ZORA results (focusing on the spin-orbit coupling effects), and the results of other available computational methods including the relativistic effects: four-component all-electron Dirac-Kohn-Sham method and effective core potentials.

a. Comparison between so-ZORA and DKS Inspection of the exact kernel results in Table I leads to the conclusion that so-ZORA reproduces the DKS results very well. Explicit

inclusion of small spinor during the calculation does not change significantly the calculated $^2J_{CC}$ couplings in comparison with two-component ZORA approximation: in most cases the differences are less than 1.5 Hz, and seem to be caused mostly by the change of the basis set (see above) rather than the picture change effects. It should be kept in mind that the comparison of ZORA and Dirac-Kohn-Sham results (or ZORA and ECP results) is not straightforward, since, out of necessity, different basis sets are used (ADF employs Slater orbital basis set, while in ReSpect and Gaussian the Gauss orbitals are used). For that reason we have also performed comparison of the results obtained using the Slater- and Gauss-type orbitals with the non-relativistic Hamiltonian. This comparison (see Table 1 in Supplementary Information) shows that in the most cases there is very good agreement between the jcpl/TZ2P basis set (Slater-type basis set) and upcJ-2/dyall.v3z basis set (Gauss-type basis set) results obtained at the non-relativistic level. While the Gauss-type basis set results systematically overestimate the Slater-type basis set ones, in most cases the differences do not exceed 1 Hz and for the 5th row compounds they are less than 0.4 Hz (except for $Cd(CCH)_2$, where the difference is 0.8 Hz). For the selected 6th row compounds, especially for -CCH derivatives, the differences are bigger (3.9 Hz , 2.2 Hz and 1.2 Hz for mercury, thallium and lead compounds respectively), but they are still only about 10 % of the relativistic term calculated at ZORA level. For the others compounds the differences do not exceed 1 Hz. Considering this, the use of different basis sets should not influence materially the comparison between the ZORA-DFT and DKS results, except when the relativistic effect is very small.

b. Fitting kernel in DKS calculations Two types of computation with DKS Hamiltonian have been performed: involving fitted kernel technique (approximate method) and involving exact kernel. Fitting kernel technique leads to somewhat overestimated spin-spin coupling constants in comparison to the exact kernel calculations. The differences are relatively small for sizeable (bigger than 10 Hz) spin-spin coupling constants, but much worse agreement is observed for small spin-spin coupling constants, where in several cases fitted kernel technique overestimate about 50% coupling constant calculated with exact form of kernel (in the case of $Po(CCH)_2$ overestimation is much bigger-fitted kernel result is 4 times bigger than result obtained with exact form of kernel). It should be concluded that fitting technique, even if faster in comparison with exact kernel technique, does not reproduce HALA effects on $^2J_{CC}$ for this compounds very well, especially when the coupling constants

are small.

c. Comparison between sc-ZORA and ECPs methods The differences between $^2J_{CC}$ spin-spin coupling constants calculated using scalar ECPs and scalar-only ZORA results are shown in Figure 1 and compared with the scalar ZORA term. Again, it should be pointed out that a different basis set has been used for the sc-ZORA and ECP calculations.

Two types of ECPs have been investigated: Los Alamos ECPs (LANL2DZ) and series of Stuttgart ECPs (MDF and MWB with small and big core replacement). LANL2DZ does not reproduce the sc-ZORA results very well, in many cases overestimating the scalar relativistic effects twice or (for $Hg(CHCH_2)_3$ and $Hg(CH_3)_2$) more. For a series of large-core MDF and MWB pseudopotentials poor agreement with the scalar ZORA results is observed again, apparently resulting mainly from replacing too many core electrons by the effective potential. In contrast to that, the small-core MWB and MDF60 results are usually in excellent agreement with sc-ZORA (provided the most recent version of MDF is used). The same has been observed before for $^1J_{CC}$ in organomercury compounds[10].

B. $^3J_{CC}$ coupling constants

The $^3J_{CC}$ coupling constants calculated using the Schrödinger, ZORA and Dirac-Coulomb Hamiltonians are shown in Table II. Comparison of $^2J_{CC}$ and $^3J_{CC}$ shows that for the vicinal coupling constants the relativistic term is much smaller (as far as the absolute value is concerned) than for the geminal coupling constants, but the relative contributions are in most cases similar (about 40% and 52% of full spin-spin coupling constant for $^2J_{CC}$ and $^3J_{CC}$, respectively).

d. Influence of the type of the heavy atom For systems containing -CCH derivatives the biggest spin-spin coupling constants are observed for 12th group elements and the smallest for 15th group elements. Interestingly, for systems containing the $-CHCH_2$ group a reverse trend is observed, the biggest spin-spin coupling constants are observed for systems containing the 16th group elements, and the smallest for systems with the 12th group elements ($^3J_{CC}$ for $Po(CHCH_2)_2$ is a bit smaller than for $Bi(CHCH_2)_3$. This is a result of the interplay between the spin-orbit coupling and scalar terms, which have opposite signs for the p-electron block metal compounds.

e. Influence of the charge of the heavy nucleus The relativistic terms for $^3J_{CC}$ in the 5th row compounds do not exceed 2.4 Hz(for $Cd(CCH)_2$). However, since spin-spin coupling constants are rather small, the percentage of the relativistic effects in the total spin spin coupling constant is still sizeable (about 25% of the so-ZORA result). For the 6th row of periodic table the relativistic effects are at most 7.4 Hz, i.e. 52% of total spin-spin coupling constant for $Hg(CCH)_2$.

f. Influence of the carbon hybridization Like for $^2J_{CC}$, the magnitude of the relativistic effect on the $^3J_{CC}$ spin-spin coupling constants depends strongly on the hybridization of carbon atoms. The largest effects are observed for series of molecules containing carbon with the sp hybridization (in the case of $Bi(CCH)_3$ the nonrelativistic value of $^3J_{CC}$ has the wrong sign and is almost 6 times too large). In the case of the couplings involving the sp^2 carbon for the systems containing elements of 5th row of periodic table the relativistic effects are generally negligible (less than 0.2 Hz). For the 6th row elements the relativistic effects are still small in terms of their absolute value (less than 0.6 Hz) but in many cases they dominate the spin-spin coupling constant (for example for $Hg(CHCH)_2$, where $^3J_{CC}$ is 0.1 Hz, the relativistic term is about 0.4 Hz).

1. The spin-orbit coupling and scalar terms

For the 5th row of periodic table the spin-orbit coupling contribution to $^3J_{CC}$ is generally small (at most 0.5 Hz). For the 6th row systems in case of mercury, thallium and lead compounds the spin-orbit coupling term is again small (0.8 Hz) and does not exceed 22% of the relativistic term, but for bismuth and polonium compounds it becomes sizeable (2.3 Hz for $Po(CCH)_2$) and dominates over the scalar term (-0.9 Hz for $Po(CCH)_2$).

The spin-orbit coupling influences $^3J_{CC}$ mainly through the FC+SD/PSO cross term (see Table IV), although for $^3J_{CC}$ in $Po(CHCH_2)_2$ the changes in the FC+SD and the FC+SD/PSO cross terms have comparable magnitudes. Again the change in the other terms (PSO and DSO) is negligible.

2. Comparison of different computational methods

a. Comparison between so-ZORA and DKS Inspection of the DKS results shows that so-ZORA reproduces DKS (with exact kernel approach) results with excellent agreement: the differences are less than 0.3 Hz and are mostly due to different basis set used.

Comparison of fitting kernel results with exact kernel shows that in case of $^3J_{CC}$ approximate method works much better than in case of $^2J_{CC}$: the differences are less than 0.4 Hz and in most cases the fitting kernel results overestimate the exact kernel results by less than 7%.

b. Comparison between sc-ZORA and ECPs methods The deviations between $^3J_{CC}$ spin-spin coupling constants calculated using scalar ECPs and scalar-only ZORA results are small when Stuttgart ECPs with small core replacement (sMWB and sMDF) are used. The LANL2DZ effective core potential is on the average rather inferior to the other pseudopotentials under study.

C. Long-range carbon-carbon coupling constants

The $^4J_{CC}$ coupling constants are the smallest among the discussed spin-spin coupling constants. They do not exceed 4 Hz, and in many cases are smaller than 1 Hz. The biggest values are observed for $Cd(CCH)_2$ and $Hg(CCH)_2$ (2.0 Hz and 3.6 Hz, respectively). Similarly as for $^3J_{CC}$, the relativistic term is sizeable only for the -CCH derivatives: from 13% for $In(CCH)_3$ to 66% for $Po(CCH)_2$. In general, the relative importance of the relativistic contributions for $^4J_{CC}$ is the same as for $^3J_{CC}$. Like for $^2J_{CC}$ and $^3J_{CC}$, the relativistic effects for the 6th row elements are about 3-5 times bigger than for analogous compounds containing 5th row elements.

In the most cases the relativistic contribution to $^4J_{CC}$ is dominated by the scalar term. Only for $Bi(CCH)_3$ and $Po(CCH)_2$ compounds spin-orbit coupling terms to $^4J_{CC}$ are sizeable and actually larger than the scalar terms. The largest contribution is the FC+SD/PSD cross term (Table IV).

1. Comparison of different computational methods

The so-ZORA method reproduces the four-component DKS results very well. In most cases the difference is lower than 0.1 Hz, and, like for the other couplings, originates to some

extent from using different basis sets. Fitting kernel technique again overestimates the exact kernel DKS results but differences are small (less than 0.2 Hz).

As for as ECPs are concerned, the small core-replacement ECPs (sMDF and sMWB) reproduce the scalar ZORA term (and the whole coupling constant, since the spin-orbit coupling terms are small) very well, while the large core-replacement Stuttgart ECPs and LANL2DZ underestimate it.

IV. SUMMARY AND CONCLUSIONS

The $^2J_{CC}$, $^3J_{CC}$, and $^4J_{CC}$ spin-spin coupling constants in the molecules with heavy atom (Cd, In, Sn, Sb, Te, Hg, Tl, Pb, Bi and Po) in the coupling path have been calculated by means of density functional theory. The relativistic effects have been accounted for by means of Dirac-Kohn-Sham calculations (with four-component Dirac-Coulomb Hamiltonian), the calculations with relativistic one-component (scalar zeroth order perturbational theory, ZORA) and two-component (spin-orbit zeroth order regular approximation ZORA) Hamiltonians, and the relativistic effective core potentials applied with non-relativistic Hamiltonians. The most important observations can be summarized as follows.

The magnitude of spin-spin coupling constants as well as importance of relativistic contribution changes significantly with the number of the bonds in coupling path, hybridization of carbon atoms, charge and electron configuration of the heavy atom. The percentage of relativistic contribution is in most cases similar for $^2J_{CC}$, $^3J_{CC}$, and $^4J_{CC}$ in the same molecule, although the magnitudes of the coupling contants vary significantly.

The value of the metal-transmitted spin-spin coupling constant depends strongly on the electron configuration of the metal. Generally the $^nJ_{CC}$ coupling constants are the biggest for the compounds containing the 12th group elements and the smallest for the compounds containing the 15 and 16th group elements. A reverse trend is observed only for $^3J_{CC}$ and $^4J_{CC}$ in $Me(CHCH_2)_n$ derivatives, where the couplings are the biggest for Te/Po compounds and the smallest for Cd/Hg compounds. $^2J_{CC}$ correlates quazi-linearly with the change of the C-Me-C bond angle.

The atomic number of the heavy atom influences significantly the value of the spin-spin coupling constant, which is visible when comparing the series of compounds containing the elements from the same group of periodic table. This variation of the coupling within

the group is mainly a relativistic effect, since nonrelativistic values of spin-spin coupling constants for these compounds are similar. For the 5th row of periodic table the relativistic contribution to $^2J_{CC}$ as a rule does not exceed 26%, whereas for 6th row elements it can reach up to 83%.

The relativistic contribution depends also on hybridization of coupled carbon atom. The value of this contribution for couplings involving the sp^3-type carbon is about 7-61% smaller than for those involving the sp-type carbon.

The ratio between the spin-orbit coupling term and the scalar term depends on the electron configuration of the heavy atom and the carbon atom hybridization. In the case of $^2J_{CC}$ in molecules containing 12-15th group elements the scalar term is the leading term in the relativistic contribution, whereas for the 16th group of periodic table the spin-orbit coupling terms are of comparable magnitude or even larger (for polonium compounds) than the scalar terms. The same is observed for $^3J_{CC}$ and $^4J_{CC}$ but here the spin-orbit coupling term dominates the relativistic correction also for the bismuth compounds. The relative importance of the spin-orbit coupling term is the biggest for compounds containing sp^3-type carbon and the smallest for compounds containing sp-type carbon. The spin-orbit coupling contribution can be correlated with the inverse of the lowest triplet excitation energy, which explains for example the large value for Po compound.

A comparison of the results obtained by means of different methods of including the relativistic effects indicates that ZORA-DFT (with the spin-orbit term included) reproduces the DKS results (calculated with the exact kernel technique) very well. In most cases the fitting kernel technique only slightly overestimates (10% or less) the exact kernel DKS results, but for several $^2J_{CC}$ coupling constants, where the value of the spin-spin coupling constant is rather small, the deviations are much bigger (30% or more).

The performance of scalar ECPs depends, obviously, on the relative weight of the scalar and spin-orbit coupling terms, but when the former are dominant, ECPs reproduce the results obtained with more elaborate relativistic methods correctly, provided the outer core electrons on the heavy atom are accounted for explicitly ('small core' types of ECPs).

ACKNOWLEDGMENTS

This work has received support from the Polish Ministry of Science and Higher Education via the ST4-270978 grant, from COST-CMTS Action CM1002 COnvergent Distributed Environment for Computational Spectroscopy (CODECS), from the Wrocław Centre for Networking and Supercomputing through a grant of computer time, and MPD/2010/4 project, realized within the MPD programme of Foundation for Polish Science, cofinanced from European Union, Regional Development Fund. O.L.M. acknowledges the financial support from the Grant Agency of the Ministry of Education of the Slovak Republic and Slovak Academy of Sciences VEGA (project No. 2/0148/13) and the Slovak Research and Development Agency (project No. APVV-0483-10 and APVV-0510-12).

REFERENCES

[1]P. Pyykkö, A. Görling, and N. Rösch, Mol. Phys. **61**, 195 (1987).

[2]M. Kaupp, V. G. Malkin, O. L. Malkina, and D. R. Salahub, Chem. Phys. Lett. **235**, 382 (1995).

[3]M. Kaupp and O. L. Malkina, J. Chem. Phys. **108**, 3648 (1998).

[4]S. Berger, W. Bock, G. Frenking, V. Jonas, and F. Mueller, J. Am. Chem. Soc. **117**, 3820 (1995).

[5]M. Kaupp, Chem. Eur. J. **2**, 348 (1996).

[6]M. Kaupp, *Relativistic Electronic Structure Theory. Part 2. Applications*, edited by P. Schwerdtfeger (Elsevier, Amsterdam, 2004) p. 552.

[7]M. Kaupp, O. L. Malkina, V. G. Malkin, and P. Pyykkö, Chem. Eur. J. **4**, 118 (1998).

[8]A. Wodyński, M. Repiský, and M. Pecul, J. Chem. Phys. **137**, 014311 (2012).

[9]A. Wodyński, A. Gryff-Keller, and M. Pecul, J. Chem. Theory Comput. **9**, 1909 (2013).

[10]A. Wodyński and M. Pecul, The Journal of Chemical Physics **140**, 024319 (2014).

[11]A. Bagno and G. Saielli, J. Am. Chem. Soc. **129**, 11360 (2007).

[12]M. Olejniczak and M. Pecul, ChemPhysChem **10**, 1247 (2009).

[13]M. Kauch and M. Pecul, ChemPhysChem **13**, 1332 (2012).

[14]S. Kirpekar, H. Jensen, and J. Oddershede, Theor. Chim. Acta **95**, 35 (1997).

[15]J. Vaara, K. Ruud, and O. Vahtras, J. Comput. Chem. **20**, 1314 (1999).

[16]A. Křístkováa, S. Komorovský, R. Michal, V. G. Malkin, and O. L. Malkina, "Relativistic four-component calculations of indirect nuclear spin-spin couplings with efficient evaluation of the exchange-correlation kernel," (in preparation 2014).

[17]L. Versluis and T. Ziegler, J. Chem. Phys. **88**, 322 (1988).

[18]"ADF2010, SCM, Theoretical Chemistry, Vrije Universiteit, Amsterdam, The Netherlands, http://www.scm.com,".

[19]S. Vosko, L. Wilk, and M. Nusair, Can. J. Phys. **58**, 1200 (1980).

[20]A. D. Becke, Phys. Rev. A **38**, 3098 (1988).

[21]J. P. Perdew, Phys. Rev. B **33**, 8822 (1986).

[22]J. P. Perdew and A. Zunger, Phys. Rev. B **23**, 5048 (1981).

[23]S. Komorovský, M. Repiský, O. L. Malkina, V. G. Malkin, I. M. Ondík, and M. Kaupp, J. Chem. Phys. **128**, 104101 (2008).

[24]J. P. Perdew, K. Burke, and M. Ernzerhof, Phys. Rev. Lett. **77**, 3865 (1996).

[25]K. G. Dyall, Theor. Chem. Acc. **112**, 403 (2004).

[26]J. Autschbach, J. Chem. Phys. **129**, 094105 (2008).

[27]Gaussian 09 Revision C.01, Gaussian Inc. Wallingford CT 2009, M. J. Frisch, G. W. Trucks, H. B. Schlegel, G. E. Scuseria, M. A. Robb, J. R. Cheeseman, G. Scalmani, V. Barone, B. Mennucci, G. A. Petersson, H. Nakatsuji, M. Caricato, X. Li, H. P. Hratchian, A. F. Izmaylov, J. Bloino, G. Zheng, J. L. Sonnenberg, M. Hada, M. Ehara, K. Toyota, R. Fukuda, J. Hasegawa, M. Ishida, T. Nakajima, Y. Honda, O. Kitao, H. Nakai, T. Vreven, Montgomery, Jr., J. A., J. E. Peralta, F. Ogliaro, M. Bearpark, J. J. Heyd, E. Brothers, K. N. Kudin, V. N. Staroverov, R. Kobayashi, J. Norm,, K. Raghavachari, A. Rendell, J. C. Burant, S. S. Iyengar, J. Tomasi, M. Cossi, N. Rega, J. M. Millam, M. Klene, J. E. Knox, J. B. Cross, V. Bakken, C. Adamo, J. Jaramillo, R. Gomperts, R. E. Stratmann, O. Yazyev, A. J. Austin, R. Cammi, C. Pomelli, J. W. Ochterski, R. L. Martin, K. Morokuma, V. G. Zakrzewski, G. A. Voth, P. Salvador, J. J. Dannenberg, S. Dapprich, A. D. Daniels, Ö. Farkas, J. B. Foresman, J. V. Ortiz, J. Cioslowski and D. J. Fox.

[28]P. J. Hay and W. R. Wadt, J. Chem. Phys. **82**, 270 (1985).

[29]D. Figgen, G. Rauhut, M. Dolg, and H. Stoll, Chemical Physics **311**, 227 (2005).

[30]B. Metz, H. Stoll, and M. Dolg, The Journal of Chemical Physics **113**, 2563 (2000).

[31]K. A. Peterson, D. Figgen, E. Goll, H. Stoll, and M. Dolg, J. Chem. Phys. **119**, 11113 (2003).

[32]D. Andrae, U. Huermann, M. Dolg, H. Stoll, and H. Preu, Theoretica Chimica Acta **77**, 123 (1990).

[33]T. Leininger, A. Nicklass, H. Stoll, M. Dolg, and P. Schwerdtfeger, The Journal of Chemical Physics **105**, 1052 (1996).

[34]F. Schautz, H.-J. Flad, and M. Dolg, Theor. Chem. Acc. **99**, 231 (1998).

[35]A. Bergner, M. Dolg, W. Küchle, H. Stoll, and H. Preuß, Mol. Phys. **80**, 1431 (1993).

[36]U. Häussermann, M. Dolg, H. Stoll, H. Preuss, P. Schwerdtfeger, and R. Pitzer, Mol. Phys. **78**, 1211 (1993).

[37]D. Andrae, U. Häussermann, M. Dolg, H. Stoll, and H. Preuss, Theor. Chim. Acta **77**, 123 (1990).

[38]T. Leininger, A. Berning, A. Nicklass, H. Stoll, H.-J. Werner, and H.-J. Flad, Chemical Physics **217**, 19 (1997).

[39]W. Küchle, M. Dolg, H. Stoll, and H. Preuss, Mol. Phys. **74**, 1245 (1991).

[40]H. Stoll, B. Metz, and M. Dolg, J. Comput. Chem. **23**, 767 (2002).

[41]"Dalton2011, a molecular electronic structure program (2011), http://www.daltonprogram.org,".

[42]M. Pecul, M. Jaszuński, and J. Sadlej, Chemical Physics Letters **305**, 139 (1999).

[43]J. Autschbach and T. Ziegler, J. Chem. Phys. **113**, 9410 (2000).

[44]M. Kaupp and O. L. Malkina, The Journal of Chemical Physics **108**, 3648 (1998).

		LANL2DZ-(sc-ZORA) [Hz]	lMDF-(sc-ZORA) [Hz]	sMDF-(sc-ZORA) [Hz]	sMDF(new)-(sc-ZORA) [Hz]	lMWB-(sc-ZORA) [Hz]	sMWB-(sc-ZORA) [Hz]	scalar term(sc-ZORA) [Hz]
Cd	$Cd(CCH)_2$	-0.33		0.77		-14.11	0.48	10.40
	$Cd(CHCH_2)_2$	4.83		0.34		-2.39	0.15	4.08
	$CdMe_2$	5.05		0.18		0.37	0.02	1.94
In	$In(CCH)_3$	-3.86		0.31		-2.96	1.19	5.97
	$In(CHCH_2)_3$	-0.65		0.09		-0.49	-0.12	2.04
	$InMe_3$	-0.26		-0.12		-0.20	-0.31	1.04
Sn	$Sn(CCH)_4$	-1.22	-0.92	0.43		-0.95		3.21
	$Sn(CHCH_2)_4$	-0.06	-0.06	0.19		-0.01		0.68
	$SnMe_4$	0.00	-0.04	0.12		0.04		0.34
Sb	$Sb(CCH)_3$	1.23	1.06	-0.14		0.38		-1.40
	$Sb(CHCH_2)_3$	0.56	0.51	-0.01		0.24		-0.61
	$SbMe_3$	0.49	0.46	0.10		0.28		-0.38
Te	$Te(CCH)_2$	0.99	0.55	-0.62		0.01		-1.59
	$Te(CHCH_2)_2$	0.48	0.35	-0.02		0.23		-0.60
	$TeMe_2$	0.36	0.30	0.02		0.27		-0.29
Hg	$Hg(CCH)_2$	3.46		-13.94	-1.11	-12.25	-1.91	30.96
	$Hg(CHCH_2)_2$	10.19		-4.50	0.10	1.46	-0.43	9.57
	$HgMe_2$	9.11		-2.26	0.81	3.88	-0.10	4.07
Tl	$Tl(CCH)_3$	-1.66		-1.53		-6.71	-1.19	23.89
	$Tl(CHCH_2)_3$	1.43		-0.42		-1.22	-0.46	7.53
	$TlMe_3$	1.33		-0.31		-0.56	-0.39	3.61
Pb	$Pb(CCH)_4$	-1.44	-2.86	-0.52		-3.74		14.00
	$Pb(CHCH_2)_4$	-0.14	-0.40	-0.09		-0.93		2.67
	$PbMe_4$	-0.14	-0.36	-0.05		-0.55		1.27
Bi	$Bi(CCH)_3$	1.26	3.44	0.57		-0.09		-5.08
	$Bi(CHCH_2)_3$	0.54	1.34	0.25		0.13		-1.96
	$BiMe_3$	0.45	0.89	0.26		0.27		-1.03
Po	$Po(CCH)_2$		0.88	-0.48		0.33		-5.01
	$Po(CHCH_2)_2$		0.44	0.07		0.27		-1.69
	$PoMe_2$		0.32	0.08		0.27		-0.68

FIG. 1. Comparison of the $^2J_{CC}$ coupling constants calculated with different types of effective core potentials on heavy atoms and pcJ-2 basis set on C and H, using PBE functional.

TABLE I. The $^2J_{CC}$ coupling constants calculated with PBE functional at different levels of theory.

	nonrel (ADF) [Hz]	sc-ZORA [Hz]	so-ZORA [Hz]	exact DKS [Hz]	fit DKS [Hz]
$Cd(CCH)_2$	38.0	48.4	48.0	47.2	50.4
$Cd(CHCH_2)_2$	25.7	29.7	29.4	28.8	31.6
$Cd(CH_3)_2$	17.6	19.5	19.3	18.7	21
$In(CCH)_3$	21.8	27.8	27.6	27.0	28.2
$In(CHCH_2)_3$	10.9	12.9	12.8	12.5	13.3
$In(CH_3)_3$	7.8	8.9	8.8	8.4	8.8
$Sn(CCH)_4$	11.4	14.6	14.5	14.3	15.4
$Sn(CHCH_2)_4$	4.0	4.7	4.7	4.1	5.2
$Sn(CH_3)_4$	3.1	3.4	3.5	3.4	3.9
$Sb(CCH)_3$	-1.5	-2.9	-2.6	-2.3	-3.4
$Sb(CHCH_2)_3$	-1.4	-2.0	-1.9	-1.7	-2.3
$Sb(CH_3)_3$	-0.8	-1.2	-0.9	-0.8	-0.7
$Te(CCH)_2$	-3.8	-5.3	-4.4	-4.2	-5.7
$Te(CHCH_2)_2$	0.7	0.1	0.6	0.8	0.7
$Te(CH_3)_2$	-0.5	-0.8	-0.3	-0.2	-0.3
$Hg(CCH)_2$	38.8	69.6	65.1	64.3	67.5
$Hg(CHCH_2)_2$	24.3	33.7	30.8	30.7	33.3
$Hg(CH_3)_2$	16.6	20.6	18.3	18.3	20.4
$Tl(CCH)_3$	19.7	43.4	40.9	40.5	42.2
$Tl(CHCH_2)_3$	10.2	17.7	16.5	16.2	17.3
$Tl(CH_3)_3$	6.9	10.4	9.8	9.5	10.2
$Pb(CCH)_4$	10.8	24.7	23.7	23.7	24.3
$Pb(CHCH_2)_4$	3.8	6.4	6.2	6.1	6.6
$Pb(CH_3)_4$	2.7	3.9	4.0	3.8	4.1
$Bi(CCH)_3$	-1.1	-6.2	-6.4	-5.6	-7.6
$Bi(CHCH_2)_3$	-1.2	-3.2	-3.4	-2.9	-4.1
$Bi(CH_3)_3$	-0.7	-1.7	-1.3	-1.0	-1.4
$Po(CCH)_2$	-3.2	-8.2	-1.5	-0.7	-2.9
$Po(CHCH_2)_2$	0.2	-1.5	0.9	1.2	0.6
$Po(CH_3)_2$	-0.4	-1.0	0.6	0.9	0.5

TABLE II. The $^3J_{CC}$ coupling constants calculated with PBE functional at different levels of theory.

	nonrel (ADF) [Hz]	sc-ZORA [Hz]	so-ZORA [Hz]	exact DKS [Hz]	fit DKS [Hz]
$Cd(CCH)_2$	6.9	9.3	9.3	9.3	9.7
$Cd(CHCH_2)_2$	-0.2	-0.1	0.0	0.0	0.2
$In(CCH)_3$	4.3	5.7	5.5	5.5	5.6
$In(CHCH_2)_3$	1.0	1.0	1.0	1.0	1.0
$Sn(CCH)_4$	2.6	3.4	3.3	3.2	3.4
$Sn(CHCH_2)_4$	1.1	1.1	1.1	0.8	1.2
$Sb(CCH)_3$	2.0	1.7	1.5	1.4	1.5
$Sb(CHCH_2)_3$	2.6	2.6	2.6	2.5	2.7
$Te(CCH)_2$	2.1	1.8	2.3	2.3	2.4
$Te(CHCH_2)_2$	3.3	3.3	3.2	3.1	3.3
$Hg(CCH)_2$	6.8	14.6	14.1	14.1	14.5
$Hg(CHCH_2)_2$	-0.3	0.0	0.1	0.3	0.3
$Tl(CCH)_3$	3.9	9.3	8.6	8.5	8.7
$Tl(CHCH_2)_3$	1.0	1.2	1.1	1.2	1.0
$Pb(CCH)_4$	2.5	5.7	5.2	5.2	5.3
$Pb(CHCH_2)_4$	1.0	1.0	1.0	0.9	0.9
$Bi(CCH)_3$	1.7	0.8	-0.3	-0.3	-0.4
$Bi(CHCH_2)_3$	2.4	2.4	2.2	2.1	2.3
$Po(CCH)_2$	1.7	0.8	3.1	3.2	3.8
$Po(CHCH_2)_2$	2.7	2.4	2.1	2.0	2.2

TABLE III. The $^4J_{CC}$ coupling constants calculated with PBE functional at different levels of theory.

	nonrel (ADF) [Hz]	sc-ZORA [Hz]	so-ZORA [Hz]	exact DKS [Hz]	fit DKS [Hz]
$Cd(CCH)_2$	1.4	1.9	2.0	2.0	2.0
$Cd(CHCH_2)_2$	0.0	0.0	0.0	0.0	0.1
$In(CCH)_3$	1.3	1.5	1.5	1.5	1.6
$In(CHCH_2)_3$	-0.2	-0.2	-0.2	-0.2	-0.2
$Sn(CCH)_4$	0.8	1.0	1.0	0.9	1.0
$Sn(CHCH_2)_4$	0.0	0.0	0.0	0.0	0.0
$Sb(CCH)_3$	0.8	0.8	0.7	0.7	0.8
$Sb(CHCH_2)_3$	0.1	0.0	0.0	0.1	0.0
$Te(CCH)_2$	0.2	0.2	0.3	0.2	0.4
$Te(CHCH_2)_2$	1.2	1.2	1.2	1.3	1.3
$Hg(CCH)_2$	1.5	3.4	3.6	3.7	3.8
$Hg(CHCH_2)_2$	-0.1	-0.2	-0.2	-0.2	-0.1
$Tl(CCH)_3$	1.2	2.4	2.2	2.2	2.2
$Tl(CHCH_2)_3$	-0.2	-0.2	-0.2	-0.2	-0.3
$Pb(CCH)_4$	0.8	1.5	1.3	1.3	1.3
$Pb(CHCH_2)_4$	0.0	0.0	0.0	0.0	-0.1
$Bi(CCH)_3$	0.7	0.7	0.3	0.3	0.4
$Bi(CHCH_2)_3$	0.0	0.0	0.0	0.0	0.0
$Po(CCH)_2$	0.2	0.1	0.6	0.5	0.6
$Po(CHCH_2)_2$	0.9	0.9	0.9	0.9	0.9

TABLE IV. The spin-orbit coupling term to FC+SD, SO(PSO+DSO) terms and FC+SD/PSO cross term to $^2J_{CC}$, $^3J_{CC}$ and $^4J_{CC}$ coupling constants

	$^2J_{CC}$				$^3J_{CC}$				$^4J_{CC}$			
	FC+SD	SO	FC+SD/PSO	SO sum	FC+SD	SO	FC+SD/PSO	SO sum	FC+SD	SO	FC+SD/PSO	SO sum
$Te(CCH)_2$	0.14	0.00	0.80	0.94	-0.04	0.00	0.60	0.56	-0.02	0.01	0.11	0.11
$Te(CHCH_2)_2$	0.04	0.00	0.51	0.54	0.00	0.00	-0.07	-0.07	0.01	0.00	-0.01	0.00
$Te(CH_3)_2$	-0.06	0.00	0.55	0.49	-	-	-	-	-	-	-	-
$Po(CCH)_2$	3.77	0.00	2.89	6.67	0.18	0.00	2.13	2.31	-0.09	0.12	0.46	0.50
$Po(CHCH_2)_2$	0.97	0.09	1.39	2.44	-0.17	0.00	-0.21	-0.39	-0.04	-0.01	0.01	-0.04
Po(CH3)2	0.40	-0.04	1.32	1.68	-	-	-	-	-	-	-	-

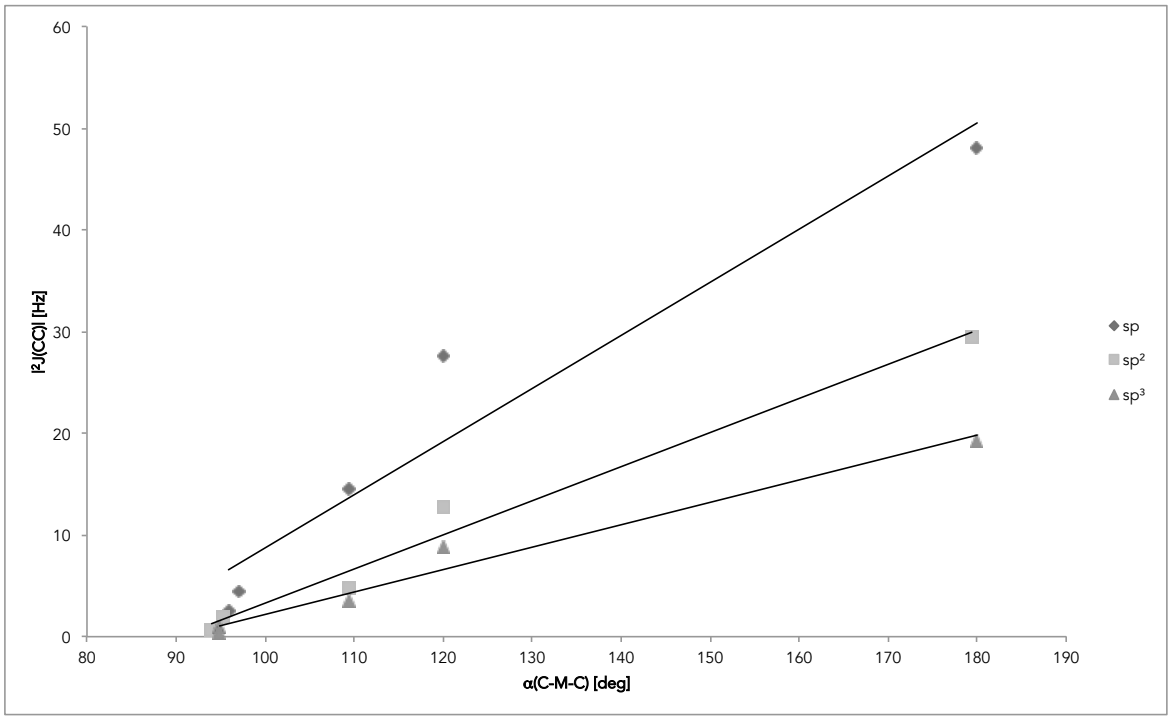

FIG. 2. Correlation of $^{2}J_{CC}$ calculated with so-ZORA level with the plane angle in the systems containing 5th row elements

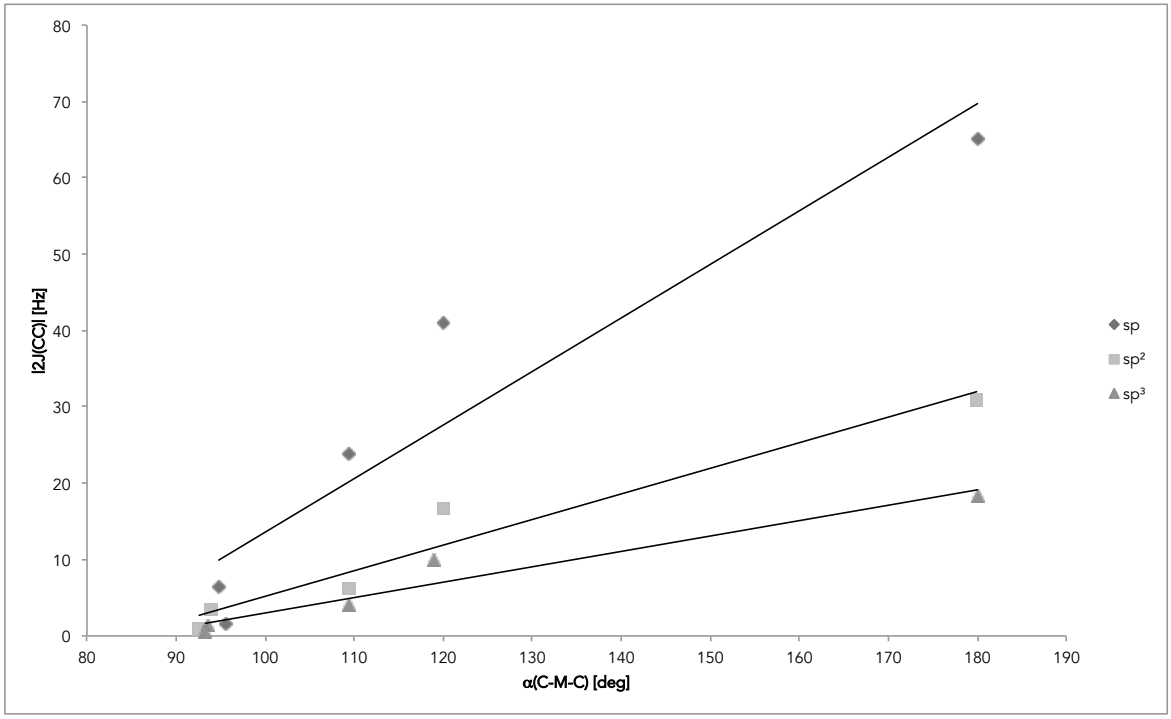

FIG. 3. Correlation of $^{2}J_{CC}$ calculated with so-ZORA level with the plane angle in the systems containing 6th row elements

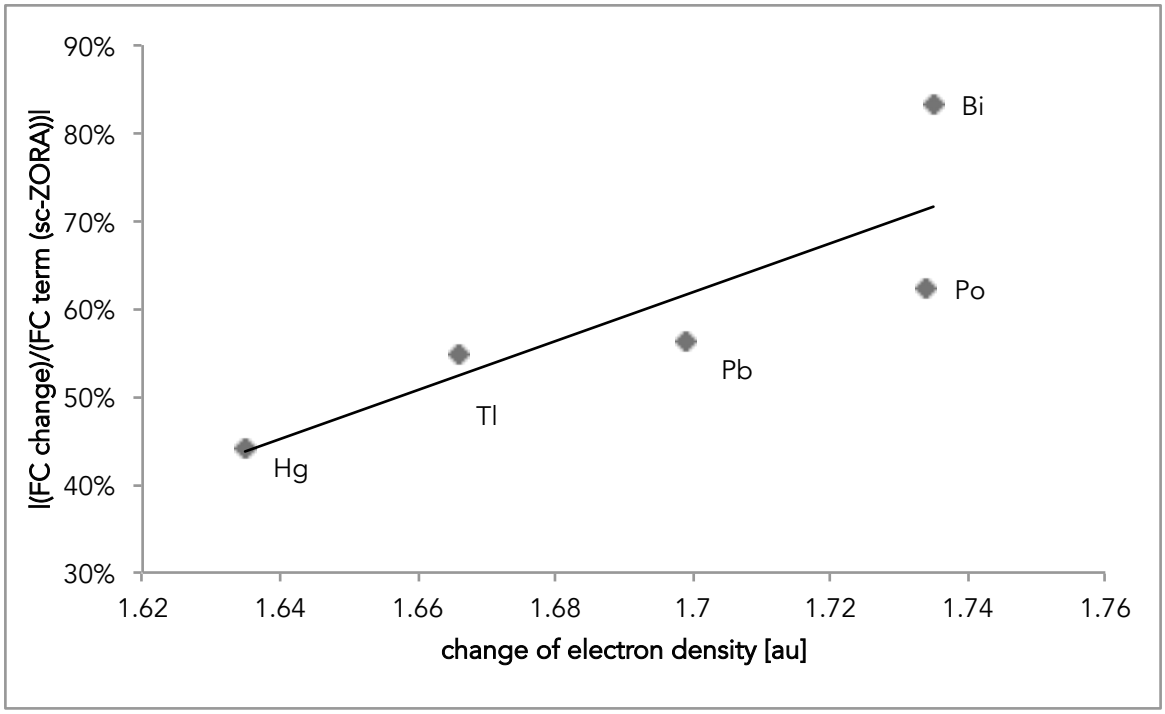

FIG. 4. Correlation of the relative contribution of the scalar relativistic effect to the FC term of $^2J_{CC}$ (shown as a percentage of the total value of the scalar FC term) for the $Me(CCH)_n$ series with the change of electron density on carbon nucleus induced by the scalar relativistic effects.

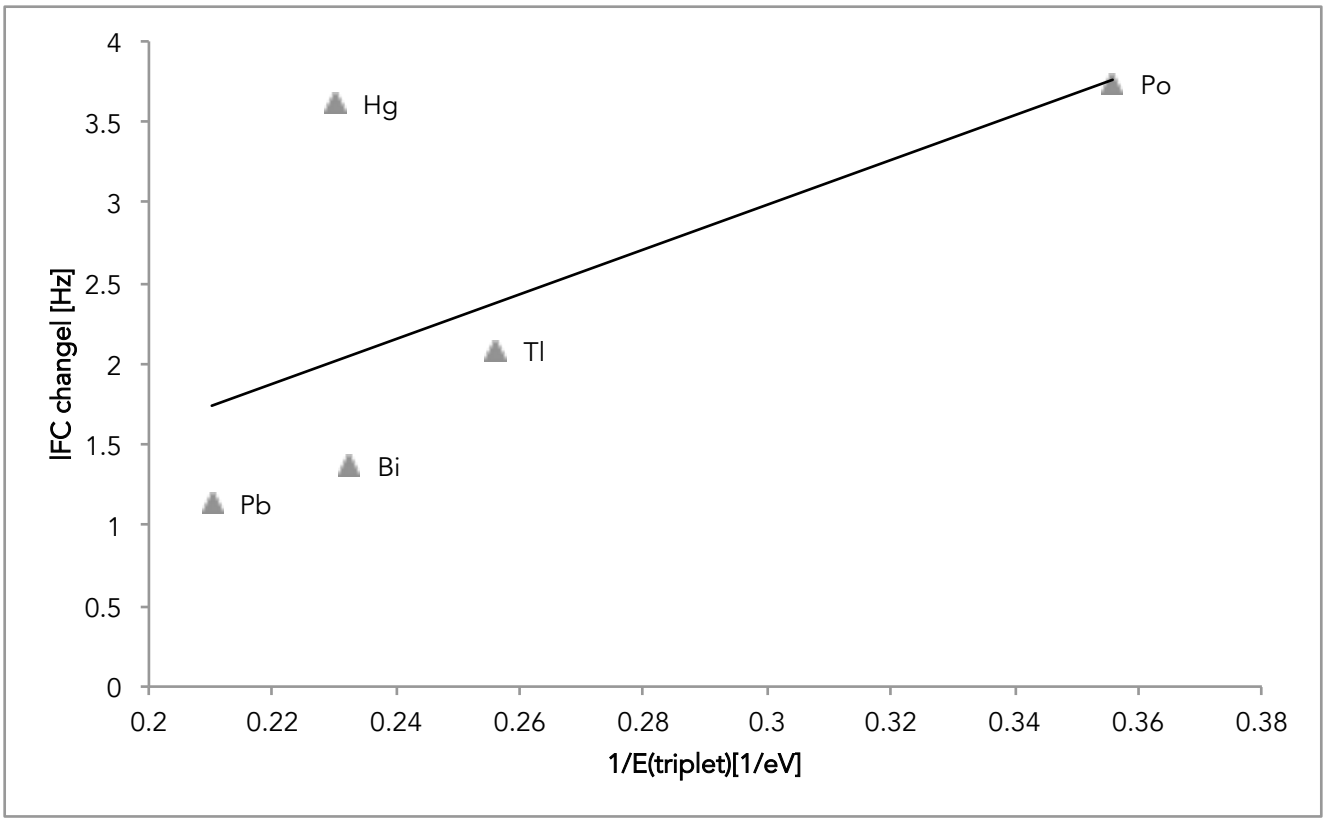

FIG. 5. Correlation of the spin-orbit coupling contributions to the FC term in $^2J_{CC}$ in the $Me(CCH)_n$ series with the inverse of the singlet-triplet HOMO-LUMO excitation energy.

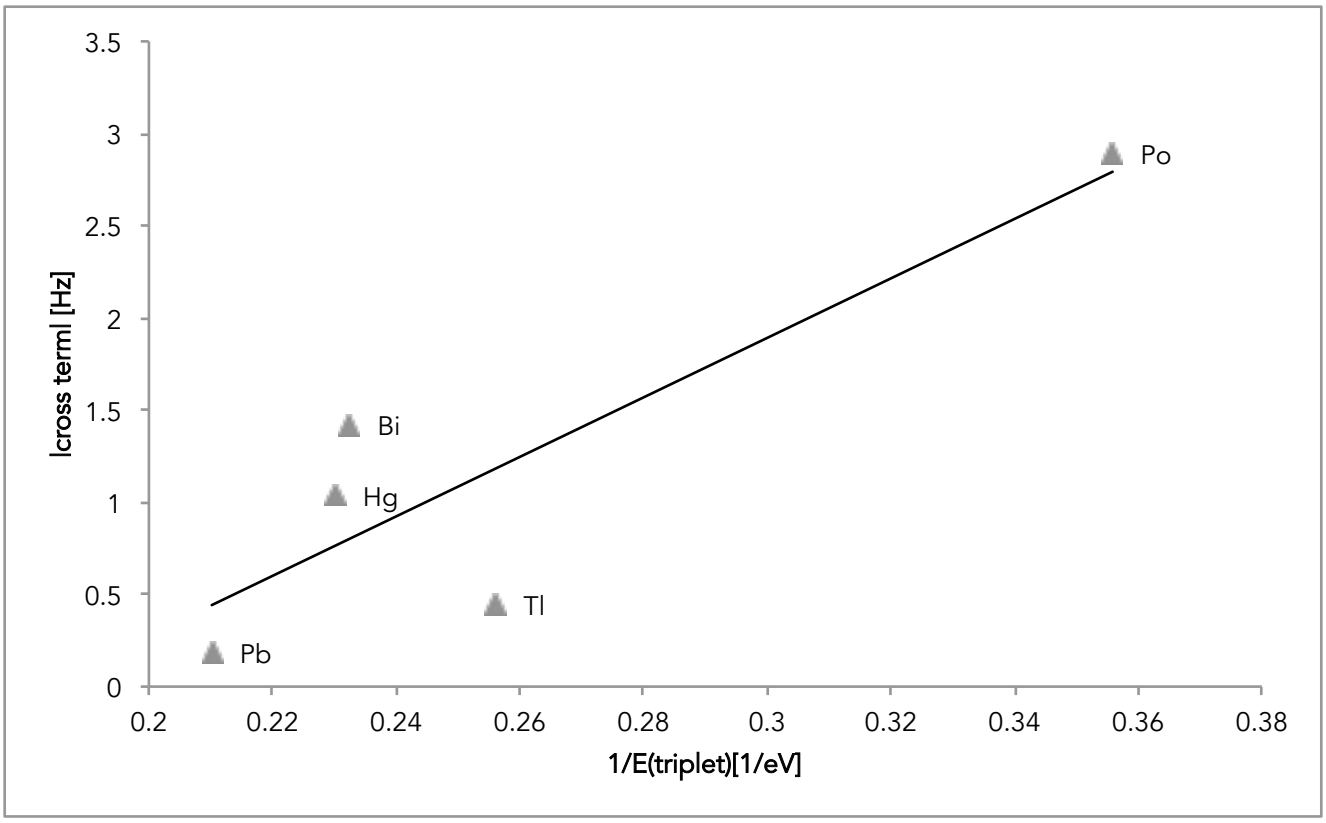

FIG. 6. Correlation of the FC+SD/PSO cross term to $^2J_{CC}$ in the $Me(CCH)_n$ series with the inverse of the singlet-triplet HOMO-LUMO excitation energy.